THE SELECTIVE STAINING AND ULTRASTRUCTURE OF THE RABBIT NUCLEUS PULPOSUS

Elizabeth Margaret Lumb

A Thesis Submitted for the Degree of PhD
at the
University of St Andrews

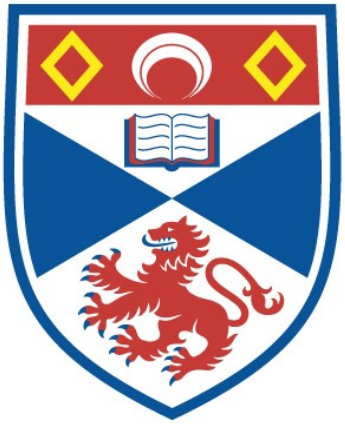

1975

The Selective Staining and Ultrastructure of the rabbit Nucleus Pulposus

being a thesis presented by

ELIZABETH MARGARET LUMB (Née RICHARDS)

to the University of St. Andrews in application for the Degree of Doctor of Philosophy.

March 1975

SUMMARY

The ultrastructure of the nucleus pulposus was studied with conventional staining methods. The multinucleated cell masses seen in toluidine blue stained thick sections could be resolved into a large number of closely packed cells at the ultrastructural level. Numerous desmosomes were observed between adjacent cells; a second type of intercellular junction was identified as a gap junction after extracellular tracer treatment. The possible functions of these junctions were discussed. The notochordal cell cytoplasmic organelles include centrioles, mitochondria, rough endoplasmic reticulum, Golgi apparatus, cytofilaments, glycogen and lysosomes. Large vesicles, a characteristic component of notochordal cells contain material which from its staining reaction was judged to be proteoglycan. Large numbers of pinocytotic vesicles were seen in the vicinity of extracellular bands of electron-dense material applied to the cells surface. Degenerating cells were occasionally seen in the young nucleus pulposus but were seen more frequently with advancing age.

The matrix contains metachromatic material which is seen after lead citrate and uranyl acetate staining as branched and unbranched beaded filaments. From its staining reaction the material was considered to represent proteoglycan. Isolated collagen fibres were occasionally seen. Banded fibres consisting of alternate dark and light bands, periodicity 84 nm were found in the pericellular matrix. From their staining reaction these structures

appear to consist of longitudinal protein filaments with transverse bands of fibrillar matrix proteoglycan. The possible relationship of this material to collagen was discussed.

With a view to selective staining and further identification of the matrix components the theory of the critical electrolyte concentration (C.E.C.) technique was outlined. The most promising organic cations containing a heavy metal for the ultrastructural application of this technique were chelates of haematein with heavy metals. Chelate formation is accompanied by a decrease in pH and in some cases a spectral change.

The characteristic absorption spectrum of indium haematein allowed the optimum molar ratio to be ascertained. Preliminary experiments of polyanions spotted on filter papers, unfixed collagen and thin sections of pancreas indicated a progressive loss of staining of sulphate, carboxyl and phosphate groups with increasing salt molarity. Unosmicated thin sections of nucleus pulposus showed loss of staining of vesicle material followed by matrix material as the salt molarity was increased; nuclear staining was largely unaffected. This staining pattern was discussed in terms of the C.E.C. theory.

Although iron, lead and uranium haematein chelates also produced staining consistant with localisation of tissue polyanions each had disadvantages which did not commend their use in the C.E.C. approach to selective staining.

DECLARATION

I hereby declare that the following thesis is based on work carried out by me, that the thesis is my own composition, and that no part of it has been presented previously for a higher degree.

The research was conducted in the Department of Anatomy, United College of St. Salvator and St. Leonard, University of St. Andrews under the direction of Professor J. W. Smith.

ACADEMIC RECORD

I first matriculated at the University of St. Andrews in October 1966 and graduated with the degree of Bachelor of Science Second Class Honours in Biochemistry in June 1970. I matriculated as a research student in the Department of Anatomy, University of St. Andrews, in October 1970.

C E R T I F I C A T E

I hereby certify that Elizabeth Margaret Lumb (née Richards) has spent 12 terms engaged in research work under my direction and that she has fulfilled the conditions of Ordinance No.12 of the University Course of the University of St. Andrews 1967 and that she is qualified to submit the accompanying thesis for the Degree of Doctor of Philosophy.

ACKNOWLEDGMENTS

I am deeply indebted to Professor J. W. Smith for his constant help and encouragement. I should like to thank Mr. R. J. Stuart for technical advice, Mr. S. Fairhurst for assistance with the photographic work and Emeritus Professor R. A. Walmsley for allowing me to work in his department during the course of this study. I should also like to thank Mrs. McAlister for preparing the typescript.

CONTENTS

	Page No.
INTRODUCTION	1
PART I	
MATERIALS and METHODS	
Tissue preparation for Light and Electron Microscopy	9
Staining procedures:-	
(1) Uranyl acetate / lead citrate	12
(2) Bismuth	13
(3) Phosphotungstic acid (P.T.A.)	14
(4) Ruthenium Red	14
(5) Lanthanum	16
(6) Acid phosphatase	19
OBSERVATIONS	
The Cells of the Nucleus Pulposus	21
The young animal	21
Specialisations of the Cell Membrane	22
Cytoplasmic Organelles	
1. Centrioles	33
2. Mitochondria	33
3. The Rough Endoplasmic Reticulum	34
4. The Golgi Apparatus	34
5. Large Vesicles	35
6. Other vesicles	38
7. Cytofilaments	39
8. Glycogen	40
9. Lysosomes.	42
Degenerating cells	44
The Matrix of the Nucleus Pulposus	46
PART II	
Theory of "critical electrolyte concentration" techniques	61
Haematein chelates	66
Indium haematein	68
C.E.C. values of polyanions adsorbed on filter paper	70
C.E.C. values for indium haematein staining of collagen and pancreas	73
C.E.C. values for indium haematein staining of the nucleus pulposus	76

C O N T E N T S

	Page No.
Iron haematein	80
Lead haematein	83
Uranium haematein	89
CONCLUSIONS	97
BIBLIOGRAPHY	101

INTRODUCTION

In mammals, intervertebral discs lie between adjacent vertebral bodies lending shape and elasticity to the spinal column. Each disc consists of a thick peripheral ring of collagenous tissue, the annulus fibrosus and a central mass of gelatinous material, the nucleus pulposus. The nucleus is separated from the adjacent vertebral bodies by plates of hyaline cartilage.

The character of the nucleus pulposus varies at different ages [Walmsley, 1953; Sylvén et al., 1951; Peacock, 1952] and in different species [Butler and Smith, 1964; Meachim and Cornah, 1970; Földes and Palfrey, 1971]. In young rabbits it is a highly viscous opalescent body which becomes increasingly fibrous with advancing age. It is entirely avascular [Smith and Walmsley, 1951] and is therefore dependent for its nutrition upon the diffusion of substances through the cartilagenous plates and/or the annulus fibrosus [Walmsley, 1951].

The histological appearance and age variation of the human nucleus pulposus has been studied extensively. Walmsley (1951) suggested, on the basis of light microscopy, the presence of large multinucleated cells having peripheral nuclei and large vesicles containing

mucoid material. The cells were embedded in a fairly extensive structureless metachromatic matrix. On the other hand, Peacock (1952) considered the multinucleated masses represented groups of singly nucleated cells, some of which showed signs of degeneration. It appears that there is a progressive loss of the cellular component with age and an increase of fibrillar material and structured elements within the matrix [Sylvén, 1951; Sylvén et al., 1951].

Previous studies on the ultrastructure of the nucleus pulposus include those by Sylvén et al. (1951), Happey et al. (1964), Smith and Serafini-Fracassini (1968), Cornah et al. (1970), Meachim and Cornah (1970), Földes and Palfrey (1971) and Meachim (1972). These have been influenced by the difficulty of fixation due to the slow diffusion rate through the proteoglycan-rich matrix [Paulson et al., 1951] and the fact that the cells of the original nucleus disappear with age and become replaced by invasion of mesenchymal cells from the annulus [Peacock, 1952]. Consequently, although the matrix components have been fairly fully described morphologically, the cellular elements of the nucleus pulposus have not yet been described in detail.

As far as the ultrastructure of the matrix components is concerned, the difficulty has been

one of biochemical identification rather than morphological description. Biochemical analysis has shown the nucleus pulposus to consist of 20% of the dry weight as collagen and 14% of the dry weight as glycosaminoglycans [Hallén, 1958; 1962]. The main glycosaminoglycan constituents have been identified as chondroitin 6-sulphate and keratan sulphate [Buddecke and Sziegoleit, 1964; Antonopoulos et al., 1964] though small amounts of hyaluronic acid [Antonopoulos, 1965] and chondroitin 4-sulphate [Ludoweig et al., 1972] have been detected in some species. In common with other tissue glycosaminoglycans, the chondroitin sulphate and keratan sulphate are associated with a non-collagenous protein as a proteoglycan. Studies by Lyons and co-workers (1964), Lowther and Baxter (1966) and Heinegård and Gardell (1967) indicate that the chondroitin sulphate and keratan sulphate are associated in the same proteoglycan which contains 22% protein.

Autoradiography, after administration of S^{35} sulphate as an index of glycosaminoglycan production, indicates a faster metabolism of glycosaminoglycans at the peripheral cells than the more central cells in the nucleus pulposus and a decrease in metabolism in older animals. However, the method did not allow sufficient resolution to localise these components

at the ultrastructural level [Souter, 1971].

Selective staining of glycosaminoglycans at the ultrastructural level by heavy metal stains has been employed by a number of authors using bismuth nitrate [Serafini-Fracassini and Smith, 1966], colloidal iron [Wetzel et al., 1966; Matukas et al., 1967], colloidal thorium [Revel, 1964], ruthenium red [Luft, 1971b], lanthanum nitrate [Khan and Overton, 1970], and Alcian blue [Thyberg et al., 1973]. The visualisation of glycosaminoglycans after staining with one of the above stains seems to be due to displacement of counterions from the anionic groups and interaction of the cationic staining molecules with these groups. The resultant neutralisation of charge permits the glycosaminoglycan to assume a coiled configuration, so increasing the density of stained anionic sites above a certain critical level, allowing their ultrastructural visualisation. This increase in electron density of glycosaminoglycans compared with other tissue components is very dependent upon the staining conditions (e.g. pH, temperature, stain concentration and prior treatment of the tissue). A further disadvantage is that the above stains do not permit a clear distinction between the three anionic groups commonly found in tissues, namely carboxyl, sulphate and phosphate.

Some distinction is possible using the technique of "pH manipulation". This is based upon the differing dissociation constants (pK values) of tissue anions. The pK values for carboxyl groups, either in the side chains of proteins or as the uronic acid residue of glycosaminoglycans, are generally considered to be greater than 3.0 [Serafini-Fracassini and Smith, 1974], whilst that of the sulphate residues is between 1.5 and 2.0 [Stimson, 1971], and the phosphate group of polynucleotides has a pK of about 1.0 [Mahler and Cordes, 1966]. Thus, although this method theoretically would allow distinction between carboxyl and sulphate groups of glycosaminoglycans by adjustment of the pH of the staining solution, in practice this is not possible since the very low pH of a number of the above staining methods is imposed by the tendency of heavy metals to hydrolyse and any increase in pH would result in their precipitation [Zobel and Beer, 1965]. In addition to this, at low pH appreciable blocking of the carboxyl groups by interaction with basic side chains of tissue proteins occurs [Szirmai, 1969]. However, this may be prevented by prior aldehyde fixation of the tissue [Serafini-Fracassini and Smith, 1974].

The "critical electrolyte concentration" (C.E.C.) approach is based upon the affinity of the organic cation R^+ for the substrate compared with that of a standard cation M^+. The concentration of standard cation required to displace R^+ from the substrate increases with increasing substrate affinity. Scott (1955) investigated the solubility of precipitates formed from interaction of long-chain quaternary ammonium salts with polyanions and showed that they were soluble in salt solutions. He found that the concentration of salt required to dissolve the precipitate or to prevent precipitation in the presence of cetylpyridinium ions depends upon the structure of the polyanion.

At first this technique was applied to the separation of glycosaminoglycans and allowed separation of closely related polyanions [Scott, 1956, 1960; Preston et al., 1965]. Scott (1968a) later applied this technique to the staining of polyanions adsorbed on filter papers using a wide variety of organic stains and showed that the molarity of salt needed to prevent staining (the critical electrolyte concentration) was dependent upon the nature of the organic cation, the electrolyte and the polyanion. Using Alcian blue in the presence of varying molarities of magnesium chloride, Scott and Stockwell (1967) investigated the localisation of glycosaminoglycans present in human cartilage.

Alcian blue staining in the presence of salt solutions has been used widely in identification and localisation of glycosaminoglycans at the light microscope level [Scott and Dorling, 1965; Scott et al., 1968]. However, no reports have been seen of its use at the ultrastructural level, although Scott (1972) suggested a possible application of Alcian blue to ultrastructural techniques, if the chelated copper was replaced by a heavier metal. Thyberg, Lohmander and Friberg (1973) have demonstrated glycosaminoglycans at the ultrastructural level using Alcian blue; however, the prior osmication of the tissue may have some effect on the Alcian blue staining by increasing its density and affecting the nature of its electrostatic interaction with the anionic groups.

It was felt that it was desirable to investigate the possibility of using the C.E.C. approach with some other organic cation containing a metal heavy enough to permit its visualisation in the electron microscope, as this might allow selective staining of carboxyl and sulphate groups. This would allow morphological identification at the ultrastructural level of the polyanions determined by biochemical analysis.

The aims of this work were broadly:

I. To determine the ultrastucture of the cells and matrix of the nucleus pulposus as demonstrated by standard staining methods.

II. To investigate the possibility of adapting the C.E.C. technique to electron microscopy to facilitate the differentiation of distinct chemical components in the matrix.

PART I

MATERIALS and METHODS

Tissue preparation for Light and Electron Microscopy

Rabbits of ages varying from 1½ days to 3 years were killed with chloroform or by injection of 1 ml. Nembutal per kg. body wt. Immediately after death, the nuclei pulposi of the lower thoracic and lumbar intervertebral discs were removed. The nuclei were easily removed without contamination because of their avascularity and structural individuality. In the youngest rabbits, whole discs were excised; most of the cartilage plate was cut away from the discs so a decalcification procedure was considered unnecessary and the discs were bisected to allow the fixative access to the interior.

For routine studies it was found that the most satisfactory fixation was effected by a mixture of 4% paraformaldehyde and 5% glutaraldehyde in 0.080 M sodium cacodylate buffer pH 7.4 for 1 hr. [Karnovsky, 1965]. The glutaraldehyde was freshly distilled after the method of Fahimi and Drochmans (1965). Fixation was carried out at room temperature since the faster penetration of the fixative was considered to outweigh the possibility of increased autolysis. The tissues were washed in three changes of buffer for a total of 15 min. Some of the blocks were post-fixed

in 1% OsO_4 in 0.05 M veronal acetate, pH 7.4 for 1 hr., the remaining blocks were stored in buffer during this procedure. The tissues were rinsed in buffer and dehydrated in a graded series of ethanols and propylene oxide and embedded in Araldite (Taab Laboratories). The resin was polymerised at 60°C overnight.

Although Araldite is a satisfactory embedding medium, its high viscosity makes complete penetration of highly hydrated tissues difficult to achieve and it requires prolonged embedding procedures. A low viscosity epoxy resin was devised by Spurr (1969) and is available from Taab Laboratories. A resin of the following formula was used.

ERL 4206 (vinylcyclohexene dioxide)	10 g
DER 736	6 g
NSA (nonylsuccinic anhydride)	26 g
S-1 (dimethylaminoethanol)	0.4 g

The fixed and dehydrated tissues were infiltrated with resin after treatment with propylene oxide and the resin was polymerised at 70°C for 8 hr. Tissues embedded in Spurr's resin were easy to cut and the thin sections showed a better penetration and embedding of the nucleus pulposus.

For some staining procedures a water-miscible embedding medium was desirable. N-butyl methacrylate

methyl methacrylate was prepared:-

N-butyl methacrylate (B.D.H.)	90 ml
Methyl methacrylate (B.D.H.)	10 ml
Benzoyl peroxide	1.0 g

The methacrylate solutions were mixed and the benzoyl peroxide added and dissolved. Since benzoyl peroxide is supplied containing 30% water, silica gel was added to the resin mixture to remove this moisture. The resin was filtered before use. After dehydration in absolute alcohol, tissues were embedded in methacrylate which was polymerised overnight at 60°C [Phillpotts, 1972]. Although the embedded tissues were easily sectioned, the ultrathin sections must be coated with carbon before examination in the electron microscope since the resin is not stable in the electron beam. Also the preservation of fine structure is often poor. This is thought to be due to uneven polymerisation. As a result of these disadvantages methacrylate embedding was used as little as possible.

The polymerised tissue blocks were trimmed and 1μm thick sections were cut on a Reichert Ultramicrotome OM U3. The sections were placed on glass slides, dried and flattened at 60°C and stained with toluidine blue at 60°C. After rinsing, the sections were dehydrated and cleared in xylene before mounting in

neutral styrene. Examination of the stained sections allowed appropriate areas to be chosen for ultrastructural study and the tissue blocks were trimmed accordingly. Ultrathin sections exhibiting interference colours between grey and pale gold, corresponding to a thickness of approximately 70 - 90 nm, were collected on copper grids. The acid solutions employed in some of the staining procedures appeared to attack the copper and so, for these methods, sections were collected on titanium grids, the titanium being unreactive under these conditions.

After suitable staining (see below), the ultrathin sections were viewed in a Zeiss E.M.9S electron microscope, operating under an accelerating voltage of 60 KeV. Photomicrographs were taken at initial magnifications varying between 1,800X and 28,000X.

Staining procedures

(1) Uranyl acetate/lead citrate

Solutions: 0.1N NaOH (CO_2 free)
0.4% (w/v) lead citrate in 0.1N NaOH
2.0% (w/v) uranyl acetate in 50% ethanol

All solutions were filtered through a millipore filter, mean pore size 0.45μm $\pm$ 0.02μm, before use.

Method: Ultrathin sections on copper grids were immersed in 2.0% uranyl acetate for 15 - 30 min. The grids were rinsed in double distilled water and floated, section side down, on the surface of 0.4% lead citrate for 5 min. Care was taken to avoid any CO_2 contamination. The grids were rinsed in 0.1N NaOH followed by double distilled water and allowed to dry on filter paper.

(2) Bismuth

Albersheim and Killias (1963) used bismuth nitrate as a stain for nucleic acids; however, under the conditions detailed below it is considered a satisfactory stain for the carbohydrate moiety of glycosaminoglycans [Serafini-Fracassini and Smith, 1966].

Solutions: 0.1M nitric acid
0.5% (w/v) bismuth nitrate (A.R.) in 0.1M nitric acid

Solutions were millipore filtered (pore size 0.45μm ± 0.02μm) before use.

Method: [Smith, 1970] Ultrathin sections of Araldite-embedded tissue collected on titanium grids were placed in 0.1M nitric acid for 15 min. After this, the grids were placed in the bismuth nitrate solution for 15 min. The grids were then rinsed in 0.1M nitric acid followed by double distilled water before being dried on filter paper.

(3) Phosphotungstic acid (P.T.A.) [Babai and Bernhard, 1971].

Studies by Marinozzi (1968) indicate that at very low pH values PTA binds to the hydroxyl groups of polysaccharides, so staining a wide variety of muco-polysaccharides as well as glycogen. The presence of the latter can be confirmed by the absence of staining after α-amylase digestion.

Solutions: 3% (w/v) PTA (A.R.) in 1.75N HCl pH 0.5
0.5% (w/v) corn diastase α-amylase

Method: Ultrathin sections of Araldite-embedded tissue collected on titanium grids were digested with 0.5% diastase for 3 hr at 37°C. The grids were rinsed in deionised water and dried.

Diastase digested and untreated sections were stained in 3% PTA pH 0.5 for 2 - 15 min. The grids were briefly rinsed in deionised water before being dried.

(4) Ruthenium Red

Ruthenium red is a large inorganic molecule which ionises in solution to form a large polyvalent cation having a net charge of +6 [Fletcher et al., 1961]. It precipitates a wide variety of polyanions from solution [Luft, 1971a] presumably by electrostatic binding to ionised carboxyl, sulphate or phosphate

groups, resulting in neutralisation and precipitation of the polyanion. Ruthenium red has been used in ultrastructural studies of tissue glycosaminoglycans by a number of workers, including Luft (1965, 1968, 1971b), Myers et al. (1969, 1973), Lagunoff (1972), Laros and Cooper (1972) and Thyberg et al. (1974). In general, they have followed the procedure devised by Luft (1964).

Method: Tissues were fixed in 2% glutaraldehyde (Taab Laboratories) in 0.1M sodium cacodylate buffer pH 7.4 containing 1500 p.p.m. ruthenium red (Gurr) for 1 - 2 hr at 0-4°C. The tissues were washed in 0.1M sodium cacodylate buffer containing 800 p.p.m. ruthenium red for 30 min at 0-4°C. The blocks were post-fixed in 1% OsO_4 in 0.05M sodium cacodylate buffer pH 7.4 containing 400 p.p.m. ruthenium red for 1 hr at room temperature. Tissues were dehydrated and embedded in Araldite.

Thick sections viewed in the light microscope without additional staining showed brownish-black deposits at the edge of the tissue block. These deposits probably represented the site at which the essential ruthenium red/ OsO_4 coupled reaction occurred [Luft 1971a]. The poor diffusion of ruthenium red into glycosaminoglycan containing tissues is probably

a result of its large size and the excluded volume effect exercised by glycosaminoglycans [page 31 Ogston and Phelps, 1961] and also due to electrostatic interaction with anionic groups. However, ultrathin sections cut from the edge of the block showed satisfactory electron density of glycosaminoglycans when viewed in the electron microscope without further staining.

Although Luft (1971a) considers that osmication is an essential feature of the method, it was noted that ultrathin sections cut from ruthenium red stained but unosmicated tissues exhibited slight electron density of polyanion containing structures. This staining could be greatly increased by exposure of ultrathin sections to 0.05% OsO_4 in distilled water or to 750 p.p.m. ruthenium red in distilled water for 20 min. at room temperature.

(5) Lanthanum

Doggenweiler and Frenk (1965) were the first to use lanthanum as a biological stain at the ultrastructural level. Although they considered it acted as a "super-Ca^{++}" in binding to cell membranes, techniques have now been developed so that it can now be used as an extracellular tracer [Revel and Karnovsky 1967; Schatzki, 1969], a cell coat stain [Lesseps, 1

Overton, 1968] and more recently as an intracellular stain [Bannister, 1972].

Method I (Extracellular tracer)

Revel and Karnovsky (1966) proposed that with this method a colloidal form of lanthanum hydroxide penetrates the tissue as a tracer via the extracellular spaces.

Lanthanum solution: [Schatzki, 1969] 3g $La(NO_3)_3.6H_2O$ (A.R.) was dissolved in 55 ml of boiled double distilled water. The solution was vigorously stirred on a magnetic stirrer whilst 0.01N NaOH was slowly added below the surface of the liquid until the solution appeared faintly opalescent and had a pH of 7.7. Vigorous stirring was necessary during the addition of alkali to prevent premature precipitation of lanthanum hydroxide. The solution was made up to 100 ml with boiled double distilled water.

The lanthanum solution was added to fixatives and buffer washes to give a final concentration of 1.3%. Tissues were then treated as described earlier in "Tissue preparation for Light and Electron Microscopy". Colloidal lanthanum penetrates tissues slowly and is easily leached out [Revel and Karnovsky, 1966] and so three regions of each tissue block were surveyed to obtain an area showing a reasonable amount of

colloidal lanthanum. Ultrathin sections were examined without further staining.

Method II (Cell Coat stain)

Shea (1971) noted that addition of Alcian blue to the aldehyde fixative greatly enhanced subsequent demonstration of the cell coat by lanthanum staining. He ascribed the staining of the cell coat by lanthanum to be due to the presence of glycosaminoglycans, perhaps in the form of proteoglycans and ascribed its enhancement by Alcian blue to the known precipitation of glycosaminoglycans by the cationic Alcian blue.

Tissues were fixed in 4% paraformaldehyde, 5% glutaraldehyde in 0.08M sodium cacodylate buffer pH 7.3 containing 0.5% Alcian blue for 2 hr at room temperature. They were rinsed in cacodylate buffer and post-fixed in a 0.08M cacodylate buffer pH 7.3 containing 1% OsO_4 and 1% $La(NO_3)_3.6H_2O$ for 1 hr at room temperature. The tissues were washed in buffer containing lanthanum, dehydrated in ethanol and propylene oxide and embedded in Spurr's resin. Thin sections were examined unstained or after lead citrate and uranyl acetate staining.

Method III (Cell Coat material)

Lesseps (1967) using a modification of the technique of Doggenweiler and Frenk (1965) demonstrated

a layer of lanthanum-stained material on the surface of embryonic chick cells. This layer could be removed by phospholipase C digestion. Although Lesseps (1967) suggests that lanthanum may be binding to the lipid [Rojas et al., 1966] protein [Srivastava, 1964] or polysaccharide [Bungenberg de Jong, 1952] present within this material, it seems probable that, from the similarity of this stained material to that obtained from Method II, in both cases lanthanum is staining the polysaccharide within the cell coat. The preservation of this material in this case is probably due to the immediate precipitation of polysaccharides by the lanthanum containing fixative.

Tissues were fixed for 4½ hr at room temperature in 0.05M veronal acetate buffer pH 7.4 containing 1% $La(NO_3)_3.6H_2O$ (A.R.) and 1% $KMnO_4$. The tissues were rinsed in veronal acetate buffer, dehydrated in ethanol and propylene oxide and embedded in Spurr's resin. Thin sections were examined unstained, after lead citrate and uranyl acetate staining and after 20 min soaking in deionised water.

(6) Acid phosphatase

Substrate solution: 0.12g $Pb(NO_3)_2$ was dissolved in 100 ml sodium acetate / acetic acid buffer pH 5.3. 0.3g glycerophosphate was dissolved in 10 ml distilled water and added to the substrate before use.

Method: Tissues were fixed in 2% glutaraldehyde in 0.067M cacodylate buffer pH 7.3 at 0 - 4°C for 1 hr. The tissues were then washed in four changes of buffer overnight. Tissues were incubated in the substrate solution at 37°C for 3 - 4 min and then rinsed in three changes of cacodylate buffer pH 7.4 containing 10% sucrose for 30 min. The blocks were post-fixed in 1% OsO_4 in 0.067M cacodylate buffer pH 7.4 for 1 hr, rinsed in buffer and dehydrated in alcohols and propylene oxide and embedded in Araldite.

Thin sections were viewed without additional staining or after lead citrate / uranyl acetate staining.

OBSERVATIONS

The Cells of the Nucleus Pulposus

There appear to be two varieties of cells in the nucleus pulposus of the young rabbit. One, which is found in the transitional zone between the nucleus and the annulus fibrosus, occurs singly and conforms morphologically to a chondrocyte, exhibiting ultrastructural characteristics similar to those found in the cells of many cartilages (Figs. 1, 2 and 3). Meachim and Cornah (1971) described similar cells in the mesenchymal component of the human nucleus pulposus.

The predominant and very highly characteristic cellular component of the tissue appears in thick araldite sections stained with toluidine blue as shown in Fig. 4. It seems probable, from studies on the development of the nucleus pulposus [Keyes and Compere, 1932; Walmsley, 1953; Wolfe *et al.*, 1965], that these are derived from the cells of the notochord and consequently, although no observations have been made in the present work on the prenatal appearance of the nucleus pulposus, these cells will be referred to, for the sake of convenience, as notochordal cells.

The young animal

In toluidine blue stained thick araldite sections

the notochordal cells appear in the light microscope as multinucleated masses of cytoplasm surrounding groups of vesicles which exhibit varying degrees of metachromasia (Fig.4). The cells are embedded in a pale homogeneous metachromatic matrix. Since the matrix is known to contain proteoglycans, the variation in vesicle metachromasia suggests that they store the glycosaminoglycans, or the proteoglycan complex, before its export to the matrix.

The question which is left unanswered by light microscope studies is whether these masses are single multinucleated cells or collections of notochordal cells in a degree of apposition which prevents their individuality being resolved by the light microscope.

This problem is clearly resolved by electron microscope studies.

The cell masses can be resolved into a large number of closely packed individual cells. Adjacent cells are separated by a relatively narrow intercellular space. In places this has a uniform width of about 25 nm, whilst in others the irregular course of the plasma membranes results in local dilatations of this space (Figs. 7 and 8).

Specialisations of the Cell Membrane

Between most adjacent notochordal cells one or two

small electron dense localised specialisations of the cell membrane are seen (Fig. 7). These when viewed at higher magnification appear as typical desmosomes (Figs. 10 and 11). In figure 11, in which the desmosome is sectioned orthogonally, its structural components can be resolved. The plasma membranes of the adjacent cells are separated by a 15-20 nm intercellular space containing material of moderate electron density and having some cross striations. This space is bisected by a central dense intermediate line. Kelly (1966) regards the cross striations as representing pillars of material projecting from the surfaces of the apposed membranes and suggests that the intermediate line may represent a condensation of this material. Continuous with the inner leaflet of the plasma membrane is an electron dense homogeneous layer, or "attachment plaque" which is separated from the feltwork of transversely sectioned cytofilaments by a paler zone. Longitudinally sectioned filaments converging on a desmosome are seen in figure 10 but in places these also appear to condense some distance from the attachment plaque. Kelly (1966), describing desmosomes of developing newt epidermis, observed that most of the cytofilaments which approach desmosomes course towards the attachment plaque and then loop, either outside the plaque or within it, and return into

the main filament tracts of the cell. He found that the majority of cytofilaments loop at a regular distance from the plaque (usually 40 - 70 nm). Although the abundant longitudinally sectioned filaments described by him were not observed in the rabbit or rat nucleus pulposus, a looping of cytofilaments could explain the failure of many filaments to attach directly onto the attachment plaque.

Another specialisation of the cell membrane is seen in figures 7, 9 and 12. The plasma membranes of adjacent cells come very close together and follow a strictly parallel undulating course. Other planes of section through these junctions may reveal bizarre profiles (Figs. 13 and 15). The junctions may be up to 1.5 μm long and they have a total thickness of 17 nm. At higher magnification of osmicated tissue sections stained on the grid with lead citrate and uranyl acetate perpendicular sections through the junctions usually reveal three electron dense lines, two thicker outer ones and a thinner inner central one which may be discontinuous or beaded in appearance (Figs. 12 and 16). These junctions resemble those described by Garant (1972) in ultrathin sections of the enamel organ. After en bloc uranyl acetate staining he described the junctions as having a seven-layered structure with a gap of approximately 2 nm

separating the outer leaflets of the adjacent cell membranes. He suggests that lead and uranyl staining of ultrathin sections obscures this gap. Goodenough and Revel (1970) showed loss of this gap after exposure of junction-rich tissue pellets to 60% acetone; also dehydrating fluids currently in use are known to extract some tissue components, particularly lipids [Hayat, 1970]. It therefore seems more probable that the inability to demonstrate the separate outer leaflets of adjacent junctional plasma membrane in ultrathin stained sections is the result of alteration of the membrane structure during dehydration and embedding procedures.

After exposure to lanthanum (Method I [Revel and Karnovsky, 1966]), perpendicular sections through the 17 nm wide junctions reveal a line of electron dense material 3.5 - 5.5 nm in thickness lying between the lightly stained inner leaflets of the apposed plasma membranes (Fig. 17). This thick electron dense line is thought to be due to permeation of lanthanum into the external leaflets of the adjacent plasma membranes as well as permeation of the 2 nm gap seen between them after *en bloc* uranyl acetate [Revel and Karnovsky, 1967; Brightman and Reese, 1969]. Further information on the structure of this type of junction is given by the lanthanum treated section shown in figure 18 in which the upper part of the junction is cut orthogonally while

the lower part appears to be sectioned more or less tangentially. In this lower region the lanthanum outlines polygonal subunits approximately 9 nm in diameter which appear at higher magnifications to exhibit a darker central dot (Fig. 19). This morphology conforms to that of the gap junction described by Revel and Karnovsky (1966, 1970).

The features which have been recognised as characteristic of gap junctions are:-

1. The presence of a 2 nm gap between the outer leaflets of adjacent plasma membranes after en bloc uranyl acetate staining.

2. The appearance of a polygonal subunit array when viewed tangentially after colloidal lanthanum treatment [Revel and Karnovsky, 1966].

3. The presence of a similar subunit pattern in freeze-cleaved junctions [Goodenough and Revel, 1970].

It was not possible to perform freeze-cleave studies on the nucleus pulposus but since these junctions fulfil the other two criteria it seems probable that they are indeed gap junctions.

After other methods of lanthanum treatment designed for cell coat demonstration different staining of the gap junction results. After aldehyde fixation in the

presence of Alcian blue and osmium post-fixation in the presence of lanthanum (Method II [Shea, 1971]), three uniformly dense lines are seen (Fig. 20). This appearance is to be expected since osmium is known to preferentially stain the inner leaflet of the plasma membrane and with this method lanthanum has been shown to stain the cell coat; since the central dense line is 5.5 nm thick it would appear that lanthanum is also staining the external laminae of adjacent plasma membranes. Slight separation of the external dense laminae is seen in places (Fig. 21). Tangential sections of gap junctions after this staining technique do not show a subunit pattern (Fig. 22).

After fixation in potassium permanganate and lanthanum nitrate (Method III [Lesseps, 1967]) an appreciably narrower 2-3 nm densely stained line is seen in the centre of the gap junction suggesting that in this case lanthanum is deposited only in the 2 nm gap between the outer leaflets. Although the fixative included potassium permanganate the thick densely stained leaflets of the plasma membrane characteristically produced by this fixative were not observed (Figs. 23 and 24). The appearance of the bizarre profiles of junctions mentioned earlier (p.24, Figs. 13 and 15) after this staining method is consistent with the view that they

represent atypically sectioned gap junctions (Fig. 14).

The variation in appearance of gap junctions after these different staining and processing techniques can be explained by the known effects of various fixatives on the plasma membrane [Farquhar and Palade, 1963], and by the fact that although lanthanum may stain the outer leaflets it does not cross intact plasma membranes [Revel and Karnovsky, 1967]. The overall thickness of the junction is constant at 17 nm and this indicates that techniques applied to tissue blocks result in the staining of different components of the junction rather than a disruption of its structure. This is in contrast to the staining of embedded osmicated tissue in which some damage may have been caused by dehydration procedures.

The gap junctions in the nucleus pulposus have to be distinguished from the tight junctions which were described earlier in a number of other tissues [Farquhar and Palade, 1963; Revel, 1968; and Staehelin *et al.*, 1969]. On the other hand they appear to be morphologically identical to those membrane specialisations described by Weiner, Spiro and Loewenstein (1964) between the cells of the drosophila salivary gland as septate junctions. Using microelectrodes Loewenstein and Kanno (1964) measured the resistance between these salivary gland cells. They found the resistance between the

interiors of adjacent cells was much lower than the resistance across the cell surface membrane or the resistance along the intercellular space to the exterior. They suggested that this low intercellular resistance may be a property of the septate junctions. Loewenstein, Socolar, Higashino, Kanno and Davidson (1965) described low resistance pathways in four epithelial tissues, and concluded that this intercellular communication was associated with the presence of certain close-junctional membrane complexes.

The co-existence of gap junctions and electrical coupling has been demonstrated in a variety of tissues. Gap junctions having a subunit pattern were first described by Robertson (1963) after uranyl and lead staining of the Mauthner cell synapses in the goldfish brain. Other workers using colloidal lanthanum have confirmed the presence of gap junctions in the heart [Revel and Karnovsky, 1967], smooth muscle [Revel et al., 1967] and liver [Revel and Karnovsky, 1967]. The cells in all these tissues have been reported to be electrically coupled (heart [Barr et al., 1965], smooth muscle [Dewey and Barr, 1964], liver [Penn, 1966], and Mauthner cells [Furshpan, 1964]). Electrical coupling between heart cells has been demonstrated by Muir (1967) following disruption of the desmosome-like junctions at the

intercalated discs and this suggests that coupling is dependent on the integrity of the remaining gap junctions.

In addition to the passage of ions between electrically coupled cells, Kanno and Loewenstein (1966) showed that molecules having a molecular weight of up to 69,000 can freely diffuse between cells of drosophila salivary gland without any leakage to the exterior. From freeze-cleave studies of gap junctions in the myocardium, McNutt and Weinstein (1970) proposed a central 1.5 - 2.0 nm hydrophilic channel within the complex subunit assembly connecting adjacent cell cytoplasms. They did not determine the maximum size of the channels but from Kanno and Loewenstein's (1966) studies, molecules having a hydrodynamic radius of 3.6 nm can pass through the junctions. Many cellular components fall within this size range and so a control of cell systems could be exerted by a flow of substances from cell to cell.

In the nucleus pulposus of the young rabbit, gap junctions have been seen between most cells within a group and it seems likely that they play an important role in the diffusion of materials between adjacent cell cytoplasms.

Since the annulus fibrosus and the nucleus pulposus

are avascular structures, the nutrition of the inter vertebral disc is therefore dependent on the diffusi of fluids into it from surrounding vascular tissues [Walmsley, 1953]. Early diffusion studies [Sylvén, 1951; Paulson et al., 1951] showed that salts, amino acids and simple sugars diffuse only half as fast in the nucleus pulposus as in water. Since th nucleus pulposus contains uronic acids and hexosamin they suggested that adsorption and salt linkage migh interfere with the free diffusion of solutes.

Recent studies by Maroudas and her associates [Maroudas 1968, 1970; Maroudas et al., 1969; Marou and Muir, 1970] on the permeability of articular car have shown that, although small molecules diffuse re through the tissue with diffusion coefficients of ab 40% of those in aqueous solutions, larger molecules a restricted, their diffusion coefficients being inver related to their molecular size. The dependence of diffusion on the molecular size of the solute is in large measure an expression of the excluded volume effect exercised by the glycosaminoglycans of the ti The greater the molecular size of the solute, the gre the exclusion volume of the glycosaminoglycans [Ogsto and Phelps, 1961], and consequently the more tortuous the route which the solute must follow through the ti

It is not surprising, therefore, that diffusion of large molecules is an inverse function of the fixed charge density, since this is determined almost exclusively by the glycosaminoglycans [Maroudas et al., 1969].

This interpretation of the slow diffusion of solutes through glycosaminoglycan-containing tissues is applicable to the matrix of the nucleus pulposus. The glycosaminoglycans of the nucleus pulposus differ from those of articular cartilage, resulting in an altered fixed charge density and consequent alteration of the diffusion coefficients of various substances. However, Sylvén (1951) concluded that diffusion alone would be too slow to supply the nutritional requirements of the nucleus pulposus and some other transport mechanism(s) must play a role. It seems probable that in the nucleus pulposus nutrients and other substances pass directly from cell to cell, crossing numerous highly permeable gap junctions rather than by slow diffusion through the extensive extracellular matrix. It is interesting to note that cells showing early degenerative changes are not connected to adjacent cells by gap junctions, suggesting a possible interruption of the proposed nutritional pathway. This aspect is further discussed on page 44 .

Desmosomes have been described in a variety of tissues including cardiac and striated muscle and various epithelia [Muir, 1965; Karrer, 1960; Farquhar and Palade, 1963]. From their morphology, it was suggested that their function is to maintain cellular adhesion [Farquhar and Palade, 1965; Karrer, 1960]. In cardiac and smooth muscle and drosophila salivary gland they are associated with gap junctions and it may be that the desmosomes maintain the close cellular apposition necessary for the integrity and proper functioning of the gap junctions.

Cytoplasmic Organelles

1. Centrioles

Centrioles are occasionally seen, either in a juxtanuclear position or near the edge of the cell (Fig. 25). In figure 26 the plane of section cuts are approximately at right angles but does not pass through the other one of the pair.

2. Mitochondria

Elongated mitochondria, having a matrix of moderate electron density and irregular cristae, are occasionally seen (Figs. 27, 28 and 29). The mitochondria become increasingly scarce in rabbits older than one month.

Large numbers of mitochondria having a similar structure are found in chick notochordal cells [Smith, 1973]. The reduction in the number of mitochondria with age probably parallels a decrease in metabolic activity as the notochordal cells degenerate and die.

3. The Rough Endoplasmic Reticulum

A limited amount of rough endoplasmic reticulum is randomly distributed and consists of a series of irregular interconnecting sacs which may be widely dilated. The cisternae are filled with homogeneous granular material of moderate electron density. Spirally arranged polysomes, which may be free or lie on the membranes of cisternae, are frequently seen (Fig. 9) and are similar to those which Ross (1968) described in fibroblast cells. In figure 29 rough endoplasmic reticulum is seen in association with mitochondria, a similar association has also been observed in fibrogenic cells [Ross, 1968].

4. The Golgi Apparatus

The stacks of flattened lamellae and vesicles of the Golgi apparatus usually occur in a juxtanuclear position (Figs. 30 and 31). The well-developed appearance of the Golgi complex in figure 31 is observed in comparatively few sections suggesting

its highly localised nature in notochordal cells. The Golgi is closely associated with the rough endoplasmic reticulum and some of the larger vesicles contain fibrillar material (Fig. 30). Labelling studies have indicated that the Golgi may be the site of glycosaminoglycan synthesis [Ross, 1968] and that in this situation the glycosaminoglycan is linked to the protein synthesised by the rough endoplasmic reticulum prior to its storage and export to the matrix.

5. Large Vesicles

Notochordal cells are invariably characterised by large vesicles [Figs. 32 and 33], which often become so enormous that the cytoplasm is displaced entirely to one side of the cell (Figs. 34, 35 and 36). Some exhibit knob-like projections protruding into their interiors, but the significance of these is unknown (Fig. 37).

In sections stained with lead citrate and uranyl acetate, the vesicles contain rather widely dispersed beaded filaments (Fig. 39). The beads vary in diameter from about 5 - 7 nm and have a centre to centre distance of about 15 nm. Although occasional larger particles of 15 - 20 nm are apparent, it seems reasonable to interpret these as being due to super-imposition of a number of smaller beads. The

filaments are frequently branched and although they reach a length of about 1 µm this measurement is probably of no significance, since the filaments appear to be randomly orientated. Similar filaments have been noted in the extracellular matrix after phosphotungstic acid staining [Smith and Serafini-Fracassini, 1968].

It is generally accepted that lead citrate and uranyl acetate do not stain glycosaminoglycans. Other staining procedures do stain this class of compounds, either selectively, as in the case of acidic phosphotungstic acid or acidic bismuth nitrate or, simultaneously with proteins as in the case of ruthenium red.

After acidic phosphotungstic acid staining the vesicle contents appear as particles with translucent centres. They vary little around an average diameter of 20 nm and many are disposed in contact with one another in the form of linear rows (Fig. 40).

If bismuth staining at low pH is followed by uranyl acetate staining the 20 nm particles appear uniformly electron-dense and are connected to one another by fine filaments (Fig. 42). A similar pattern is noted after ruthenium red staining (Fig. 41).

It seems entirely possible that the particles and beaded filaments, seen after specific staining and lead citrate and uranyl acetate respectively, represent two components of the same structural elements. Indeed a valid interpretation would be that the 20 nm particles represent the glycosaminoglycan chains in coiled configuration after destruction of their net charge by staining, while the beaded filaments represent a protein core to which the glycosaminoglycans are periodically attached. However, although such an interpretation would be in keeping with the metachromasia of the vesicles in light microscope preparations, it cannot be definitely proved with available evidence.

With all the methods of staining the amount of visible material varies considerably in different vesicles (Figs. 37 and 38), and this is obviously in keeping with the distinct variations in metachromasia already noted in suitably stained light microscope preparations (p.22, Fig.4).

It is known from autoradiographic studies that the similar though smaller proteoglycan-containing vesicles in chondrocytes are derived from the Golgi apparatus and it seems probable that the large vesicles in the notochordal cells of the nucleus

pulposus have a similar derivation. This view is supported by the frequent observations of smaller vesicles with morphologically similar contents in close spatial relationship with the Golgi apparatus (Fig. 30).

6. Other vesicles

Many of the notochordal cells exhibit numerous pinocytotic vesicles. They are usually situated close to the cell membrane and indeed often open onto its surface. Observations in the present investigation indicate that they occur only in those areas in which dense extracellular material is associated with the cell membrane (page 58 , Figs. 45 and 95). The continuity of many of these pinocytotic vesicles with the extracellular space is clearly demonstrated after lanthanum staining (Method III). In this method the stain does not cross the cell membrane and yet many stained vesicles can be seen distributed along either side of the narrow intercellular spaces, both at low magnification (Fig. 43) and at high magnification (Fig. 44).

Many notochordal cells also contain vesicular profiles which are much larger than pinocytotic vesicles but differ from the proteoglycan-containing vesicles described above in the nature of their contents.

Their contents are morphologically identical to the dense extracellular material to which the pinocytotic vesicles are invariably related (see above, Fig. 45). These structures seem open to three interpretations. First, they may represent a packaging of extracellular material for export during its passage from either the rough endoplasmic reticulum or the Golgi apparatus. Secondly, they may represent heterophagic vesicles of the lysosome system which are ingesting extracellular material for digestion within the cells. Neither of these explanations are regarded as entirely satisfactory and it is suggested that despite their frequency these apparent vesicles are in fact invaginations of the cell surface. This view is favoured by the frequent association of pinocytotic vesicles with their limiting membranes (Figs. 45, 46 and 47) and also by their invasion by lanthanum staining (Fig. 43).

7. Cytofilaments

Notochordal cells contain bundles of unbranched parallel pale-stained cytofilaments (Figs. 30 and 48) 5 nm in diameter. The cytofilaments appear more regular than the filaments observed converging on the attachment plaque of desmosomes (Fig. 10), and the fibrillar network sometimes seen just below the cell

surface (Fig. 49) and it may be that they represent different classes of cellular filaments.

Kelly (1966) and Fawcett (1958) consider that the filaments associated with desmosomes and the fibrillar network provide intracellular tensile support. It seems likely that the reduced quantity of these filaments in the nucleus pulposus, by comparison with epithelia, is a result of the decreased strength necessary to maintain cellular adhesion, since the notochordal cells undergo equilateral compressive forces rather than the stretching forces experienced by epithelial cells.

Ross (1968) describes filaments in the fibrogenic cell and suggests a possible contractile function; however, this seems unlikely to be the case in notochordal cells.

8. Glycogen

The smaller glycogen β-particles are similar in size to free ribosomes and, since both appear electron dense after lead citrate and uranyl acetate staining, specific stains are necessary for glycogen demonstration. Baba[illegible] and Bernhard (1971) used phosphotungstic acid (P.T.A.) solutions at low pH for the localisation of glycogen. Although proteins do not stain with P.T.A. at low pH since their carboxyl groups are undissocia

the authors showed that the method stains a variety of polysaccharides and subsequently pre-digestion of glycogen in ultrathin sections by diastase was employed to distinguish glycogen particles from other polysaccharides.

Figure 50 shows the localisation of polysaccharides stained by P.T.A. at pH 0.5 in notochordal cells. The cytoplasm contains large numbers of stained particles which have an irregular outline and are 25-30 nm in diameter. They may occur singly (β-glycogen) or in loose aggregates (α-glycogen) (Figs. 51 and 52). After diastase-digestion and P.T.A. staining the centres of these particles appear completely electron-lucent although the periphery still stains intensely (Fig. 53).

This peripheral staining could result from incomplete removal of digestion products although this seems unlikely since the remaining material is located peripherally. A second possibility is that the peripheral glucose molecules are resistant to α-amylase digestion owing to their linkage to other components. This could occur either *in vivo* or be a result of the cross-linking action of the fixatives employed.

9. Lysosomes

A few acid phosphatase-positive vesicles were observed in some of the notochordal cells. Some of these were small and appeared to contain only reaction product, and have consequently been regarded as primary lysosomes (Fig. 54). Others contained additional material and appear to conform to secondary lysosomes (Fig. 55). In older degenerating cells, a very large number of vesicles containing myelin bodies and other material were acid phosphatase-negative and were considered to be postlysosomes (Fig. 56).

The small number of acid phosphatase-positive bodies in the notochordal cells is perhaps surprising on several counts. First, these are cells which undergo physiological cell death at an early age. The early view that cell death was due to intercellular rupture of primary lysosomes [De Duve, 1959; Brachet et al., 1958] is no longer accepted, but the present concept that it is due to a programmed cessation of anabolic functions in the cell still involves an intercellular digestion of worn-out cytoplasmic components by the lysosome system. Secondly, it has been shown that there is a rather rapid turnover of matrix components [Lohmander et al., 1973]. Using labelled sulphate as a precursor the

authors demonstrated two metabolic pools of chondroitin sulphate, having half-lives of 3 and 30 days, and keratan sulphate, also with a half-life of 30 days. It has been suggested that in several connective tissues, matrix turnover is dependent on the extracellular export of lysosomal enzymes. Dingle (1969) suggested primary lysosomes liberate their contents to the exterior where the lysosomal enzymes, although presumably working above their pH optima, cause some degradation of non-collagenous protein. He proposed that the partially degraded material is then ingested into the cell for further breakdown by lysosomal digestion. If this were the case in the nucleus pulposus, the zones of dense extracellular material in association with the cell surface and with vesicles already described (p.38 Figs. 45, 46 and 47) could represent partially digested glycosaminoglycan complexes and its ingestion by numerous pinocytotic vesicles. On this ground also, therefore, one would expect a more profuse lysosomal system in the notochordal cells.

Indeed, the fact that there is a lysosome system in these cells, more profuse than that indicated by the acid phosphatase reaction in the present investigation, is strongly suggested by the gross disparity between the number of acid phosphatase-positive bod..

in young cells and the numbers of postlysosomes in older cells. And the most probable explanation of this phenomenon is a failure of the substrate to reach the notochordal cells during incubation owing to the very slow diffusion rate of solutes through the extracellular matrix [Sylvén, 1951; Paulson et al., 1951].

Degenerating Cells

Some notochordal cells contain large numbers of vesicles in their cytoplasm, many of which resemble the postlysosomes described earlier (p.42 Fig. 56). These cells also have an amorphous granular cytoplasm with very few cytoplasmic organelles (Fig. 57). This appearance is consistent with a reduction or cessation of anabolic cellular activities and a continual normal rate of catabolism effected by the lysosome system. The cell surface has complex infoldings and, although these cells still appear to lie within a group of notochordal cells, no membrane specialisations are seen connecting them to adjacent cells. Gap junctions found between normal cells allow communication of their cytoplasmic interiors and it has been suggested that notochordal cells receive their nutrients by intercellular passage through successive gap junctions, rather than by

slow diffusion through the matrix (p. 31). Although the degenerating cell may be in close proximity to a group of healthy cells (Fig. 57), nutrients may be unable to cross the intervening area of matrix. This may be either because the nutrients do not cross the plasma membrane of healthy cells to reach the matrix or, if they do reach the matrix, their diffusion may be so restricted that they cannot supply the nutritional needs of the separated cell. Desmosomes which are thought to assist in maintaining cellular adhesion are absent from degenerating notochordal cells. It is, therefore, not surprising that, in time, the degenerate cell gradually separates from the group in which it originally lay and this could perhaps be a result of the forces normally experienced by the nucleus pulposus.

Cells showing further degenerative changes are found as individual entities quite apart from cell groups. The nuclei become pyknotic and the darkly stained cytoplasm encompasses a variety of membranous bodies, the plasma membrane and vesicle limiting membrane are discontinuous (Figs. 58 and 59). Cell death results in karyolysis of the nucleus and the break-up of cytoplasm bounding the large vesicles, the vesicle contents become indistinguishable from the extracellular matrix (Fig. 59). The last recognisable

remains of a degenerated notochordal cell is an amorphous mass of densely stained material. (Fig. 60).

The Matrix of the Nucleus Pulposus

The cells of the young nucleus pulposus are embedded in a matrix which in the light microscope, after toluidine blue staining, exhibits uniform pale metachromasia (Fig. 4). In the matrix of older animals the metachromasia becomes patchy and contains varying amounts of densely stained metachromatic material (Figs. 5 and 6). The metachromatic nature of the matrix indicates the presence of glycosaminoglycans. Whether the variation in metachromasia observed in older animals is due to asymmetric distribution of existing components can be resolved by electron microscope studies.

At this level the matrix of the nucleus pulposus consists of a filamentous meshwork in which other matrix components are embedded.

1. After lead citrate uranyl acetate staining the extracellular matrix contains widely dispersed branched and unbranched fine beaded filaments which can be seen in Fig. 61. The beads are 5 - 7 nm in diameter and have a centre to centre distance of 15 nm. Occasional larger beads 25 nm in diameter are seen, but this could

well be due to the superimposition of several of the finer beads. Meachim (1972) has described a similar meshwork of filaments in the human nucleus pulposus, and Smith and Serafini-Fracassini (1968) have demonstrated similar beaded filaments in the rabbit nucleus pulposus after staining with phosphotungstic acid at neutral pH.

After other methods of staining, particles occupy the same areas occupied by the filamentous meshwork. Ruthenium red localises particles 15 - 20 nm in diameter. The particles are interconnected by filaments (Fig. 62). Similar particles were observed in rabbit articular cartilage after ruthenium red staining by Myers, Highton and Rayns (1973). They showed that after extraction with 4M guanidinium chloride, 60% of the proteoglycans were removed and very little ruthenium red-positive material remained. It seems probable therefore that these particles in the nucleus pulposus represent glycosaminoglycan.

It has been shown that glycosaminoglycans are stained by solutions of phosphotungstic acid or bismuth nitrate at low pH [Babaï and Bernhard, 1971; Serafini-Fracassini and Smith, 1966]. After staining with acidic phosphotungstic acid, the matrix of the nucleus pulposus exhibits rows of particles of rather varying sizes, although many have a diameter of 20 nm (Fig. 63).

Bismuth nitrate staining at low pH reveals discrete particles 30 nm in diameter, many of which have a more densely stained periphery. These particles seem to be randomly distributed although occasional rows of particles may be seen (Figs. 80 and 81).

Fixation with 1% potassium permanganate and 1% lanthanum nitrate (Method III) results in a very dense staining of the matrix components. The beaded filaments seen after lead and uranyl staining are densely stained (arrows Fig. 64), but in most areas densely stained particles 15 - 20 nm in diameter are seen, although these may often be superimposed, resulting in larger stained aggregates. Since lanthanum may bind to proteins under certain conditions [Srivastava, 1964] as well as glycosaminoglycans [Bungenberg de Jong, 1952; Mathews, 1960], it appears that lanthanum staining results in localisation of the proteoglycan.

The particles which are demonstrated by these several methods are broadly similar in appearance and distribution and it seems reasonable, from what is known of the selectivity of the methods, to postulate that they represent a similar tissue component in each case. It is considered that the particles represent glycosaminoglycan chains of the proteoglycan complex which have collapsed into a coiled configuration, owing to destruction of their net charge by the binding of

staining cations to their anionic groups. In this view, each particle represents not necessarily the whole glycosaminoglycan chain, but that part of the chain which is sufficiently tightly coiled to concentrate a critical amount of heavy metal. The size of each particle would obviously depend on a number of factors such as the atomic number of the staining metal, the size of the staining molecule, the tightness of the coiling produced by stain binding and whether the staining produces binding between adjacent glycosaminoglycan chains. The fact that the particles produced by bismuth staining are appreciably larger than those seen after the other staining methods may be due to some of these factors. Thus bismuth has a higher atomic number than tungsten, lanthanum or ruthenium so that a larger proportion of the coiled glycosaminoglycan chain may be rendered visible by that stain, and the trivalent nature of the bismuth ion may favour interchain binding so that many particles may contain more than one glycosaminoglycan chain.

The particles, seen after staining with bismuth, ruthenium red, lanthanum or phosphotungstic acid at low pH, have the same distribution as the network of beaded filaments localised after lead citrate and uranyl acetate staining and so it seems probable that

they represent different components of a single structure. If the particles do consist of glycosaminoglycan, the fibrillar network may represent the protein core of the proteoglycan occurring in the nucleus pulposus matrix.

Low magnifications of sections of the young nucleus pulposus indicate a more or less uniform distribution of the features regarded as representative of proteoglycan (Fig. 1) and this is in keeping with the uniformity of toluidine blue staining of similar material (Fig. 4). However, at higher magnification it becomes apparent that the concentration of these elements does vary gradually between adjacent areas (Figs. 65, 66 and 67). In the nucleus pulposus of older animals the distribution of proteoglycan appears to be less uniform. Indeed at higher magnifications, there are fairly abrupt changes in concentration between closely related areas (Fig. 68). And again, this patchiness may be regarded as the ultrastructural counterpart of the uneven metachromasia of the matrix in light microscope preparations (Figs. 5 and 6).

2. A few individual fibrils are widely dispersed in the nucleus pulposus matrix of 4 week old rabbits (Figs. 69 and 70). In older animals, they are found

in increasing numbers and may surround degenerating notochordal cells (Fig. 71). They follow a straight course and vary in diameter from 10 - 30 nm. Some cross striations of the fibrils are evident, but clear periodic cross striations of the collagen type could not be discerned. However, on the basis of their general appearance and the results of chemical analysis of the nucleus pulposus [Hallén, 1962], it is suggested that they are in fact collagenous.

3. Banded fibres are a characteristic feature of the rabbit nucleus pulposus matrix; they become increasingly abundant with age. They are usually found in the pericellular matrix, near a healthy or degenerating cell (Fig. 72) or, they may lie in whorls surrounding necrotic notochordal cell remains (Fig. 71). The banded structures may occur singly, or in groups (Figs. 73 and 74), and they vary in width from fibres of 100 nm to wide sheets up to 1μm wide.

After conventional fixation, lead and uranyl staining of ultrathin sections show banded fibres having a regular repeat pattern of light and dark bands with a mean periodicity of 84 $\pm$ 8 nm. The light bands are 30 nm wide and are traversed longitudinally by fine filaments about 4 nm wide (Figs. 75

and 76). In figure 77, the free fine filaments can be seen extending beyond the end of the banded fibre. The 4 nm longitudinal fine filaments are also continuous through the dark bands, but in this zone they are partially obscured by the presence of beaded filamentous material similar to that found in the matrix and described above. A similar staining of the banded fibres by phosphotungstic acid at neutral pH was noted by Smith and Serafini-Fracassini (1968).

After phosphotungstic acid staining at low pH, the dark bands of the banded fibres contain material very similar to the 20 nm stained particles described previously in the matrix after this treatment. Very faint longitudinal striae are visible within the light bands and probably represent the unstained, osmicated 4 nm axial filaments (Figs. 78 and 79). A similar result was obtained after bismuth staining, but in this case additional uranyl acetate staining confers electron density on the longitudinal filaments (Figs. 80 and 81).

Ruthenium red or lanthanum stains material within the dark bands of the banded fibres, and this material is similar in appearance to the particles seen in the matrix after these staining methods (Figs. 82, 83, 84 and 85).

The similarity of the protein components (visualised after lead citrate and uranyl acetate or after neutral phosphotungstic acid staining) and the glycosaminoglycan components (stained by bismuth or acidic phosphotungstic acid) of the material within the dark bands of the banded fibres, to the proteoglycan found in the matrix suggests that the dark bands may also contain proteoglycan. Since the longitudinal filaments are stained by lead citrate and uranyl acetate and neutral phosphotungstic acid solutions it seems probable that they are protein in nature. After water extraction of the rabbit nucleus pulposus, Smith and Serafini-Fracassini (1968) observed the appearance of large native collagen fibres as well as a variety of fibrous forms. They proposed that these forms represent stages in aggregation of the 4 nm filaments eventually producing larger collagen fibres than are found in the intact nucleus. They suggested that either the extracted proteoglycan, or some other component extracted with it, is responsible for the failure of the 4 nm collagenous filaments to aggregate *in vivo*.

The longitudinal filaments are of similar dimensions to the primary collagen filament consisting of five quarter-staggered tropocollagen molecules proposed by Smith (1968). The absence of banding

of the 4 nm filaments is due to their small size and it seems possible that adjacent filaments are cross-linked only once in each collagen period, at the level of the dark bands. This is in contrast to the seven cross links and tighter aggregation of tropocollagen molecules producing the characteristically banded native collagen fibre. X-ray diffraction studies have suggested a possible supercoiling of tropocollagen molecules within the native collagen fibre [Miller and Wray, 1971]. An absence of this supercoiling within the 4 nm axial filaments observed in the banded fibres could explain their longer collagen period. Banded fibres having a period appreciably longer than the collagen period have been described in a variety of tissues [Cornah et al., 1970]. Recently Ludoweig and Parker (1973) prepared striated fibres having a beaded appearance from the insoluble collagen residues of the foetal nucleus pulposus and noted the similarity of this material to the banded fibres of the intact nucleus. The striated fibres have a 100 nm axial repeat distance. The authors suggested that this material could be a variety of fibre long spacing collagen, or it may represent proteoglycan intimately associated with collagen.

Although the net charge of collagen above pH 4 is almost zero, electron microscope and amino acid sequence studies have shown that cationic and anionic side chains are localised in narrow regions within the collagen period, separated by non-polar regions. And so regions of positive and negative overall charge could exist within the collagen period. It seems probable that in the nucleus pulposus the proteoglycan is attached to 30 nm wide zones of overall positivity within each collagen period.

Formations consisting of parallel strips of electron-dense material occur in the pericellular matrix; an exceptionally well ordered example is seen in figure 86. This material is often found in association with banded fibres (Fig. 87). The electron-dense strips may show considerable variations in width (8 - 150 nm) and distance apart (18 - 200 nm) but in any one area, the ratio of distance apart to width of electron-dense strip is constant. The variations of dimensions within a group of parallel strips are usually slight although gradual variations may occur (Fig. 86). The electron-dense strips may be up to 500 nm long and several show continuity with adjacent bands at their ends. The staining of the parallel strips with lead citrate and uranyl acetate,

ruthenium red or lanthanum (Figs. 86, 87 and 88) is very similar to the staining of the dark bands of the banded fibres after these methods.

The similarity of size, and location, and the frequent association of the parallel electron-dense strips with the banded fibres, coupled with the similarity of staining, suggests that they may represent different planes of section through the same structures. If the banded fibres were arranged as parallel sheets about 10 nm thick and of considerable length and width, an orthogonal section would reveal the material within the dark bands as parallel strips. The axial filaments would not be visible due to their small size and the oblique angle of sectioning. Figure 87 illustrates this, a longitudinal section along a banded fibre reveals the typical banded structure, but where the structure becomes orthogonal to the plane of section, parallel electron-dense strips are seen continuous with the dark bands of the banded fibres. Continuity between the ends of the parallel electron-dense strips could also account for the continuity between adjacent dark bands of the banded fibres seen in figure 87. If this interpretation is correct, the variation in width and spacing of the electron-dense strips is a result of the angle of sectioning of the banded fibre.

4. Distributed throughout the fibrillar matrix, but particularly concentrated in the neighbourhood of the notochordal cells are masses of highly electron-dense osmophilic material. In most situations this appears as groups of stellate particles 90 - 120 nm in diameter, while in others it takes the form of elongated zones closely applied to the cell surface for distances of up to 6 μm.

After fixation in osmium and staining with lead citrate and uranyl acetate, the structure of the stellate particles of the matrix varies with section thickness and length of staining. With normal staining times, a dense amorphous centre is surrounded by a rim of separate projections and dense bodies (Figs. 65 and 89). On the other hand, when very thin sections are lightly stained, the central part of the particle appears to be composed of a feltwork of very narrow filaments of about 4 nm diameter, and many of these can be traced as individual elements for some distance into the surrounding matrix (Figs. 90 and 91). The particles are not stained by acidic phosphotungstic acid (Fig. 92) or ruthenium red (Fig. 93) and there appears to be no evidence in previous investigations that they are stained by acidic bismuth nitrate [Smith and Serafini-Fracassini, 1968]. Occasionally the larger stellate particles appear to have electron-lucent

centres which may contain a central amorphous dense spot (Figs. 91 and 95).

The chemical nature of these stellate particles is presently unknown but their staining reactions strongly suggest that they are not proteoglycan while their filamentous ultrastructure suggests that they may be proteinaceous in nature.

Large areas of electron-dense material are frequently seen in the older nucleus pulposus matrix. These masses are often found associated with the surface of banded fibres (Fig. 94); other masses may contain an irregular array of electron-lucent spaces (Fig. 94). Considering the similarity of staining of this material with the stellate particles, it could be interpreted as the result of fusion of a number of stellate particles; an irregular or incomplete fusion could result in isolated areas of matrix within the electron-dense material appearing as electron-lucent spaces. The decrease in the number of stellate particles and the appearance of these electron-dense masses with age also points to this explanation.

The similarity of the stellate particles to strips of electron-dense material associated with the cell surface is illustrated in figure 95. This material occurs as zones 25 - 50 nm wide, and, although

it is occasionally closely applied to the cell surface (Fig. 45), usually it is seen separated from the cell membrane by a distance of 10 - 20 nm. Similar material is also seen within large apparent vesicles, but it seems probable that this represents an association of electron-dense material with the cell surface which has become invaginated (page 39, figs. 45, 46 and 47). After osmium fixation this material stains very densely and appears to be covered with extremely fine filaments. Fixation with glutaraldehyde and lead and uranyl staining of ultrathin sections reveals the filamentous surface in continuity with a rather amorphous centre (Fig. 47). This amorphous appearance could result from close packing and superimposition of the fine filaments observed at their periphery.

The similar appearance and staining of the stellate particles and the areas of electron-dense material, either free in the matrix, or associated with the surface of banded fibres, or found in narrow zones closely applied to the cell surface, suggest that they all consist of similar proteinaceous filaments. The pericellular distribution of the zones of extracellular electron-dense material and the stellate particles suggest that they have been recently synthesized by the notochordal cells and exported into the matrix. Larger areas of electron-dense material are found only

in older animals suggesting an aggregation and maturation of stellate particle material producing large aggregates which may become associated with the banded fibres.

P A R T II

Theory of "critical electrolyte concentration" techniques

- as developed by Scott (1960, 1970)

The precipitation of polyanions from solution by organic cations can be represented:-

$$P^{z-}{}_zM^+ + zR^+ \leftrightarrows P^{z-}{}_zR^+ + zM^+$$

where P^{z-} is a polymer with z anionic sites, M^+ is the counterion and R^+ is the organic cation. Applying the Law of Mass Action and ignoring activity coefficients results in

$$\frac{[P^{z-}{}_zR^+]}{[P^{z-}{}_zM^+]} \cdot \frac{[M^+]^z}{[R^+]^z} = K$$

where K is the equilibrium constant and the square brackets denote concentrations. Rearranging this gives

$$\frac{[P^{z-}{}_zR^+]}{[P^{z-}{}_zM^+]} = K \frac{[R^+]^z}{[M^+]^z}$$

and $\frac{[P^{z-}{}_zR^+]}{[P^{z-}{}_zM^+]}$ is the ratio of the insoluble to the soluble form of the polyanion, i.e. the extent of precipitation or staining. A plot of this ratio against $\frac{[R^+]}{[M^+]}$ shows increasingly sharp inflections as the value of z increases [Scott, 1968b]. For the polyanions being considered in the present study, z is of the order of 100 - 10,000. If the value of R^+ is kept constant, the position of inflection on the $\frac{[R^+]}{[M^+]}$ axis is expressable

in terms of $[M^+]$, and is termed the critical electrolyte concentration (C.E.C.). The C.E.C. is dependent upon the magnitude of K, the equilibrium constant, which in turn is governed by the relative affinities of M^+ and R^+ for the anionic groups of the polyanion; this 'affinity' may be composed of coulombic and van der Waal's forces, hydrogen bonding and charge transfer mechanisms.

Scott (1968a; 1968b) tested the reaction of a number of polyanions with different organic cationic stains and counterions. He showed that for a particular salt/stain system the C.E.C. values depended primarily upon the type of anionic site on the polymer (e.g. $-COO^-$, $=PO_4^-$ or $-SO_4^-$). The molecular weight and charge density of the polyanion may affect the C.E.C., this effect is less important for large polyanions.

The size and nature of the organic cation affects the relative order of C.E.C. values for particular anionic groups. The stains used can be divided into two groups [Scott and Willett, 1966]. Organic stains of low electrostatic field and polarising power interact with polyanions mainly by coulombic forces and their C.E.C. values are grouped in the order

$$\text{C.E.C.}(-COO^-) < \text{C.E.C.}(=PO_4^-) < \text{C.E.C.}(-SO_4^-).$$

Polarising organic cations include haematein and mucicarmine chelates and exhibit a C.E.C. sequence:-

$$\text{C.E.C.}(-SO_4^-) < \text{C.E.C.}(-COO^- + SO_4^-) < \text{C.E.C.}(-COO^-) < \text{C.E.C.}(=PO_4^-).$$

Scott (1968b) explained these differences by an extension of the observations of Bungenberg de Jong (1949) on the affinity of inorganic ions for sulphate, carboxyl and phosphate groups. Bungenberg de Jong observed that inorganic cations had less "affinity" for sulphate groups and suggested an order of polarisability:-

$$-COO^- > =PO_4^- > H_2O > -SO_4^-.$$

A solvated, highly polarising cation could accept carboxyl or phosphate into its solvation shell, but not sulphate which, being less polarisable than the solvation water, would not displace it from the solvation shell. Non-polarising organic cations would not differentiate between more or less polarisable anions and the pattern of C.E.C. values for these is dependent upon the affinity of the inorganic counterion for the anionic group. Organic cations with a polarising charge, which include metal chelates, have a greater affinity for the more polarising carboxyl and phosphate groups than sulphate which explains the reversal of their C.E.C. sequences.

The C.E.C. values may be measured in a variety of ways. If the organic cation is colourless, the C.E.C. is that concentration of electrolyte resulting in formation or dissolution of the insoluble organic

cation-polyanion complex. Scott (1968a) measured the C.E.C. of polyanion solutions spotted on filter paper as that electrolyte concentration at which the spot (containing 2 - 10 µg polyanion) ceases to stain. Staining experiments with Alcian blue on a variety of tissues, which contain predominently or characteristically members of each group of polyanions [Scott and Dorling, 1965], show a staining pattern similar to that determined for polyanions adsorbed on filter paper, although the C.E.C. values for polyanions within tissues are generally 30 - 50% higher than those adsorbed on filter paper. This is probably due to the higher molecular weight of tissue polyanions as well as a greater charge density resulting from the higher concentration of polyanions within tissues [Scott and Dorling, 1965].

This technique has not been successfully applied to tissues at the ultrastructural level to my knowledge. The basic problem appears to be to find an organic cation containing sufficient heavy metal atoms to produce adequate scattering of the electron beam, which binds readily to tissue anionic groups and which is not significantly altered in composition by the presence of high concentrations of inorganic salts. A number of such compounds have been tested but the most promising results have been obtained from haematein

chelates of heavy metals. This finding was not surprising since a number of coloured organic chelates of light metals, including those of haematein have been used at the light microscope level [Lillie, 1969]. The subsequent text refers entirely to such compounds.

Haematein chelates

Haematoxylin is the most commonly used histological stain; however, haematoxylin (I), as supplied, has no staining properties until it has been 'ripened' by oxidation to haematein (II) [Palmer and Lillie, 1965; Marshall and Horobin, 1972].

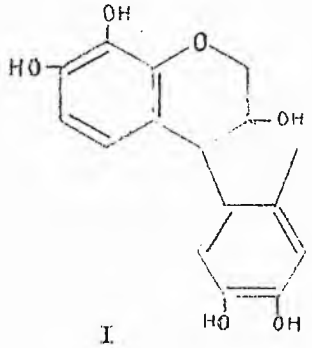

I

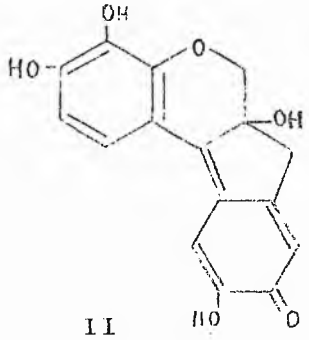

II

Haematein is not in common use, since the purity of commercial preparations may be suspect [Lillie, 1969; Imes et al., 1969].

It has been known for many years that haematein forms chelates with a large number of heavy metals and that, although in certain circumstances the charge characteristics of some of these are doubtful [Berube et al., 1965], the majority are cationic and may therefore bind to anionic tissue groups. The available evidence [Berube et al., 1965; Arshid et al., 1954] suggests that with the formation of haematein-metal complexes the metal is chelated by hydroxy-oxo groupings

and that this results in a liberation of hydrogen ions. Consequently an increase in the hydrogen ion concentration may be taken as presumptive proof of chelate formation [Martell and Calvin, 1952] and conversely the addition of hydrogen ions will tend to suppress chelate formation.

$$M^{++} + nHem \leftrightharpoons [M\ Hem_n]^{m\pm} + nH^+$$

Solutions of haematein exhibit an absorption spectrum with a maximum at 430 nm. Fortunately the majority of haematein chelates are intensely coloured [Pizzolato and Lillie, 1967] and many have maximum absorptions at wavelengths differing from that of haematein. This fact allows the determination of the molar ratios of haematein and heavy metal which may be associated as chelates. This information is vital to ensure optimum cationic chelate formation and to ensure that any staining produced by a mixture of haematein and an inorganic metal salt results from the chelate and not from excess free inorganic salt.

Indium haematein

Chelates of aluminium with haematein are routinely used in staining methods for light microscopy [Lillie, 1965; 1969]. They appear to be stable in the presence of salt solutions and in conjunction with a variety of inorganic salts have been used in C.E.C. determinations of polyanions adsorbed on filter paper [Scott and Willett, 1966; Scott, 1968a]. However aluminium chelates do not provide sufficient electron density for use at the ultrastructural level. It was felt that a haematein chelate of a heavier metal from Group III of the periodic table might show a similar stability towards salt solutions whilst providing enough electron density for use in the electron microscope.

The progressive addition of a 1% haematein solution to a 1% indium nitrate solution results in a progressive decrease in pH to below that of either of the original solutions (Fig. 96). This increase in hydrogen ions as haematein is added is presumptive proof of chelation.

The violet solution formed from the brown haematein solution and the colourless indium solution showed two visible absorption maxima, one at 426 nm and a larger one at 572 nm (Fig. 97). Preliminary studies indicated that the visible absorption spectrum was unaffected by incorporation of up to 4.0M magnesium chloride. In

the absence of added salt, the chelate stained a variety of polyanions adsorbed on filter papers, as well as tissue components viewed at the light microscope level in paraffin sections and visualised at the ultrastructural level. It therefore appears to conform to the criteria necessary for use in the C.E.C. approach.

It can be shown that the absorbance at 426 nm is largely due to haematein and that neither haematein alone or indium nitrate alone absorbs at 572 nm. Consequently the absorbance at 572 nm can be taken as a measure of the concentration of the indium haematein chelate. The absorbance at this wavelength was therefore measured for solutions containing indium nitrate and haematein in molar ratios varying from 0.25 to 6.0 (Fig. 98). It is evident that the absorbance at 572 nm increases progressively as the molar ratio of indium: haematein approaches 3:1. The absorbance thereafter levels off and finally begins to decrease as the ratio reaches 6:1. This suggests that chelate formation is maximal at a ratio of 3 of indium to 1 of haematein and that the final decrease in absorbance beyond a ratio of 5:1 reflects possible polymeric chelate formation. Likewise the ratio of 3:1 does not infer that the resulting chelate is a combination of three indium nitrate molecules with one haematein molecule. Methods are available [Imes et al., 1969; Marshall and Horobin,

1974] for the estimation of the haematein content of commercial preparations which would allow calculation of the exact molar ratio in the chelate but it was considered that this refinement was outside the scope of the present study. All the indium haematein chelates used in the following studies had a nominal molar ratio of 3:1 (In:H).

C.E.C. values of polyanions adsorbed on filter paper

The method of assessing the effect of inorganic salts on the staining of polyanions by organic cations by using samples adsorbed on filter paper was introduced by Scott and Dorling (1965). In the present study the effects of varying molarities of magnesium chloride on the staining of a number of polyanions by indium haematein chelate was studied in the same way. The polyanion substances employed were alginate, gelatin and hyaluronate as examples of polycarboxylates, heparin as an example of a polysulphate, chondroitin sulphate and PPL-3 as examples of polyanions containing both carboxyl and sulphate groups, and RNA and DNA as examples of polyphosphates. The results varied somewhat with stain concentration and duration of staining. In the present experiments the clearest C.E.C. values (i.e. no background staining and dark staining of polyanion 'spots') were

obtained by staining for 16 hrs. at 0°C in the dark with low stain concentrations of about 0.01%. The absence of light largely prevents background staining and consequently accentuates the clarity of the polyanion staining though the reason for this is not known.

The results of one experiment are shown in figure 99. The C.E.C. values, expressed as molarity of magnesium chloride, of alginate, gelatin and hyaluronate were 0.4, 1.6 and 0.2 respectively. Heparin had a C.E.C. value of 0.2. Chondroitin sulphate and PPL-3 had C.E.C. values of 3.0 and 1.4 while those for RNA and DNA were above 3.4, the highest salt molarity employed in this experiment. The rather large variations of C.E.C. values of polyanions containing the same anionic group is probably due to the differences in their molecular weights. Despite this variation the polyanion sequence appears to be

$$\text{C.E.C.}(-SO_4^-) < \text{C.E.C.}(-COO^-) \lesssim \text{C.E.C.}\ (-COO^- + -SO_4^-) < \text{C.E.C.}(=PO_4^-)$$

Scott (1968a) found similar C.E.C. values for aluminium haematein staining of polysulphates and polyphosphates on filter paper in the presence of magnesium chloride although his higher values for polycarboxylates (1.0-3.0) and lower values for carboxyl and sulphate containing polyanions (<0.1 - 0.2) resulted in a slightly different C.E.C. sequence:

$$\text{C.E.C.}\ (-SO_4^-) < \text{C.E.C}\ (-COO^- + -SO_4^-) < \text{C.E.C.}(-COO^-) < \text{C.E.C.}(=PO_4^-)$$

He regards this sequence as characteristic of the cationic metal chelate dyes of Group II. The differences between the C.E.C. values obtained with indium haematein and those determined by Scott (1968a) for aluminium haematein may be partly due to variations in the molecular weight of the polyanion substrates employed since log C.E.C. α M. Wt. In addition, for dyes of Group II the character of the electrostatic interaction is determined by the nature of the chelated ion [Scott and Willett, 1966] and so, although aluminium and indium are both trivalent metals from Group III of the periodic table the larger size of indium may explain these differences.

Glutaraldehyde and/or osmium fixation has little effect upon the C.E.C. of most polyanions; however, after fixation gelatin staining could not be abolished by incorporation of up to 4.2M magnesium chloride into the staining solution. It is not clear how the extensive crosslinking produced by glutaraldehyde or osmium could cause the gelatin to bind the chelate so strongly. The staining of chondroitin sulphate and hyaluronate was reduced after fixation although their C.E.C. values were unaffected. This finding is compatible with the well known lack of fixation of glycosaminoglycans by glutaraldehyde or osmium [Hayat, 1970].

C.E.C. values for indium haematein staining of collagen and pancreas

I. It was considered that it might be of value to study the staining properties of native collagen fibrils, an example of a normal tissue component carrying repeating carboxyl groups. The staining properties of the acinar cells of the pancreas in which the phosphate groups are exemplified by the nuclear DNA and the very numerous ribosomes of the endoplasmic reticulum and carboxyl groups by the enzymes contained within the zymogen granules were also examined.

When unfixed collagen is stained on formvar filmed grids with indium haematein the band pattern is readily evident in low concentrations of magnesium chloride but disappears at higher concentrations. In figure 100 a) is the standard pattern exhibited by a collagen fibril after staining with many standard cationic stains such as uranyl acetate or lead citrate. Figure 100 b) shows a similar fibril unstained. Figure 100 c) - g) shows the staining pattern obtained with indium haematein in the presence of molarities of magnesium chloride varying from 0.2 to 3.8. It is evident that distinct staining of bands ceases at about 3.0M magnesium chloride. It must be assumed that the chelate is binding to carboxyl groups on the collagen fibrils and that the extinction

value of 3.0M magnesium chloride represents the C.E.C. value for these groups in collagen. Prior fixation of the collagen has little effect upon the banding pattern observed with indium haematein or the molarity of salt required to abolish it.

It will be noted that this C.E.C. value for collagen carboxyl groups is appreciably higher than those found for carboxyl containing polyanions on filter paper. A similar disparity between C.E.C. values in filter paper experiments and tissue staining was noted by Scott and Dorling (1965) and was ascribed by them to the greater polymerisation and concentration of the polyanions in the tissues. In the present context the collagen was stained by a 0.25% solution of indium haematein compared with the 0.01% concentration used in filter paper experiments and this may be an additional factor.

II. Osmication although not interfering with polyanion C.E.C. determinations as seen from the results of C.E.C. determinations of polyanions adsorbed on filter paper does confer electron density to a variety of other tissue structures which at the ultrastructural level would tend to mask any C.E.C. effect. The technique of staining tissues prior to embedding was investigated but it was found that the technical difficulties encountered when

sectioning tissues stained en bloc with indium haematein and the laborious task of preparing the large numbers of tissue blocks did not commend this approach.

The best ultrastructural staining was obtained by exposure of ultrathin unosmicated tissue sections to 0.25% indium haematein at pH 4.6 at 0°C in the dark for 2 hrs. Attempts to stain ultrathin sections under the optimum conditions determined for demonstration of C.E.C. of polyanions adsorbed on filter papers, namely 0.01% indium haematein pH 4.6 at 0°C for 2-3 days resulted in paler staining which would not allow easy identification of C.E.C. values at the ultrastructural level.

Figure 101 shows the appearance of an unstained section of unosmicated pancreas. Figures 102 and 103 show similar sectioned material stained with indium haematein in the presence of molarities of magnesium chloride between 0.2 and 3.0. In the presence of 0.2M magnesium chloride the nuclei, ribosomes and zymogen granules are well stained. Addition of up to 3.0M magnesium chloride has little or no effect on the ribosomal or nuclear staining (Figs. 103, 104 and 106); however, the staining of the zymogen granules is markedly reduced in the presence of 1.4M magnesium chloride (Fig. 107). It must be assumed that in the case of zymogen granules the cationic indium haematein chelate is binding to the carboxyl groups of aspartate

and glutamate residues in the contained enzyme precursors.

The C.E.C. value for these carboxyl groups is somewhat higher than those found for polycarboxylates in filter paper experiments and the possible reasons for such a difference have already been noted. However, the value for the pancreatic zymogen granules is obviously considerably lower than the value of 3.0M found for collagen. It may be that this difference is again a reflection of a difference in molecular weights. It is also possible that an excess of acidic over basic amino acids in collagen compared with an excess of basic over acidic in enzymes of the zymogen granules [Green et al., 1963; Tristram and Smith, 1963] may be a relevant factor.

The C.E.C. values for the phosphate groups in the pancreatic acinar cells are certainly above 3.0M and thus are in conformity with those determined from filter paper experiments.

C.E.C. values for indium haematein staining of the nucleus pulposus

Figure 108 shows the appearance of unstained, unosmicated rabbit nucleus pulposus; figures 109 and 110 illustrate the staining pattern obtained after exposure to indium haematein in the presence of 0.2M

and 2.6M magnesium chloride. In the presence of 0.2M magnesium chloride, indium haematein stains a wide variety of structures. The nuclei and sparsely distributed rough endoplasmic reticulum are well stained (Fig. 111). Material within the large vesicles is also stained (Figs. 111, 113) and appears as particles 20 nm in diameter arranged in rows; some particles appear to touch or overlap while others appear to be connected by fine filaments (Fig. 113, inset a). Their location, arrangement and similar size to material stained with ruthenium red or bismuth and uranyl acetate suggests that they represent proteoglycan. Darkly stained clumps of material are frequently seen within notochordal cells, these are located towards the cell periphery and at the edge of large vesicles (Figs. 111, 113); however, their precise localisation could not be determined since the cell membranes are not stained. The filamentous meshwork within the extracellular matrix is densely stained by indium haematein (Fig. 113) and appears as linear rows of particles approximately 30 nm in diameter (Fig. 113). Similarly stained particles are seen within the dark bands of the banded fibres (Fig. 115). Bands of electron-dense material and stellate particles previously described in the matrix of the nucleus pulposus (page 57) are not stained by indium haematein although the 30 nm diameter stained matrix particles

appear to be closely applied to the surface of these masses (Figs. 118, 119).

Incorporation of 0.6M magnesium chloride into the staining solution completely abolishes all staining of particles within the large vesicles as well as reducing the density of staining of matrix material (Fig. 112). The staining of material either free in the extracellular matrix (Fig. 114), within the dark bands of banded fibres (Fig. 116) or, applied to the surface of electron-dense masses (Fig. 120) is gradually reduced as the salt molarity is increased from 0.6M but is not completely abolished until a salt molarity of 2.0M is attained (Fig. 117).

The staining of clumps of dense material at the periphery of notochordal cells is also reduced in a similar fashion to the staining of matrix material and is abolished by incorporation of 2.0M magnesium chloride. This observation coupled with the distribution of this material suggests that these clumps may represent either condensed extracellular matrix material during its export from the notochordal cell, or matrix proteoglycans undergoing ingestion and breakdown during the normal metabolic turnover of matrix components (page 43).

Nuclear staining was not markedly reduced even at the highest salt molarities attained (Fig. 110).

This is in keeping with the observations on the staining of pancreas with indium haematein at high salt molarities and the model experiments performed on filter papers in which the C.E.C. value of the phosphate groups in DNA and RNA was found to be above 3.8M.

The material within the large vesicles exhibited a C.E.C. value of less than 0.6M while the extracellular matrix material and clumps of stained material found at the cell periphery exhibited a C.E.C. value between 1.4 and 2.0M. Correlation of these values with the actual C.E.C. values of polyanions determined from filter paper experiments is of little value since the observed C.E.C. value is affected by the differing physical state of the polyanion, the different stain concentration and different criteria used in assessing the C.E.C. value; however, the sequence of C.E.C. values for the anionic groups does provide a guide to the nature of residues staining at the ultrastructural level.

The C.E.C. value for the matrix material is similar to the value also determined at the ultrastructural level for carboxyl groups in collagen (3.0M) and within pancreatic zymogen granules (1.4M). It is probable that the matrix staining is due to binding of indium haematein by dissociated carboxyl

groups within the proteoglycan. While the role of sulphate groups in the matrix staining cannot be discounted it is extremely unlikely that they participate since from the filter paper experiments it was determined that the sulphate residues have the lowest C.E.C. values.

As has been mentioned earlier the staining characteristics of the vesicle material suggest that it consists of proteoglycans. The staining is probably again due to dissociated carboxyl groups. The much lower C.E.C. value would seem to be a reflection of the low molecular weight of this material prior to its aggregation and export.

Iron haematein

Lillie (1965) modified Weigert's iron haematein stain by doubling the hydrochloric acid content and reducing the amount of haematoxylin. Addition of ferrous sulphate stabilises the solution. Although freshly dissolved haematoxylin is used, its rapid oxidation by ferric salts means the solution can be used immediately; the solution had a pH of 1.0.

A second staining solution was prepared from the above formula with the omission of the concentrated hydrochloric acid. This solution had a pH of 1.8.

After 30 minutes exposure to iron haematein pH 1.0, ultrathin sections of rabbit articular cartilage show staining of chondrocyte nuclei and ribosomes as well as dense matrix staining (Fig. 121). At higher magnification the matrix is visualised as stained particles 25 nm in diameter which may be interconnected by fine filaments (Fig. 122). This appearance is almost identical to that of cartilage stained with ruthenium red or Alcian blue, both of which are considered to localise cartilage proteoglycans [Thyberg et al., 1973; Luft, 1968]. The similarity of the iron haematein staining pattern to that of other cationic stains would seem to indicate that iron haematein binds to free tissue anionic groups such as the phosphate groups of DNA and RNA and the sulphate and the few dissociated carboxyl groups of proteoglycans within the matrix.

The matrix of the rabbit nucleus pulposus after treatment with iron haematein pH 1.0 is seen as 25 - 30 nm diameter particles which may be arranged in rows. The dark bands of the banded fibres are also stained (Fig. 124). In contrast to this the moderate density of the electron-dense masses (Fig. 123) would seem to be a result of prior osmication of the tissue (page 58). The staining of 30 nm diameter particles and banded fibres within the nucleus pulposus matrix is similar to that produced by exposure to phosphotungstic acid at low pH,

ruthenium red and bismuth as has been noted earlier (pages 47 and 52). This observation, coupled with the cartilage staining, suggests that iron haematein is localising the free carboxyl and/or sulphate groups within the matrix proteoglycans.

Raising the pH of the staining solution from 1.0 to 1.8 resulted in an appreciable increase in density of the stained material within the nucleus pulposus matrix (Figs. 125 and 126).

This increase in density is probably the result of two mechanisms operating. Firstly, chelate formation can be represented

$$M^{++} + nHem \leftrightarrows [MHem_n]^{m+} + nH^+$$

and so, from consideration of the Law of Mass Action it can be seen that raising the pH would favour chelate formation thus increasing the chelate concentration. Secondly, since the pK of sulphate and carboxyl groups within glycosaminoglycans is about 1.5 to 3.0 respectively, any increase in pH would result in further dissociation of sulphate and carboxyl groups, rendering them free to react with cationic molecules.

There is a possibility that the observed staining may result from the excess ferric and ferrous ions present in solution since the molar ratio of iron to haematein is 7.6:1. Sprumont and Musy (1971) using iron-tartrate complex ions considered that below pH 4.5

there were some free ferric ions which were complexed by phosphate and sulphate radicals within the tissue and conferred electron density upon nuclei and basement membranes. However, Berube et al. (1965) determined that iron haematein solutions in which the molar ratio of iron to haematein was between 40:1 and 7:1 combined with the phosphate groups of nucleic acids and deduced that the staining was due to cationic chelates having the form $[Fe_nHem]^{m+}$.

In the present study it appears that the observed staining at anionic tissue sites (nuclei, ribosomes and matrix glycosaminoglycans) is due to a cationic iron haematein chelate with a possible contribution to the electron density by the binding of free ferric and ferrous ions also. Since the electron density resulting from this staining was not very marked it was felt that cationic chelates of haematein with heavier metals might be worth investigation.

Lead haematein

A lead haematein stain was adapted from the formula of MacConaill (1949). He used it as a constituent of a polychrome stain for nervous tissue.

The standard lead haematein solution was made by mixing equal volumes of i) 2% (w/v) haematoxylin (Hopkin and Williams Ltd., Batch No. 82246B19349) in distilled water, and ii) 5% (w/v) $Pb(NO_3)_2$ (A.R.) in distilled water.

The mixture was allowed to stand for 1 hr and filtered. The resulting orange solution had a pH of 3.0 and was millipore filtered (mean pore size 0.45 $\pm$ 0.02 μm) before use.

Exposure of ultrathin sections of rabbit nucleus pulposus to this stain resulted in a similar localisation of electron density (Figs. 127 and 128) to that observed with iron haematein and is considered to stain matrix glycosaminoglycans. The denser staining observed with lead haematein compared with iron haematein is in part due to the heavier metal and also the longer exposure to stain (4 hrs). Experiments showed that staining density was increased up to 4 hr exposure and further prolongation of the staining period did not result in any increase of electron-density.

The possibility that unchelated lead ions remaining in solution may confer electron-density on tissue structures was investigated by staining sections in a series of lead haematein solutions in which the molar ratio of lead to haematein was varied between 0.4:1 and 6.8:1. As can be seen from figs. 129 and 130 varying the lead : haematein molar ratio within these limits has very little effect upon the staining of the rabbit nucleus pulposus matrix.

Lowering the pH of the standard lead haematein staining solution to pH 0.5 by addition of nitric acid

had a profound effect upon the appearance of stained sections (Fig. 131). Glycosaminoglycan staining was abolished as evidenced by the loss of staining of 30 nm particles within the matrix and 6 nm particles within the dark bands of the banded fibres (Figs. 132 and 133). The residual electron-density of the notochordal cells (Fig. 131) and electron-dense masses within the matrix would appear to be a result of prior osmication of the tissue. Raising the pH of the staining solution to pH 4.4 by addition of sodium hydroxide does not alter the staining pattern appreciably compared with the staining produced by the standard lead haematein pH 3.0 (Fig. 134). The matrix particles and material within the dark bands of the banded fibres are densely stained while the appearance of the electron-dense masses is unaffected (Fig. 135). It was noted that raising the pH of the staining solution increased the tendency of stain to precipitate on the sections. This is in keeping with the findings of Berube et al. (1965) who showed that increasing the pH of an iron haematoxylin staining solution favoured the formation of polymeric iron haematein chelates with consequent precipitation.

Addition of various molarities of inorganic salts to lead haematein solutions and its effect upon tissue staining was observed. Sodium nitrate was the salt chosen for study since addition of chlorides resulted in precipitation of lead chloride and addition of magnesium

salts caused excessive pH alteration. Varying amounts of sodium nitrate were added to millipore filtered 10 ml aliquots of the standard lead haematein staining solution and dissolved by rotation, resulting in staining solutions containing between 0.0 and 2.0M sodium nitrate. Addition of up to 1.6M sodium nitrate had little apparent effect upon the staining of the nucleus pulposus matrix (Figs. 136 and 137). However, further increases in salt molarity resulted in decreased staining of 30 nm diameter matrix particles and 6 nm particles seen within the dark bands of the banded fibres (Fig. 138). Addition of sodium nitrate to give a resultant molarity of 2.0M in the staining solution prevents any staining of matrix glycosaminoglycans, although the masses of amorphous electron-dense material are still visible due to osmication of the tissue (Fig. 139). The nuclear staining is largely unaffected by addition of up to 2.0M sodium nitrate (Fig. 140).

The reduction and eventual abolition of matrix staining by addition of sodium nitrate to the staining solution could be the result of several mechanisms operating. One possibility is that increased addition of sodium nitrate could gradually lower the pH of the staining solution until in 2.0M sodium nitrate the pH has been lowered below the pK values for the carboxyl and sulphate groups and so only the phosphate groups

having a lower pKa would be free to accept the staining molecule. Since the pH of these staining solutions was not measured, this possibility cannot be discounted. Secondly, since the ultraviolet and visible absorption spectrum of the lead haematein solution was so similar to that of haematoxylin it was difficult to ascertain to what extent a stable lead haematein chelate was formed. If appreciable dissociation of the chelate occurred, the observed electron density of tissue structures could be due to binding of free lead ions with the addition of sodium nitrate producing a reduction in electron density by displacement of lead by sodium. In an attempt to elucidate this problem, tissues were stained with lead nitrate in the presence and absence of 2.0M sodium nitrate. As can be seen from figure 141, staining with 5% lead nitrate is much less dense than with lead haematein. This difference can be attributed to the fact that only one lead ion can bind to each anionic group whereas binding by lead haematein chelate may involve several lead atoms. Incorporation of 2.0M sodium nitrate into the lead nitrate solution results in only a very slight reduction in the intensity of staining (Fig. 142). This is not surprising since glycosaminoglycans appear to have a higher affinity for divalent ions than univalent ions [Scott, 1968c]. It therefore seems probable that the lead haematein chelate does not dissociate but that any reduction in

staining by addition of sodium nitrate is due to a true critical electrolyte concentration (C.E.C.) effect.

The results are in agreement with C.E.C. values determined by Scott and Willett (1966) for aluminium haematein polyanion complexes absorbed on filter paper. Assuming that the material staining in the nucleus pulposus matrix is glycosaminoglycan, the C.E.C. value of 1.7 (expressed as molarity of sodium nitrate) is rather higher than Scott's value of 0.4 to 0.6 (expressed as molarity of sodium chloride) [Scott, 1968a]. This difference can be largely attributed to the chelate concentration since Scott (1968a) used a 0.01% (w/v) aluminium haematein solution and the present experiments employed 1.0% (w/v) lead haematein. The C.E.C. value is theoretically an expression of $\frac{[R^+]}{[M^+]}$ and can only be expressed in terms of $[M^+]$ if $[R^+]$ is kept constant (p. 61). Although the C.E.C. values cannot be compared directly with Scott's values (1968a), the order of C.E.C. values found upon staining with lead haematein in the presence of sodium nitrate was found to be:-

$$\underset{1.7}{\text{C.E.C. } (-COO^- + -SO_4^-)} < \underset{> 2.0}{\text{C.E.C. } (= PO_4^-)}$$

and is similar to the order of C.E.C. values determined by Scott and Willett (1966) for aluminium haematein complexes adsorbed on filter papers.

Although addition of sodium nitrate to lead haematein staining solutions does seem to produce a C.E.C. effect the absence of a characteristic absorption spectrum for lead haematein solutions made accurate estimation of the chelate concentration impossible. It was felt that chelation of a heavy metal atom by haematein resulting in a definite spectral change might be advantageous. With this in view a variety of other metal haematein chelates were tested.

Uranium haematein

Another haematein chelate which has been investigated is that formed with uranium salts. Although the chelate itself exhibited strong cationic staining properties, difficulties were encountered in the establishment of suitable salt molarities for the C.E.C. technique and the method was consequently discontinued. However, some of the observations made on the uranium haematein chelate seem to be of general interest and will be described.

Addition of a uranyl acetate solution to an orange/brown solution of haematoxylin or haematein produces a dark purple solution which has a characteristic visible absorption spectrum which is different from that of either of the original components (Fig. 143). The appearance of a new absorption maximum at 560 nm indicates the presence of a new chemical species - probably a chelate

of uranyl ions with haematein. It is generally considered that haematoxylin must be 'ripened' and oxidised to haematein before chelate formation can occur [Marshall and Horobin, 1972]. However, the similarity of absorption spectra and the speed with which the purple chelate was formed upon mixing uranyl acetate and haematoxylin would indicate that either oxidation of haematoxylin occurs almost instantaneously upon mixing with uranyl acetate, or that the haematoxylin preparation itself was appreciably oxidised. It was hoped that the use of haematein to form the chelate would overcome the rather variable effects of ripening haematoxylin [Marshall and Horobin, 1972] and allow more accurate determinations of chelate concentrations and binding to polyanions [Terner et al., 1964].

The effect of staining chondroitin sulphate with uranium haematein produced from uranyl acetate and haematoxylin or haematein was investigated. Varying quantities of chondroitin sulphate (Sigma Grade II) were added to staining solutions and shaken for 5 min. The solutions were centrifuged and the absorbence of the supernatant read directly on a Unicam SP 600 spectrophotometer at 560 nm. A plot of the reduction in absorbence at 560 nm of the residual staining solution against the amount of chondroitin sulphate being stained is shown in figure 144. Addition of chondroitin sulphate

to the chelate formed by mixing haematein and uranyl acetate resulted in a greater reduction in absorbence at 560 nm than addition to the chelate formed by mixing haematoxylin and uranyl acetate. This was possibly due to the greater proportion of cationic chelate available for binding in solutions made with haematein as evidenced by the greater absorbence at 560 nm in the absence of added polyanion. As a result of this, the uranium haematein chelates used for further studies were produced from haematein.

In an effort to determine the relative amounts of uranyl acetate and haematein for optimum chelate formation, the absorption spectra of solutions containing various molar ratios of uranyl acetate to haematein were analysed and the absorbence of these solutions at various wavelengths is illustrated (Fig. 145). The absorbence at 340 nm is largely due to charge transfer mechanisms within the uranyl ion although a small contribution by the haematein molecule is indicated from the appreciable absorption at this wavelength in the absence of uranyl ions. That the contribution due to haematein is only small is indicated by the curve showing that absorbence at 340 nm is proportional to the concentration of uranyl acetate. The absorbence at 430 nm was thought to be characteristic of haematein; however there is a minor contribution by a peak at 415 nm due to $d\text{-}d^{*}$ transformations

within the uranyl ion. The sharp drop in absorbance at 430 nm and similar increase in absorbence at 560 nm upon addition of a relatively small amount of uranyl acetate to the haematein solution indicates an initial alteration in a larger proportion of haematein molecules than could be accounted for by a 1:1 interaction (assuming Beer's Law is obeyed). If absorbence at 560 nm is indicative of chelate formation and since previous experiments have shown that this compound obeys Beer's Law the optimum molar ratios may be determined. The haematein preparation being used had a moisture content of 8.96 $\pm$ 0.16% and when dissolved under standardised conditions a residue which amounted to 27.24 $\pm$ 0.39% remained. Assuming that the soluble material was pure haematein the molar ratios of a range of solutions was computed. The variation of absorbence at 560 nm for solutions containing different molar ratios of uranium: haematein is illustrated (Fig. 146). The absorbence at 560 nm increases sharply as the uranium:haematein ratio is increased to 2.5, further increases in the amount of uranyl acetate have relatively little effect. That the uranium:haematein ratio producing maximum absorption at 560 nm and presumably similar chelate formation is not unity may be attributed to several causes. Firstly, the material which dissolved (63.80 $\pm$ 0.55%) upon stirring 0.1 g haematein in 100 ml distilled water for 30 min was not pure haematein since

the purity of commercial preparations may be very low (Imes et al., 1969). Secondly, the equilibria governing chelate formation are often of a complex nature and so it seems unlikely that all the uranyl ions added will be chelated; it was felt that determination of the extent of chelation other than by spectrophotometric means was outwith the scope of this work. A solution having a molar ratio of 2:1 (uranium: haematein) was used, this molar ratio was chosen as a compromise between the maximum chelate formation and the presence of unchelated uranyl ions which would affect the staining of tissues at the ultrastructural level.

Tissue staining was observed using a 1% uranium haematein solution having a molar ratio of 2:1. The solution had a pH of 4.2 and was millipore filtered (mean pore size 0.45 $\pm$ 0.02 μm) before use. Exposure of ultrathin sections of osmicated rabbit nucleus pulposus to this stain for 4 hr produced clear nuclear and ribosomal staining as well as staining of granular material present within the large vesicles (Fig. 147). In addition 30 nm diameter particles within the extracellular matrix and material within the dark bands of the banded fibres were also stained (Fig. 148). This distribution of staining is consistent with the view that the chelate is binding to tissue polyanions.

Exposure of unfixed collagen to uranium haematein solution at pH 4.2 resulted in a periodic cross banding pattern (Fig. 149). The close resemblance of collagen after exposure to uranium haematein with normal positively stained collagen (Fig. 150) suggests that the chelate is binding to the same acidic residues that are rendered electron dense by positive staining. However, the possibility that this staining is due to binding of free uranyl ions perhaps produced by dissociation of the chelate remains.

To show that the staining is due to the chelate and not to excess uranyl ions, a quantitative estimation of uranium haematein binding by collagen was attempted. Varying quantities of freeze-dried collagen, up to 0.5 g, were added to 10 ml of 0.017M uranium haematein. The solutions were placed in a rotary mixer for 1½ hr and then centrifuged. The absorbence at 560 nm of duplicated aliquots of the supernatant staining solution was determined, after suitable dilution, on a Unicam SP 600 spectrophotometer. Since a calibration curve of uranium haematein obeys Beer's Law, the concentration of the supernatant staining solution could be calculated. The values obtained were plotted against the quantity of collagen being stained (Fig. 151). It was found that provided the stain was present in reasonable excess, the amount of chelate removed from solution was proportional

to the amount of freeze-dried collagen added. The stained collagen was a purple colour due to the bound chelate and so it seems that the periodic banding pattern of collagen observed at the ultrastructural level after exposure to uranium haematein must be due to binding of the chelate to anionic sites on the collagen molecule.

Addition of formate, acetate or maleate buffers to maintain the original pH of 4.2 were unsuccessful and resulted in a partial loss of absorbence at 560 nm. Addition of 1.0M sodium or magnesium chloride to acetate buffered uranium haematein solutions resulted in further loss of absorbence at 560 nm (Fig. 152) and the appearance of a precipitate, the amount of which was proportional to the stain concentration. The precipitate is probably a complex acetate of uranium and sodium having the general formula $Na(CH_3COO).M(CH_3COO)_2.3UO_2(CH_3COO)_2.6H_2O$ in which M can be a variety of divalent metal ions including those of magnesium, cobalt, nickel, manganese and zinc. This complex salt is only sparingly soluble 5.85g/100ml at 21°C [Charlot and Bézier, 1954; Kolthoff and Sandell, 1952]. That addition of magnesium salts caused a greater decrease in absorbence can be explained by assuming that the amount of sodium ions (introduced by addition of buffer) is limiting for complex acetate formation and so further additions of magnesium do not

result in any further loss of absorbence at 560 nm, or increase in precipitation. In a similar way the amount of precipitate produced on addition of sodium chloride is limited by the amount of divalent metal ions present. In an effort to overcome problems of complex acetate formation a chelate was made from uranyl nitrate and haematein, the resultant blue/black solution was characterised by an absorption maximum at 510 nm; however the solution had an unattractively low pH of 2.9. Since uranium forms a wide variety of insoluble salts it appears that addition of salt and/or buffer to uranium haematein solutions results in a loss of chelated uranyl ions characterised by a decrease in absorbence at 560 nm.

The cationic chelate formed from uranyl acetate and haematein binds to polyanions conferring a visible purple colour enabling their quantitative estimation and sufficient electron density for their ultrastructural localisation. However, this stain could not be used in the C.E.C. technique due to the wide variety of insoluble salts formed by uranyl ions.

CONCLUSION

Although the C.E.C. theory has received widespread application in industrial processes and in biochemical and histochemical investigations, recently Marshall and Horobin (1973a) have cast doubts upon certain aspects of the theory. They measured the affinities of cationic dyes for various tissue substrates and interpreted their results for dyes of Group I (low polarising power) as being contrary to the C.E.C. theory. However, as Scott (1974) observed, this discrepancy was solely due to their erroneous interpretation of the C.E.C. theory, namely that the C.E.C. of Group I dyes is determined by their affinity for the anionic tissue groups. In fact, the correct interpretation is that the affinity of the inorganic cation for tissue anionic groups dictates the sequence of dyes of Group I and this is in fact supported by Marshall and Horobin's (1973a) affinity data. Marshall and Horobin (1973a) also suggest that their affinity data for dyes of Group II conflict with the C.E.C. theory but doubt is thrown upon this interpretation by the low pH values and arbitrary ratio of metal to haematein in the staining solutions employed as well as the wide variation in results for dyes of Group II [Marshall and Horobin, 1973a; 1973b].

All the metal haematein chelates examined in the present investigation produced tissue staining at the

ultrastructural level. The localisation of electron density in collagen, pancreas and nucleus pulposus is suggestive of staining of sites having high concentrations of anionic groups. For reasons discussed earlier, further staining properties of iron haematein or uranium haematein were not investigated.

When increasing molarities of salt are added to lead haematein or indium haematein staining solutions there is a progressive and differential loss of staining of ultrastructural components. This, together with data from model experiments performed on filter papers was highly suggestive of a C.E.C. effect and gave the following sequence of C.E.C. values for both lead and iron chelates.

$$C.E.C.(-SO_4^-) < C.E.C.(-COO^- + -SO_4^-) < C.E.C.(-COO^-) < C.E.C.(=PO_4^-)$$

This is in keeping with previous observations of the C.E.C. sequence of aluminium haematein chelates [Scott and Willett, 1966; Scott, 1968a]. Such chelates are considered to be characteristic of dyes of Group II in which the high polarising power of the chelate affects its electrostatic interactions.

Although the C.E.C. values of tissue polyanions at the ultrastructural level using indium haematein could be determined, these could not be correlated with the values obtained from model experiments. This was because

the optimum stain concentration for ultrastructural staining and staining of polyanions on filter paper differed, which in turn affects the C.E.C. values [Scott and Dorling, 1965]. In addition the C.E.C. value of the model filter paper experiments was judged on the basis of the extinction of visible purple colouration whereas that at the ultrastructural level was judged on the decrease in density of bound indium to a certain critical level at which there was no observable increase in electron density. Also although the pattern of C.E.C. values follows that determined by Scott and Willett (1966) and Scott (1968a) for aluminium haematein chelates the precise values cannot be compared since the nature of electrostatic interaction depends primarily on the nature of the chelated ion [Scott and Willett, 1966].

The variable purity of haematein and haematoxylin commercial preparations [Imes et al., 1969; Marshall and Horobin, 1974] and the apparent lack of any simple purification procedures may partly explain the lack of interest in the use of haematein chelates as ultrastructural stains for application to the C.E.C. technique. In addition the very variable nature of haematein chelates [Berube et al., 1965] makes any use of them at the ultrastructural level rather uncertain. Despite this it was felt that indium haematein would

be a valuable ultrastructural stain. The large size of the indium ion, the spectral change upon chelate formation and the pH of the chelate solution of 4.2 are valuable advantages over those of other haematein chelates. The fact that the chelate does not appear to be affected by addition of magnesium chloride is important for C.E.C. determination. The indium haematein staining could be more fully characterised by prior purification of the haematein preparation, electrophoretic separation and spectral studies of the chelates formed and 'model' experiments using resin embedded polyanions to determine their ultrastructural C.E.C. values. Indium haematein chelates could then be used for ultrastructural characterisation of tissue polyanions by determination of their C.E.C. values.

BIBLIOGRAPHY

Albersheim, P. and Killias, U. (1963)

The use of bismuth as an electron stain for nucleic acids.
J. Cell Biol. 17, 93-103.

Antonopoulos, C.A. (1965)

Glycosaminoglycans of human nucleus pulposus, identification and variation in their concentration with age.
Acta Univ. Lund. Section II no.35, 1-7.

Antonopoulos, C.A., Gardell, S., Szirmai, J.A. and De Tyssonsk, E.R. (1964)

Determination of glycosaminoglycans from tissues on the microgram scale.
Biochim. biophys. Acta 83, 1-19.

Arshid, F.M., Connelly, R.F., Desai, J.N., Fulton, R.G., Giles, C.H. and Kefalas, J.C. (1954)

A study of certain natural dyes: II. The Structure of the metallic lakes of the brazilwood and logwood colouring matters.
J. Soc. Dyers Colour. 70, 402-412.

Babai, F. and Bernhard, W. (1971)

Détection cytochimique par l'acide phosphotungstique de certains polysaccharides sur coupes à congélation ultrafines.
J. Ultrastruct. Res. 37, 601-617.

Bannister, L.H. (1972)

Lanthanum as an intracellular stain.
J. Microscopy 95, 413-419.

Barr, L., Dewey, M.M. and Berger, W. (1965)

Propergation of action potentials and the structure of the nexus in cardiac muscle.
J. gen. Physiol. 48, 797-823.

Berube, G.R., Powers, M.M. and Clark, G. (1965)

Iron hematoxylin chelates I. The Weil staining bath.
Stain Technol. 40, 53-62.

Brachet, J., Decroly-Briers, M. and Hoyez, J. (1958)

Contribution a l'étude des lysosomes au cours du développement embryonnaire.
Bull. Soc. Chim. biol. 40, 2039-2048.

Brightman, M.W. and Reese, T.S. (1969)

Junctions between ultimately apposed cell membranes in the vertebrate brain.
J. Cell Biol. 40, 648-677.

Buddecke, E. and Sziegolet, M. (1964)

Isolierung, chemische zusammensetzung und altersabhangige. Verteilung von mucopoly-sacchariden menschlicher zwischenwirbelscheiben.
Hoppe-Seyler's Z. physiol. Chem. 337, 66-78.

Bungenberg De Jong, H.G. (1952)

In "Colloid Science" Ed. H.R. Kruyt.
American Elsevier Pub. Co., Inc., New York, 2, 259.

Butler, W.F. and Smith, R.N. (1964)

The nucleus pulposus of the intervertebral disc of the newborn cat.
Res. vet. Sci. 5, 71-74.

Charlot, G. and Bézier, D. (1954)

Quantitative Inorganic Analysis.
Methuen, London p.579.

Cornah, M.S., Meachim, G. and Parry, E.W. (1970)

Banded structures in the matrix of human and rabbit nucleus pulposus.
J. Anat. 107, 351-362.

De Duve, C. (1959)

Lysosomes, a new group of cytoplasmic particles.
In "Subcellular Particles". Ed. T. Hayashi.Ronald Press. New York. pp.128-159.

Dewey, M.M. and Barr, L. (1964)

A study of the structure and distribution of the nexus.
J. Cell Biol. 23, 553-585.

Dingle, J.T., Fell, H.B. and Glauert, A.M. (1969)

Endocytosis of sugars in embryonic skeletal tissues in organ culture IV. Lysosomal and other biochemical effects. General discussion. J. Cell Sci. 4, 139-153.

Doggenweiler, C.F. and Frenk, S. (1965)

Staining properties of lanthanum on cell membranes. Proc. natn. Acad. Sci. U.S.A. 53, 425-430.

Fahimi, H.D. and Drochmans, P. (1965)

Essais de standardisation de la fixation au glutaraldehyde I. Purification et determination de la concentration du glutaraldehyde. J. Microscopie 4, 725-736.

Farquhar, M.G. and Palade, G.E. (1963)

Junctional complexes in various epithelia. J. Cell Biol. 17, 375-412.

Farquhar, M.G. and Palade, G.E. (1965)

Cell junctions in amphibian skin. J. Cell Biol. 26, 263-291.

Fawcett, D.W. (1958)

Structural specialisations of the cell surface. In "Frontiers in Cytology" Ed. S.L. Palay. Yale University Press, New Haven. pp.19-41.

Fletcher, J.M., Greenfield, B.F., Hardy, C.J., Scargill, D. and Woodhead, J.L. (1961)

Ruthenium red. J. chem. Soc. (1961) 2000-2006.

Földes, I. and Palfrey, A.J. (1971)

Ultrastructure of rat intervertebral disc and epiphyseal cartilage. J. Anat. 110, 167.

Furshpan, E.J. (1964)

"Electrical transmission" at an excitatory synapse in a vertebrate brain. Science, N.Y. 144, 878-880.

Garant, P.R. (1972)

The demonstration of complex gap junctions between the cells of the enamel organ with lanthanum nitrate.
J. Ultrastruct. Res. 40, 333-348.

Goodenough, D.A. and Revel, J.P. (1970)

A fine structural analysis of intercellular junctions in the mouse liver.
J. Cell Biol. 45, 272-290.

Greene, L.J., Hirs, C.H. and Palade, G.E. (1963)

On the protein composition of bovine pancreatic zymogen granules.
J. biol. Chem. 238, 2054-2070.

Hallén, A. (1958)

Hexosamine and ester sulphate content of the human nucleus pulposus at different ages.
Acta chem. scand. 12, 1869-1872.

Hallén, A. (1962)

The collagen and ground substance of human intervertebral disc at different ages.
Acta chem. scand. 16, 705-710.

Happey, F., Johnson, A.G., Naylor, A. and Turner, R.L. (1964)

Preliminary observations concerning the fine structure of the intervertebral disc.
J. Bone Jt. Surg. 46B, 563-567.

Hayat, M.A. (1970)

"Principles and Techniques of Electron Microscopy". Vol.I. Biological Applications. Van Nostrand Reinhold Co. N.Y.

Heinegård, D. and Gardell, S. (1967)

Studies on protein-polysaccharide complex (proteoglycan) from human nucleus pulposus.
I. Isolation and preliminary characterisation.
Biochim. biophys. Acta 148, 164-171.

Imes, N.K. Jr., Sanders, D.C., Crane, C.R. and Clark, G. (1969)

Assaying actual hematein content of commercial hematoxylins and hemateins.
Stain Technol. 44, 167-172.

Kahn, T.A. and Overton, J. (1970)

Lanthanum staining of developing chick cartilage and reaggregating cartilage cells.
J. Cell Biol. 44, 433-438.

Kanno, Y. and Loewenstein, W.R. (1966)

Cell-to-cell passage of large molecules.
Nature, Lond. 212, 629-630.

Karnovsky, M.J. (1965)

A formaldehyde-glutaraldehyde fixative of high osmolarity for use in electron microscopy.
J. Cell Biol. 27, 137A.

Karrer, H.E. (1960)

The striated musculature of blood vessels II. Cell interconnections and cell surface.
J. biophys. biochem. Cytol. 8, 135-150.

Kelley, D.E. (1966)

Fine structure of desmosomes, hemidesmosomes, and an adepidermal globular layer in developing newt epidermis.
J. Cell Biol. 28, 51-72.

Keyes, D.C. and Compere, E.L. (1932)

The normal and pathological physiology of the nucleus pulposus of the intervertebral disc.
J. Bone Jt. Surg. 14, 897-938.

Kolthoff, I.M. and Sandell, E.B. (1952)

"Textbook of Quantitative Inorganic Analysis".
3rd Edn. MacMillan p.400.

Lagunoff, D. (1972)

Vital staining of mast cells with ruthenium red.
J. Histochem. Cytochem. 20, 938-944.

Laros, G.S. and Cooper, R.R. (1972)

Electron microscopic visualisation of protein-polysaccharides.
Clin. Orthop. 84, 179-192.

Lesseps, R.J. (1967)

The removal by phospholipase C of a layer of lanthanum-staining material external to the cell membrane in embryonic chick cells.
J. Cell Biol. 34, 173-183.

Lillie, R.D. (1965)

"Histopathologic Technic and Practical Histochemistry". 3rd Edn. McGraw-Hill Book Co. N.Y.

Lillie, R.D. Ed. (1969)

"H.J. Conn's Biological Stains". 8th Edn. Williams and Wilkins Co., Baltimore.

Loewenstein, W.R. and Kanno, Y. (1964)

Studies on an epithelial (gland) cell junction. I. Modifications of surface membrane permeability.
J. Cell Biol. 22, 565-586.

Loewenstein, W.R., Nakas, M. and Socolar, S.J. (1967)

Junctional membrane uncoupling. Permeability transformations at a cell membrane junction.
J. gen. Physiol. 50(ii) 1865-1891.

Loewenstein, W.R., Socolar, S.J., Higashino, S., Kanno, Y. and Davidson, N. (1965)

Intercellular communication: Renal, urinary bladder, sensory and salivary gland cells.
Science, N.Y. 149, 295-298.

Lohmander, S., Antonopoulos, C.A. and Friberg, V. (1973)

Chemical and metabolic heterogeneity of chondroitin sulfate and keratan sulfate in guinea pig cartilage and nucleus pulposus.
Biochim. biophys. Acta 304, 430-448.

Lowther, D.A. and Baxter, E. (1966)

Isolation of chondroitin sulphate protein complex from bovine intervertebral discs.
Nature, Lond. 211, 595-597.

Ludoweig, J.J., Sharma, M.L., Hashimoto, A., Emmons, E., Nishizawa, I. and Okazaki, K. (1972)

The mammalian intervertebral disc: composition of the nucleus pulposus of whales during development and ageing.
Connect. Tissue Res. 1, 79-91.

Ludoweig, J.J. and Parker, J. (1973)

The mammalian intervertebral disc: fibrous structures of the whale nucleus pulposus.
J. Cell Sci. 12, 925-932.

Luft, J.H. (1964)

Electron microscopy of cell extraneous coats as revealed by ruthenium red staining.
J. Cell Biol. 23, 55A.

Luft, J.H. (1965)

The fine structure of hyaline cartilage matrix following ruthenium red fixative and staining.
J. Cell Biol. 27, 61A.

Luft, J.H. (1968)

Selective staining of acid mucopolysaccharides by ruthenium red.
26th Proc. Electron Microsc. Soc. Amer. pp.38-39.

Luft, J.H. (1971a)

Ruthenium red and violet. I. Chemistry, purification, methods of use for electron microscopy and mechanisms of action.
Anat. Rec. 171, 347-368.

Luft, J.H. (1971b)

Ruthenium red and violet. II. Fine structural localisation in animal tissues.
Anat. Rec. 171, 369-416.

Lyons, H., Jones, E., Quinn, F.E. and Sprunt, D.H. (1964)

Protein-polysaccharide complexes of normal and herniated human intervertebral discs.
Proc. Soc. exp. Biol. Med. 115, 610-614.

MacConaill, M.A. (1949)

The myelothecal apparatus of human nerves.
Proc. R. Ir. Acad. 53 Sect.B No.1,1-14.

Mahler, H.R. and Cordes, E.H. (1966)

"Biological Chemistry". Harper and Row, New York, Evanston and London.

Marinozzi, V. (1968)

Phosphotungstic acid as a stain for polysaccharides and glycoproteins in electron microscopy. 4th Eur. Reg. Conf. Electron Microsc., Rome. Ed. D.S. Bocciarelli. pp.55-56.

Maroudas, A. (1968)

Physiochemical properties of cartilage in the light of ion exchange theory. Biophys. J. 8, 575-595.

Maroudas, A. (1970)

Effect of fixed charge density of the distribution and diffusion coefficients of solutes in cartilage. In "Chemistry and Molecular Biology of the Intercellular Matrix". Vol. III. Ed. E.A. Balazs. Academic Press, London. pp.1389-1401.

Maroudas, A. and Muir, H. (1970)

The distribution of collagen and glycosaminoglycans in articular cartilage and the influence on hydrolytic permeability. In "Chemistry and Molecular Biology of the Intercellular Matrix". Vol. III. Ed. E.A. Balazs. Academic Press, London. pp.1381-1387.

Maroudas, A., Muir, H. and Wingham, J. (1969)

The correlation of fixed negative charge with glycosaminoglycan content of human articular cartilage. Biochim. biophys. Acta 177, 492-500.

Marshall, P.N. and Horobin, R.W. (1972)

The oxidation products of haematoxylin and their role in biological staining. Histochem. J. 4, 493-503.

Marshall, P.N. and Horobin, R.W. (1973a)

Measurements of the affinities of basic and "mordant" dyes for various tissue substances. Histochemistry 36, 303-312.

Marshall, P.N. and Horobin, R.W. (1973b)

The influence of inorganic salts when staining with preformed metal complex dyes. Histochemistry 37, 299-311.

Marshall, P.N. and Horobin, R.W. (1974)

A simple assay procedure for mixtures of hematoxylin and hematein. Stain Technol. 49, 137-142.

Martell, A.E. and Calvin, M. (1952)

"Chemistry of the Metal Chelate Compounds". Prentice-Hall Inc. New Jersey.

Mathews, M.B. (1960)

Trivalent cation binding of acid mucopolysaccharides. Biochim. biophys. Acta 37, 288-295.

Matukas, V.J., Panner, B.J. and Orbison, J.L. (1967)

Studies on ultrastructural identification and distribution of protein-polysaccharide in cartilage matrix. J. Cell Biol. 32, 365-377.

McNutt, N.S. & Weinstein, R.S. (1970)

The ultrastructure of the nexus. A correlated thin-section and freeze-cleave study. J. Cell Biol. 47, 666-688.

Meachim, G. (1972)

Meshwork patterns in the ground substance of articular cartilage and nucleus pulposus. J. Anat. 111, 219-227.

Meachim, G. and Cornah, M.S. (1970)

Fine structure of juvenile human nucleus pulposus. J. Anat. 107, 337-350.

Miller, A. and Wray, J.S. (1971)

Molecular packing in collagen.
Nature, Lond. 230, 437-439.

Muir, A.R. (1965)

Further observations on the cellular structure of cardiac muscle.
J. Anat. 99, 27-46.

Muir, A.R. (1967)

The effects of divalent cations on the ultra-structure of the perfused rat heart.
J. Anat. 101, 239-261.

Myers, D.B., Highton, T.C. and Rayns, D.G. (1969)

Acid mucopolysaccharides closely associated with collagen fibrils in normal human synovium.
J. Ultrastruct. Res. 28, 203-213.

Myers, D.B., Highton, T.C. and Rayns, D.G. (1973)

Ruthenium red-positive filaments interconnecting collagen fibrils.
J. Ultrastruct. Res. 42, 87-92.

Ogston, G.G. and Phelps, C.F. (1961)

The partition of solutes between buffer solutions and solutions containing hyaluronic acid.
Biochem. J. 78, 827-833.

Overton, J. (1968)

Localised lanthanum staining of the intestinal brush border.
J. Cell Biol. 38, 447-452.

Palmer, R.W. and Lillie, R.D. (1965)

Spectroscopic and staining studies of the ripening and over-ripening of aluminium hematoxylins.
Histochemistry 5, 44-54.

Paulson, S., Sylvén, B., Hirsch, C. and Snellman, O. (1951)

Biophysical and physiological investigations on cartilage and other mesenchymal tissues. III. The diffusion rate of various substances in normal bovine nucleus pulposus. Biochim. biophys. Acta 7, 207-213.

Peacock, A. (1952)

Observations on the postnatal structure of the intervertebral disc in man. J. Anat. 86, 162-179.

Penn, R.D. (1966)

Ionic communication between liver cells. J. Cell Biol. 29, 171-174.

Phillpotts, C.J. (1972)

The preparation of thin methacrylate embedded sections of renal biopsies for light microscopy. Med. Lab, Technol. 26, 66-70.

Pizzolato, P. and Lillie, R.D. (1967)

Metal salts-hematoxylin staining of skin keratohyalin granules. J. Histochem. Cytochem. 15, 104-110.

Preston, B.N., Davies, M. and Ogston, A.G. (1965)

The composition and physicochemical properties of hyaluronic acids prepared from ox synovial fluid and from a case of mesothelioma. Biochem. J. 96, 449-474.

Revel, J-P. (1964)

A stain for the ultrastructural localisation of acid mucopolysaccharides. J. Microscopie 3, 535-544.

Revel, J.P. (1968)

Studies on the fine structure of intercellular junctions. 26th Proc. Electron Miscrosc. Soc. Amer. pp.40-41.

Revel, J-P. and Karnovsky, M.J. (1966)

Fine structure of tight junctions. Biol. Bull. mar. biol. Lab., Woods Hole 131, 380.

Revel, J.P. and Karnovsky, M.J. (1967)

Hexagonal array of subunits in intercellular junctions of the mouse heart and liver.
J. Cell Biol. 33, C7-C12.

Robertson, J.D. (1963)

The occurrence of a subunit pattern in the unit membranes of club endings in Mauthner cell synapses in goldfish brains.
J. Cell Biol. 19, 201-221.

Rojas, E., Lettvin, J.Y. and Pickard, W.F. (1966)

A demonstration of ion-exchange phenomena in phospholipid mono-molecular films.
Nature, Lond. 209, 886-887.

Ross, R. (1968)

The connective tissue fiber forming cell. In "Treatise on Collagen" Vol.II, Part A. Ed. B.S. Gould.Academic Press, London and New York pp. 1-75.

Schatzki, P.F. (1969)

Bile canaliculus and space of Disse. Electron microscopic relationships as delineated by lanthanum.
Lab. Invest. 20, 87-93.

Scott, J.E. (1955)

The solubility of cetylpyridinium complexes of biological polyanions in solutions of salts.
Biochim. biophys. Acta 18, 428-429.

Scott, J.E. (1956)

The preparation and fractionation of acidic polysaccharides using long-chain quaterniary ammonium compounds.
Biochem. J. 62, 31P.

Scott, J.E. (1960)

Aliphatic ammonium salts in the assay of acidic polysaccharides from tissues.
Meth. biochem. Analysis 8, 145-197.

Scott, J.E. (1968a)

Specificity in the interaction of organic cations with biological polyanions. In "Solution Properties of Natural Polymers".
Chemical Soc. (Lond.) Special Pub. No.23, 263-272.

Scott, J.E. (1968b)

Patterns of specificity in the interaction of organic cations with acid mucopolysaccharides.
In "The Chemical Physiology of Mucopolysaccharides" Ed. G. Quintarelli, Churchill, London. pp. 219-229.

Scott, J.E. (1968c)

Ion binding in solutions containing acid mucopolysaccharides. In "The Chemical Physiology of Mucopolysaccharides". Ed. G. Quintarelli, Churchill, London. pp.171-186.

Scott, J.E. (1970)

Critical electrolyte concentration (C.E.C.) effects in interactions between acid glycosaminoglycans and organic cations and polycations. In "Chemistry and Molecular Biology of the Intercellular Matrix" Vol.2. Ed. E.A. Balazs. Academic Press, London and New York. pp.1105-1119.

Scott, J.E. (1972)

Histochemistry of Alcian blue. III. The molecular biological basis of staining by Alcian blue 8GX and analogous phthalocyanins.
Histochemistry 32, 191-212.

Scott, J.E. (1974)

Comment on the paper by Marshall and Horobin "Measurements of the affinities of basic and "mordant" dyes for various tissue substrates."
Histochemistry 39, 195-196.

Scott, J.E. and Dorling, J. (1965)

Differential staining of acid glycosaminoglycans (mucopolysaccharides) by Alcian blue in salt solutions.
Histochemistry 5, 221-233.

Scott, J.E., Dorling, J. and Stockwell, R.A. (1968)

Reversal of protein blocking of basophilia in salt solutions. Implications in the localisation of polyanions using Alcian blue.
J. Histochem. Cytochem. 16, 383-386.

Scott, J.E. and Stockwell, R.A. (1967)

On the use and abuse of the critical electrolyte concentration approach to the localisation of tissue polyanions.
J. Histochem. Cytochem. 15, 111-113.

Scott, J.E. and Willett, I.H. (1966)

Binding of cationic dyes to nucleic acids and other biological polyanions.
Nature, Lond. 209, 985-987.

Serafini-Fracassini, A. and Smith, J.W. (1966)

Observations on the morphology of the proteinpolysaccharide complex of bovine nasal cartilage and its relationship to collagen.
Proc. R. Soc. B.165, 440-449.

Serafini-Fracassini, A. and Smith, J.W. (1974)

"The Structure and Biochemistry of Cartilage".
Churchill Livingstone, London and Edinburgh.

Shea, S.M. (1971)

Lanthanum staining of the surface coats of cells. Its enhancement by the use of fixatives containing Alcian blue or cetylpyridinium chloride.
J. Cell Biol. 51, 611-620.

Smith, J.W. (1968)

Molecular pattern in native collagen.
Nature, Lond. 219, 157-158.

Smith, J.W, (1970)

The disposition of proteinpolysaccharide in the epiphyseal plate cartilage of the young rabbit.
J. Cell Sci. 6, 843-864.

Smith, J.W. (1973)

Personal Communication.

Smith, J.W. and Serafini-Fracassini, A. (1968)

The distribution of the protein-polysaccharide complex in the nucleus pulposus matrix in young rabbits.
J. Cell Sci. 3, 33-40.

Smith, J.W. and Walmsley, R. (1951)

Experimental incision of the intervertebral disc.
J. Bone Jt. Surg. 33B, 612-625.

Souter, W.A. (1971)

Sulphated acid mucopolysaccharide metabolism in the rabbit intervertebral disc. An autoradiographic study.
Ann. rheum. Dis. 30, 202-203.

Sprumont, P. and Musy, J-P. (1971)

Ph effect on electron microscopical contrast with iron salt solutions.
Histochemistry 26, 228-237.

Spurr, A.R. (1969)

A low viscosity embedding medium for electron microscopy.
J. Ultrastruct. Res. 26, 31-43.

Srivastava, S.N. (1964)

Effect of metal ions on bovine serum albumin-stabilised emulsions with particular regard to specific flocculation effect and cation binding.
J. Indian chem. Soc. 41, 203-211.

Staehelin, L.A., Mukherjee, T.M. and Williams, A.W. (1969)

Freeze-etch appearance of the tight junctions in the epithelium of small and large intestines of mice.
Protoplasma 67, 165-184.

Stimson, W.H. (1971)

Personal Communication.

Sylvén, B. (1951)

On the biology of nucleus pulposus.
Acta orthop. scand. 20, 275-279.

Sylvén, B., Paulson, S., Hirsch, C. and Snellman, O. (1951)

Biophysical and physiological investigations on cartilage and other mesenchymal tissues.
II. The ultrastructure of bovine and human nuclei pulposi.
J. Bone Jt. Surg. 33A, 333-340.

Szirmai, J.A. (1969)

Structure of cartilage. In "Aging of Connective and Skeletal Tissue". Thule International Symposia. Ed. A. Engel and T. Larsson.
Nordiska Bokhandelns Förlag, Stockholm. pp.169-184.

Terner, J.Y., Gurland, J. and Gaer, F. (1964)

Phosphotungstic acid - hematoxylin : Spectrophotometry of the lake in solution and in stained tissue.
Stain Technol. 39, 141-153.

Thyberg, J., Lohmander, S. and Friberg, U. (1973)

Electron microscopic demonstration of proteoglycans in guinea pig epiphyseal cartilage.
J. Ultrastruct. Res. 45, 407-427.

Tristram, G.R. and Smith, R.H. (1963)

Amino acid composition of certain proteins.
In "The Proteins. Composition, Structure and Function" 2nd Edn. Vol.1. Ed. H. Neurath.
Academic Press, London and New York. pp.46-51.

Trump, B.F. and Ericsson, J.L.E. (1964)

Electron microscopic observations on the localisation of acid phosphatase in mouse hepatic parenchymal cells.
Exptl. Cell Res. 33, 598-601.

Walmsley, R. (1953)

The development and growth of the intervertebral disc.
Edinb. med. J. LX, 341-364.

Weiner, J., Spiro, D. and Loewenstein, W.R. (1964)

Studies on an epithelial (gland) cell junction II. Surface structure.
J. Cell Biol. 22, 587-598.

Wetzel, M.G., Wetzel, B.K. and Spicer, S.S. (1966)

Ultrastructural localisation of acid muco-substances in the mouse colon with iron-containing stains.
J. Cell Biol. 30, 299-315.

Wolfe, H.J., Putschar, W.G.J. and Vickery, A.L. (1965)

Role of the notochord in human intervertebral disc. I. Fetus and Infant. Clin. Orthop. 39, 205-212.

Zobel, C.R. and Beer, M. (1965)

The use of heavy metal salts as electron stains.
Int. Rev. Cytol. 18, 363-400.

Figures:

Unless otherwise stated all figures are from rabbit nucleus pulposus fixed in paraformaldehyde and glutaraldehyde in cacodylate, post-fixed in osmium and thin sections stained on the grid with lead citrate and uranyl acetate.

Figure 1. Transitional zone between the annulus fibrosus (top of figure) containing a chondrocyte (c), lipid granules (l) and collagen fibres (arrowed) and the nucleus pulposus (bottom of figure) containing notochordal cells (n) embedded in fibrillar matrix. x 2,500.

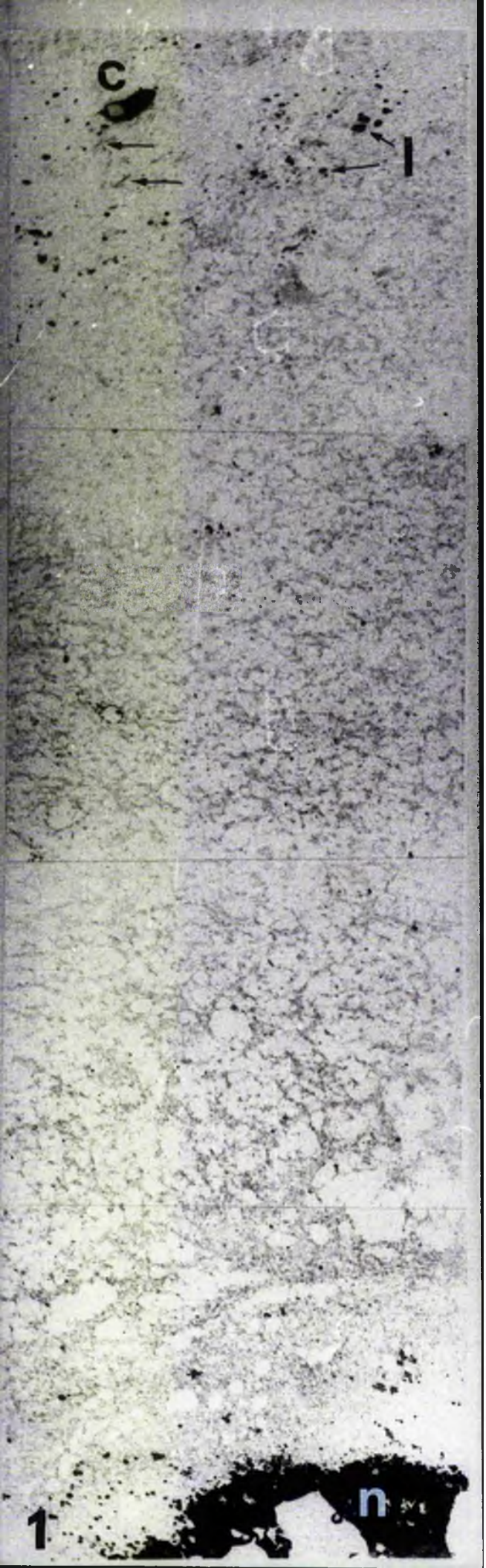
c
l
n
1

Figure 2. Group of cells within the annulus fibrosus.
Note prominent endoplasmic reticulum with dilated cisternae. x 4,250.

Figure 3. Cell within annulus fibrosus showing similarity to a chondrocyte x 15,350.

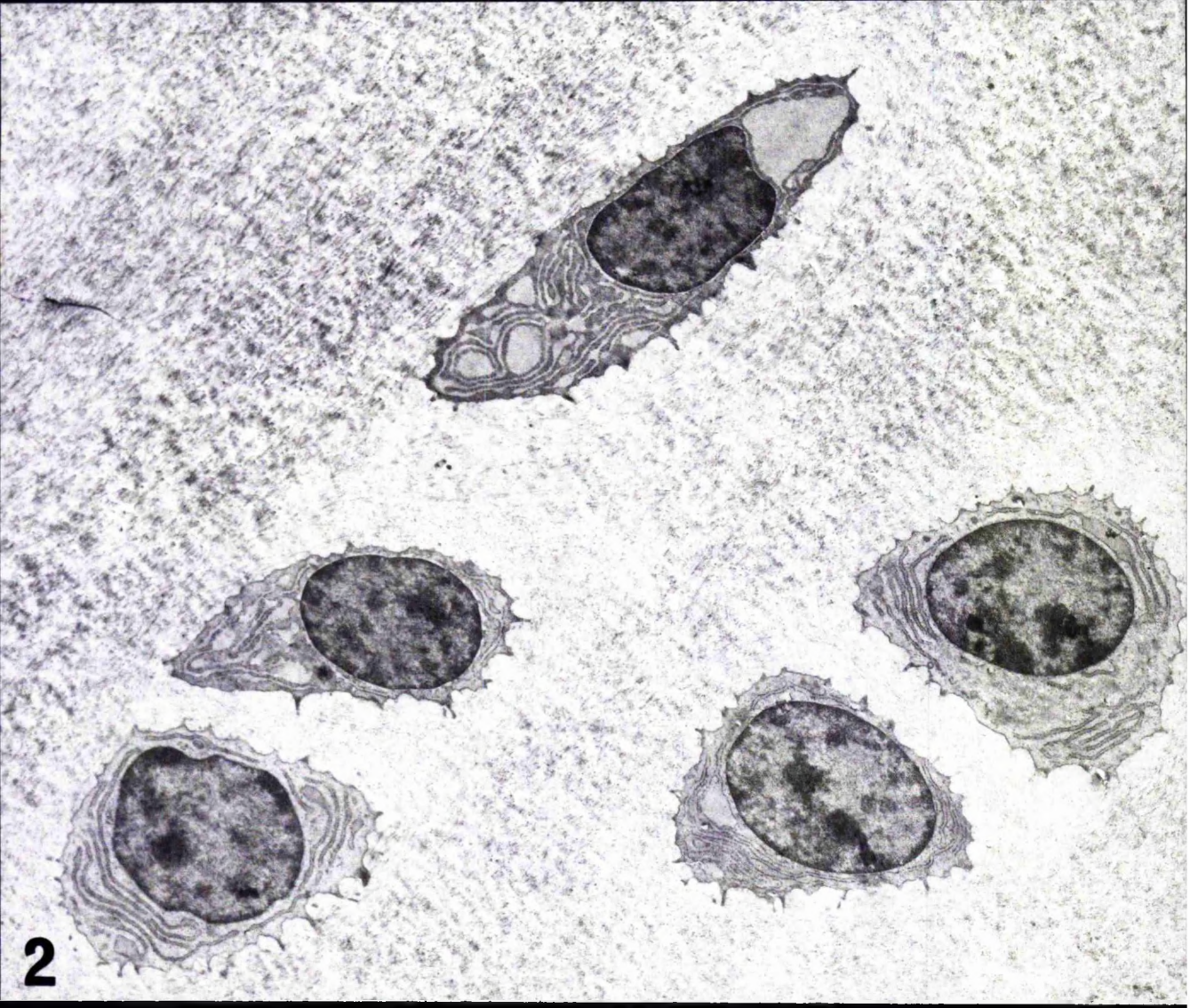

2

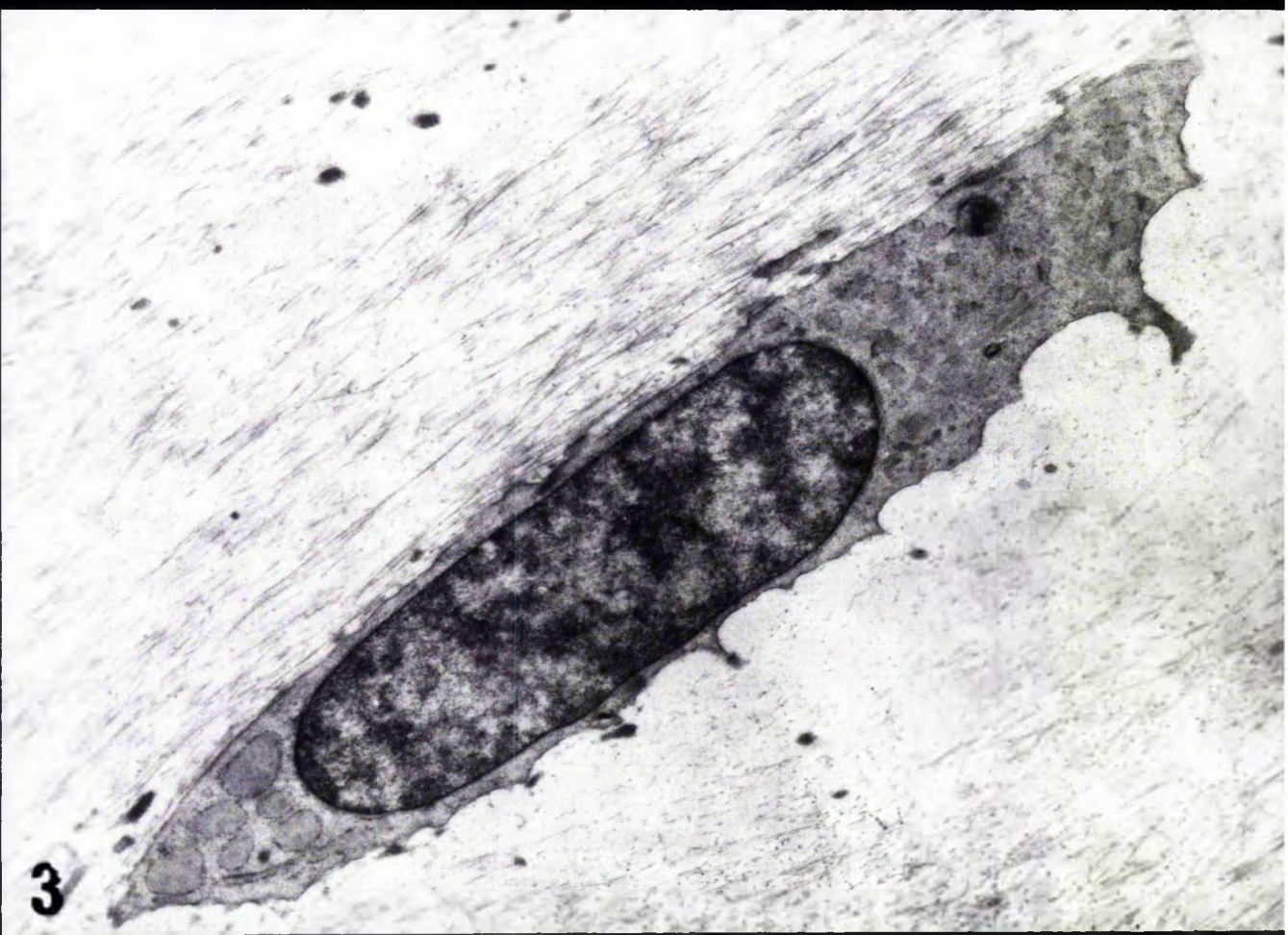

3

Figure 4. Very young rabbit nucleus pulposus containing multinucleated masses of cytoplasm surrounding vesicles exhibiting varying degrees of metachromasia. Note pale stained homogeneous matrix. Thick araldite section stained with toluidine blue. x 356.

Figure 5. Adult rabbit nucleus pulposus showing groups of notochordal cells surrounded by metachromatically stained fibrillar material. Thick araldite section stained with toluidine blue x 356.

Figure 6. Very old rabbit nucleus pulposus showing a few necrotic remains of notochordal cells within the fibrillar matrix. Thick araldite section stained with toluidine blue x 356.

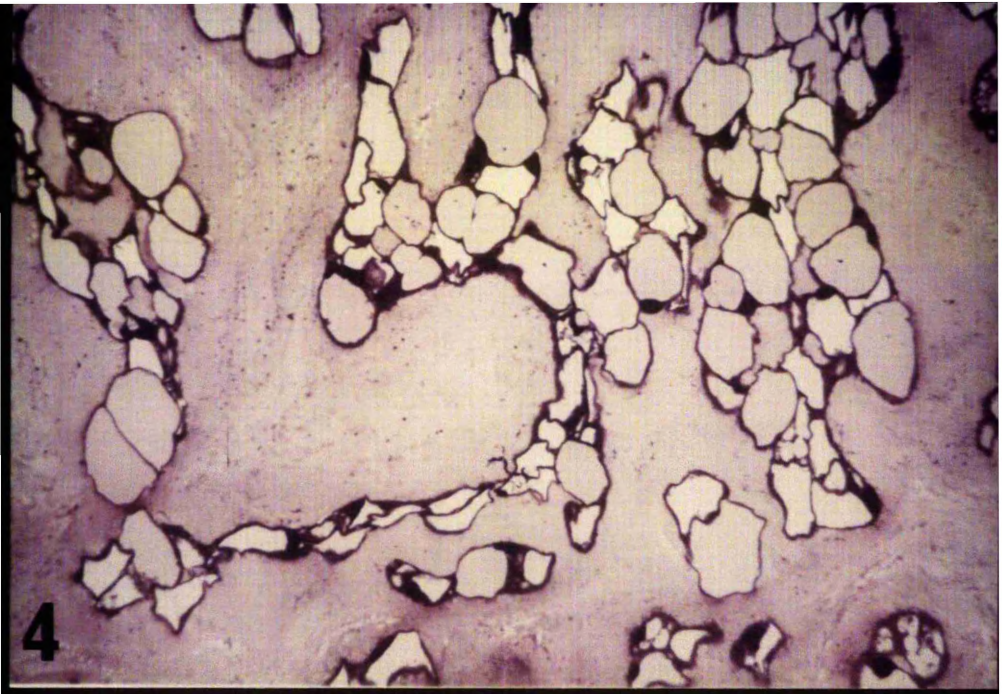
4

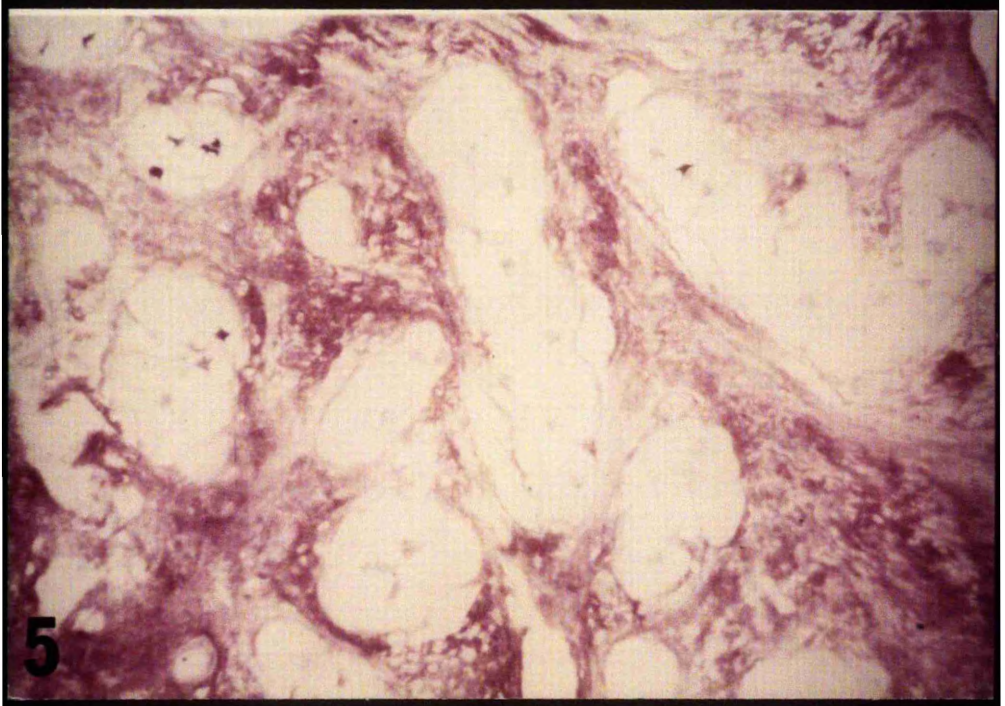
5

Figure 7. Within the junction between two apposed notochordal cells is seen a transversely sectioned desmosome (d) and two gap junctions (arrowed)

x 35,500


d
7

Figure 8. Part of two notochordal cells separated by a relatively uniform gap of 25 nm. The large vesicles (v) contain fibrillar material. x 40,000.

Figure 9. A gap junction (g) is seen between two cells. Numerous ribosomes are seen free in the cytoplasm and on the surface of the endoplasmic reticulum. x 31,560.

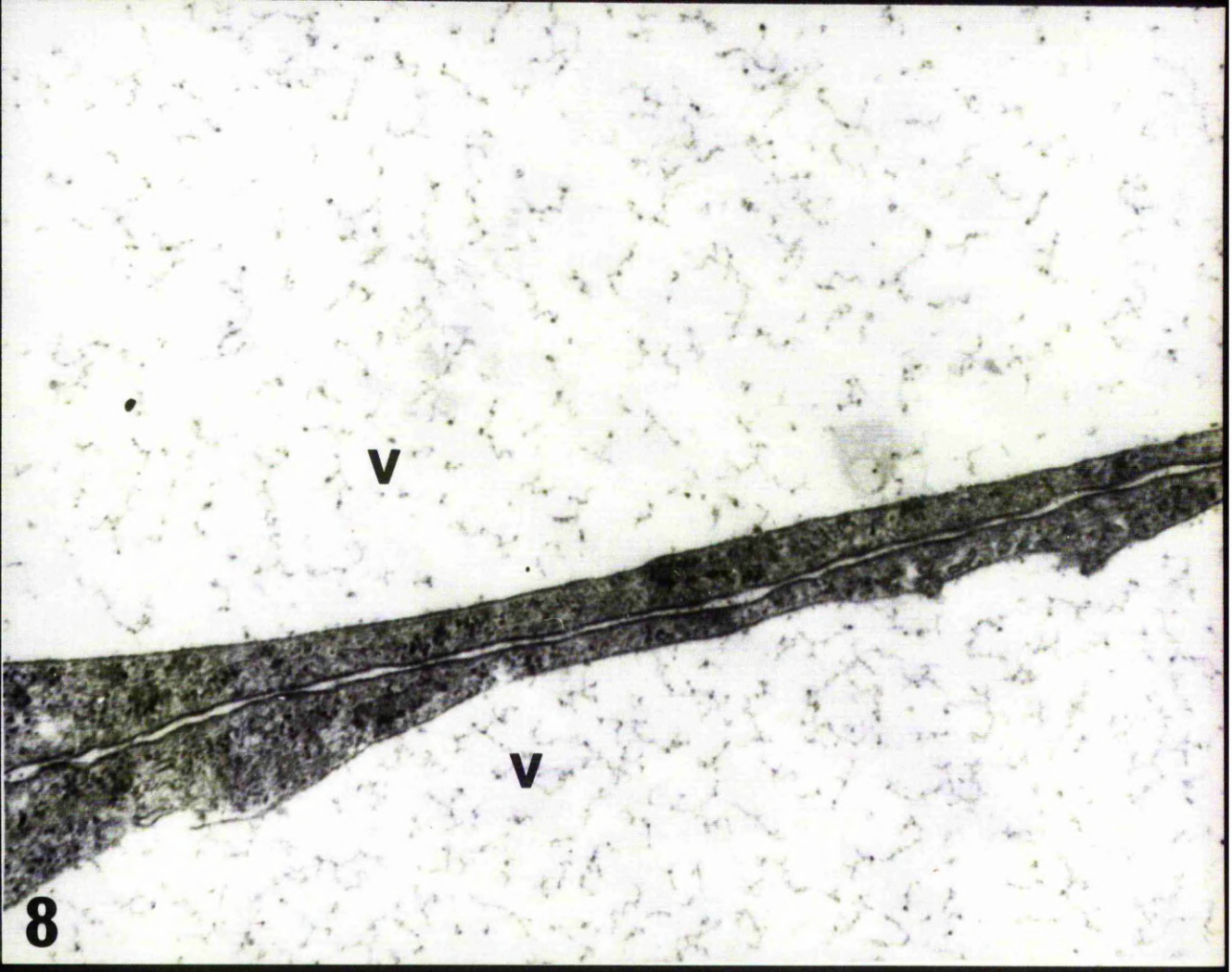
v
v
8

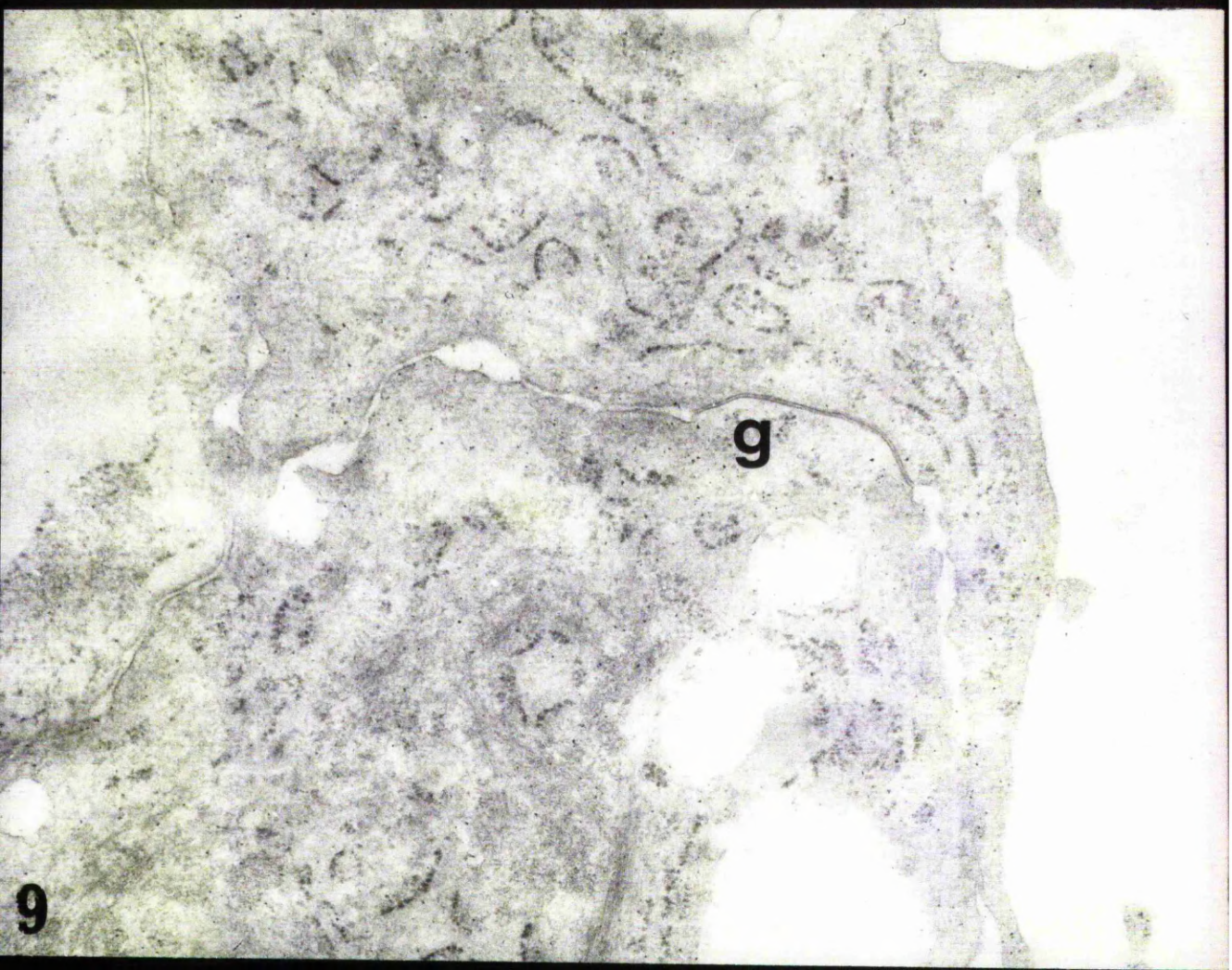
g
9

Figure 10. A desmosome in which the cytofilaments are seen to converge upon the attachment plaque.

x 112,000.

Figure 11. Orthogonally sectioned desmosome revealing the structural components (page 24)

x 112,000.

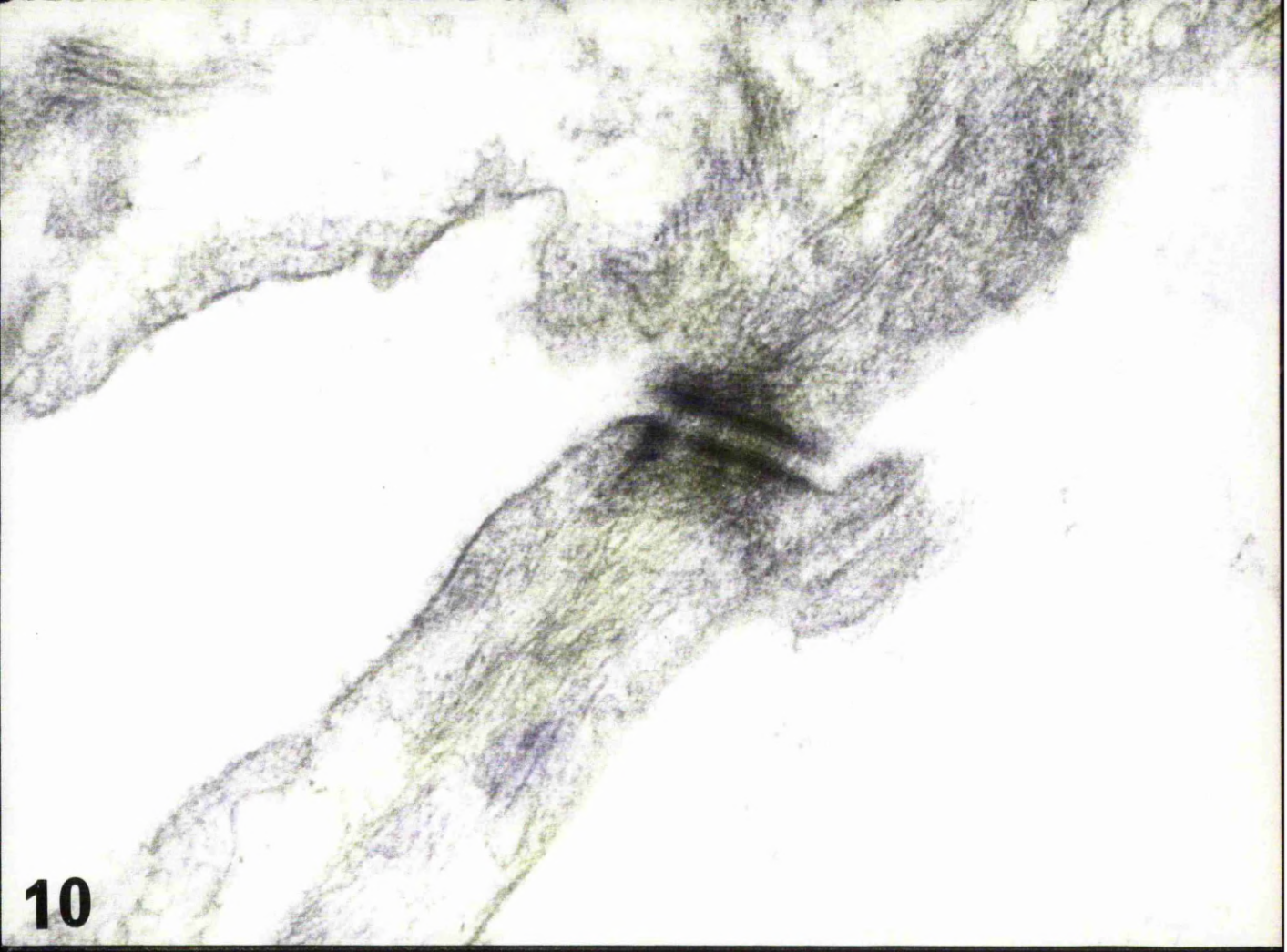

10

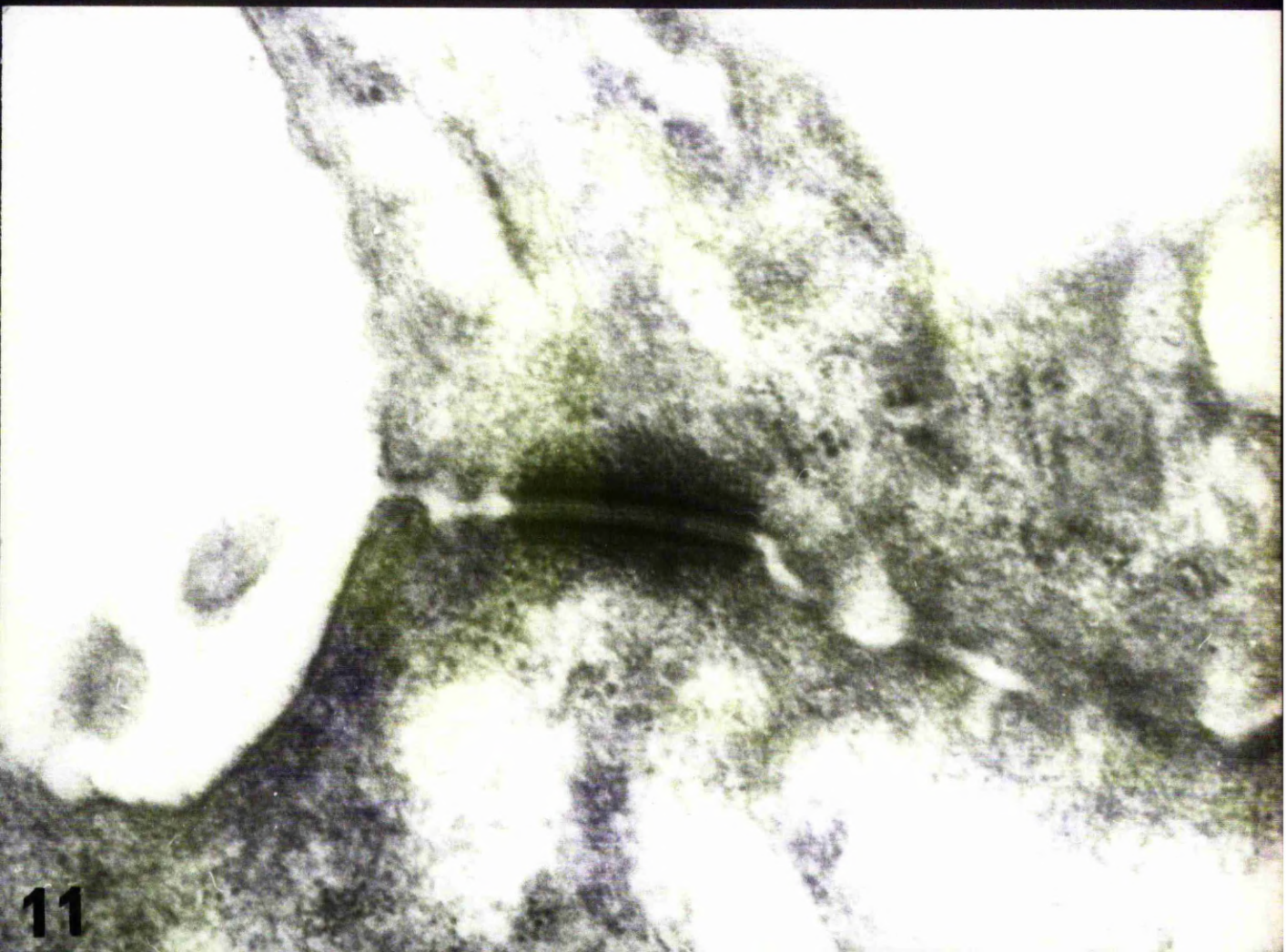

11

Figure 12. Gap junction with two outer electron dense lines and a thinner discontinuous or beaded central line (arrowed) x 140,000

12

Figure 13. Plane of section through a gap junction revealing a bizarre profile x 98,000.

Figure 14. Similarly sectioned gap junction seen after fixation with potassium permanganate and lanthanum nitrate (Method III). x 125,500.

Figure 15. Note similarity of bizarre profile to the gap junction above it. x 39,500.

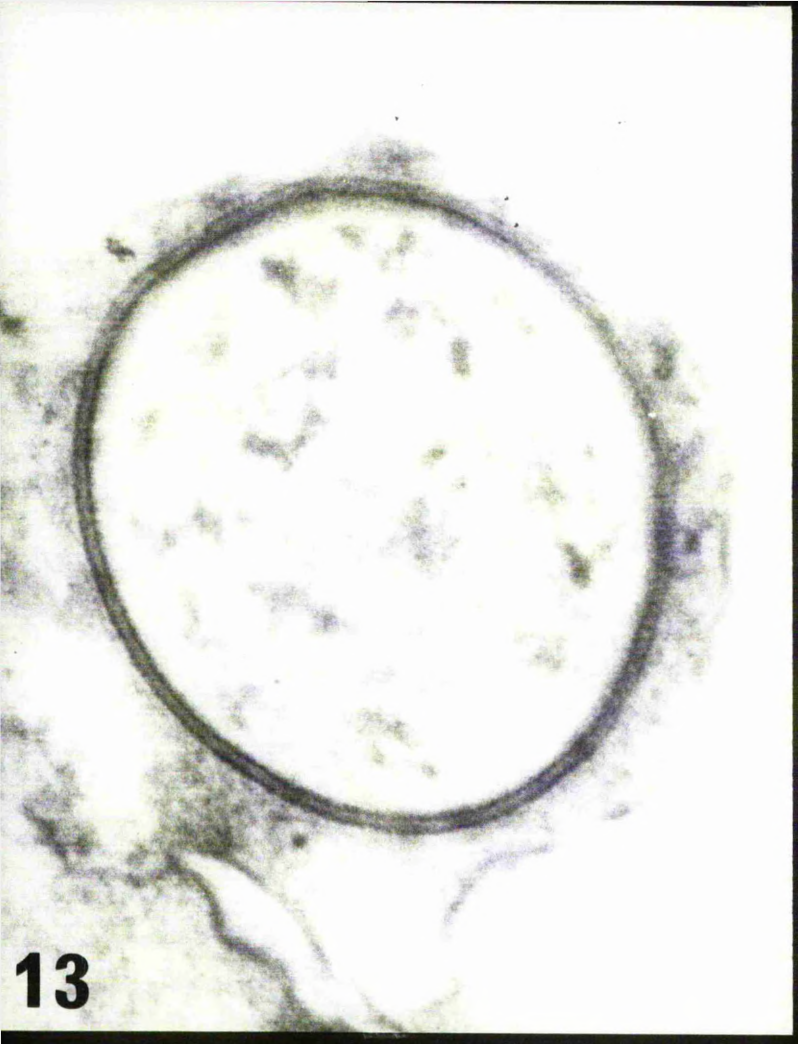

13

14

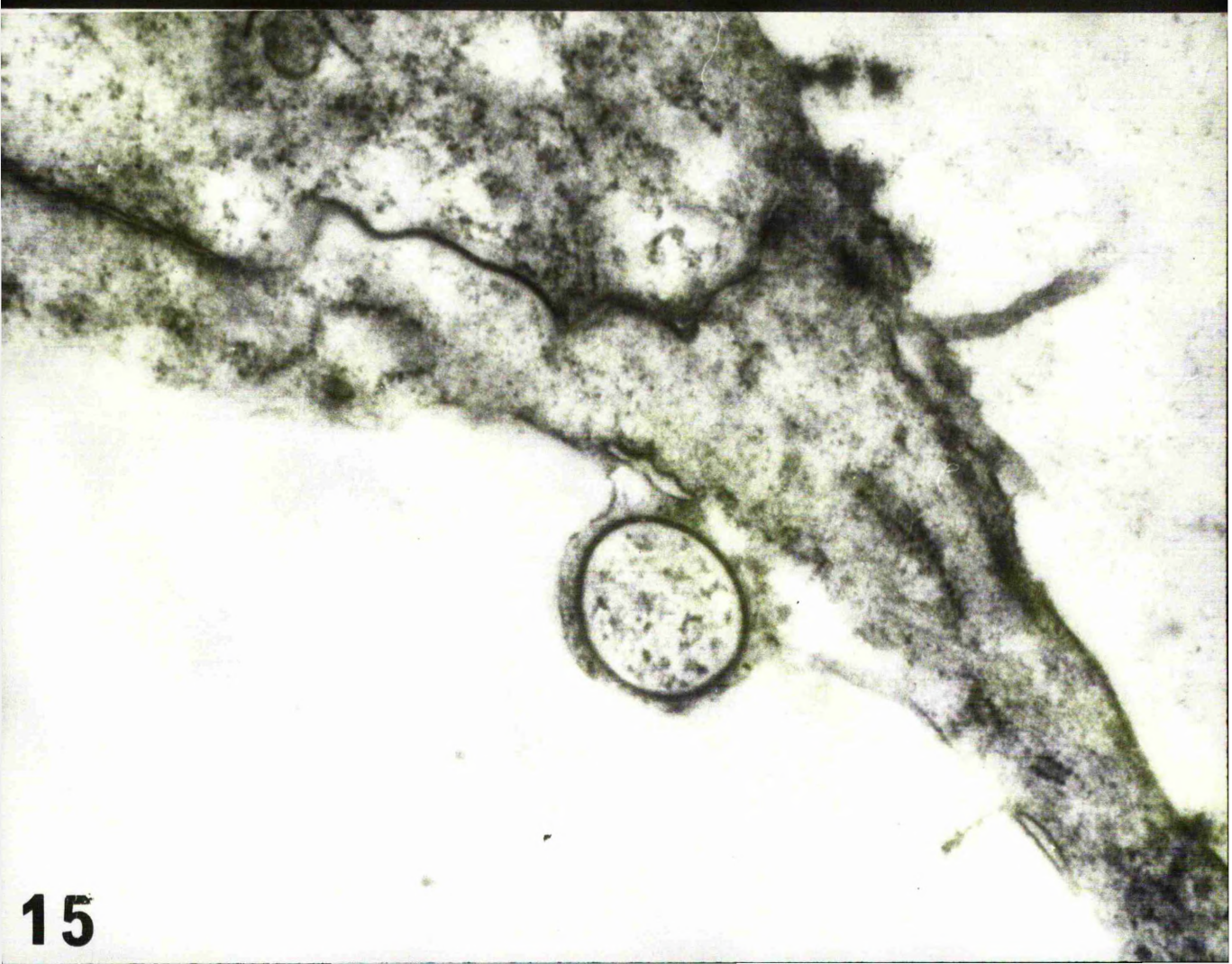

15

Figure 16. Gap junction between two notochordal cells. Note the relatively empty appearance of the large vesicles (v). x 80,000.

Inset of gap junction at higher magnification allows structural components to be discerned.

x 160,000.

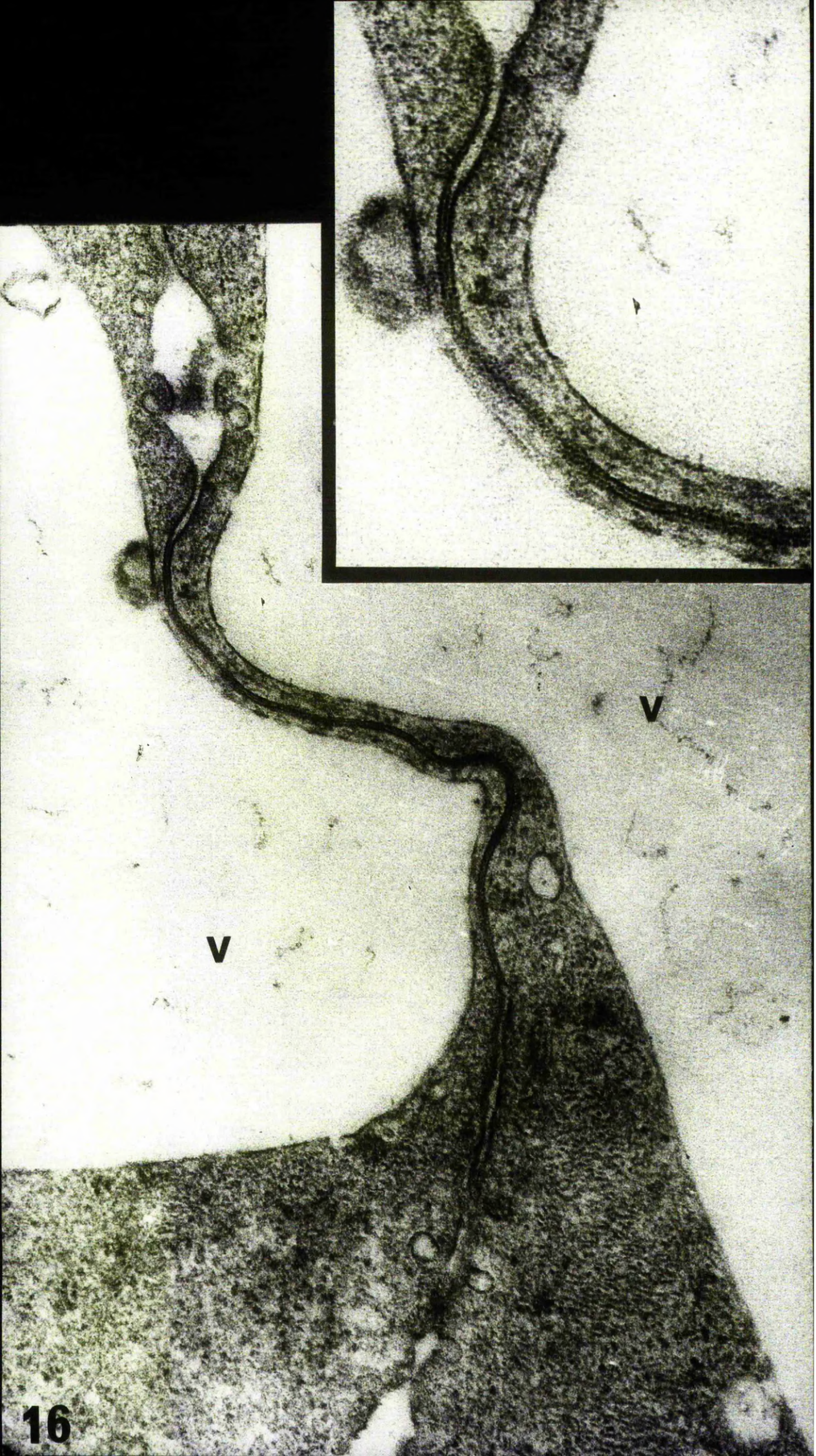

16

Figure 17. Orthogonally sectioned gap junction seen after exposure to lanthanum (Method I)

x 139,500

Figure 18. Lower portion of gap junction is sectioned tangentially revealing polygonal subunit pattern. Lanthanum staining (Method I)

x 139,500

Figure 19. Tangentially sectioned gap junction revealing polygonal subunits, some of which exhibit a central dot (arrows) x 350,000

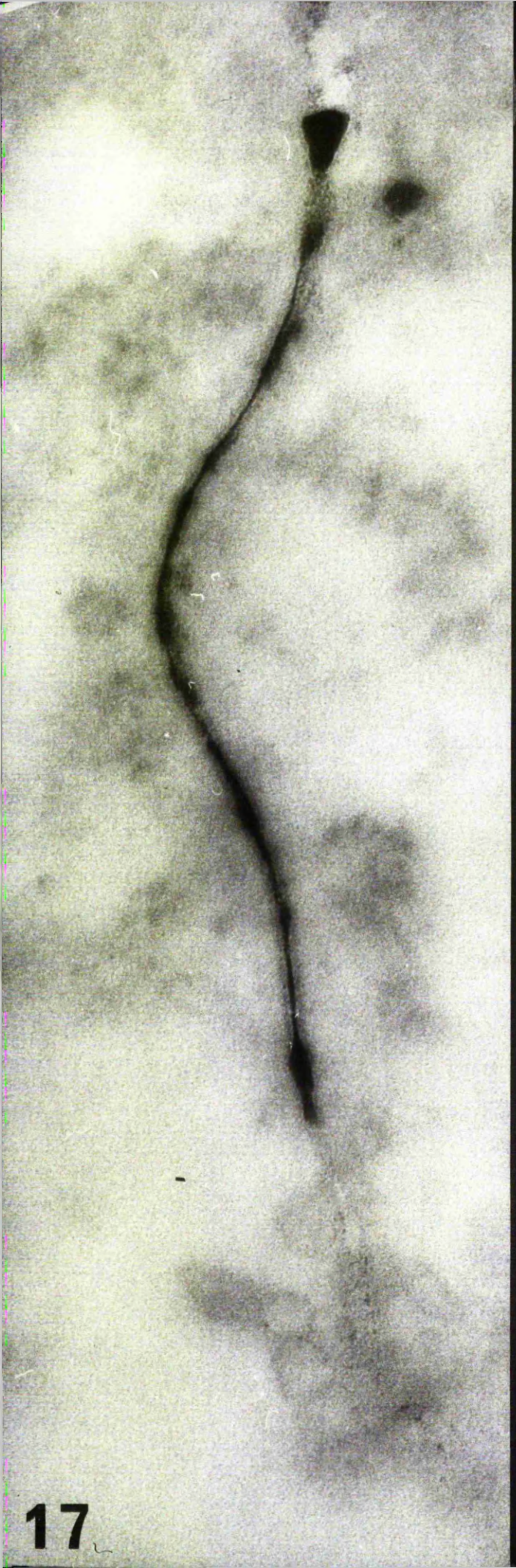

17

18

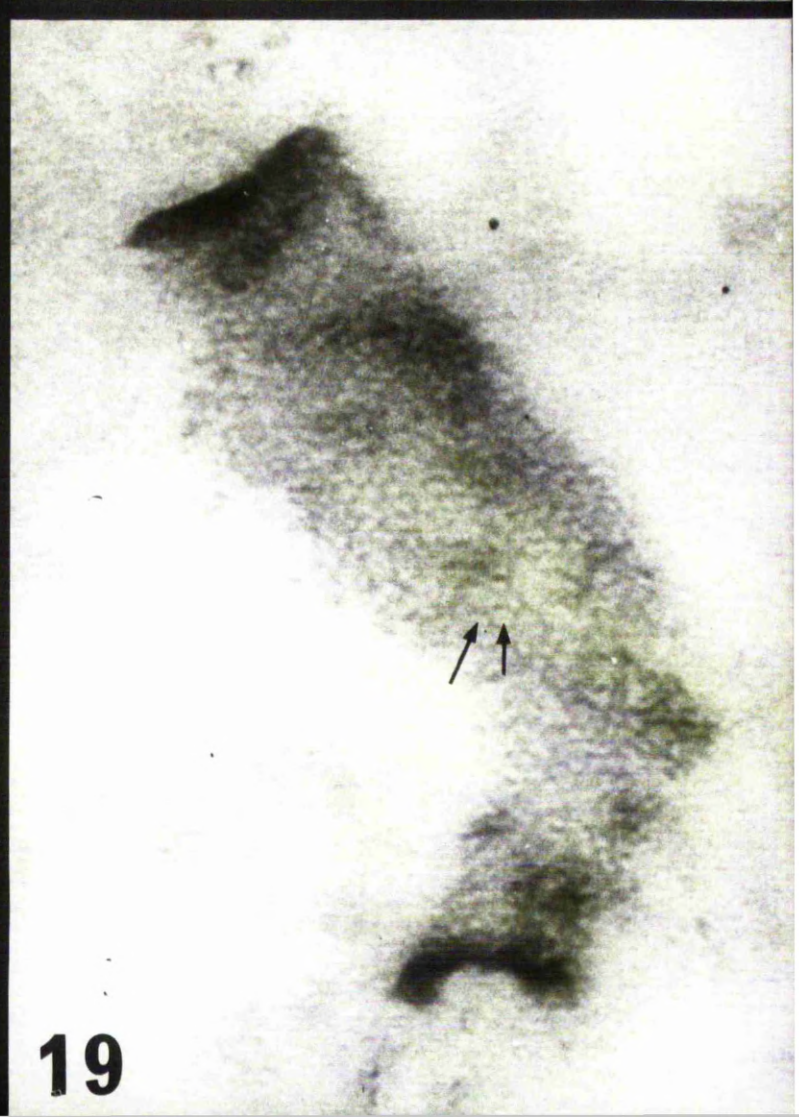

19

Figure 20. Gap junction seen after aldehyde fixation in the presence of Alcian blue and osmium post-fixation in the presence of lanthanum (Method II). x 125,500

Figure 21. Orthogonally sectioned gap junction seen after lanthanum treatment (Method II). Slight separation of the external leaflets of the plasma membrane is seen in places (arrow)

x 125,500

Figure 22. A tangential section through a gap junction after lanthanum treatment (Method II) does not reveal any subunit structure.

x 192,000


20


21


22

Figure 23. Orthogonally sectioned gap junction seen after fixation in potassium permanganate and lanthanum nitrate (Method III) x 268,900

Figure 24. Gap junction seen after lanthanum treatment (Method III). Darkly stained circular profiles are considered to be pinocytotic vesicles.

x 117,000

23

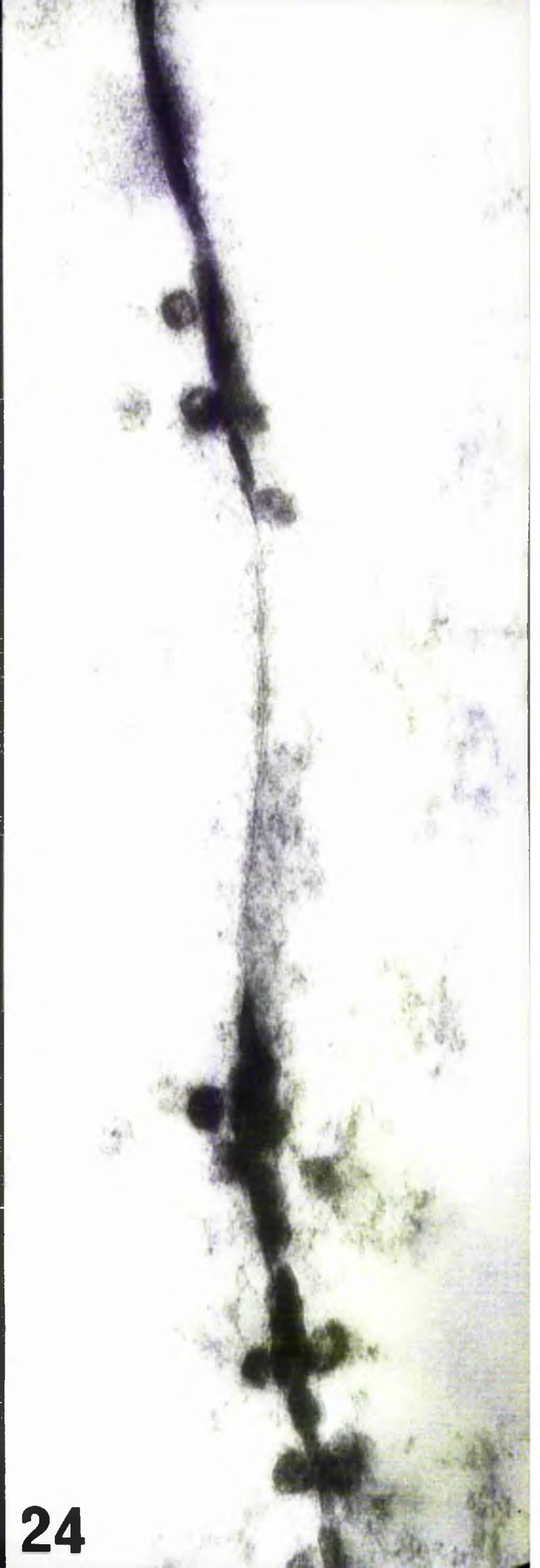

24

Figure 25. A pair of centrioles are seen in the juxtanuclear position. x 35,000

Figure 26. An orthogonally sectioned centriole reveals the subunit structure. x 35,000

Figure 27. Longitudinally sectioned mitochondrion x 84,000

Figure 28. Transversely sectioned mitochondrion x 84,000


25


26


27

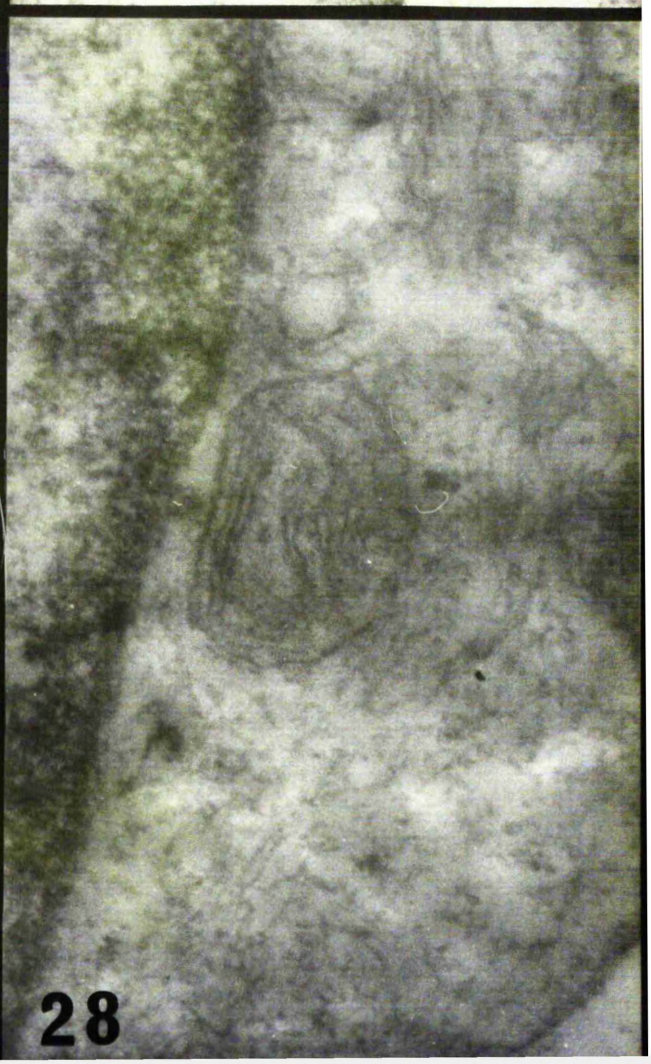
28

Figure 29. Two notochordal cells containing mitochondria closely associated with rough endoplasmic reticulum, free ribosomes and cytofilaments are also seen in the cytoplasm.

x 28,000

Figure 30. Portion of a notochordal cell showing the Golgi apparatus in a juxtanuclear position; the larger vesicles contain fibrillar material. Note also the bundles of transversely and longitudinally sectioned cytofilaments.

x 37,500

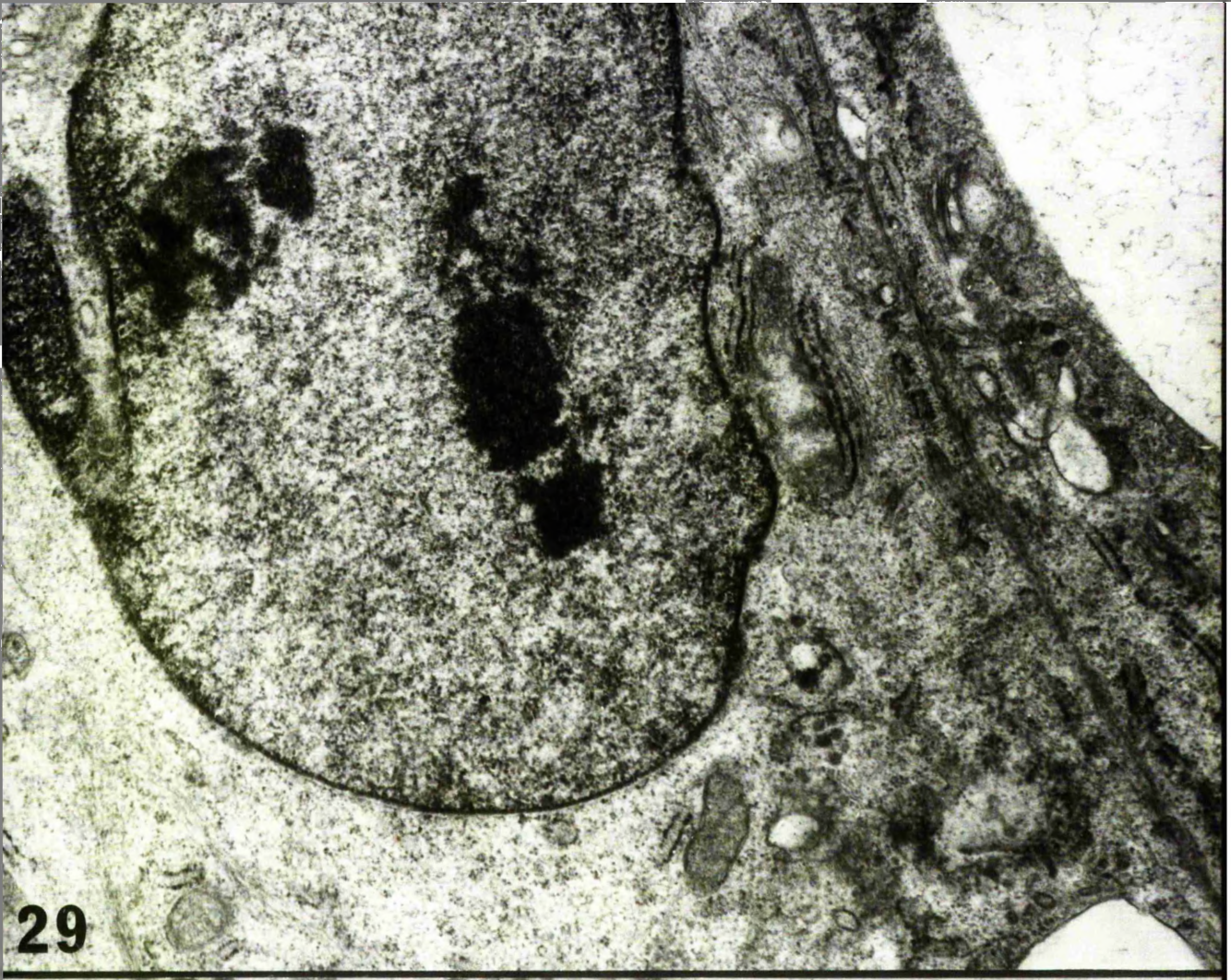

29

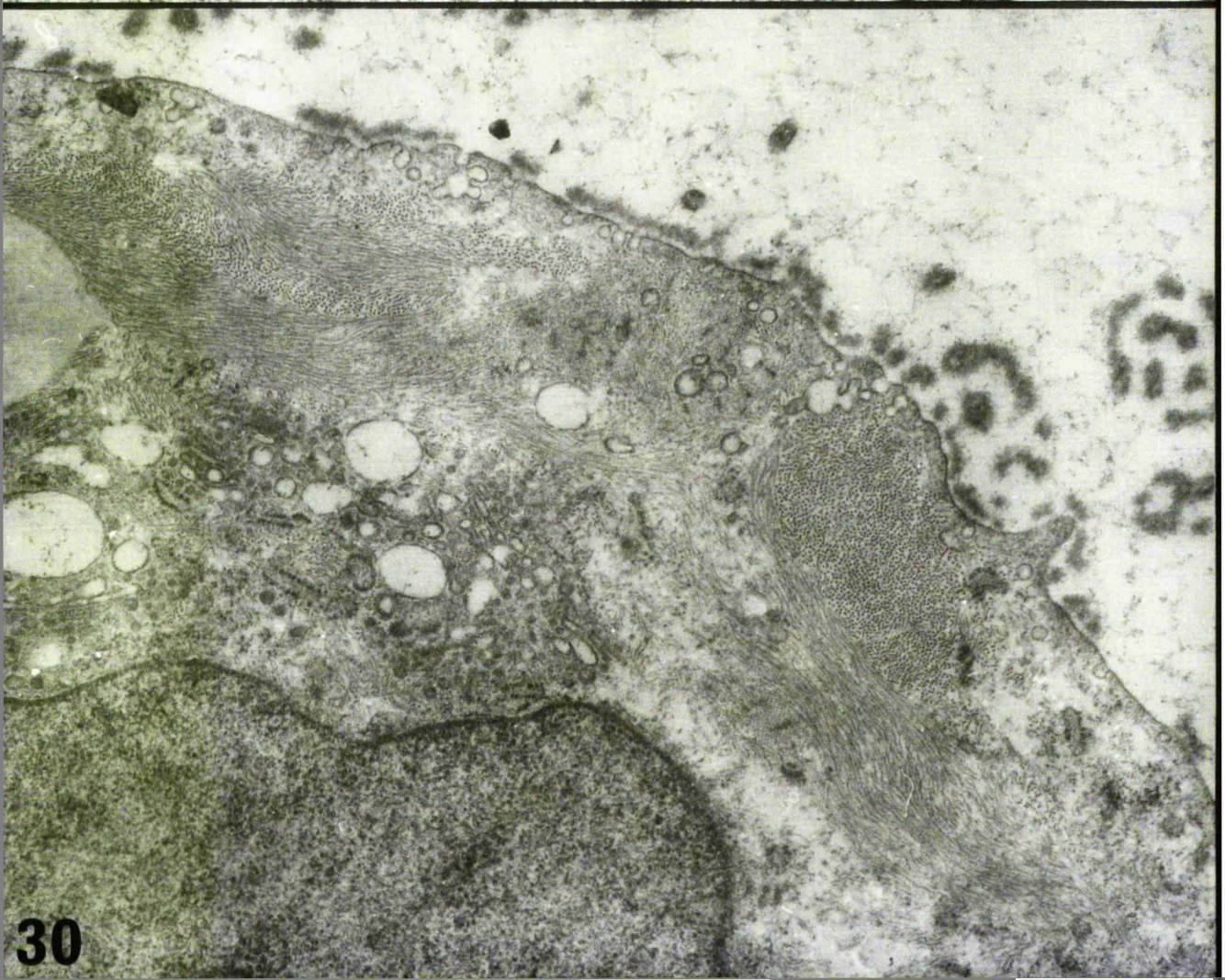

30

Figure 31. A group of notochordal cells surrounded by densely stained extracellular matrix material. The Golgi apparatus (g) is seen within one cell. Lanthanum (Method III)

x 8,300

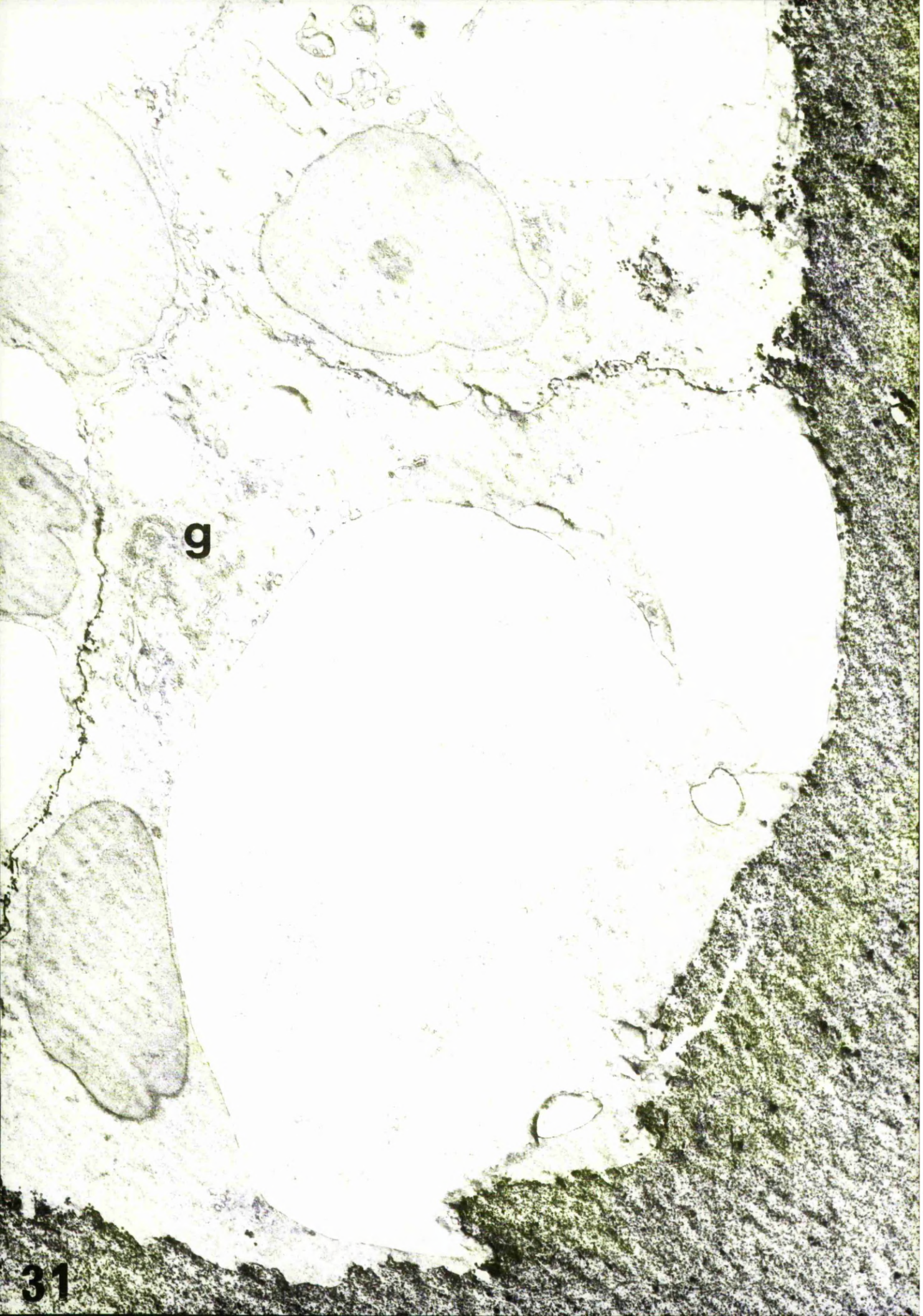
g

Figure 32. A group of two notochordal cells containing many vesicles. x 7,440

Figure 33. Notochordal cell containing a relatively large vesicle. x 7,440

Figure 34. Notochordal cells in which the large vesicles have displaced the cytoplasm to one side. x 7,440

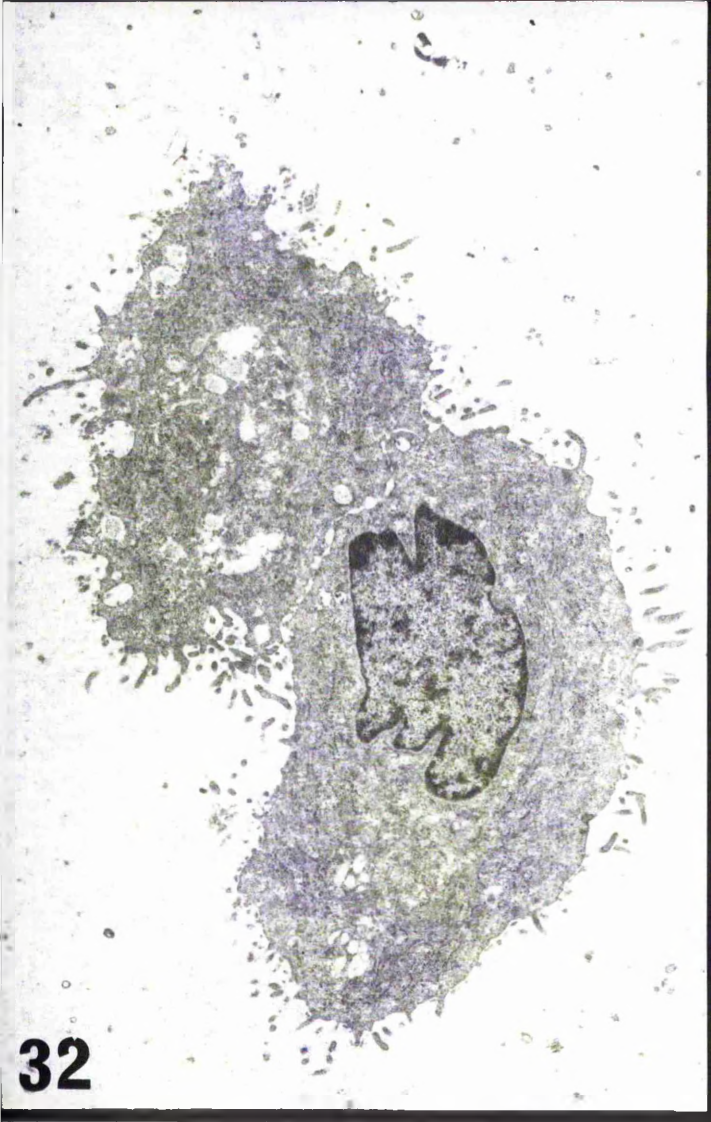

32

33

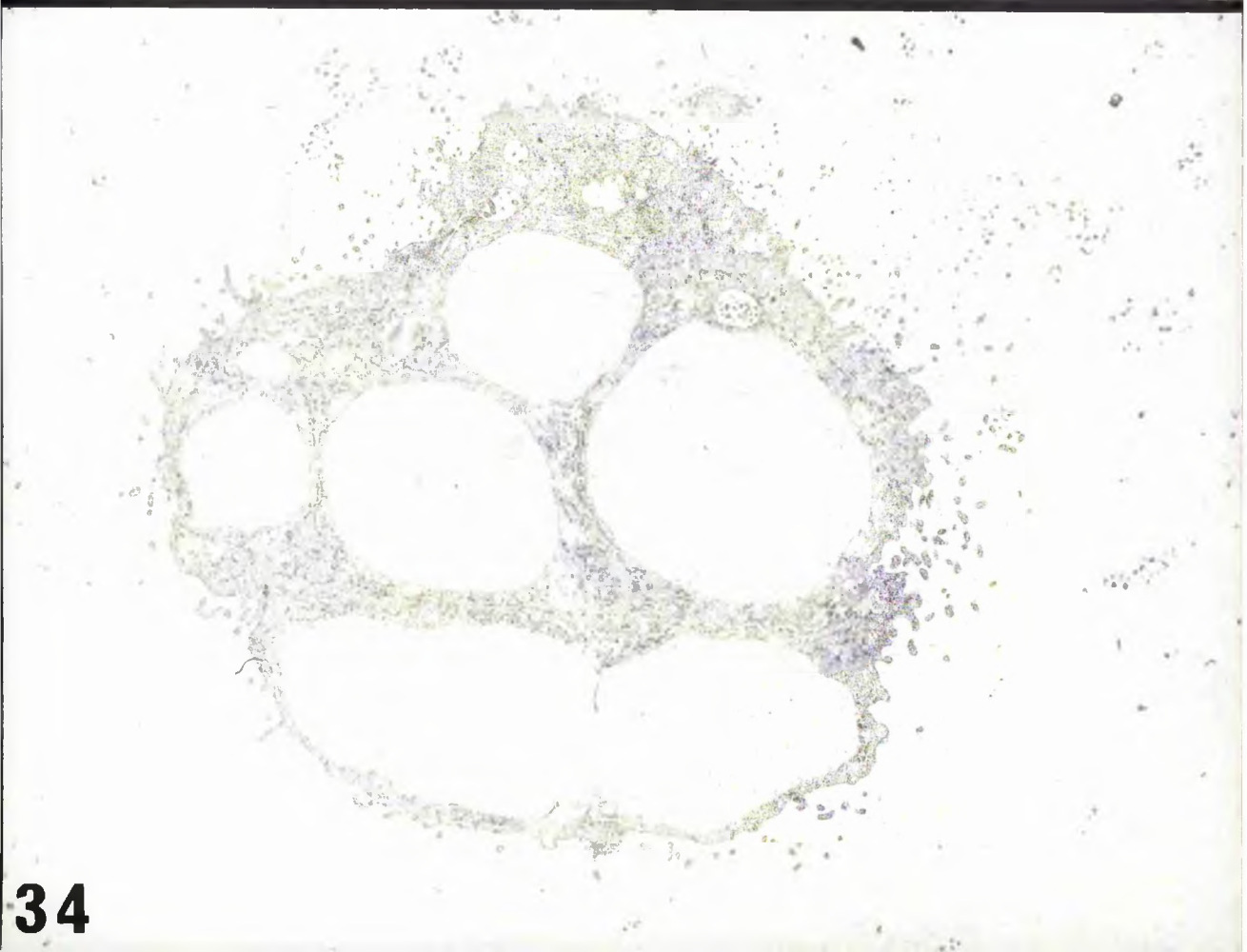

34

Figure 35. A group of notochordal cells in which the large vesicles have displaced the cytoplasm to the periphery. x 4,500

Figure 36. Large vesicles within notochordal cells. Some of the vesicles contain fibrillar material. x 5,700

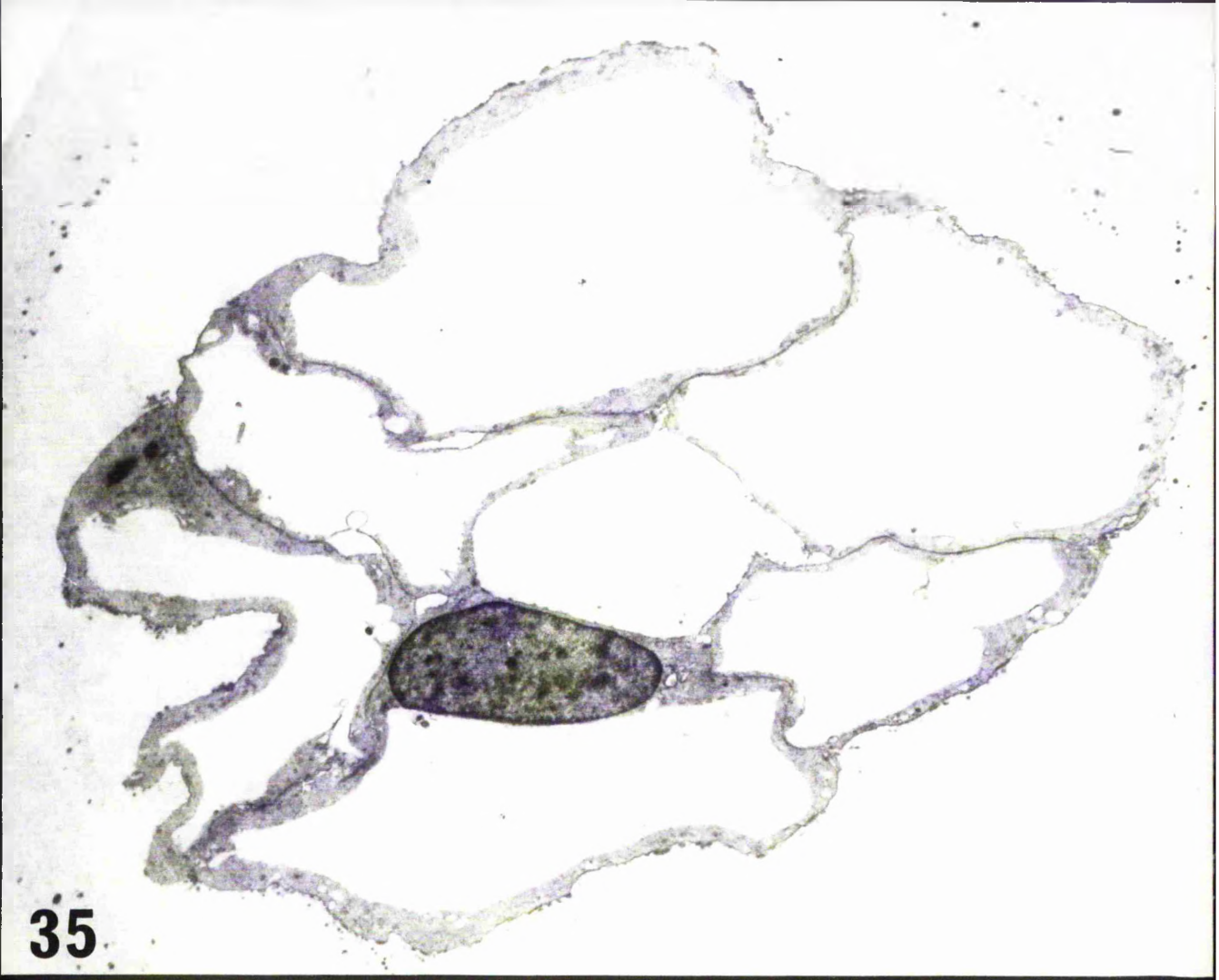

35

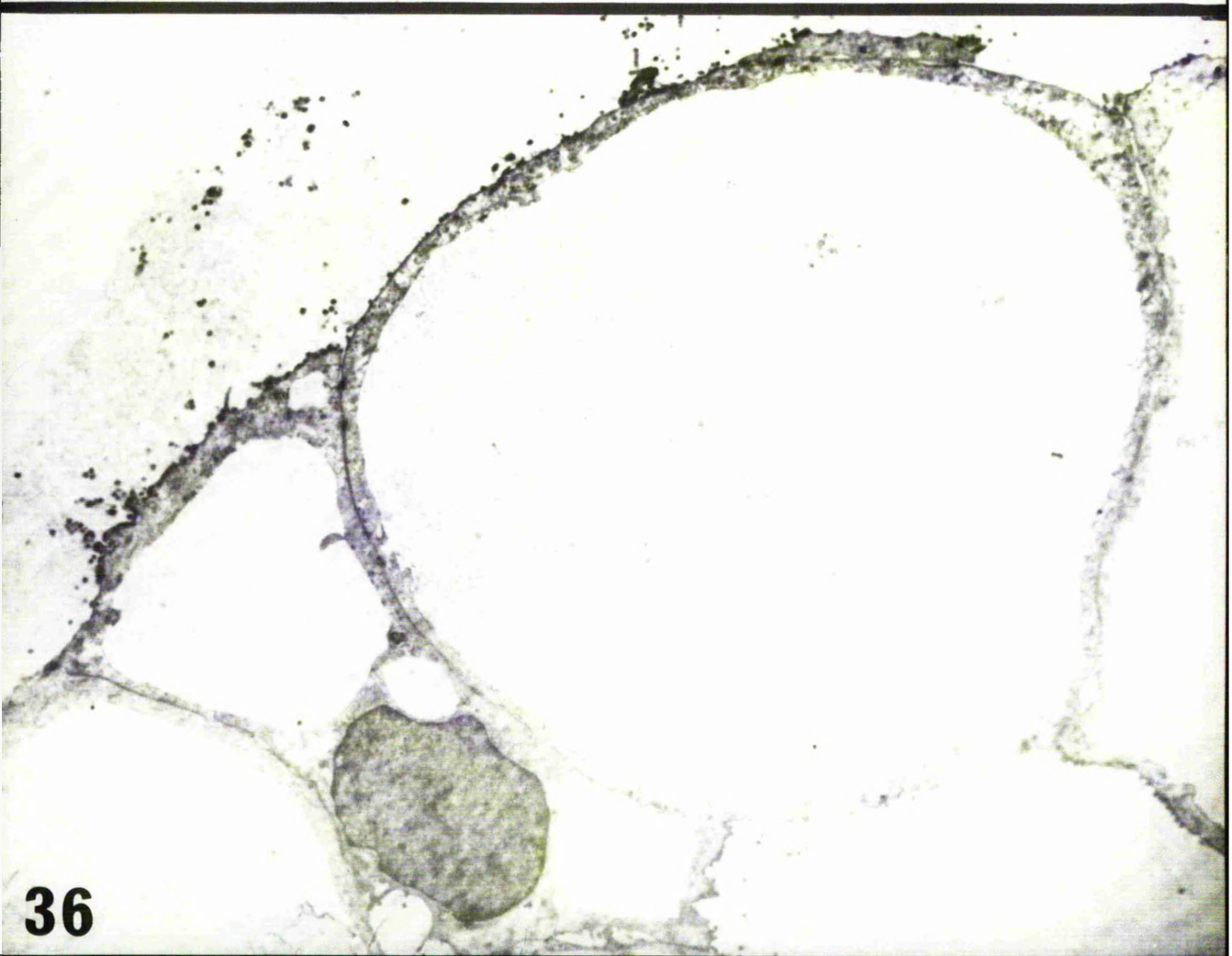

36

Figure 37. Knob-like projection into a large vesicle (v) x 39,450

Figure 38. Note variation in contents of large vesicles in adjacent notochordal cells.

x 39,000

37

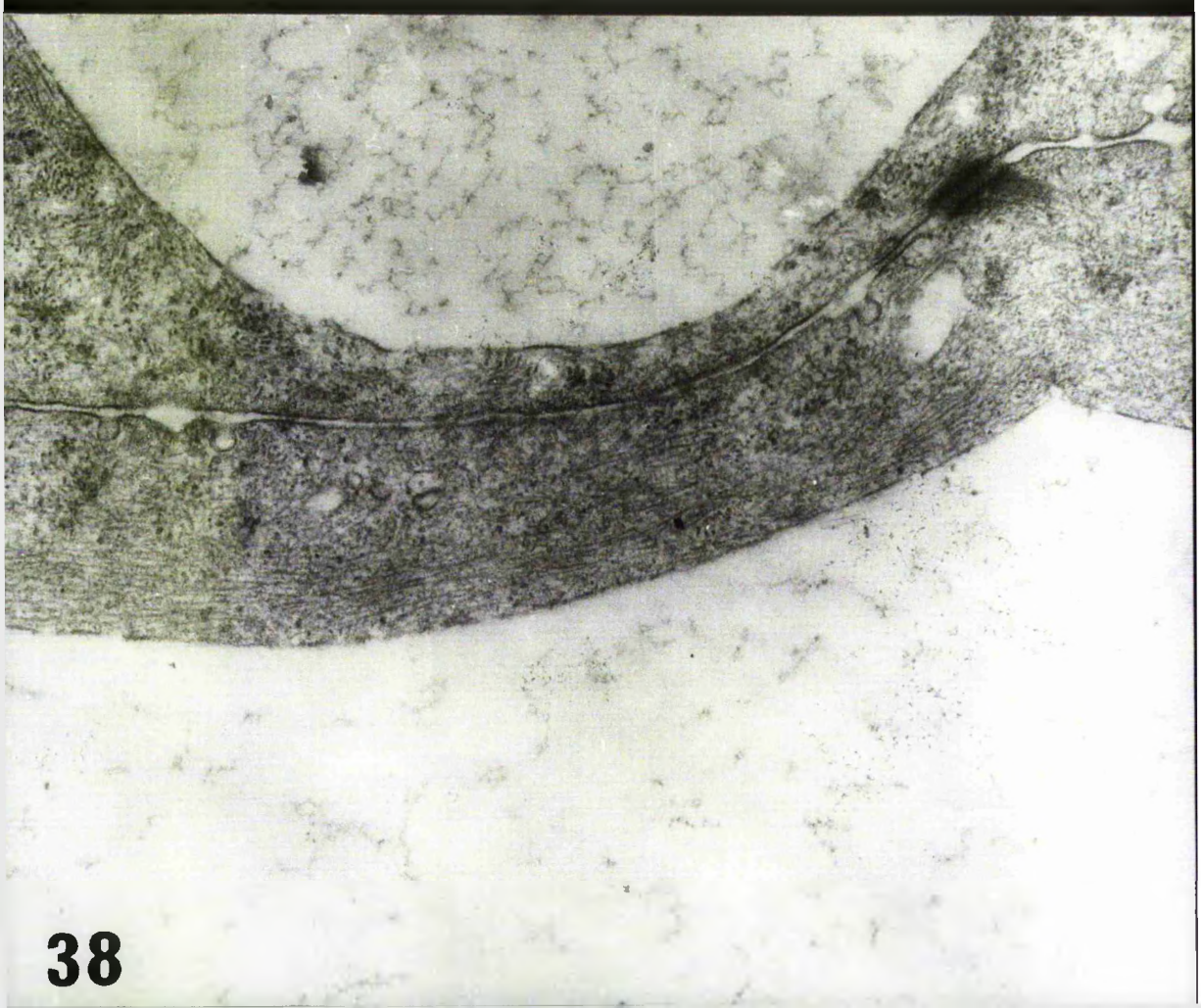

38

Figure 39. Fibrillar material within large vesicles seen after staining with lead citrate and uranyl acetate. x 35,000

Figure 40. Similar material after staining with phosphotungstic acid pH 0.5. x 35,000

Figure 41. Vesicle material seen after staining with ruthenium red. x 35,000

Figure 42. Vesicle material seen after staining with bismuth and uranyl acetate. x 35,000


39


40


41

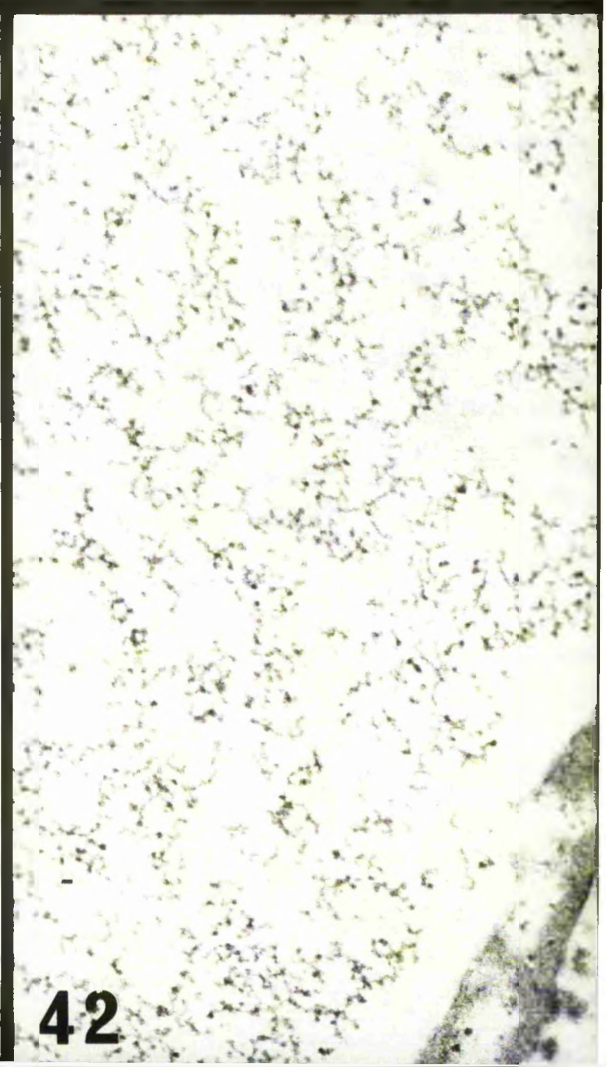
42

Figure 43. Dense staining of extracellular material deliniates intercellular spaces communicating with the matrix. Lanthanum treatment (Method III).

x 5,760

Figure 44. At higher magnification the electron dense circular profiles interpreted as pinocytotic vesicles are seen to be continuous with the intercellular space. x 112,000

43

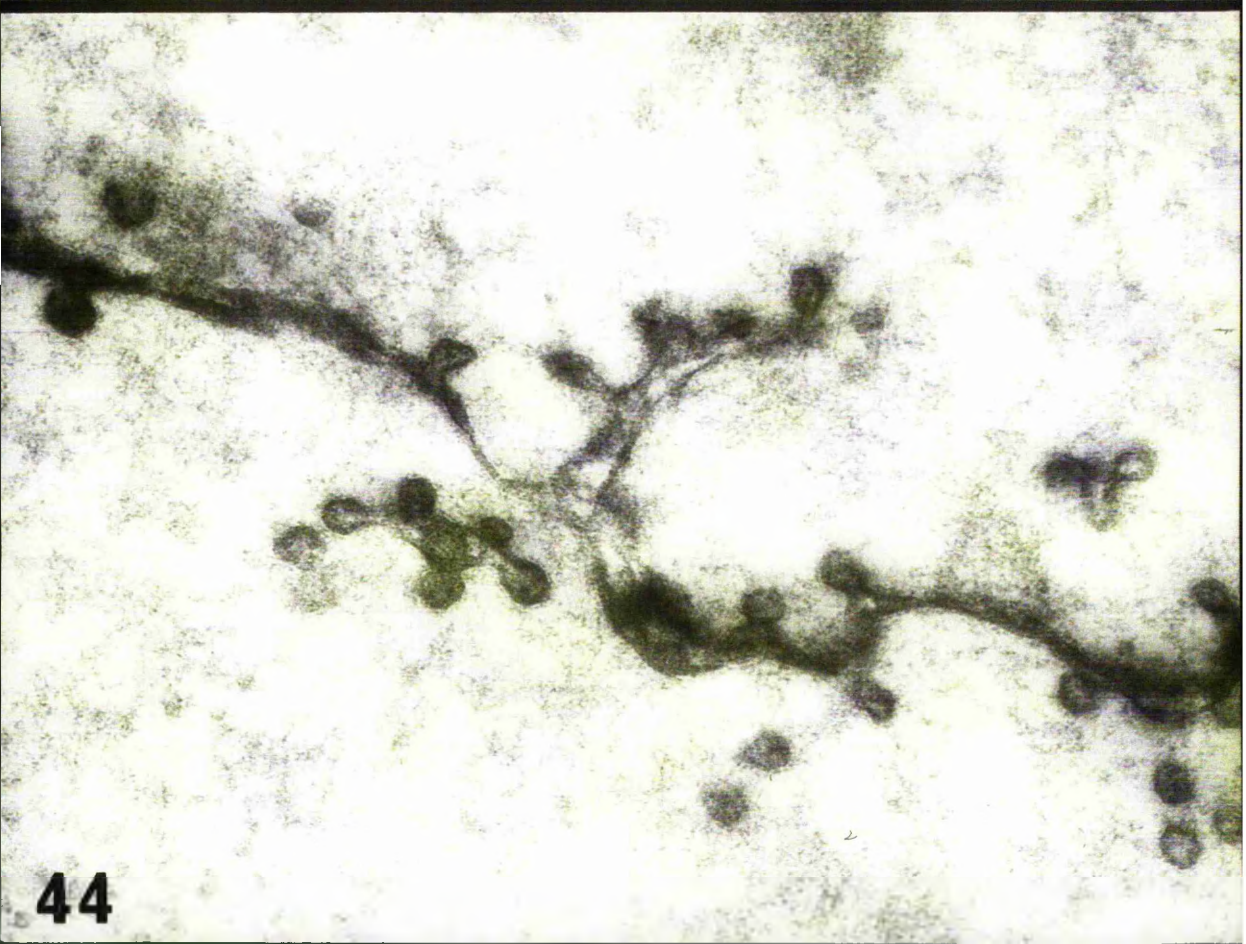

44

Figure 45. Pinocytotic vesicles opening onto the cell surface in the vicinity of extracellular dense material (e). Note other apparent vesicles containing similar material. x 33,140

Figure 46. Extracellular dense material and pinocytotic vesicles associated with an invagination of the cell surface. x 33,140

Figure 47. Apparent vesicle containing electron dense material with pinocytotic vesicles opening into it. x 111,500

45

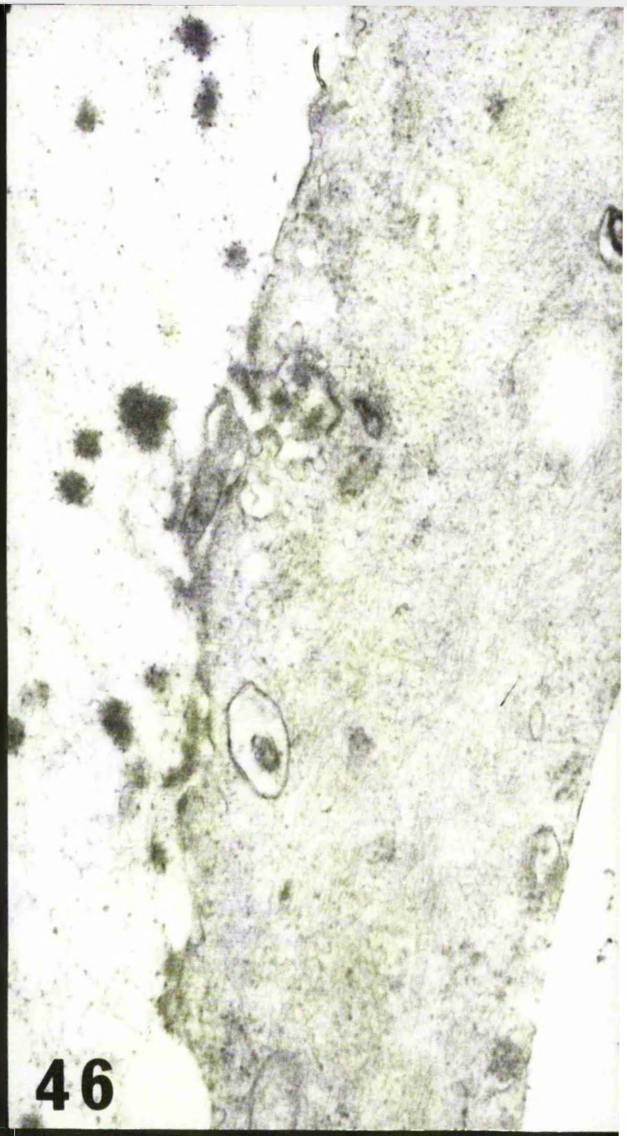

46

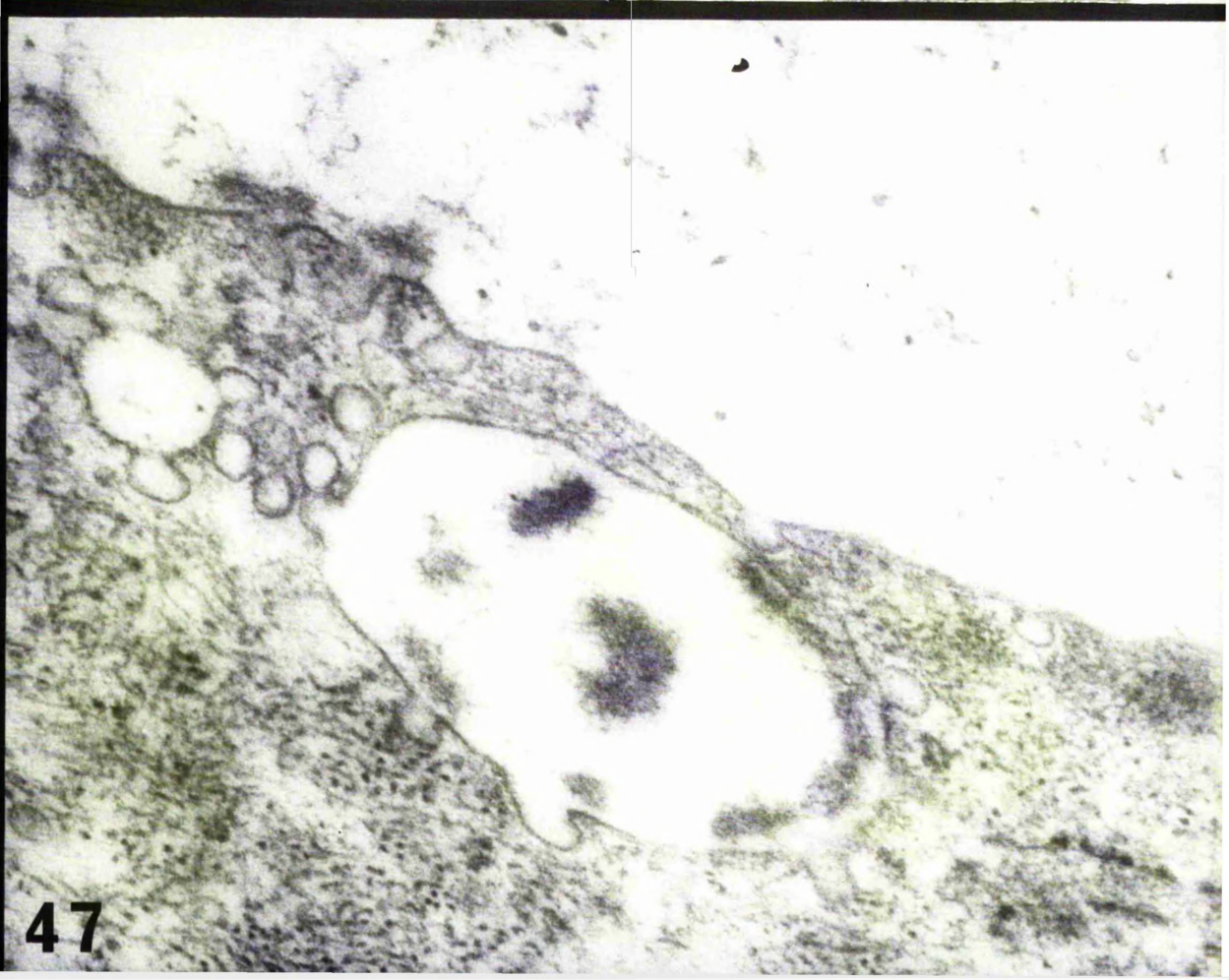

47

Figure 48. Cytofilaments within a notochordal cell.
x 70,000

Figure 49. Condensed cytofilaments beneath the cell surface. x 35,500

Figure 50. Notochordal cells showing localisation of particles within the cytoplasm stained by P.T.A. at low pH (arrows). x 7,440

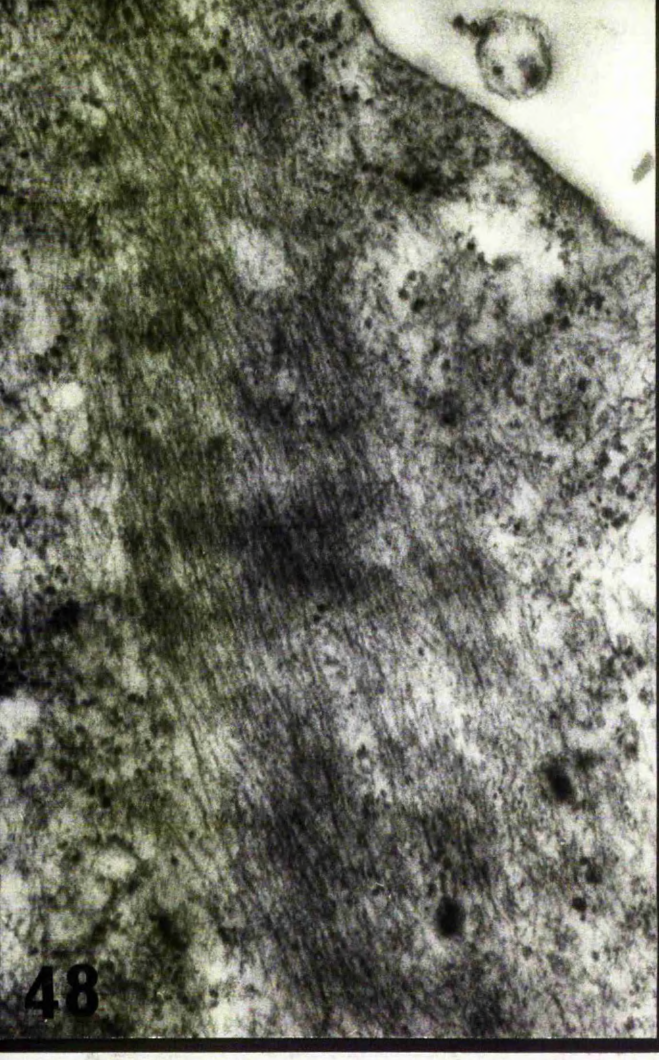

48

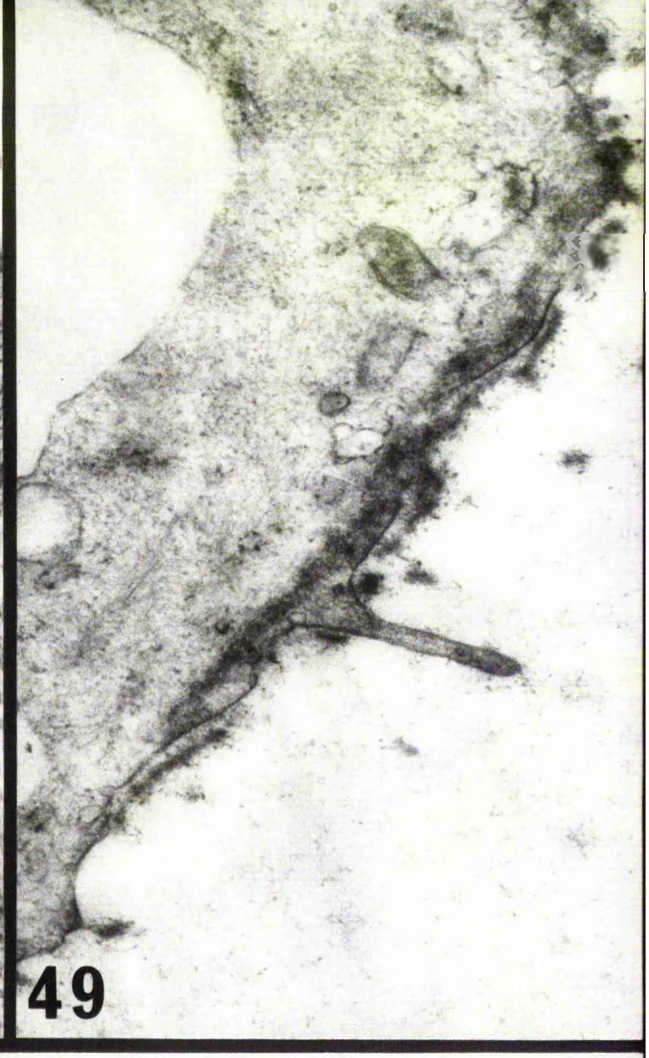

49

50

Figure 51. Stained material resembling β-glycogen particles seen after staining with P.T.A. at low pH.

x 31,560

Figure 52. Aggregated particles (α-glycogen) seen after staining with P.T.A. at low pH.

x 31,560

Figure 53. Residual peripheral staining of particles after diastase-digested sections were stained with P.T.A. at low pH. x 31,560

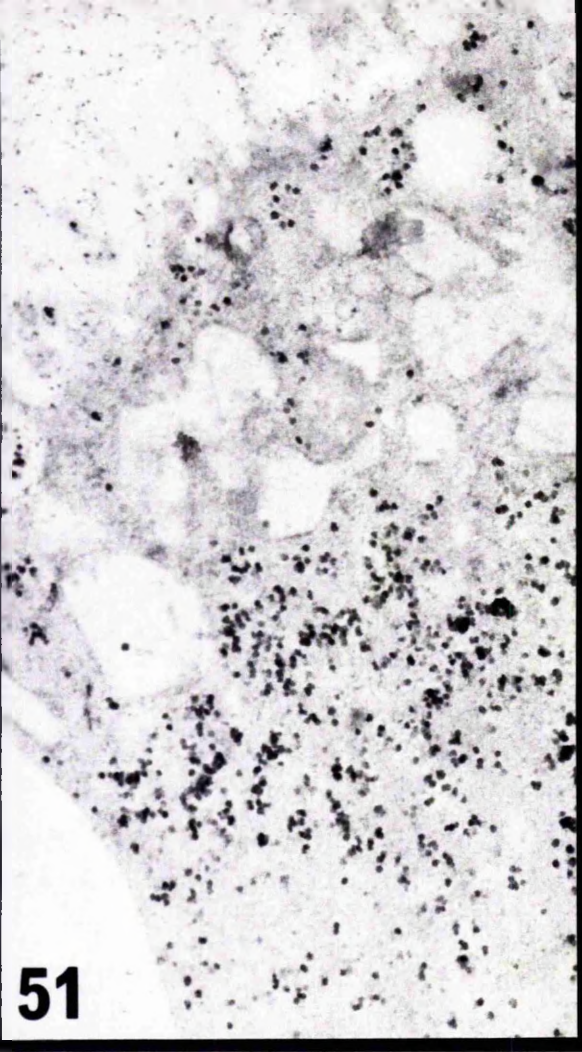
51

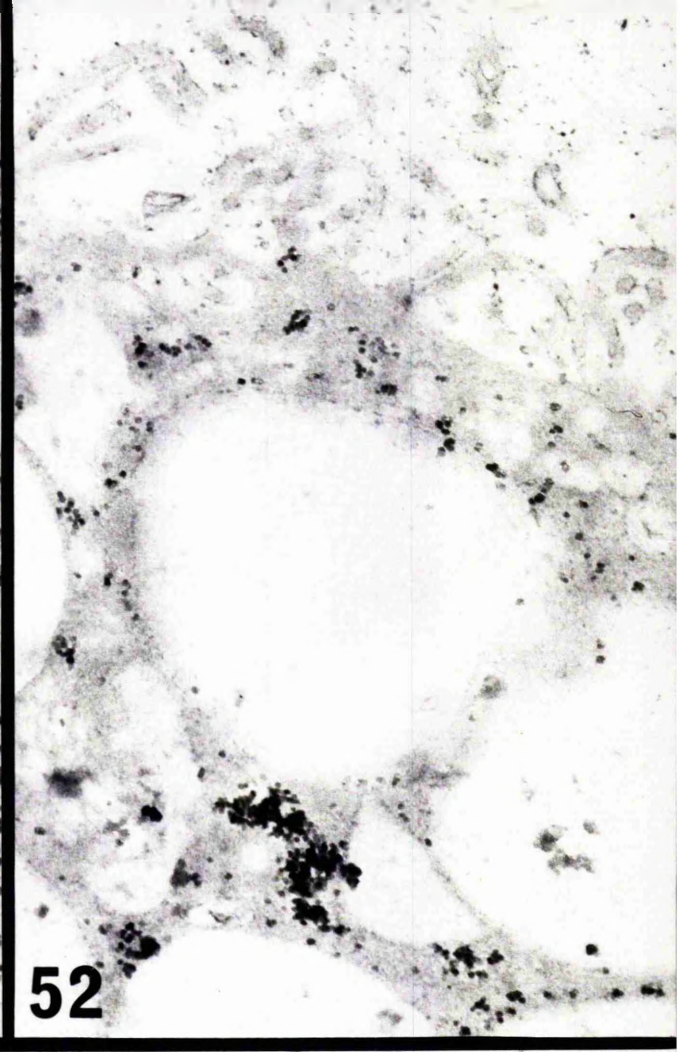
52

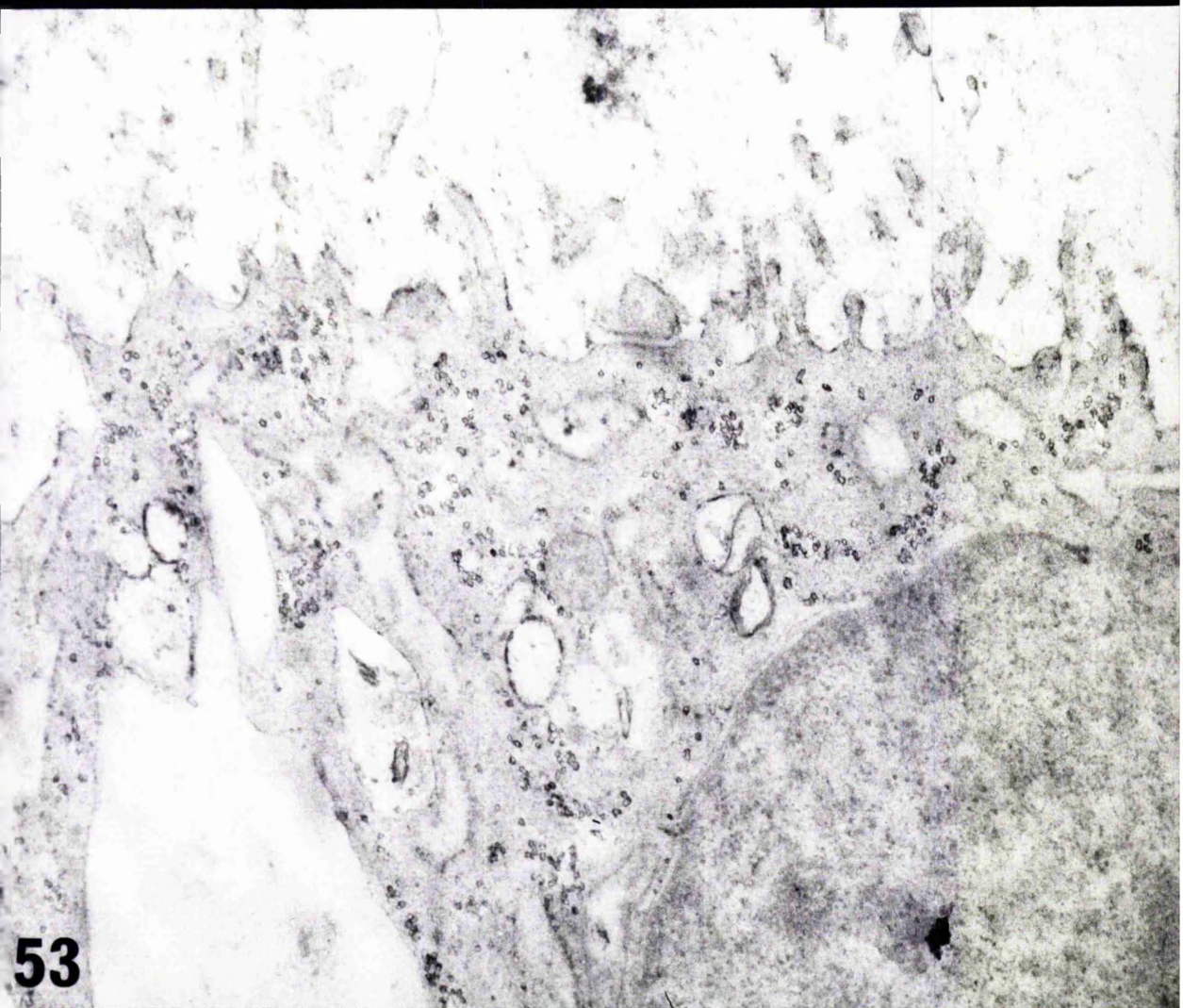
53

Figure 54. Small vesicle (primary lysosome) containing reaction product. Acid phosphatase. x 31,560

Figure 55. Vesicle containing additional material (secondary lysosome). Acid phosphatase. x 31,560

Figure 56. Acid phosphatase - negative vesicles containing myelin bodies. x 31,560

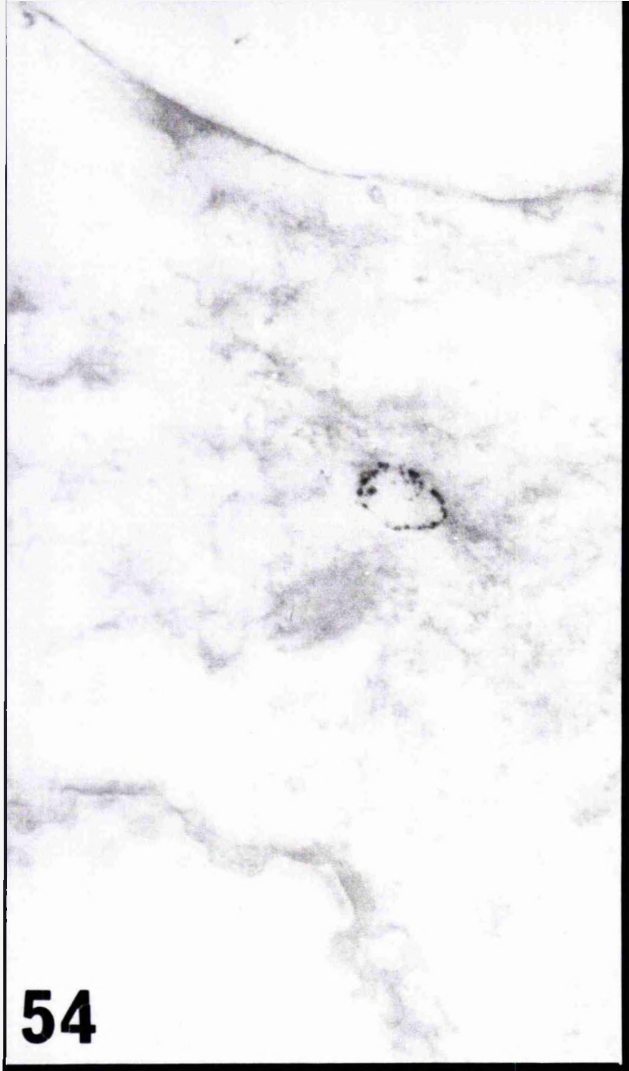

54

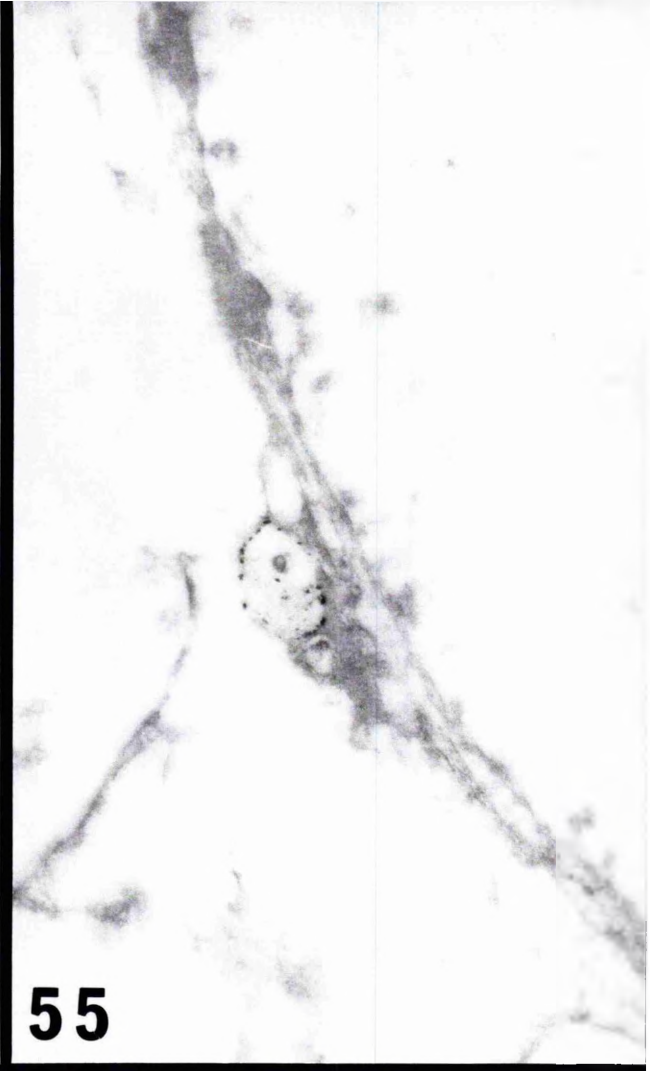

55

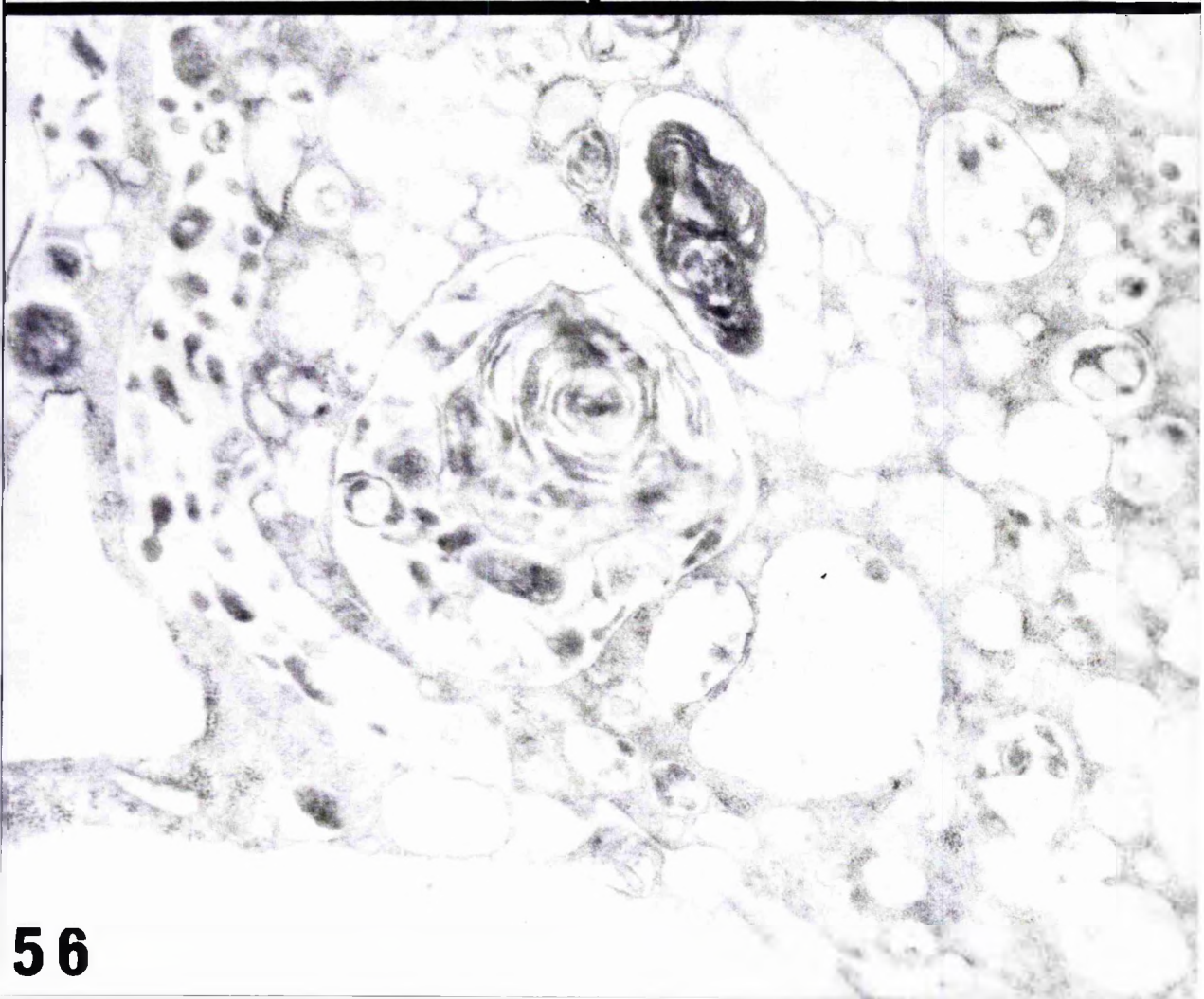

56

Figure 57. Notochordal cell group containing two degenerating notochordal cells. x 4,200

Figure 58. Degenerating notochordal cell. x 7,500

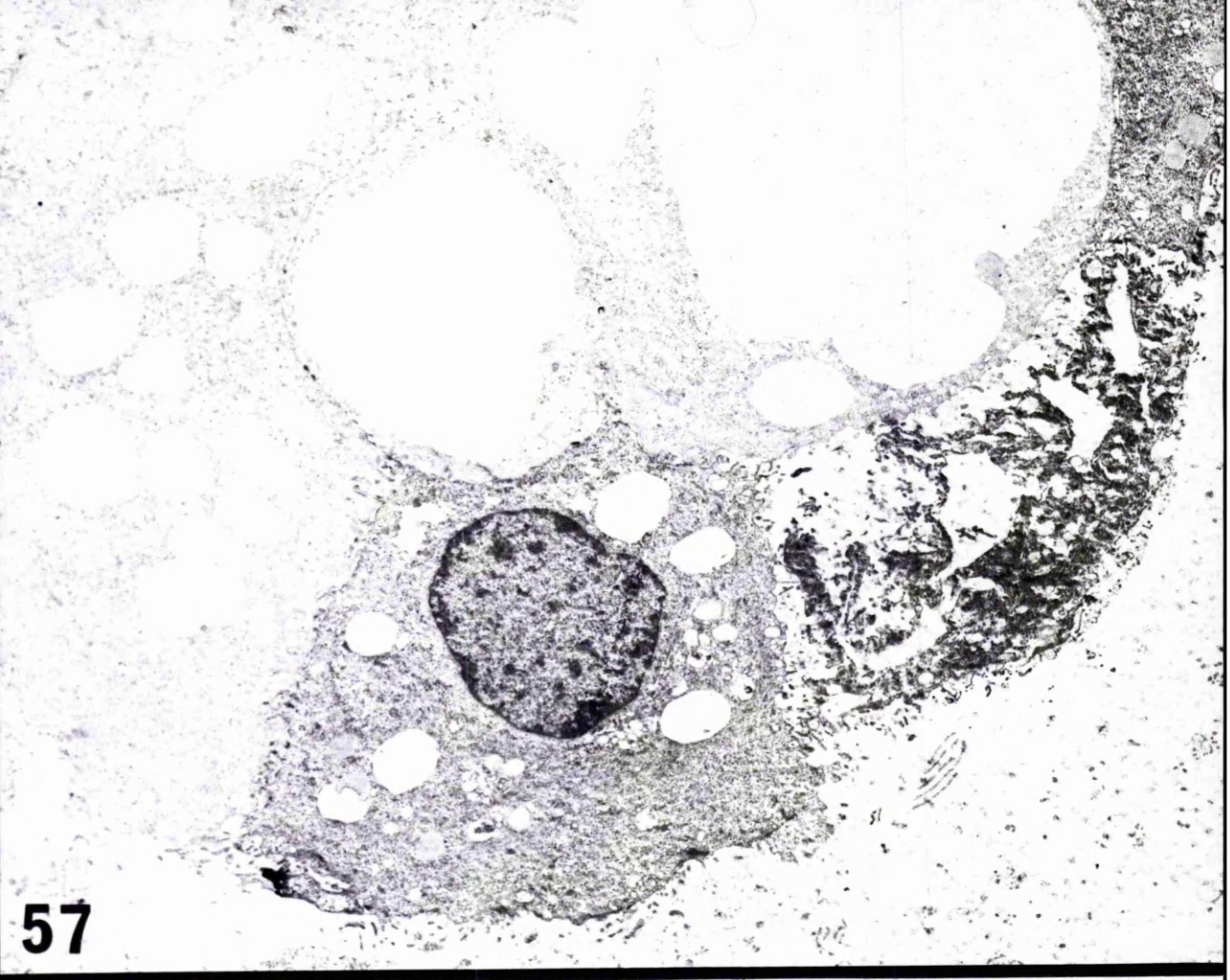

57

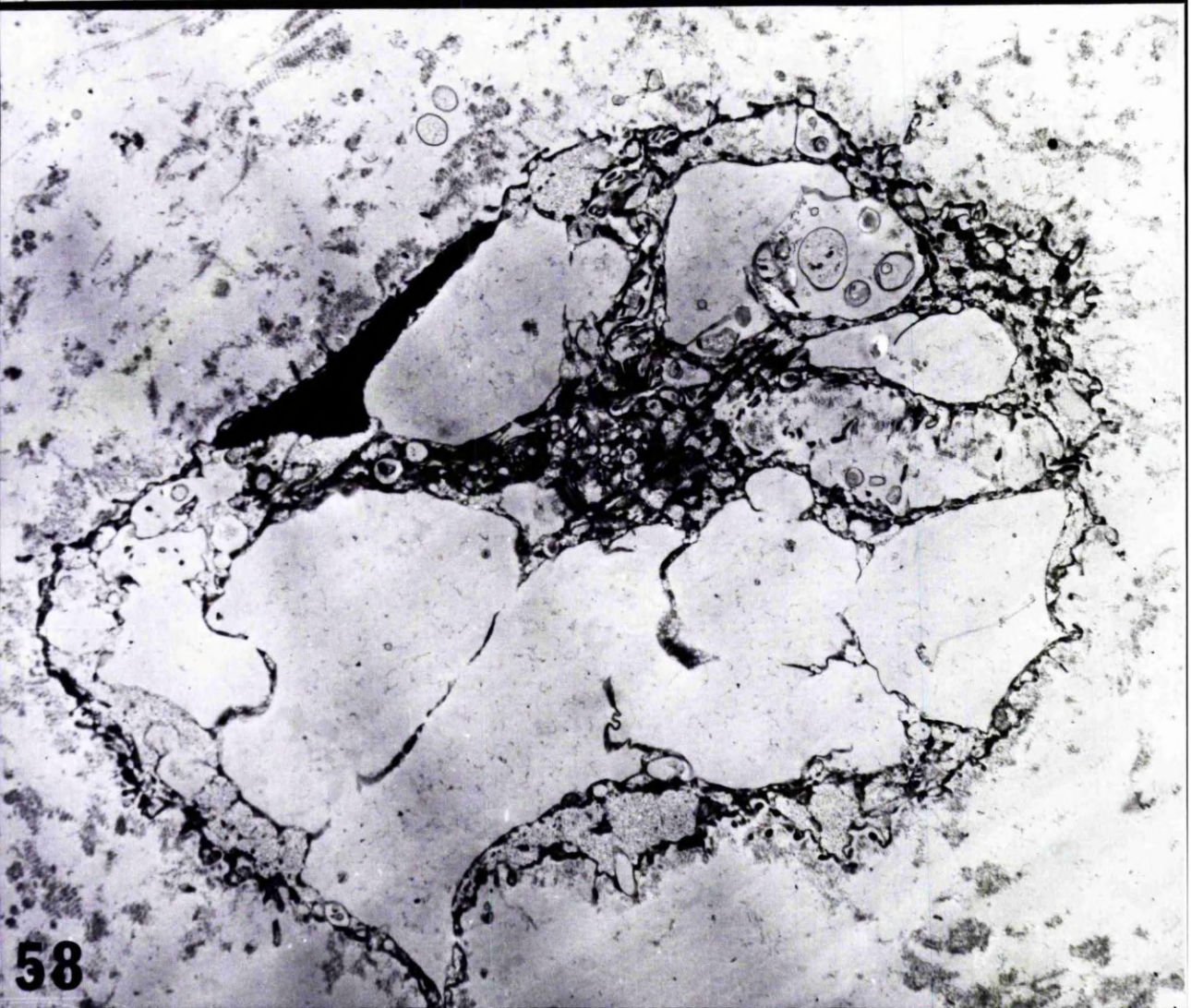

58

Figure 59. Degenerating notochordall cell. Note banded fibre within a vesicle at the right of the figure. x 6,500

Figure 60. Notochordal cell remains lying in the extracellular matrix between two healthy notochordal cells. x 9,000

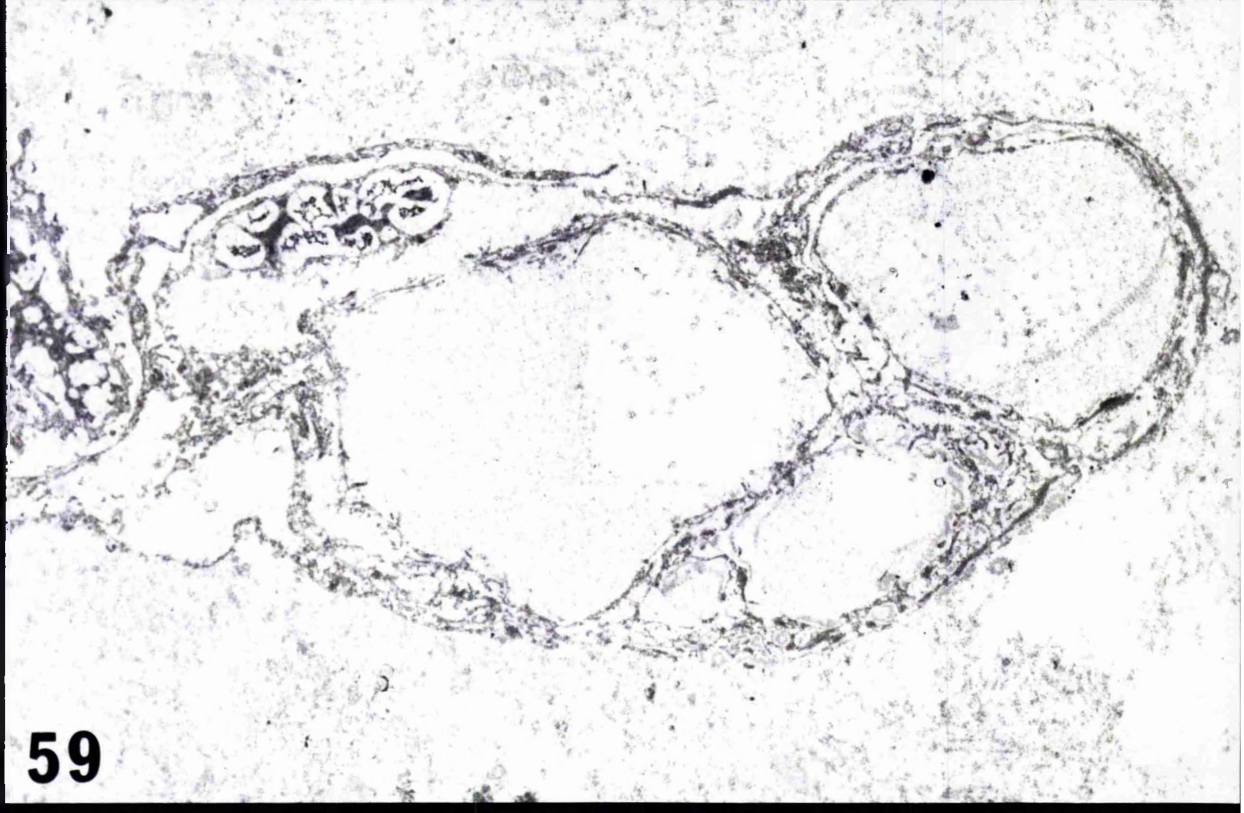

59

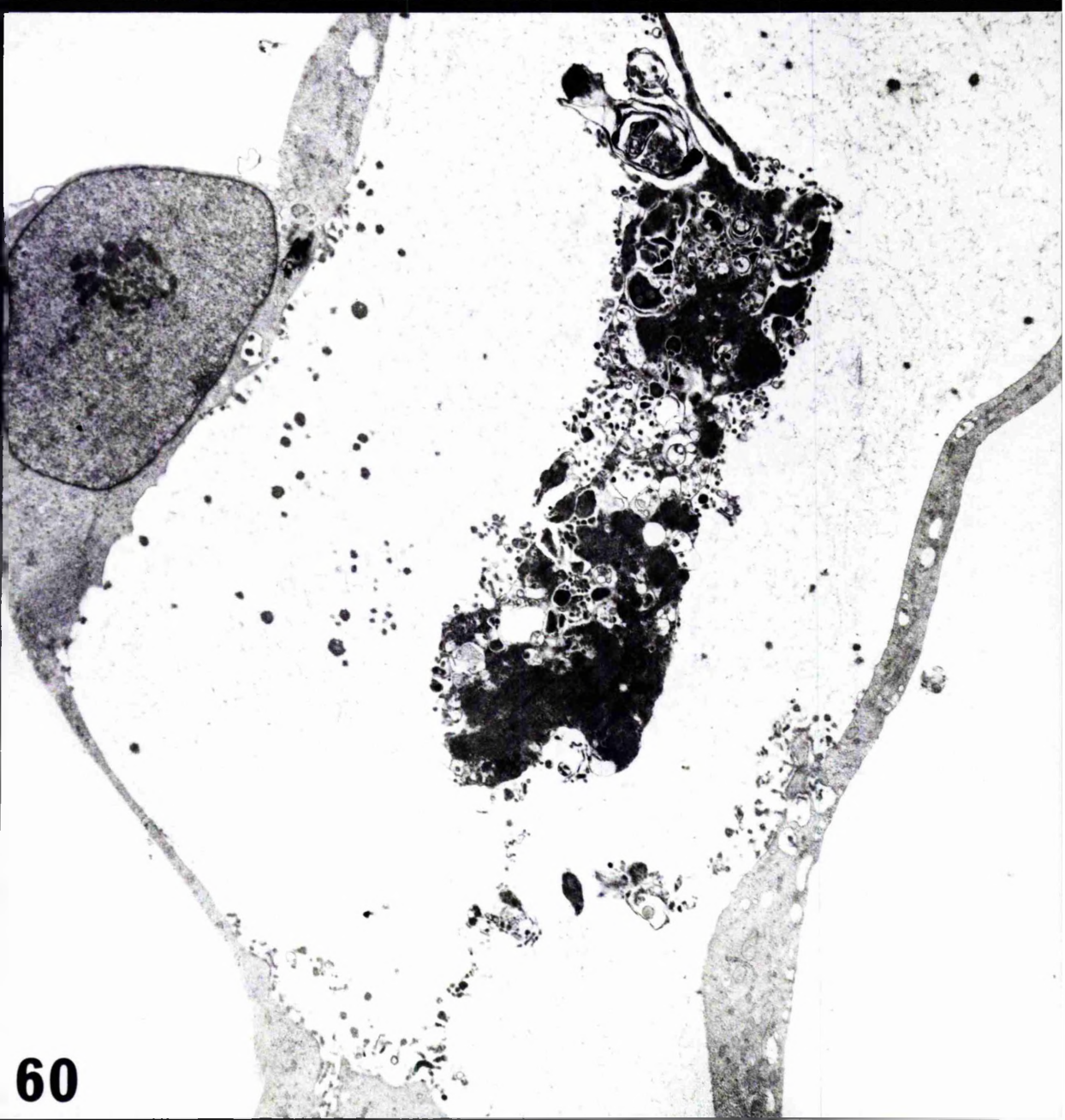

60

Figure 61. Material within the extracellular matrix seen after lead citrate and uranyl acetate staining. x 35,000

Figure 62. Extracellular matrix material. Ruthenium red. x 35,000

Figure 63. Extracellular matrix material. Phosphotungstic acid pH 0.5 x 35,000

Figure 64. Extracellular matrix material seen after fixation in potassium permanganate and lanthanum nitrate (Method III). x 35,000


61

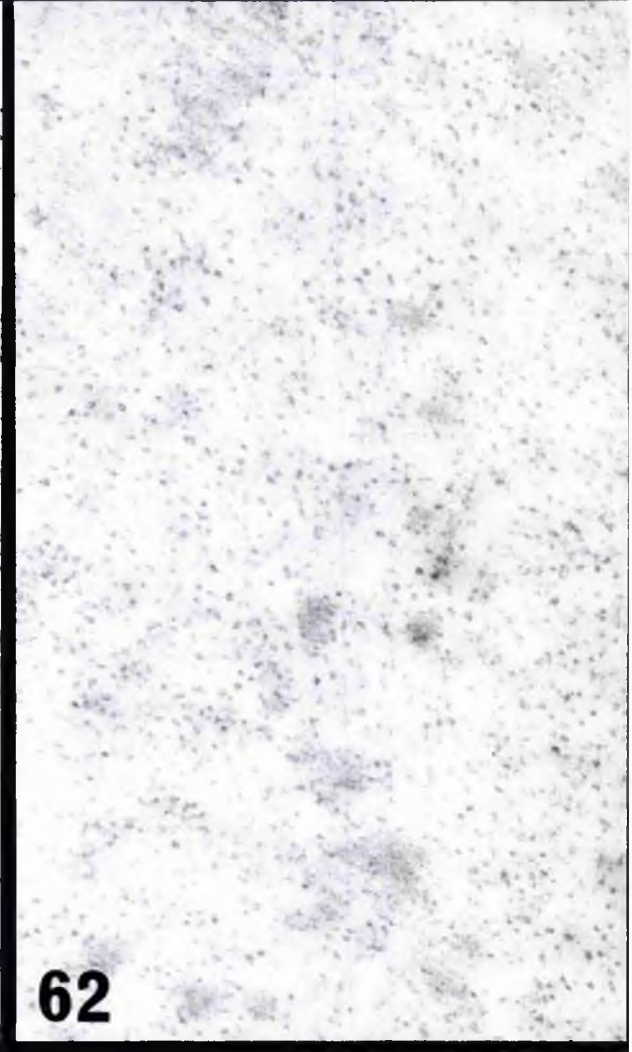
62


63

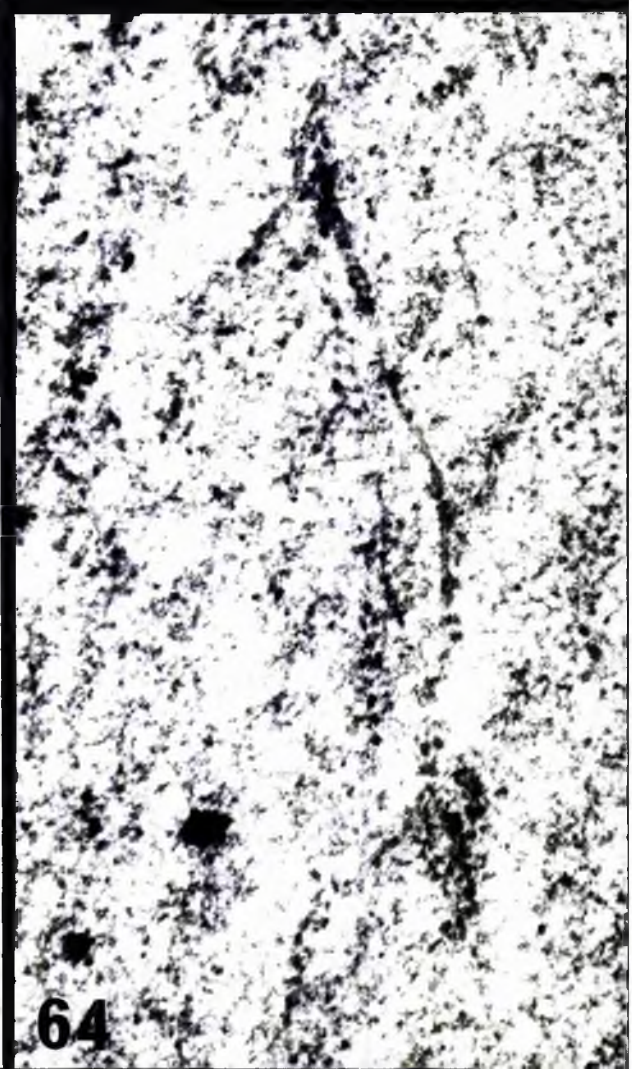
64

Figures 65, 66 and 67. Different areas at the surface of notochordal cells illustrating the variation in density of beaded filamentous material within the extracellular matrix. Note also the stellate particles within the extracellular matrix and the similarity of this material to bands of electron dense material adjacent to the cell surface.

x 33,000

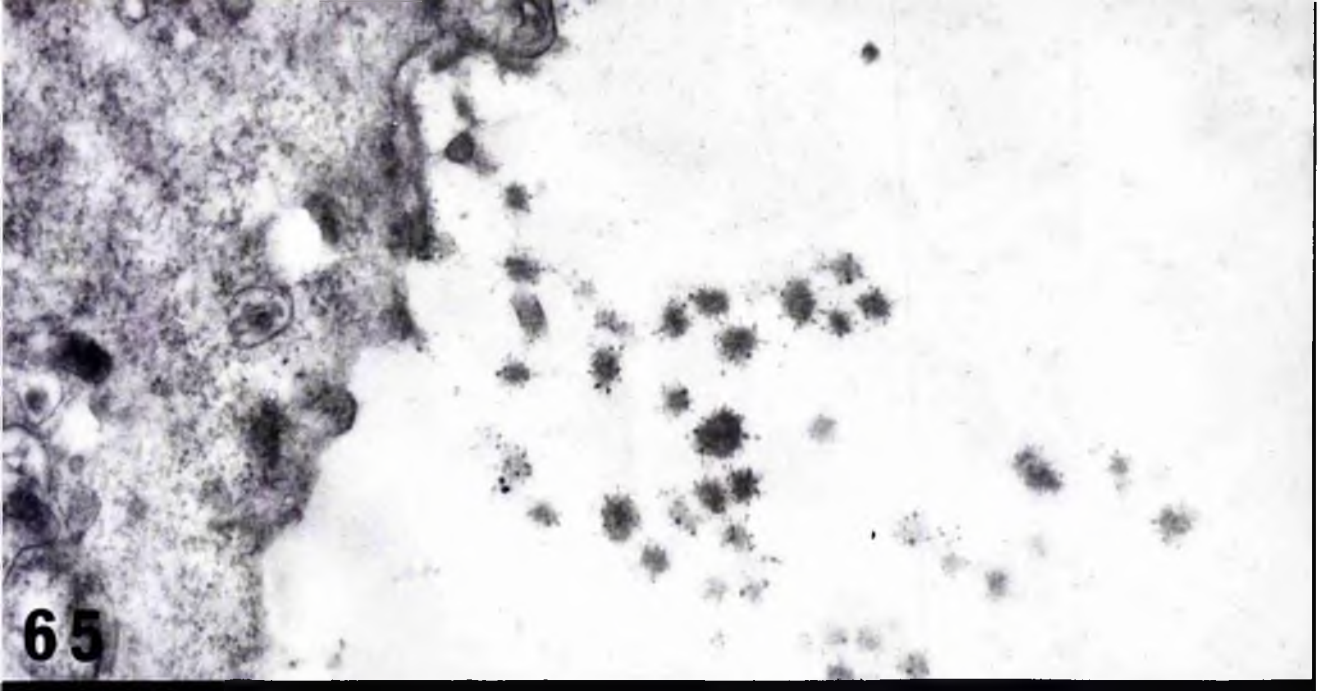
65

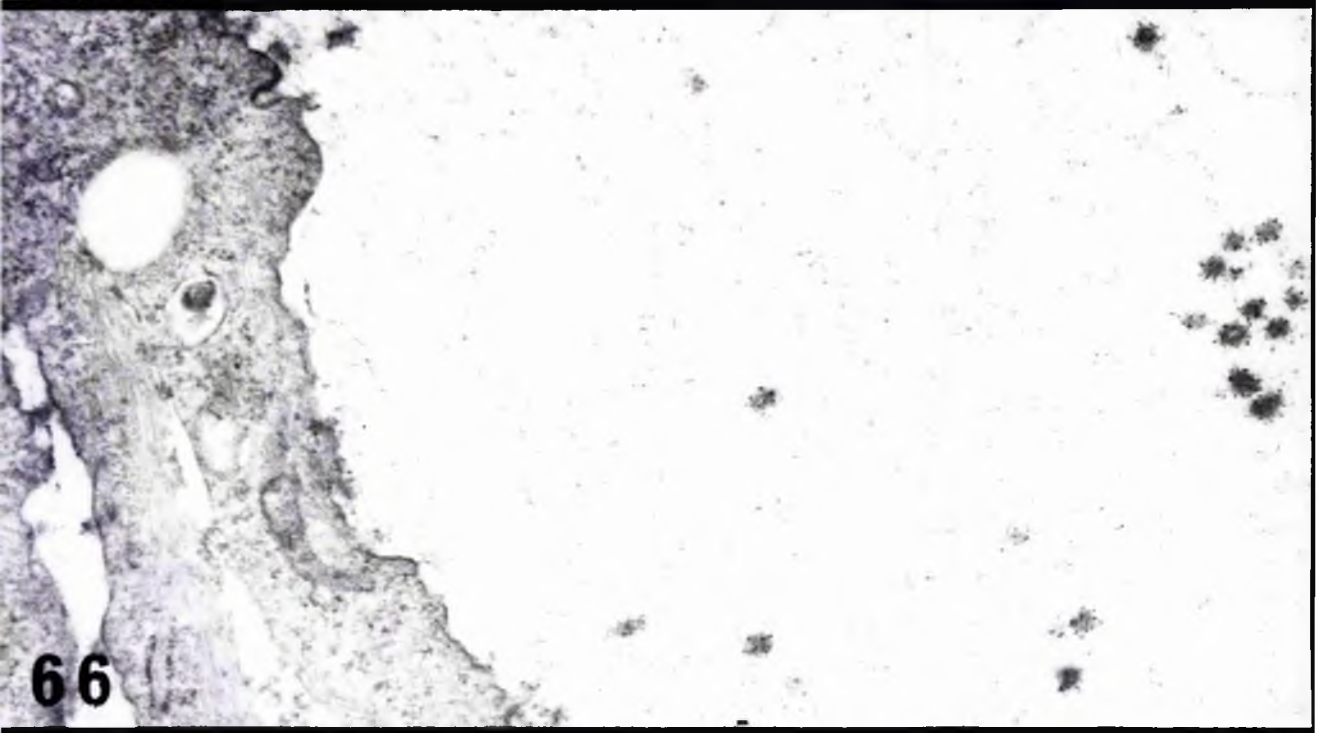
66

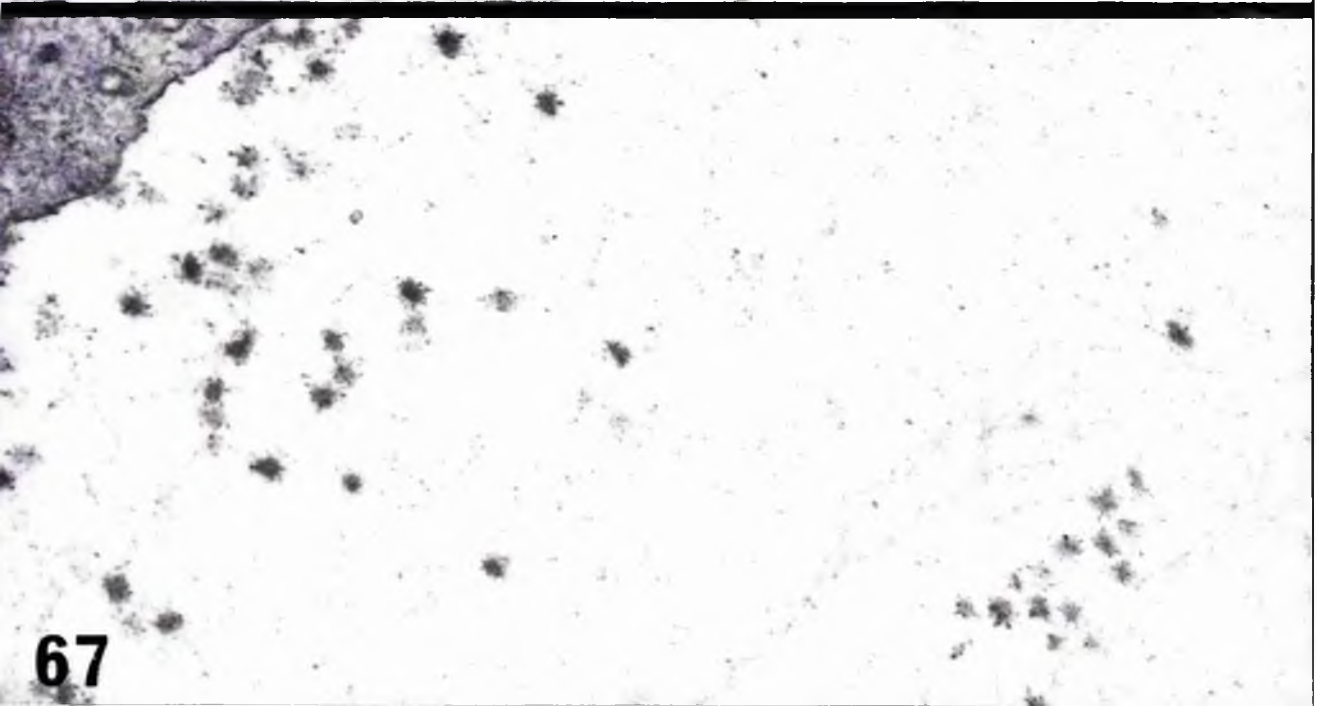
67

Figure 68. Extracellular matrix containing stellate particles. Note abrupt variation in density of beaded filamentous material.

x 33,100

Figures 69 and 70. Isolated groups of fibrils lying within the matrix. x 33,100

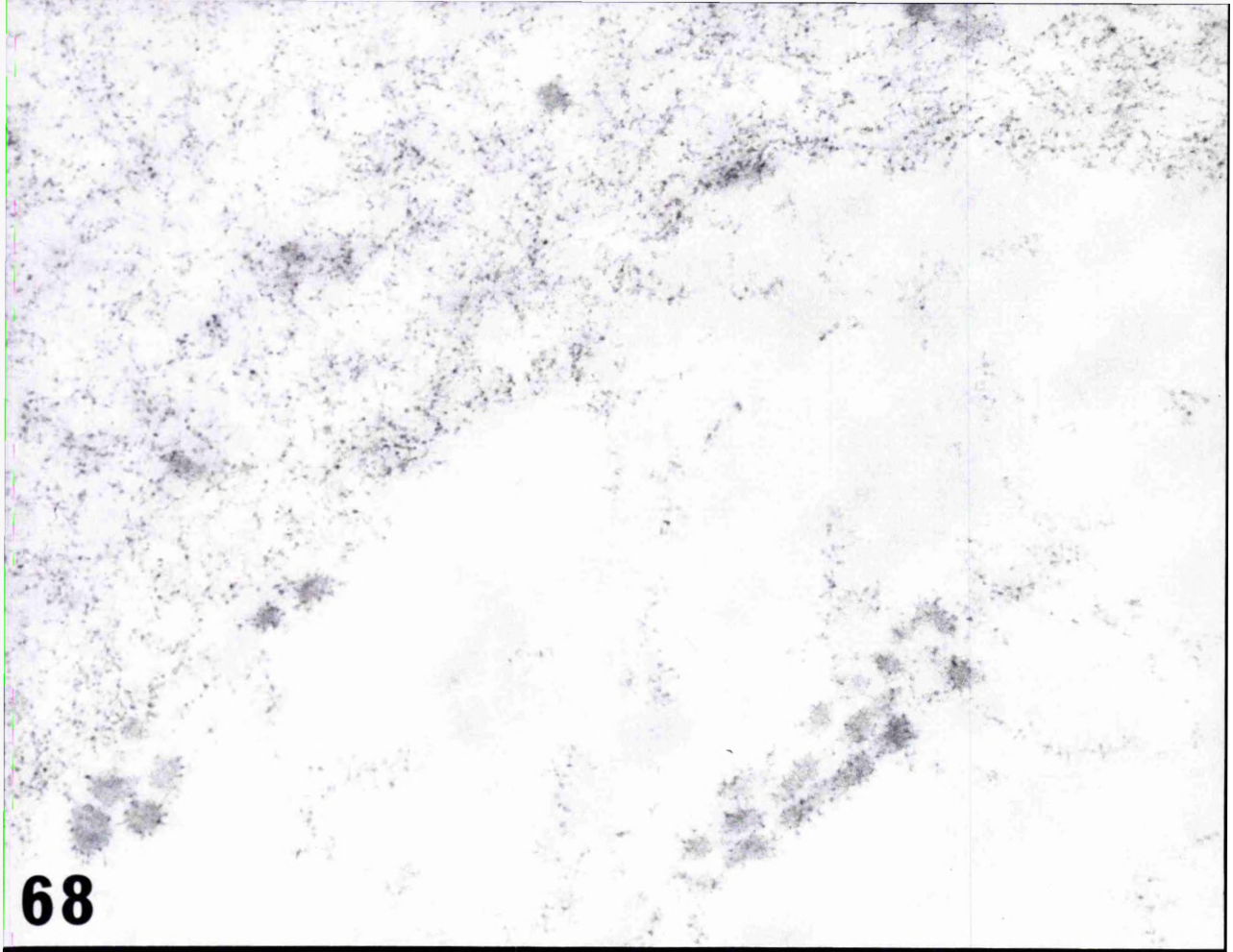

68

69

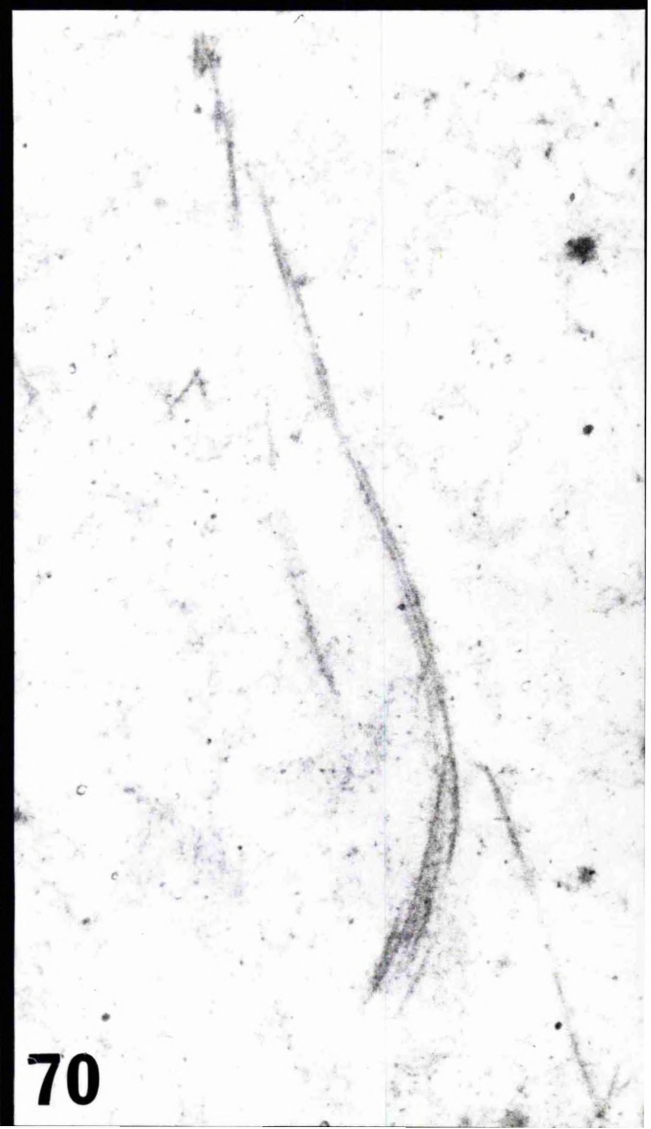

70

Figure 71. Degenerating notochordal cell surrounded by whorls of fibres. x 9,000

Figure 72. Large numbers of banded fibres in vicinity of degenerating notochordal cell x 9,000

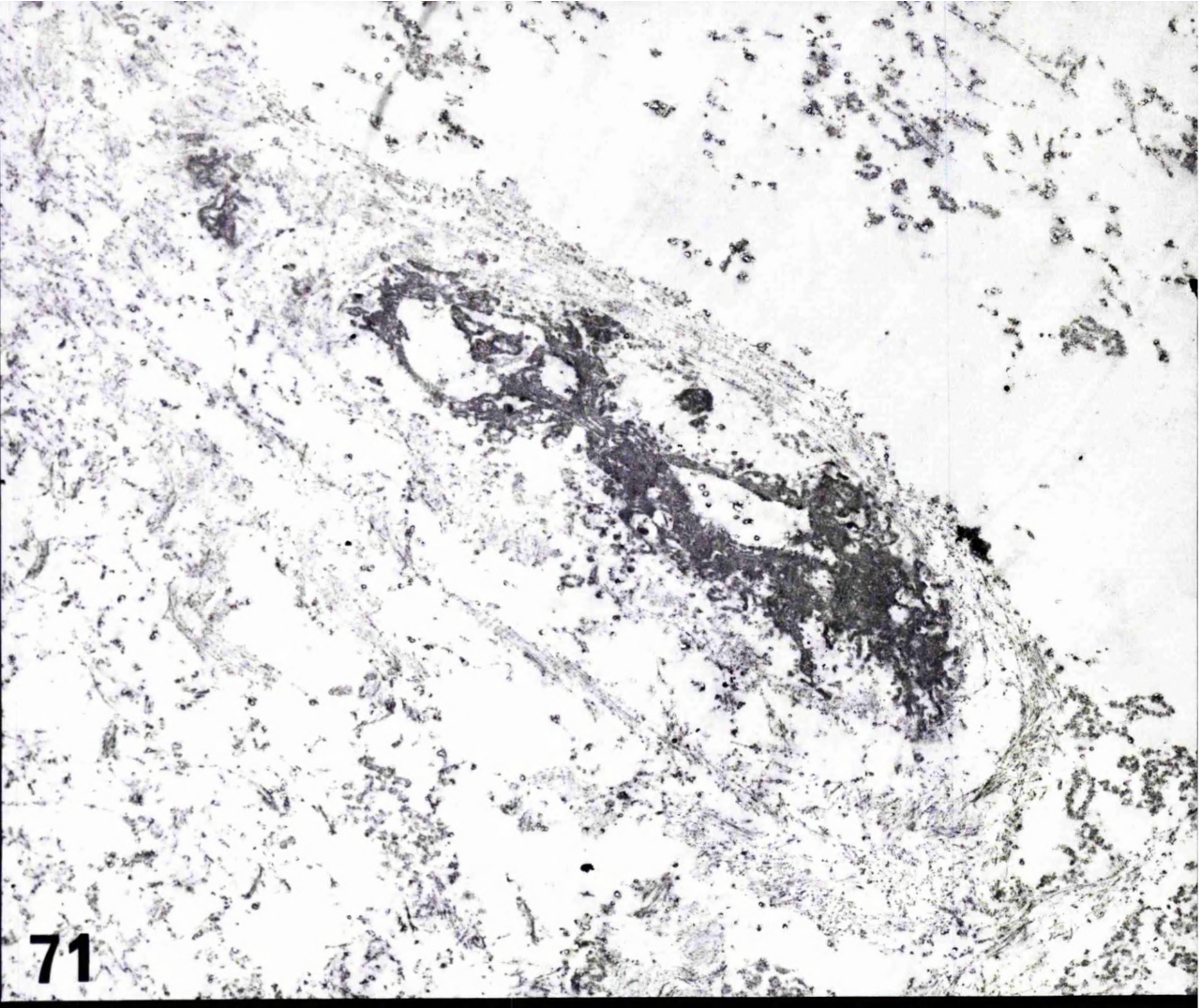

71

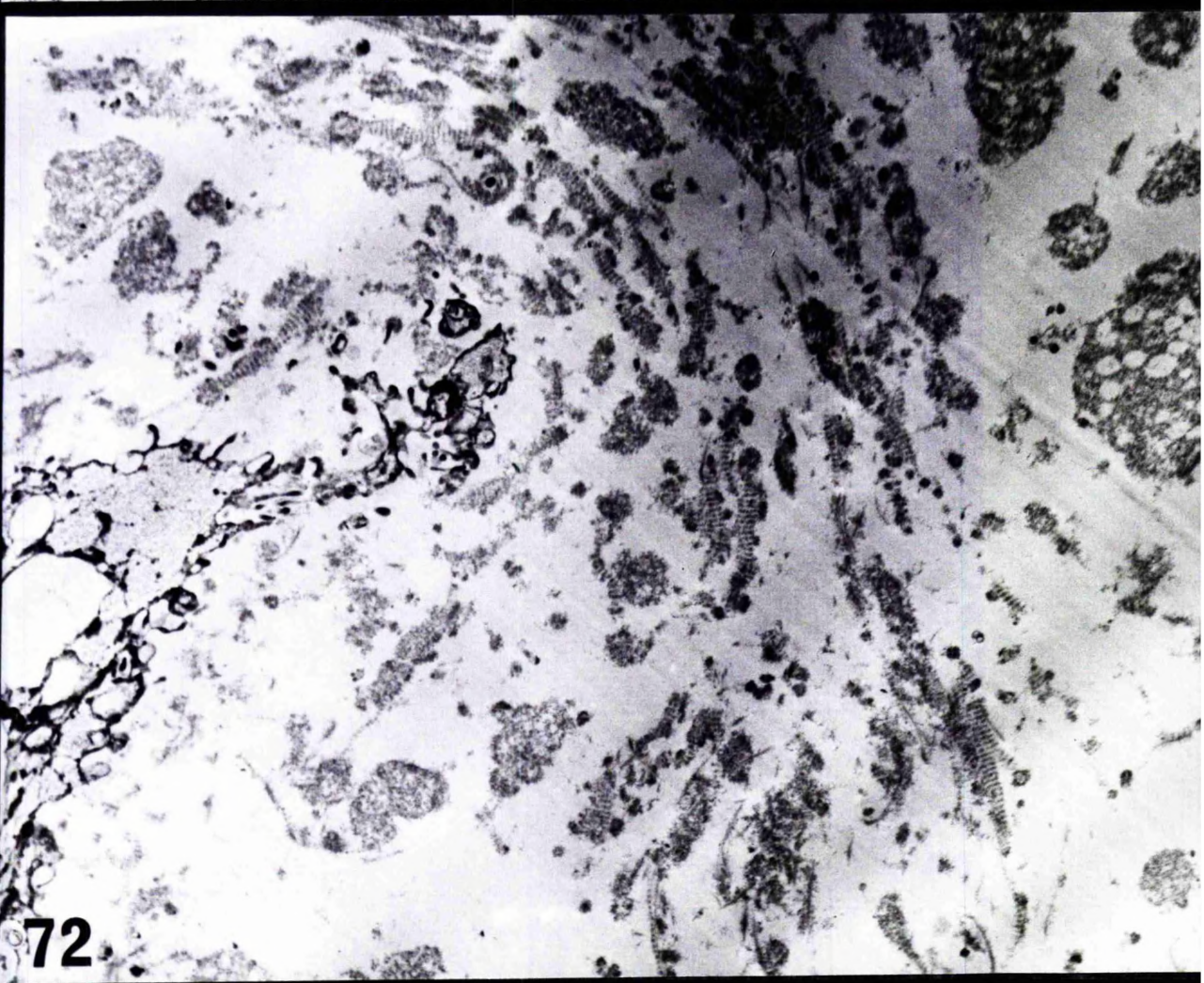

72

Figures 73 and 74. Banded fibres within nucleus pulposus matrix. x 32,500

Figure 75. Banded fibre x 49,000

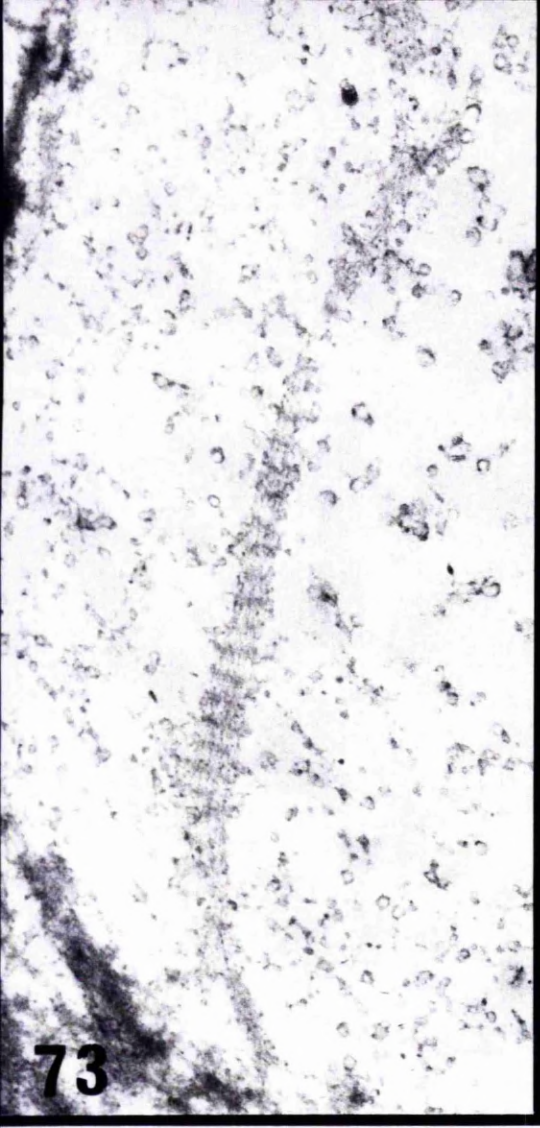
73

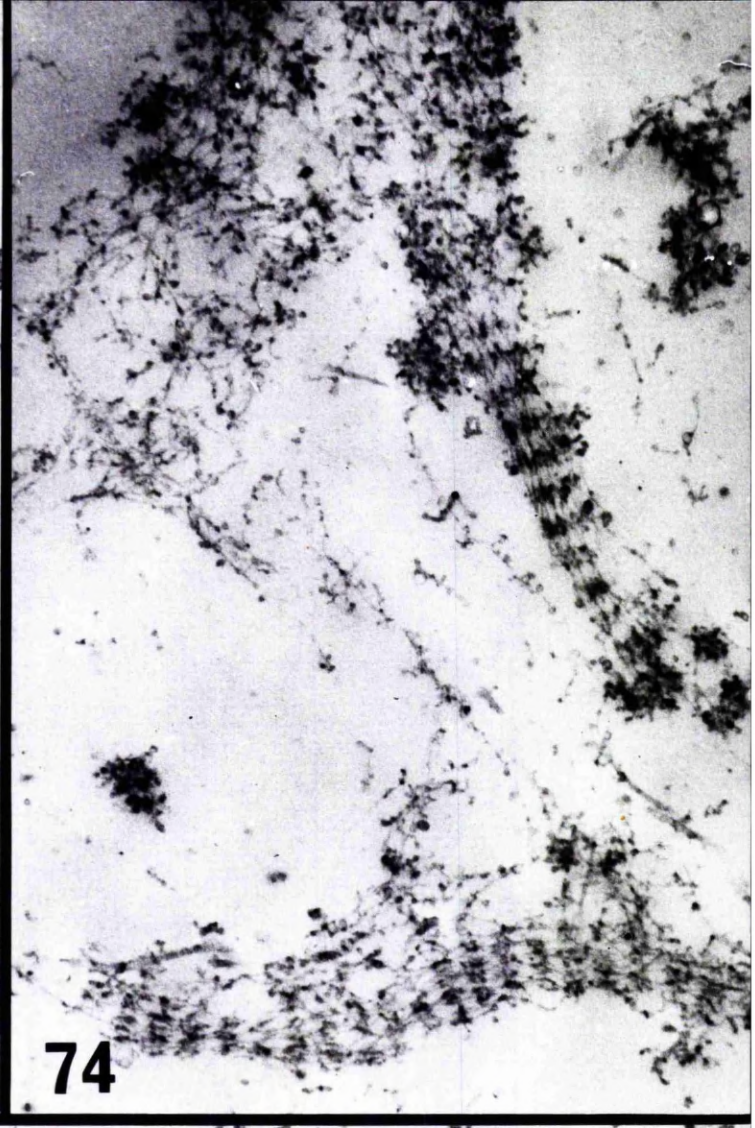
74

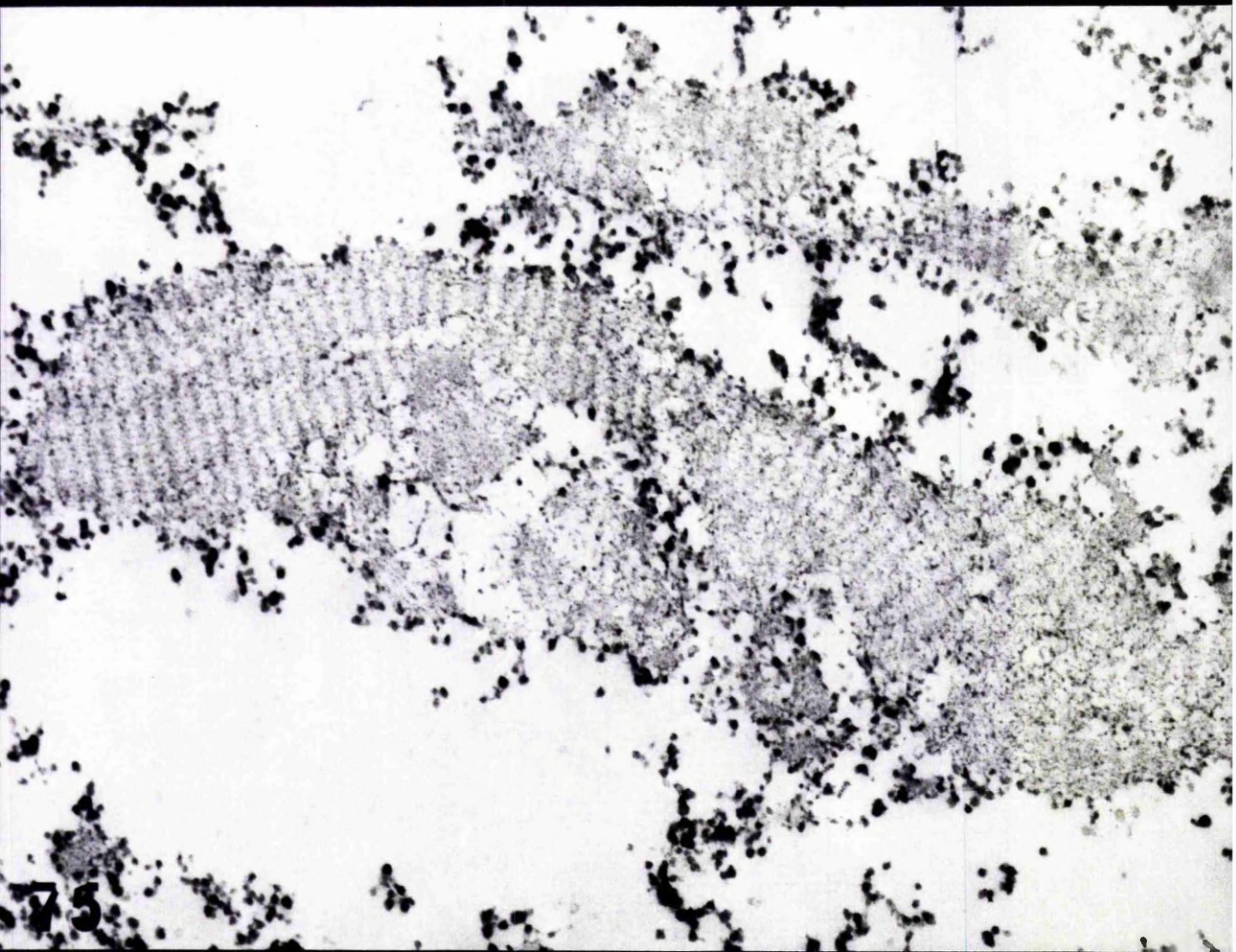
75

Figure 76. Banded fibre. x 90,000

Figure 77. Banded fibres and electron dense strips. x 35,000

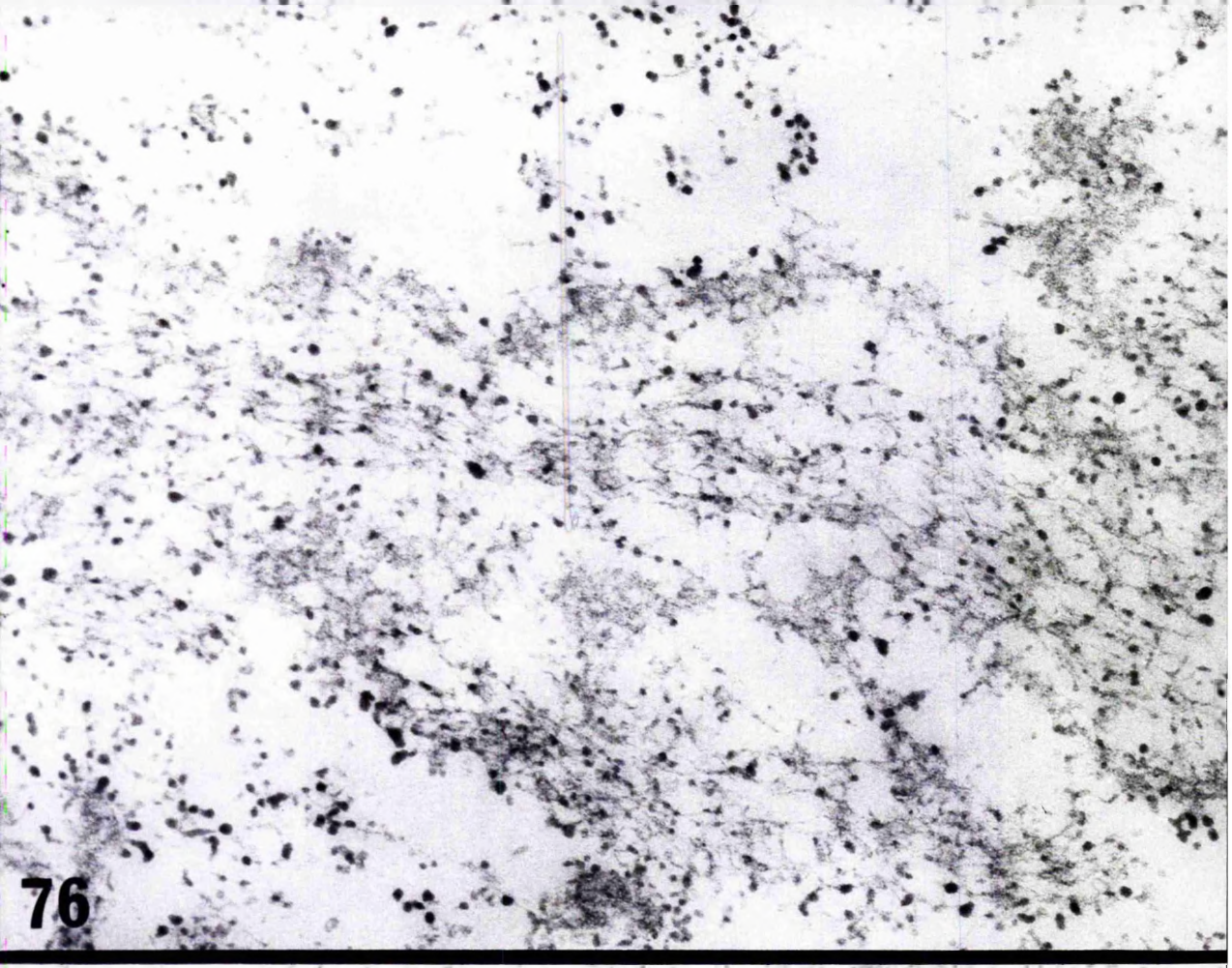
76


77

Figure 78. Banded fibre stained with phosphotungstic acid at low pH. x 36,000

Figure 79. Banded fibre. Phosphotungstic acid pH 0.5. x 50,000

Figure 80. Banded fibres. Bismuth nitrate and uranyl acetate. x 36,000

Figure 81. Banded fibre. Bismuth nitrate and uranyl acetate. x 50,000

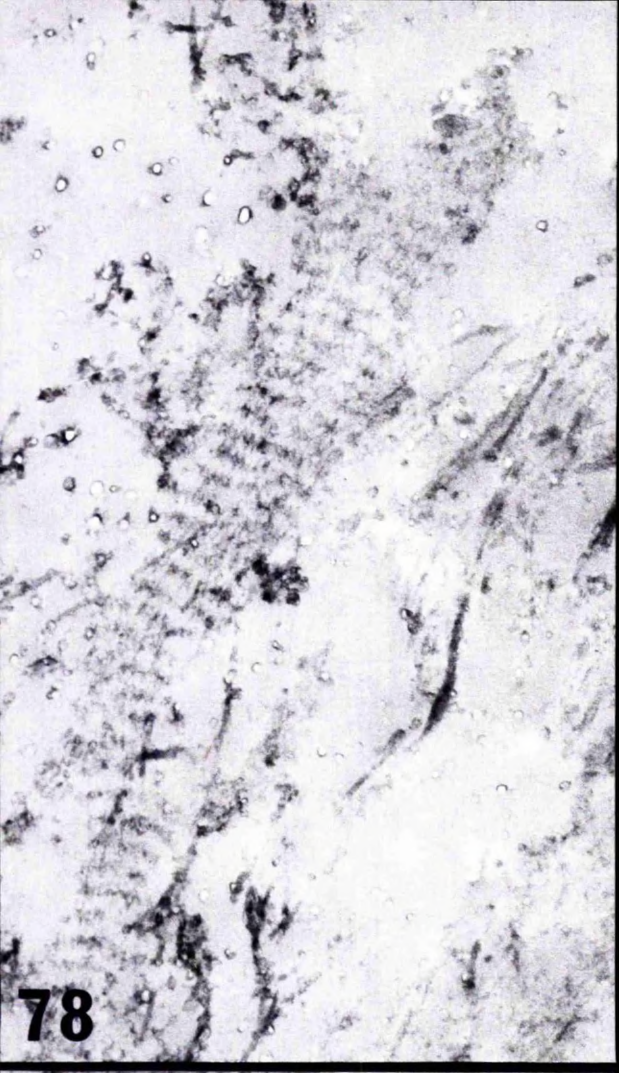
78

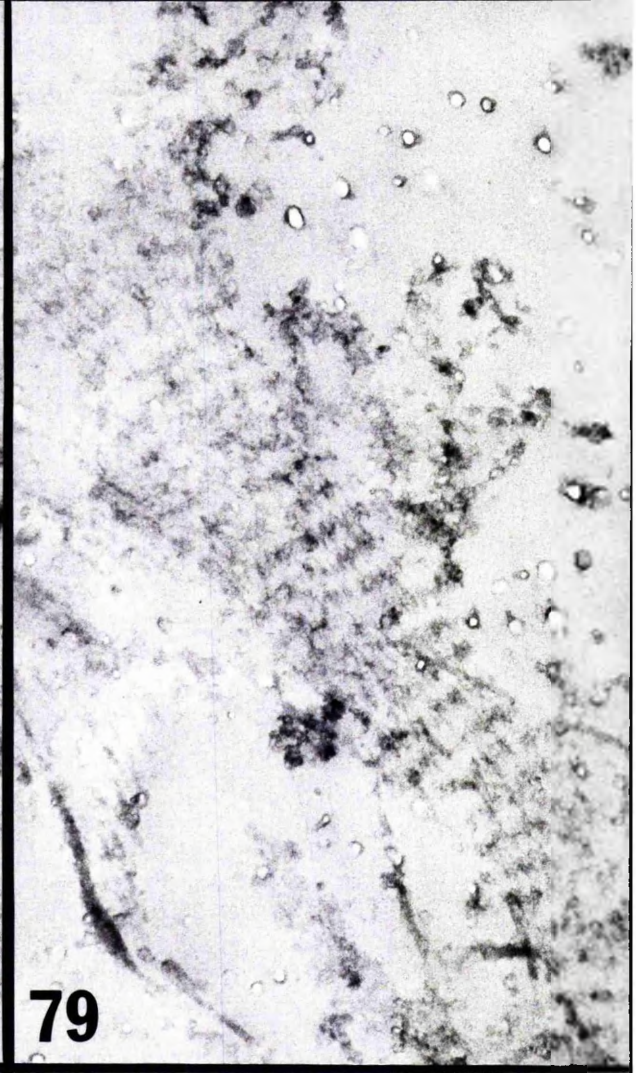
79

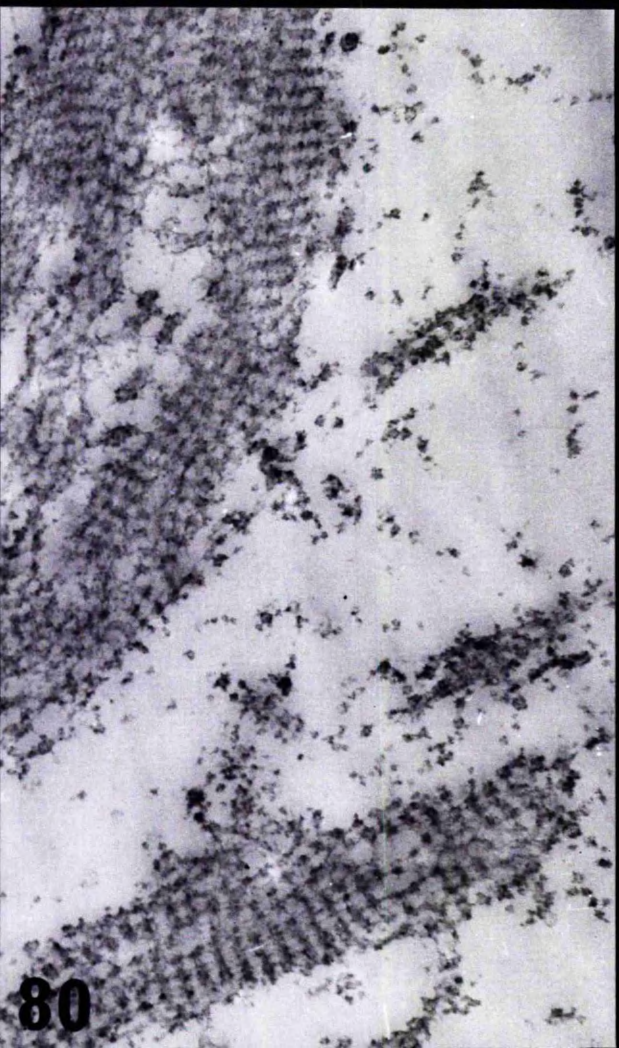
80

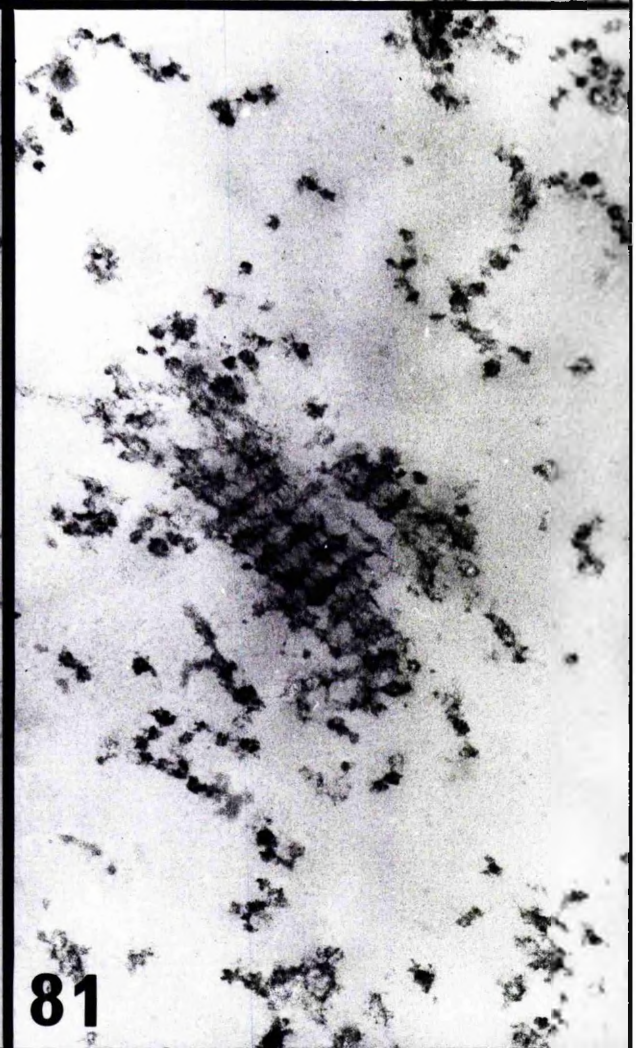
81

Figure 82. Banded fibre. Ruthenium red.

x 36,000

Figure 83. Banded fibre. Ruthenium red.

x 50,000

Figure 84. Banded fibre. Lanthanum treatment (Method I) x 55,000

Figure 85. Banded fibre seen after fixation in potassium permanganate and lanthanum nitrate (Method III) x 55,000


82


83

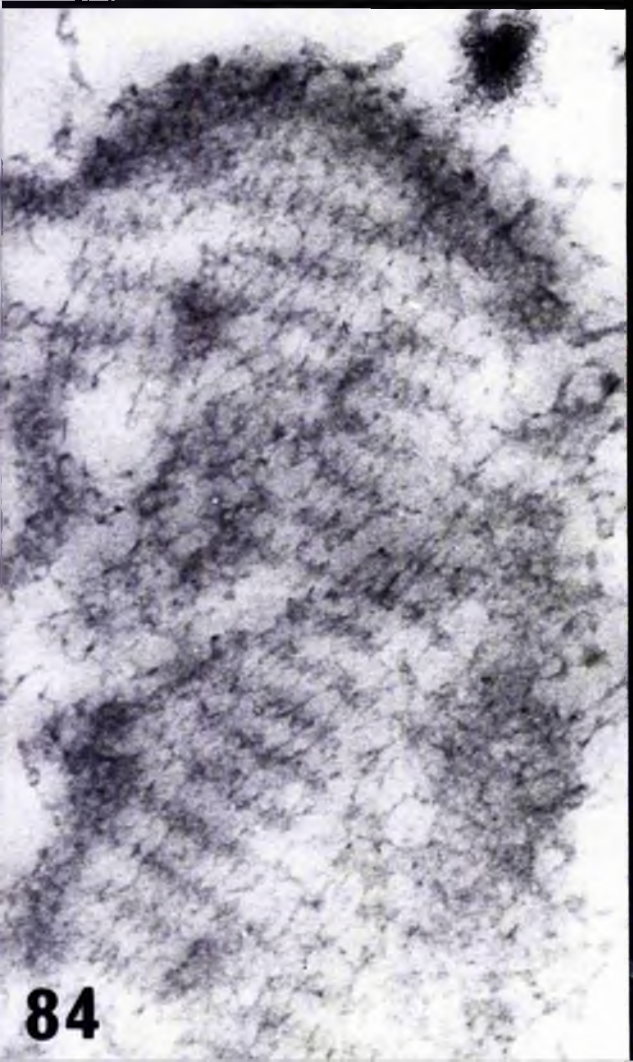
84

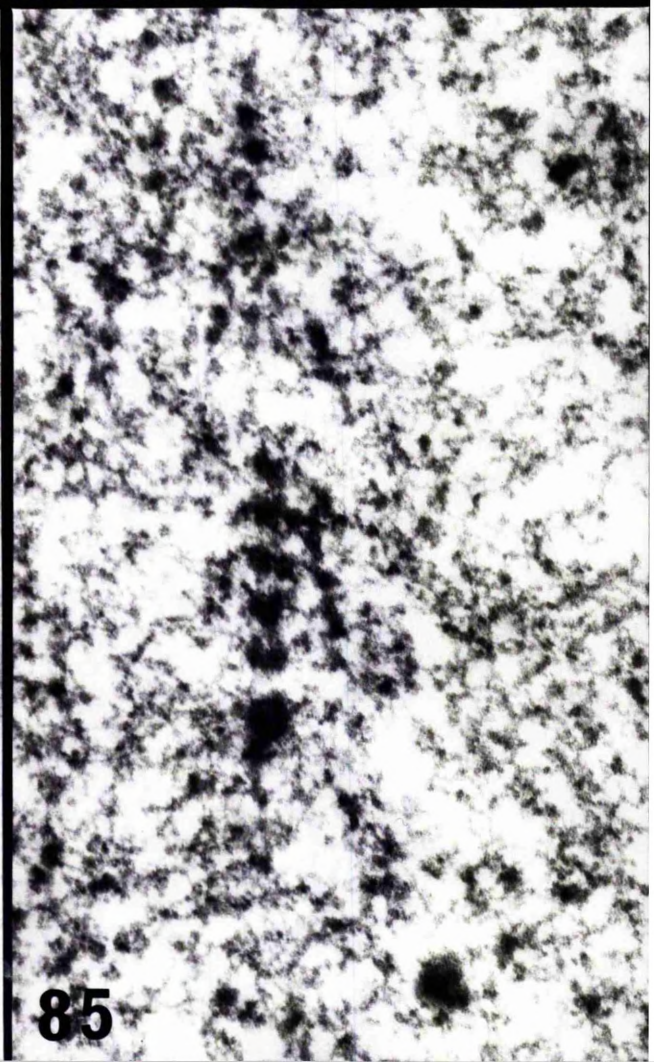
85

Figure 86. Electron dense material within extracellular matrix. x 13,000

Figure 86a, in which the structure is seen at higher magnification reveals the beaded filamentous material applied to the edge of the electron dense strips. x 35,000

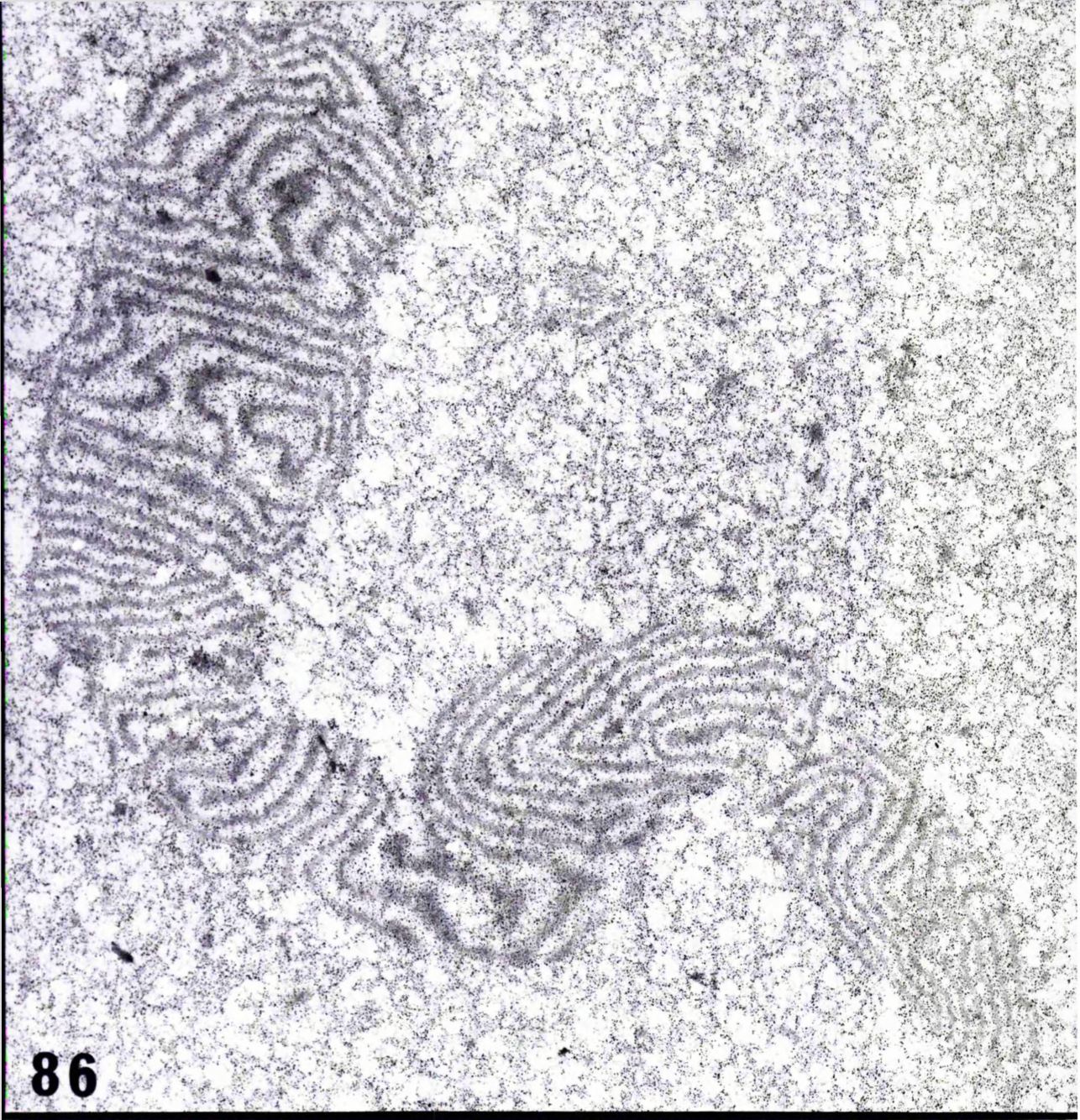
86

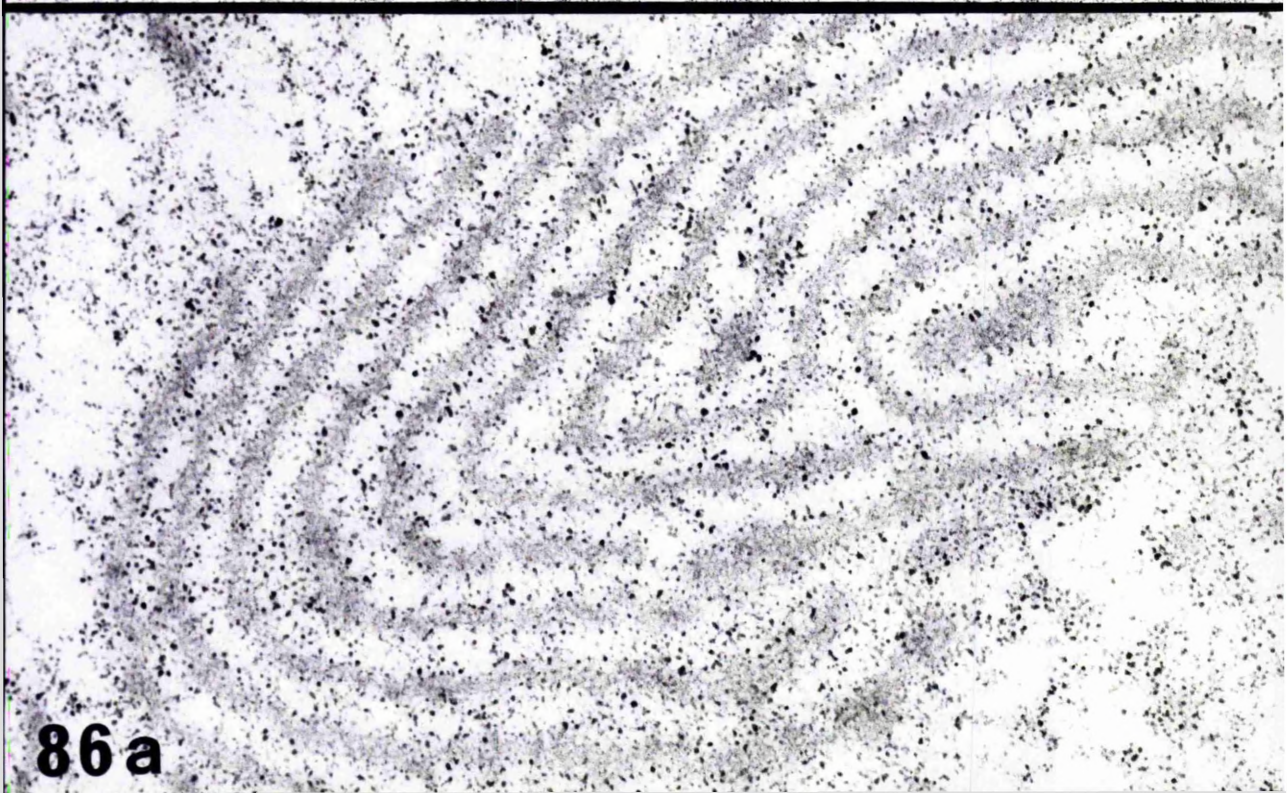
86a

Figure 87. Electron-dense strips in association with banded fibres. Lanthanum (Method I)

x 22,000

Figure 88. Electron-dense strips in association with the cell surface. Lanthanum (Method I)

x 22,000

87

88

Figure 89. Stellate particles within the extracellular matrix seen after conventional fixation and staining. x 100,000

Figure 90. Stellate particles seen after fixation in 1% OsO_4 in veronal acetate pH 7.4 and lead citrate and uranyl acetate staining of ultrathin sections. x 100,000

89

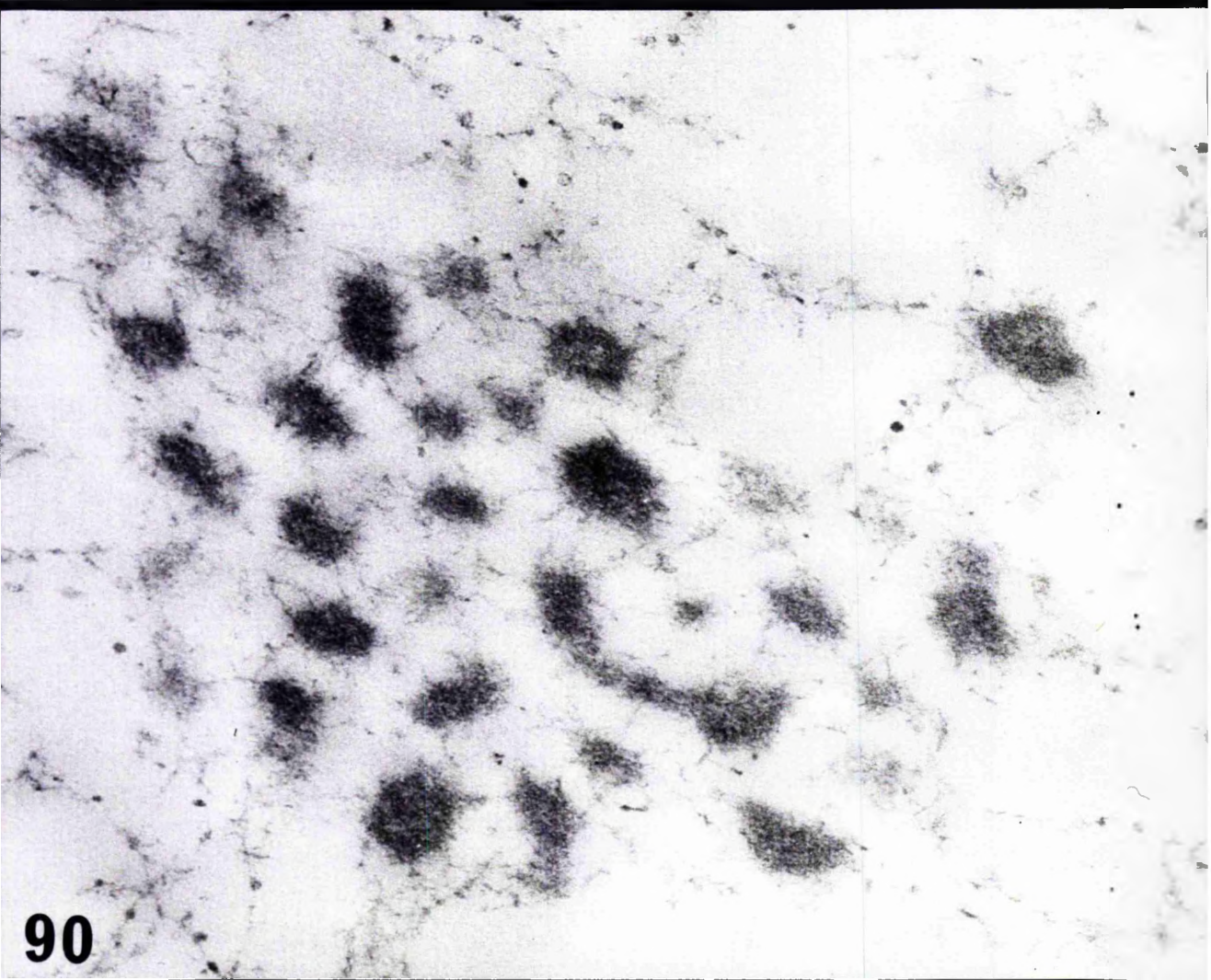

90

Figure 91. Stellate particles. Aldehyde fixed, unosmicated tissue stained on the grid with lead citrate and uranyl acetate. x 100,000

Figure 92. Stellate particles. Phosphotungstic acid pH 0.5. x 35,000

Figure 93. Stellate particles. Ruthenium red. x 35,000

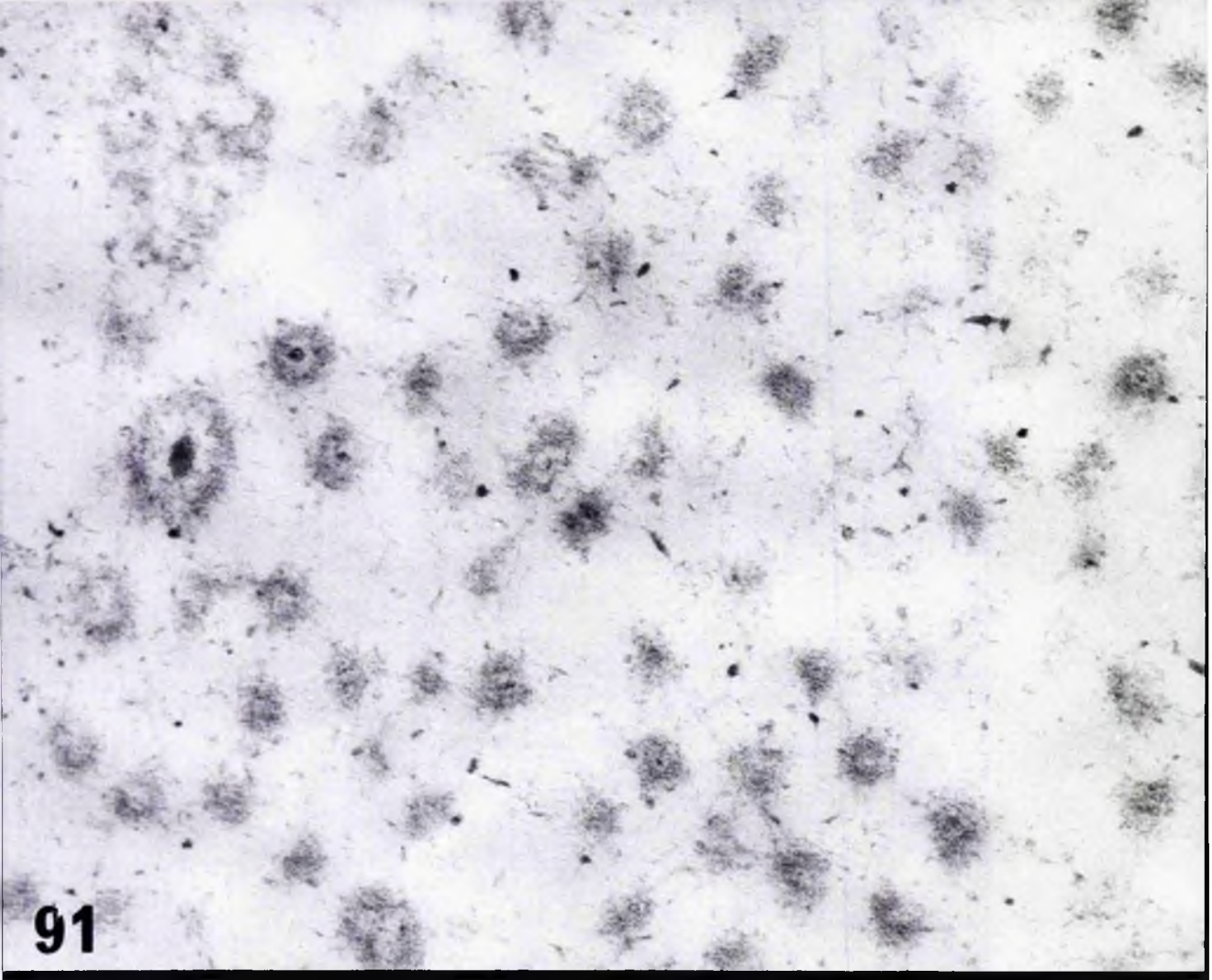
91

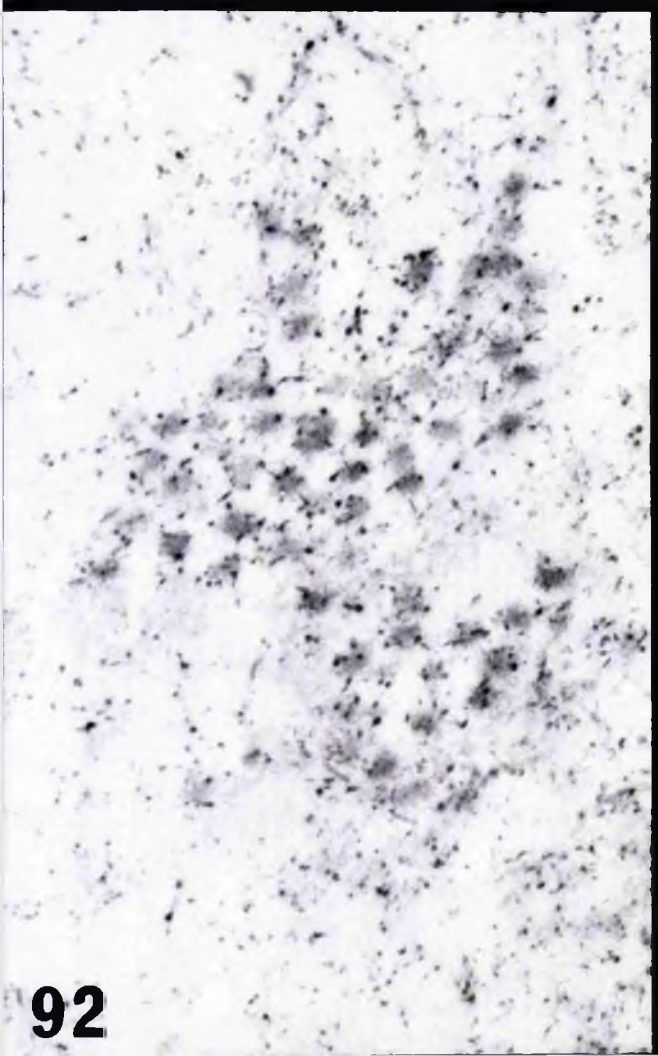
92

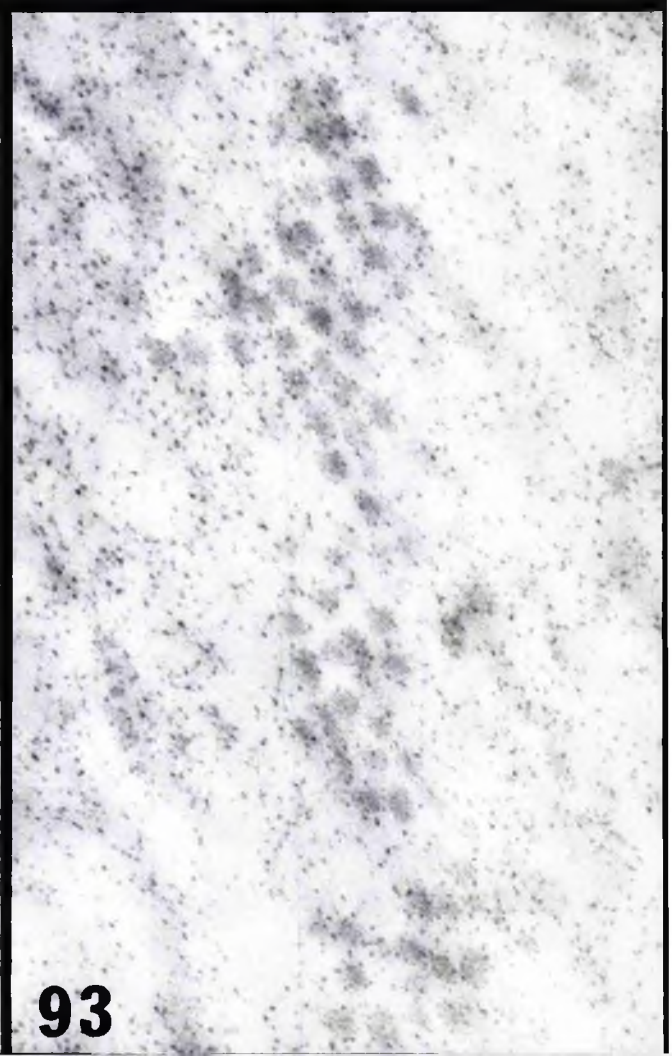
93

Figure 94. Electron-dense material free in the matrix and associated with the surface of a banded fibre. x 30,000

Figure 95. Strips of electron-dense material associated with the cell surface. Numerous pinocytotic vesicles open onto the cell surface in the vicinity of this material.

x 30,000

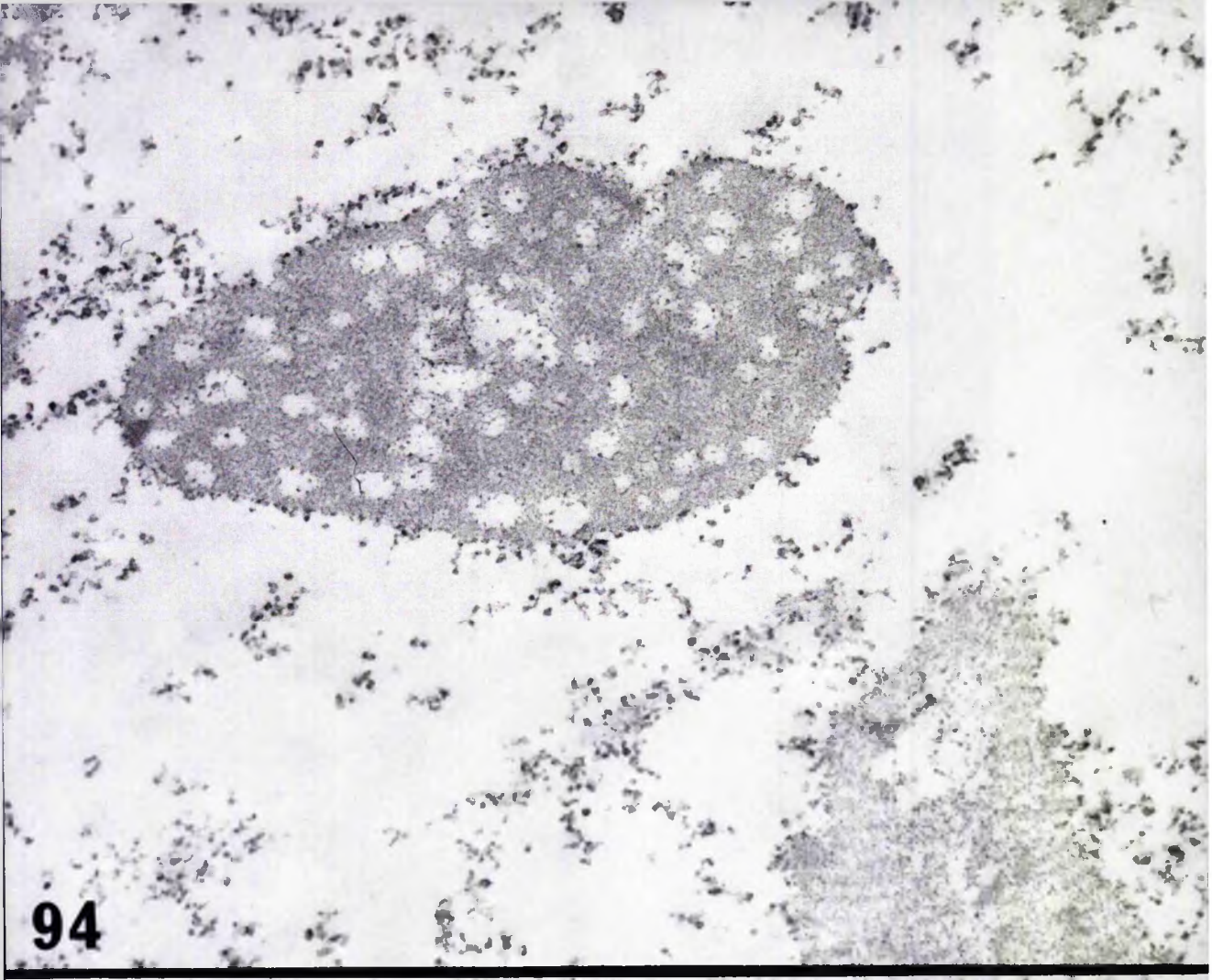
94

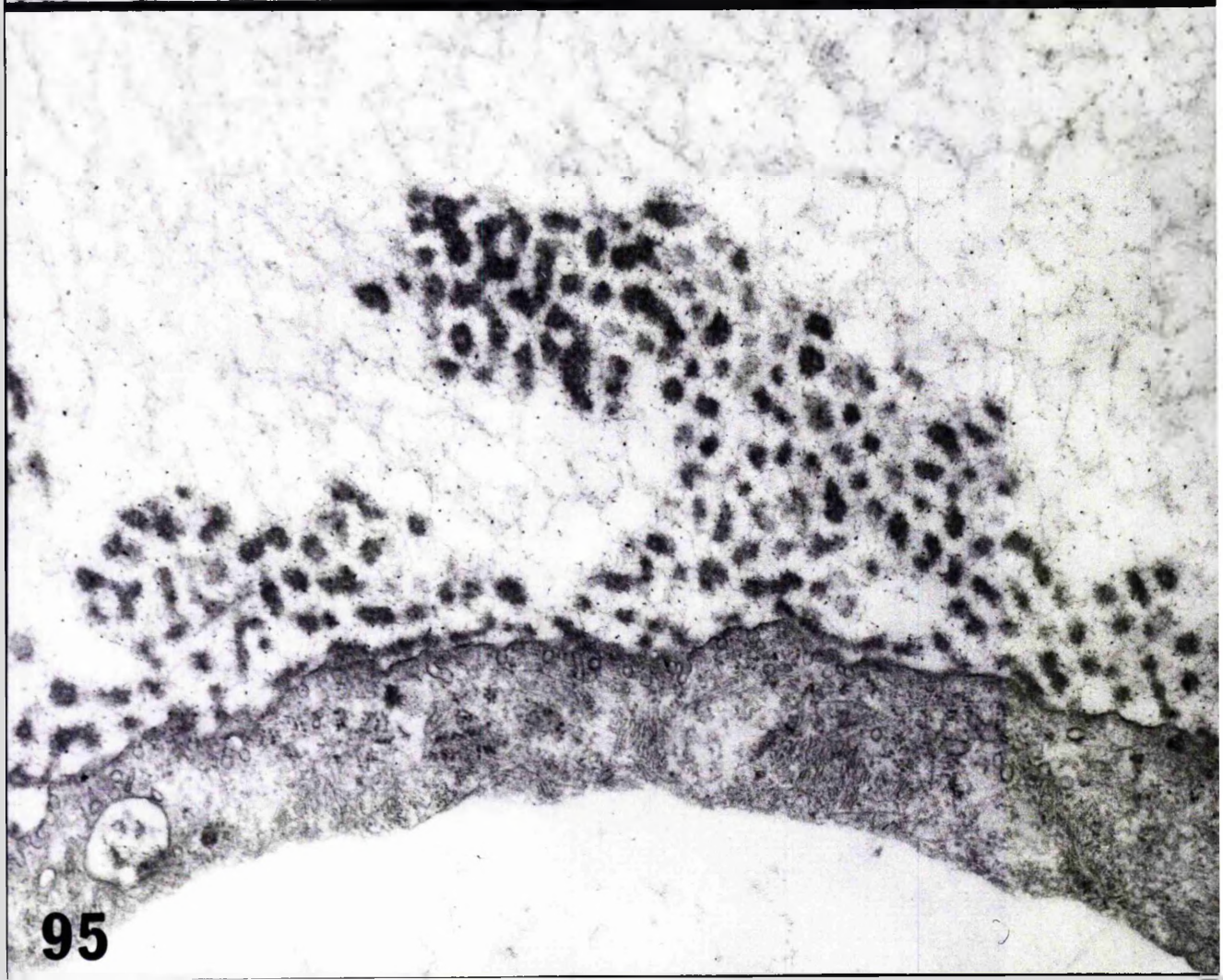
95

Figure 96. pH change during addition of 1% haematein to 25 ml. 1% indium nitrate.

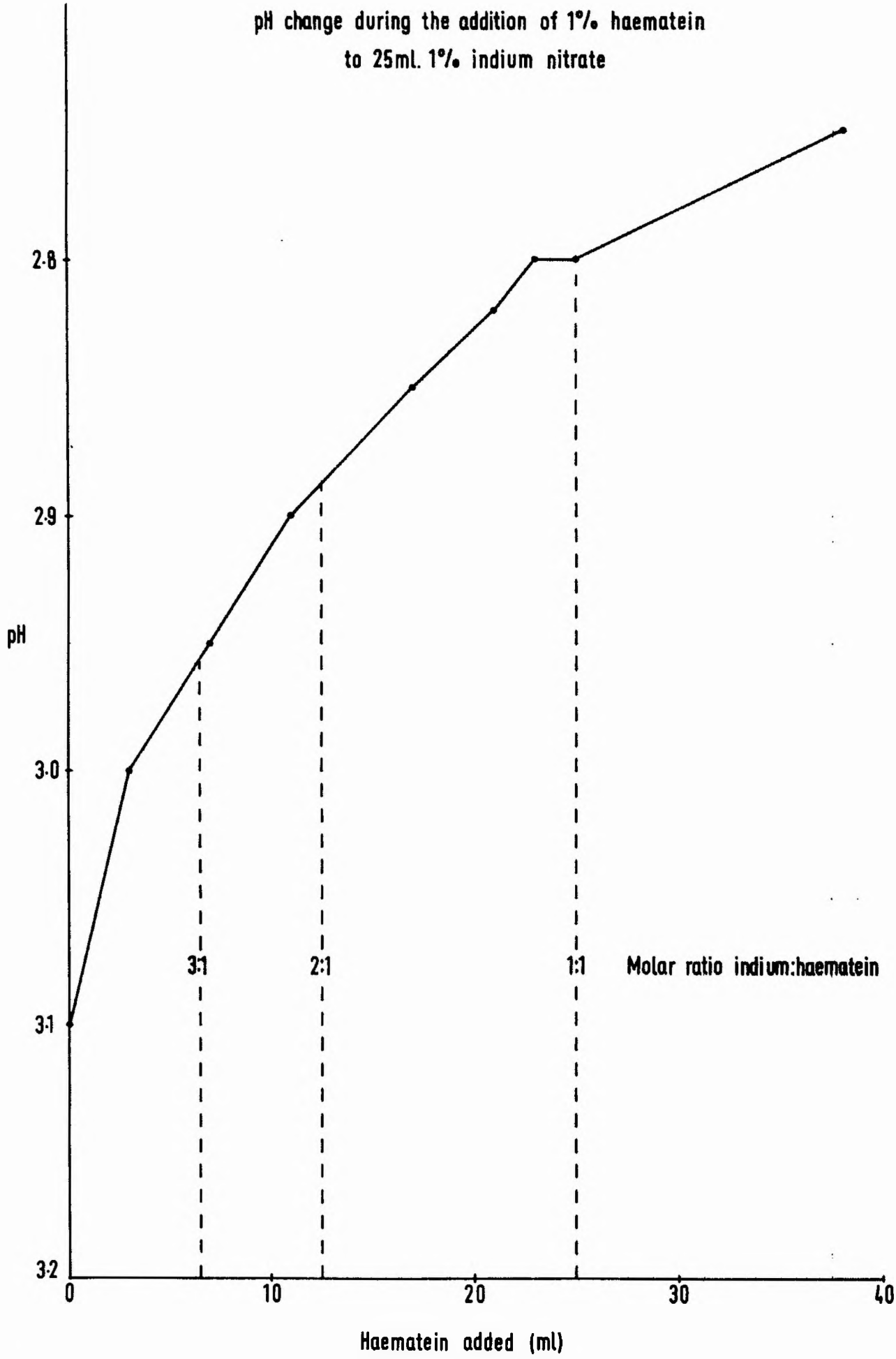
pH change during the addition of 1% haematein
to 25ml. 1% indium nitrate
2·8
2·9
pH
3·0
3·1
3·2
3:1
2:1
1:1
Molar ratio indium:haematein
0
10
20
30
40
Haematein added (ml)

Figure 97. Absorption spectra of 1% haematein (a) and 1% indium haematein (b).

Figure 98. The absorbence at 572 nm. of solutions containing different molar ratios of indium:haematein.

Absorption spectra of 1% haematein (a) and 1% indium haematein (b).

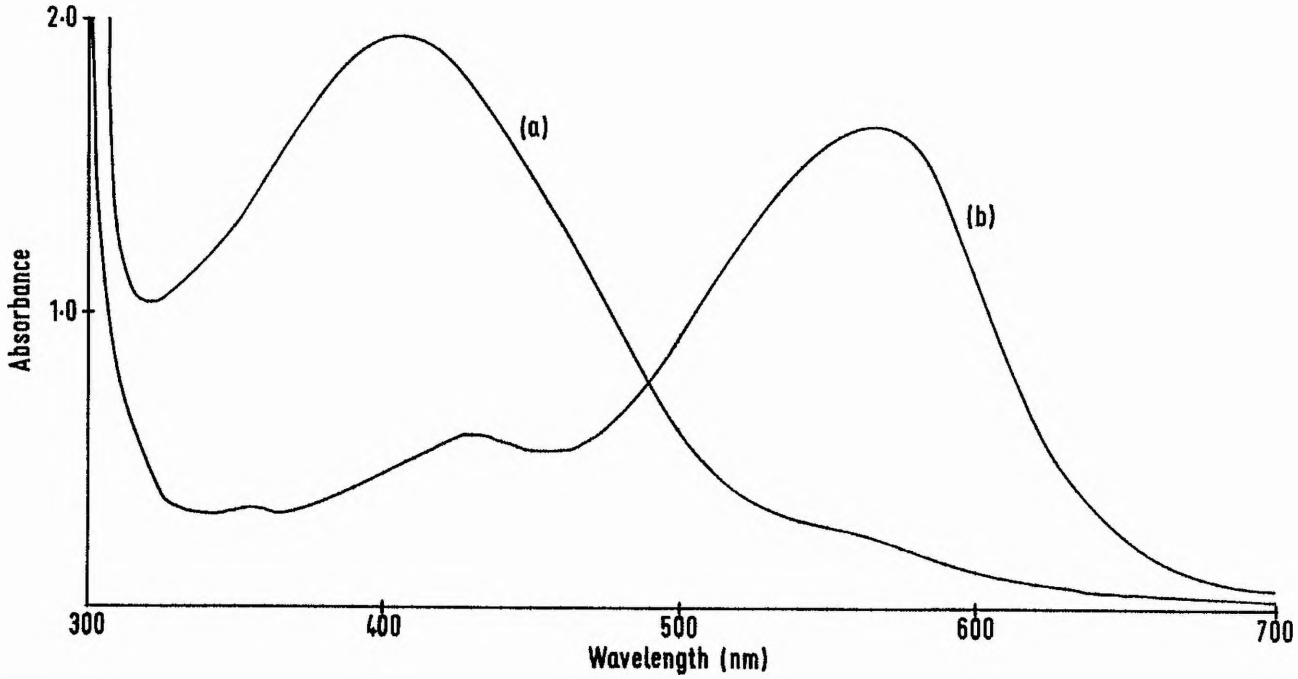

97

The absorbance at 572nm of solutions containing different molar ratios of indium:haematein

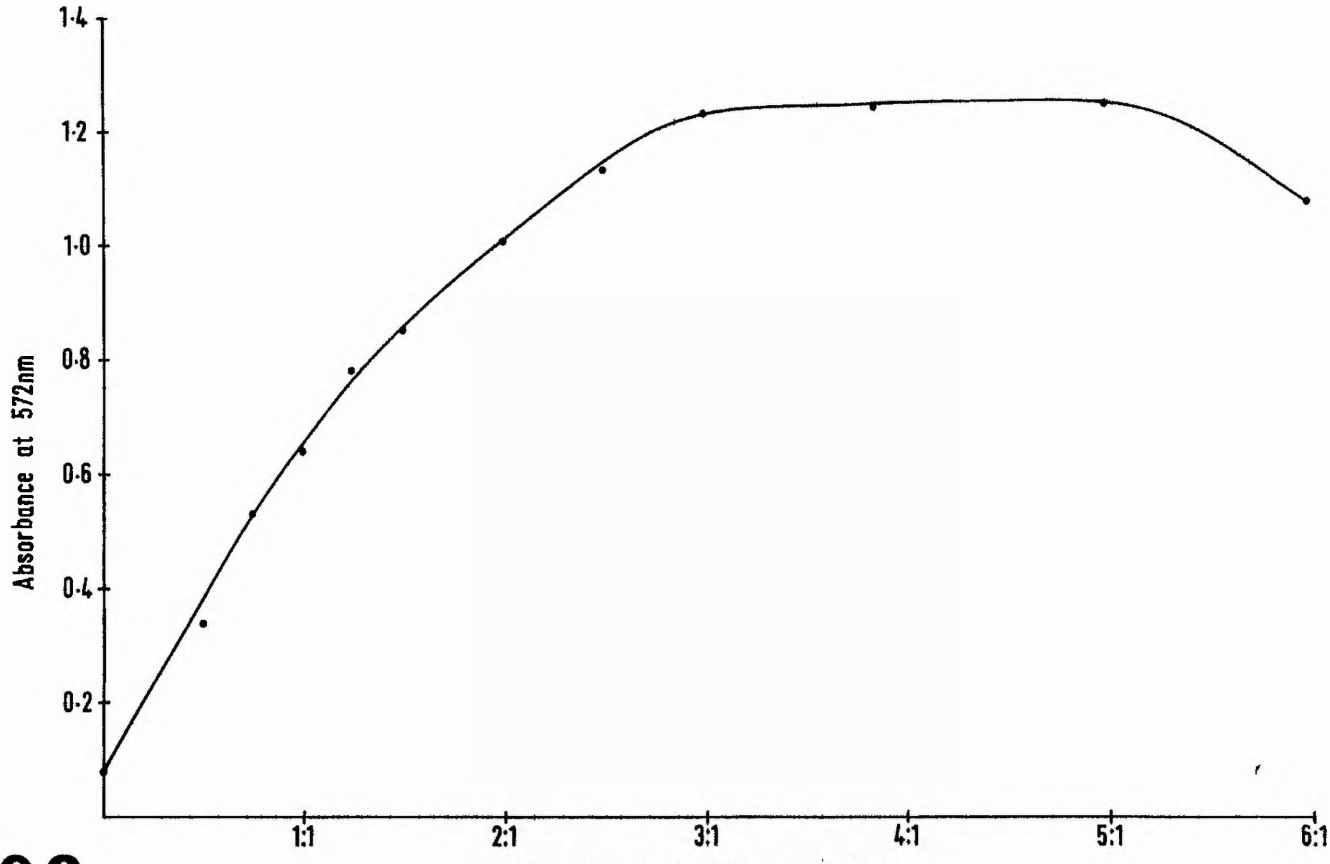

98

Figure 99. Filter papers spotted with polyanion solutions and stained in 0.01% indium haematein solutions containing varying molarities of magnesium chloride up to 3.4M. The papers were stained in the dark at 0°C for 16 hrs.

Alginate
Xylan
Chondroitin sulphate
Pectin
Gelatin
Milk
DNA
BSA
Alginate
Xylan
Chondroitin sulphate
Pectin
Gelatin
Milk
DNA
BSA

Figure 100 a) Collagen fibre. Lead citrate and uranyl acetate. x 150,000

b) Unstained collagen fibre. x 150,000

c) Collagen fibre stained with indium haematein + 0.2M $MgCl_2$ pH 4.6 x 150,000

d) Collagen fibre. Indium haematein + 1.0M $MgCl_2$ pH 4.6. x 150,000

e) Collagen fibre. Indium haematein + 2.6M $MgCl_2$ pH 4.6. x 150,000

f) Collagen fibre. Indium haematein + 3.0M $MgCl_2$. pH 4.6. x 150,000

g) Collagen fibre. Indium haematein + 3.8M $MgCl_2$. pH 4.6. x 150,000

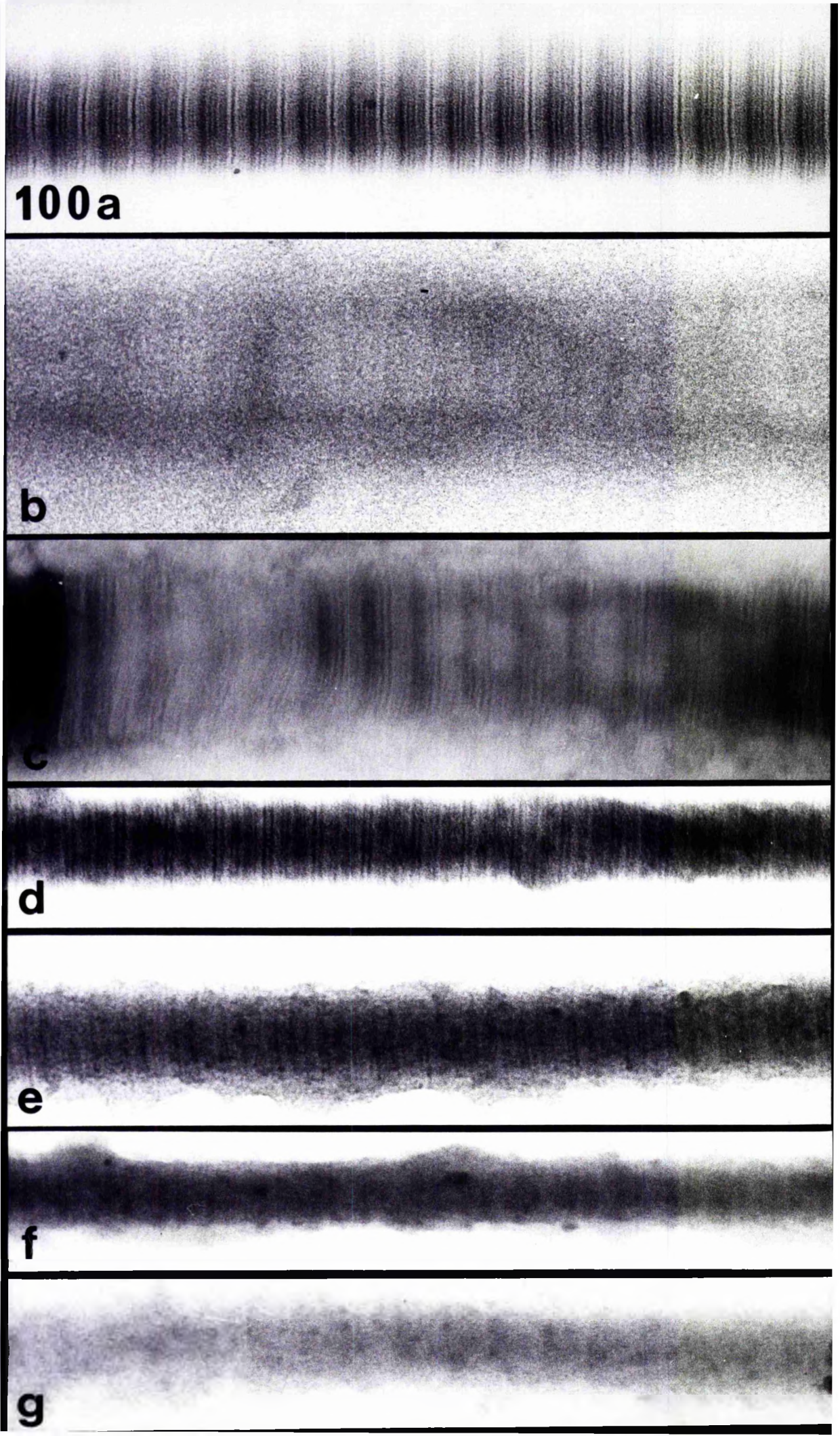
100a
b
c
d
e
f
g

Figure 101. Unstained unosmicated pancreas

x 7,000

Figure 102. Unosmicated pancreas stained in 0.25% indium haematein + 0.2M $MgCl_2$, pH 4.6

x 7,000

Figure 103. Unosmicated pancreas stained in 0.25% indium haematein + 3.0M $MgCl_2$, pH 4.6

x 7,000

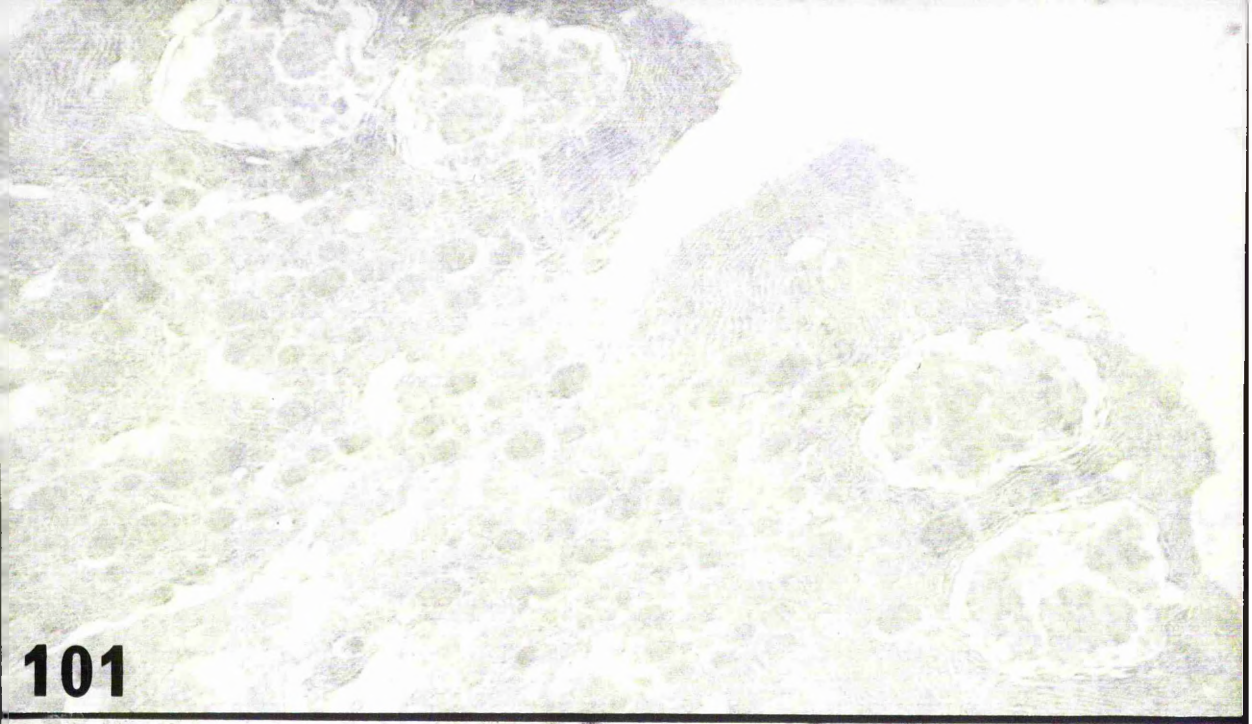
101

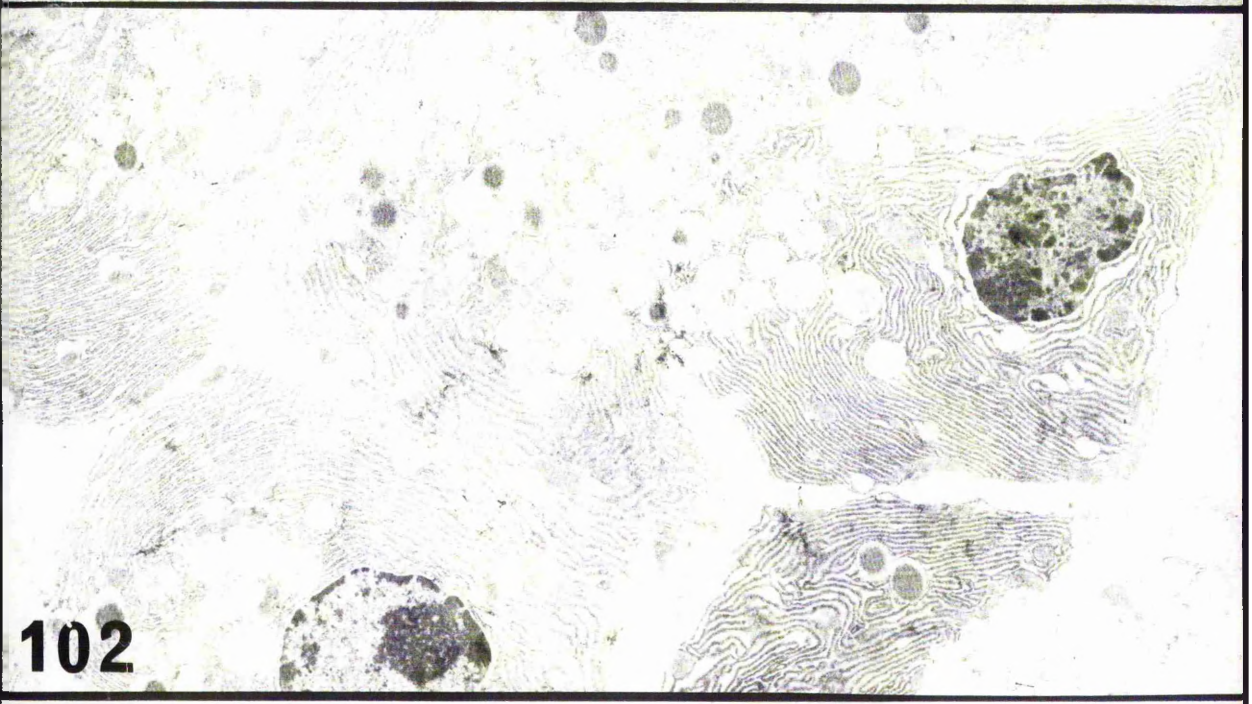
102

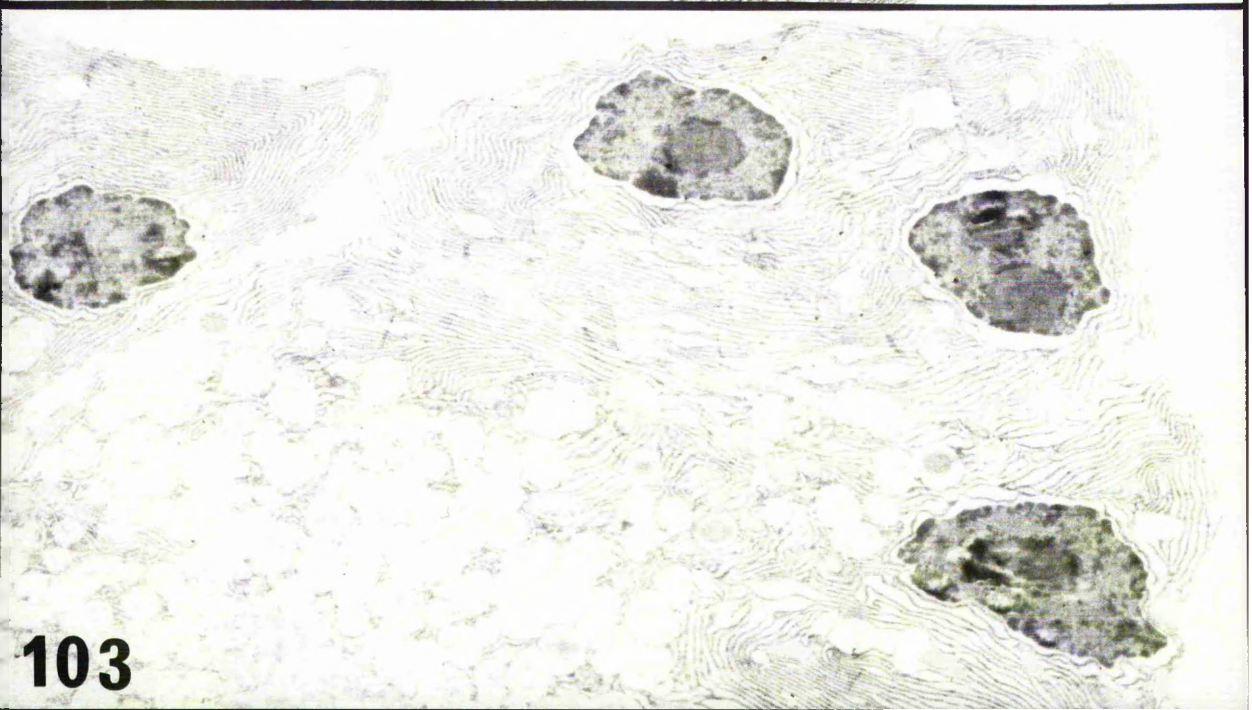
103

Figure 104. Endoplasmic reticulum of a pancreatic acinar cell. Indium haematein + 1.0M $MgCl_2$, pH 4.6

x 111,500

Figure 105. Zymogen granules within a pancreatic acinar cell. Indium haematein + 1.0M $MgCl_2$, pH 4.6

x 28,000

Figure 106. Endoplasmic reticulum of a pancreatic acinar cell. Indium haematein + 1.4M $MgCl_2$, pH 4.6

x 111,500

Figure 107. Zymogen granules within a pancreatic acinar cell. Indium haematein + 1.4M $MgCl_2$, pH 4.6.

x 28,000


104

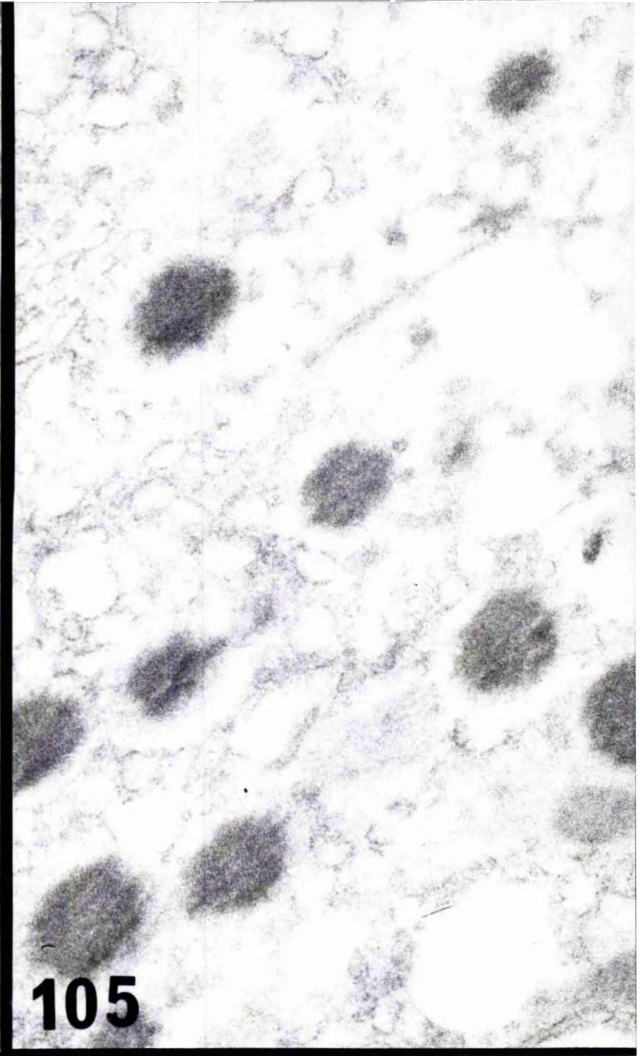
105

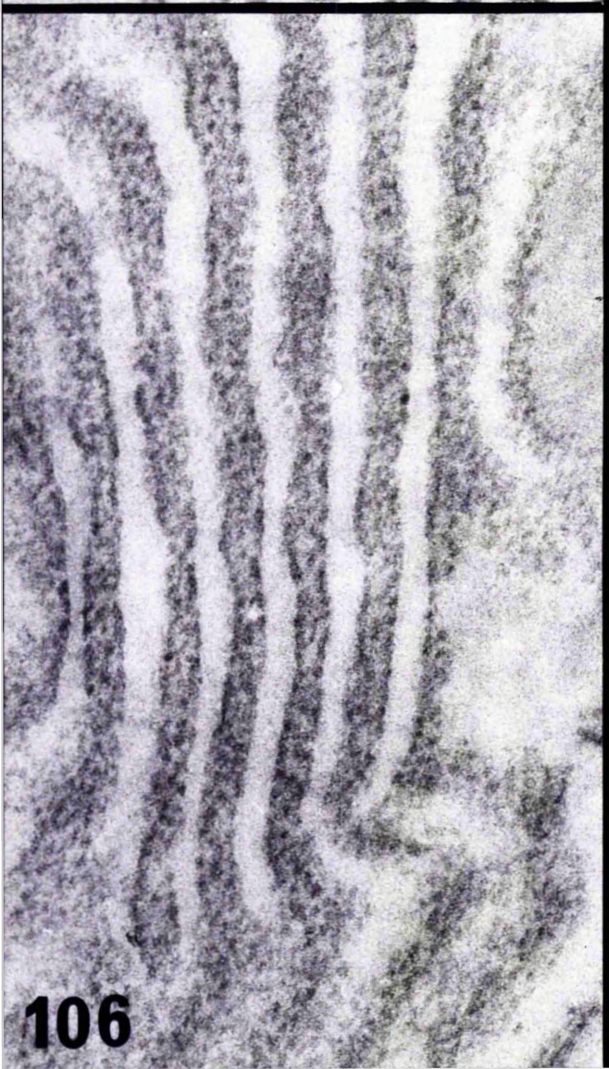
106

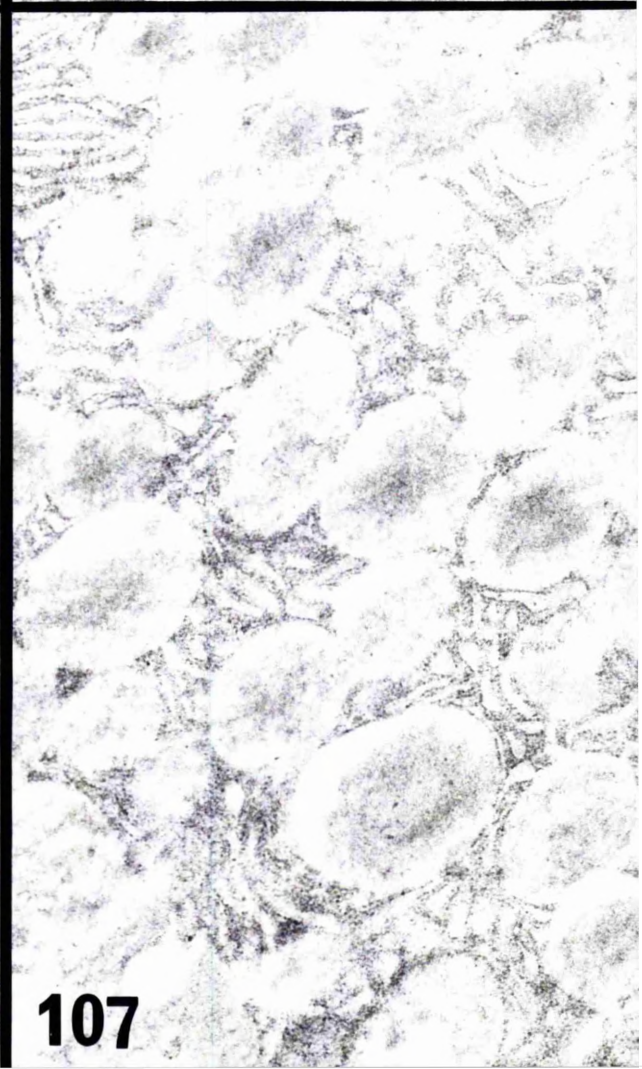
107

Figure 108. Unstained unosmicated nucleus pulposus

x 4,000

Figure 109. Unosmicated nucleus pulposus stained with indium haematein + 0.2M $MgCl_2$ pH 4.6.

x 4,000

Figure 110. Unosmicated nucleus pulposus stained with indium haematein + 2.6M $MgCl_2$. pH 4.6.

x 4,000

108

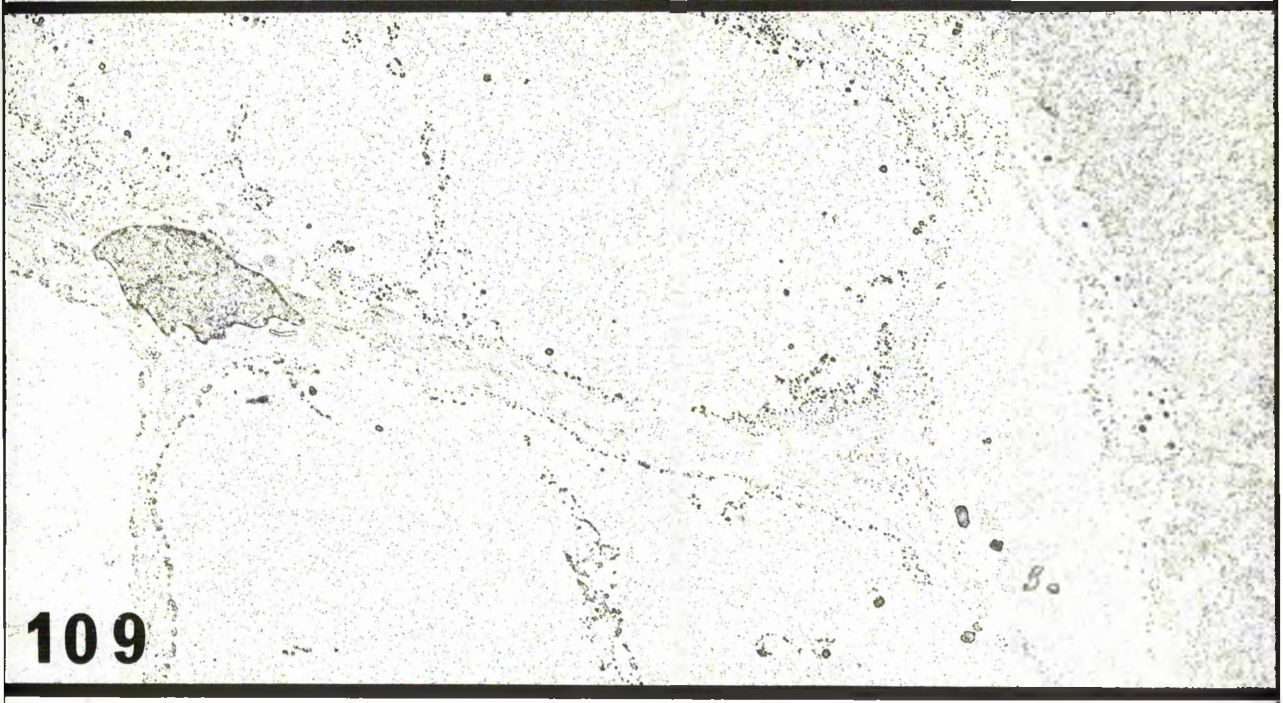

109

110

Figure 111. Unosmicated nucleus pulposus stained with indium haematein + 0.2M $MgCl_2$. pH 4.6.

x 15,000

Figure 112. Unosmicated nucleus pulposus stained with indium haematein + 0.6M $MgCl_2$. pH 4.6.

x 15,000

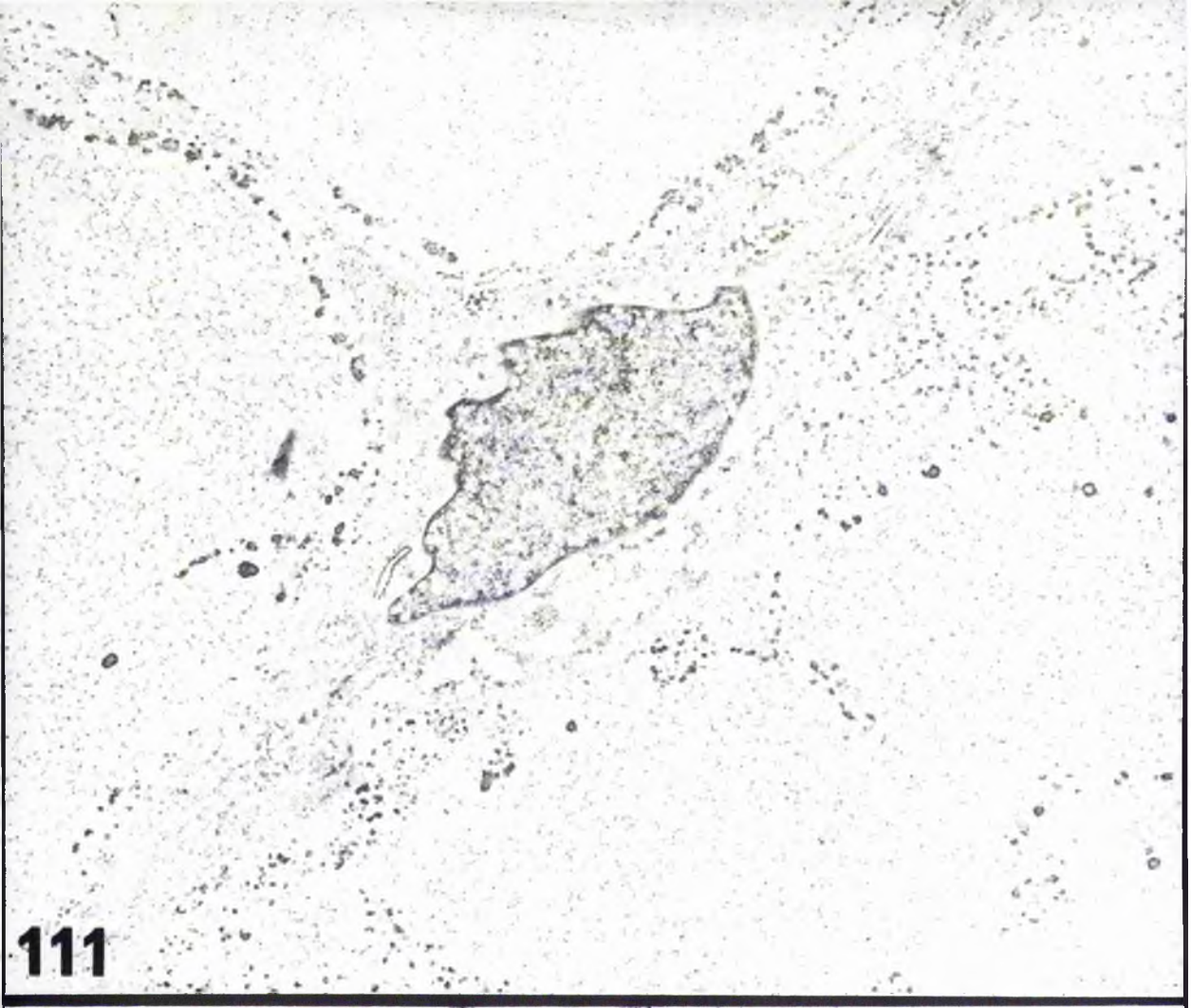
111

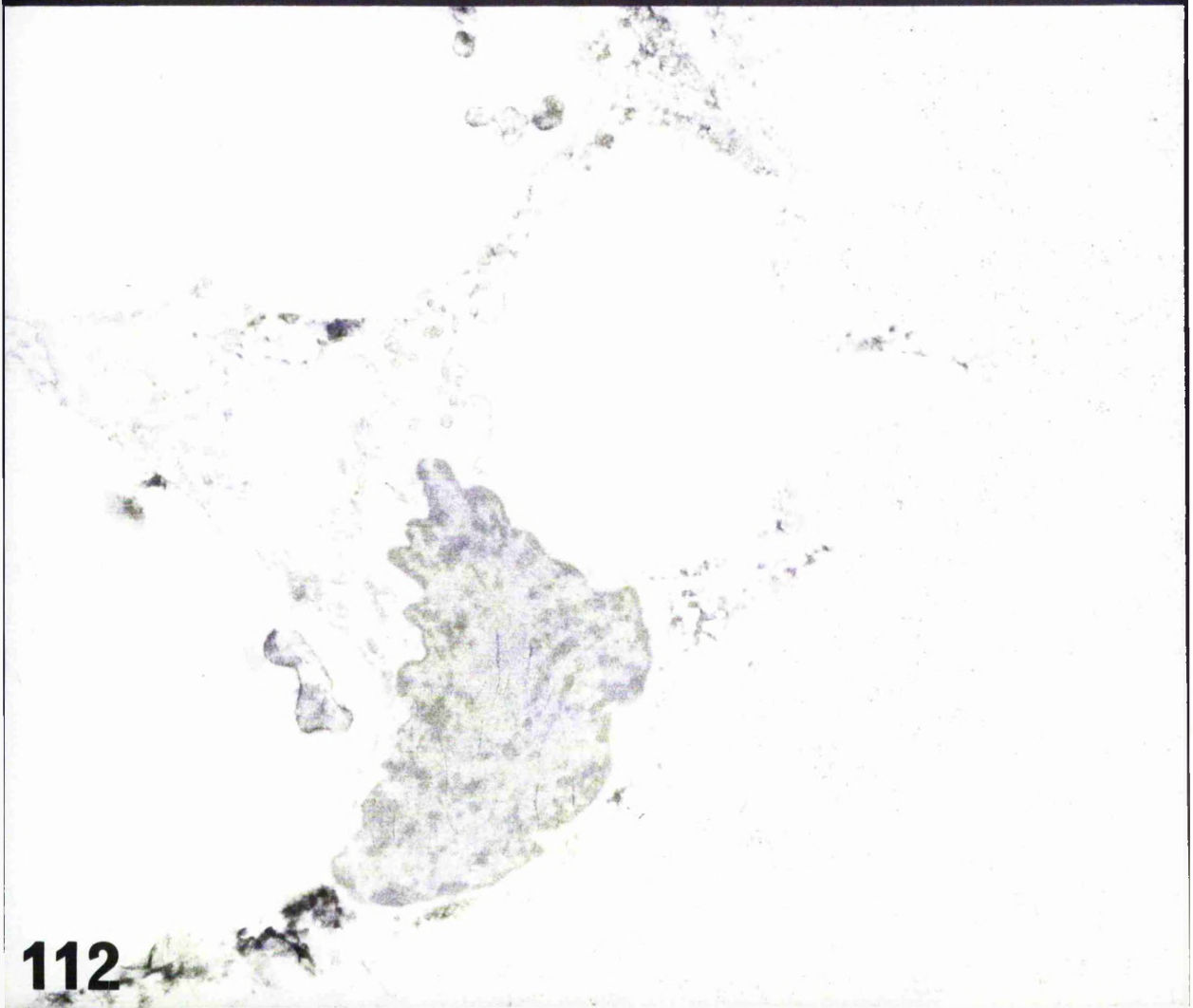
112

Figure 113. Edge of a notochordal cell containing large vesicle (v). Unosmicated tissue stained on the grid with indium haematein + 0.2M $MgCl_2$, pH 4.6.

x 20,000

Inset a) shows appearance of contents of large vesicle. x 35,000

Figure 114. Edge of notochordal cell containing a large vesicle. Note absence of vesicle staining and reduced staining of extracellular matrix material. Indium haematein + 1.0M $MgCl_2$, pH 4.6.

x 20,000

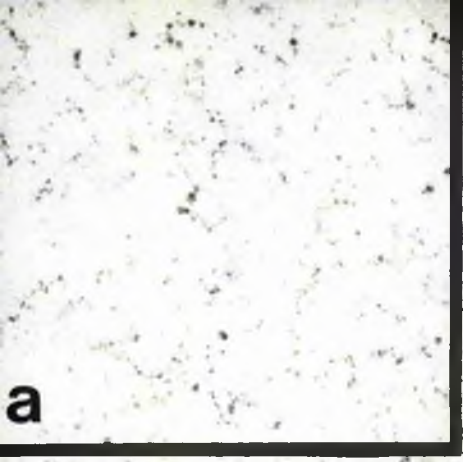

a

113

114

Figure 115. Banded fibre. Unosmicated tissue stained with indium haematein pH 4.6 without added magnesium chloride. x 25,000

Figure 116. Banded fibre. Unosmicated tissue stained with indium haematein + 1.4M $MgCl_2$. pH 4.6. x 25,000

Figure 117. Banded fibre and electron dense parallel strips near the cell surface. Unosmicated tissue stained with indium haematein + 2.0M $MgCl_2$ pH 4.6. x 20,000

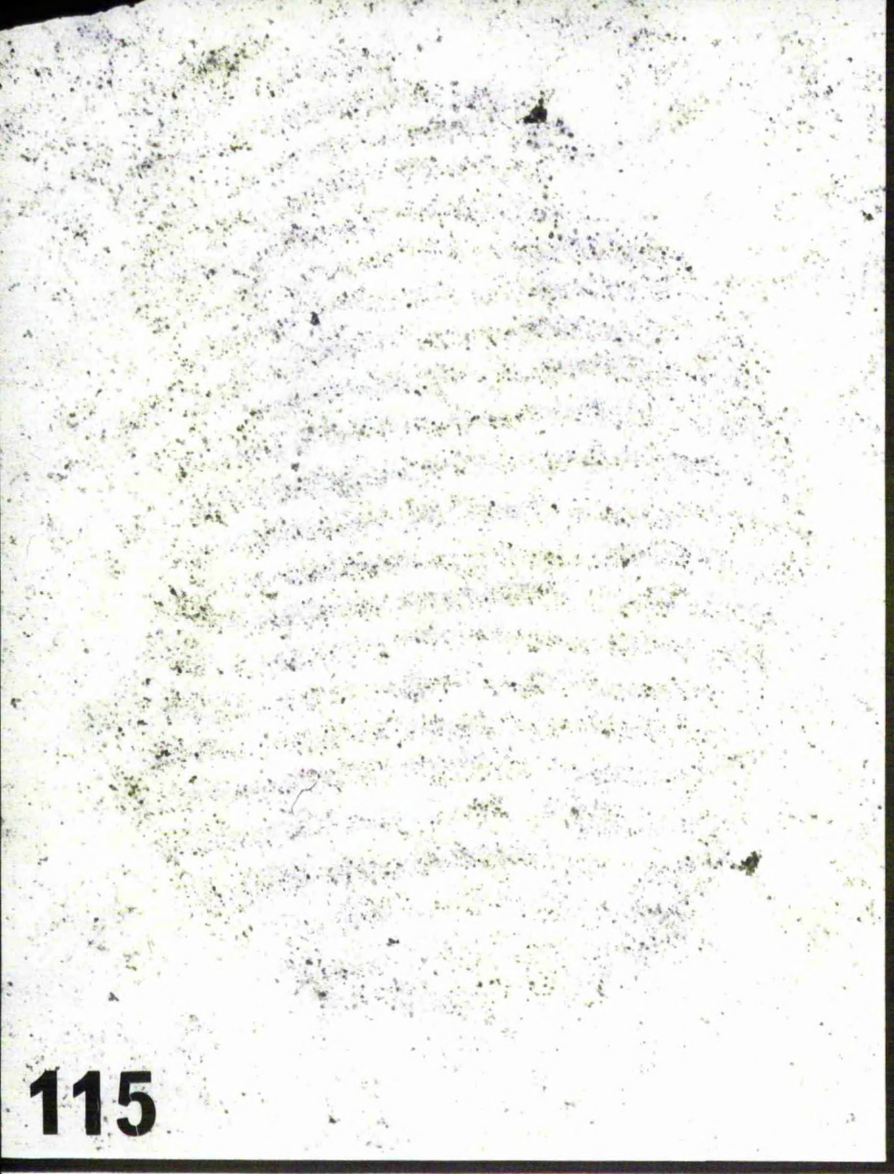
115

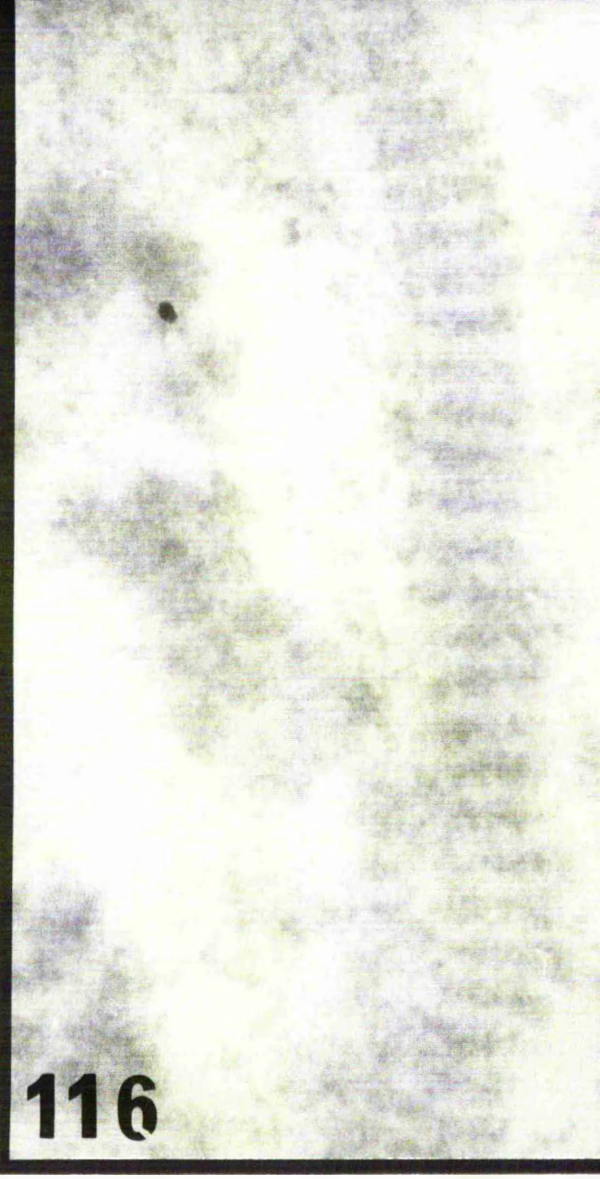
116


117

Figure 118. Parallel electron-dense strips in the matrix. Unosmicated tissue stained with indium haematein + 0.2M $MgCl_2$. pH 4.6.

x 25,000

Figure 119. Stellate particles within the matrix. Unosmicated tissue stained with indium haematein + 0.2M $MgCl_2$, pH 4.6. x 25,000

Figure 120. Stellate particles within the matrix. Unosmicated tissue stained with indium haematein + 1.0M $MgCl_2$, pH 4.6. x 25,000

118

119

120

Figure 121. Chondrocyte of rabbit articular cartilage. Iron haematein pH 1.0. x 10,000

Figure 122. Rabbit articular cartilage matrix. Iron haematein pH 1.0. x 84,000

121

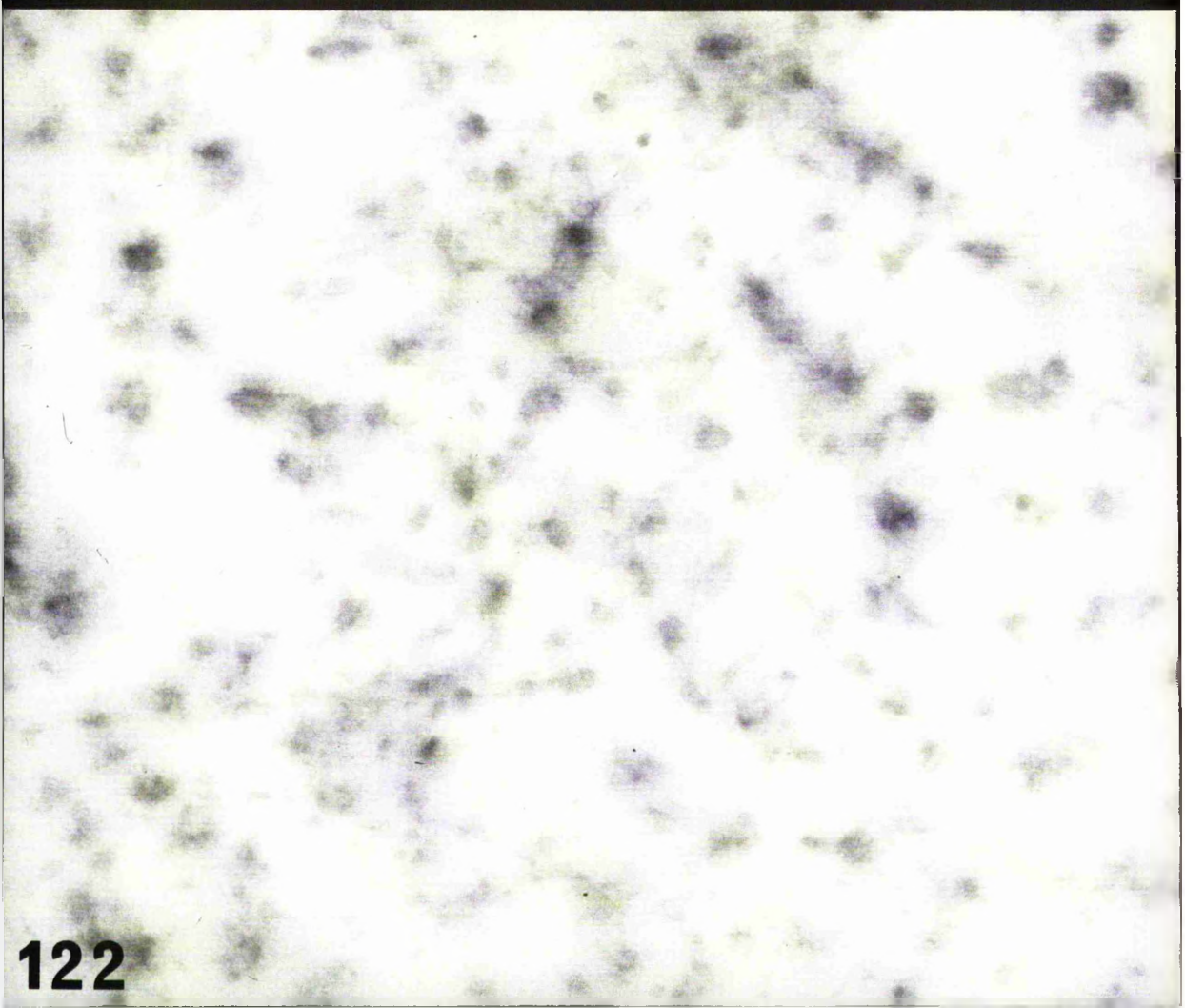

122

Figure 123. Electron-dense masses within the matrix. Iron haematein pH 1.0. x 10,000

Figure 124. Banded fibre. Iron haematein, pH 1.0. x 33,000

Figure 125. Banded fibre. Iron haematein, pH 1.8. x 10,000

Figure 126. Electron-dense masses. Iron haematein, pH 1.8. x 33,000

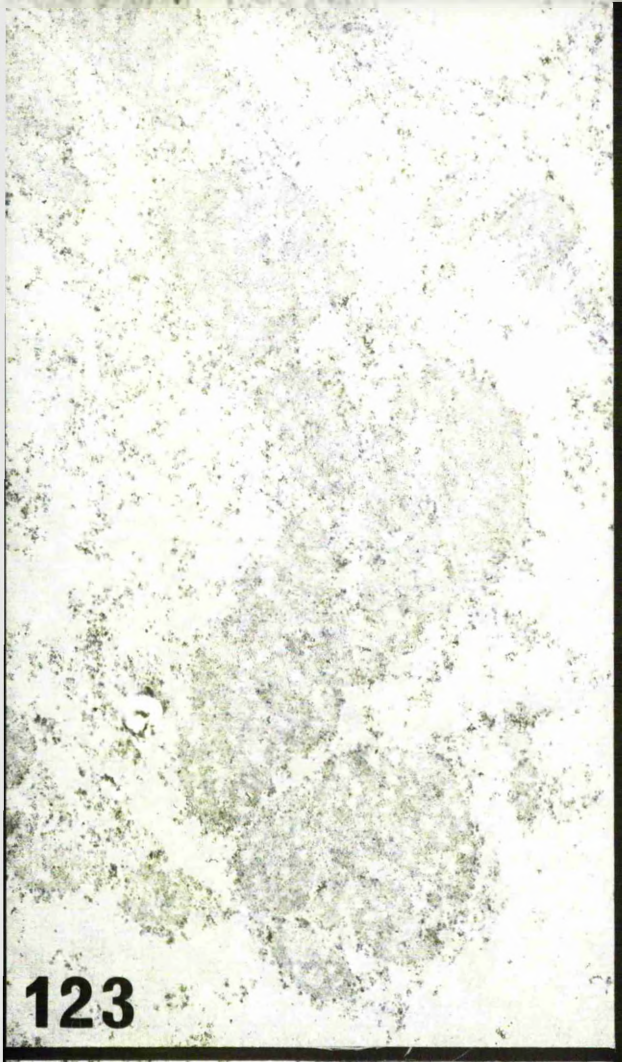
123

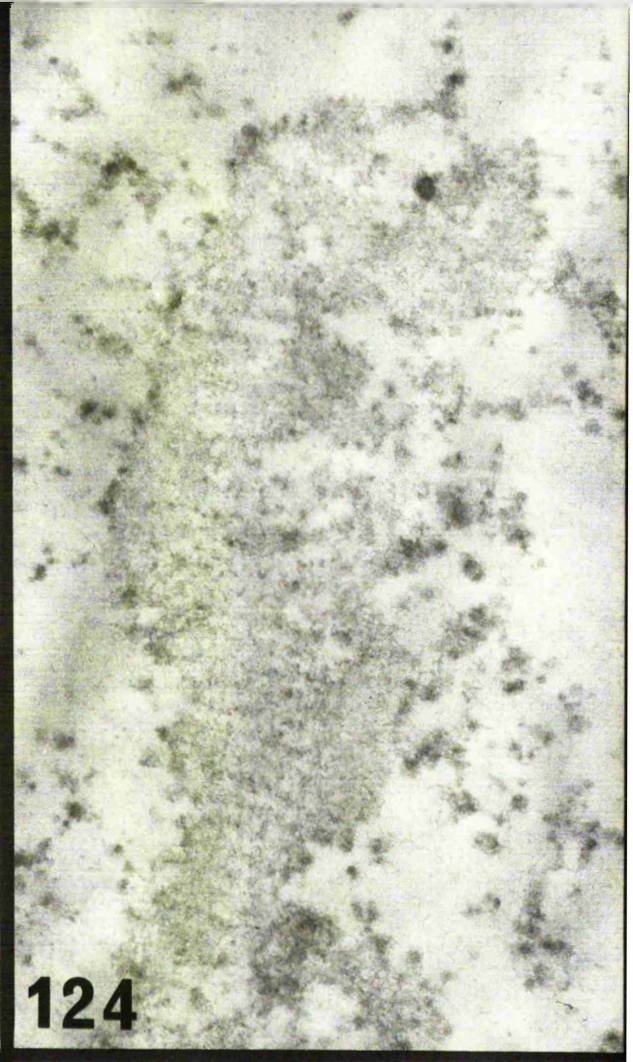
124

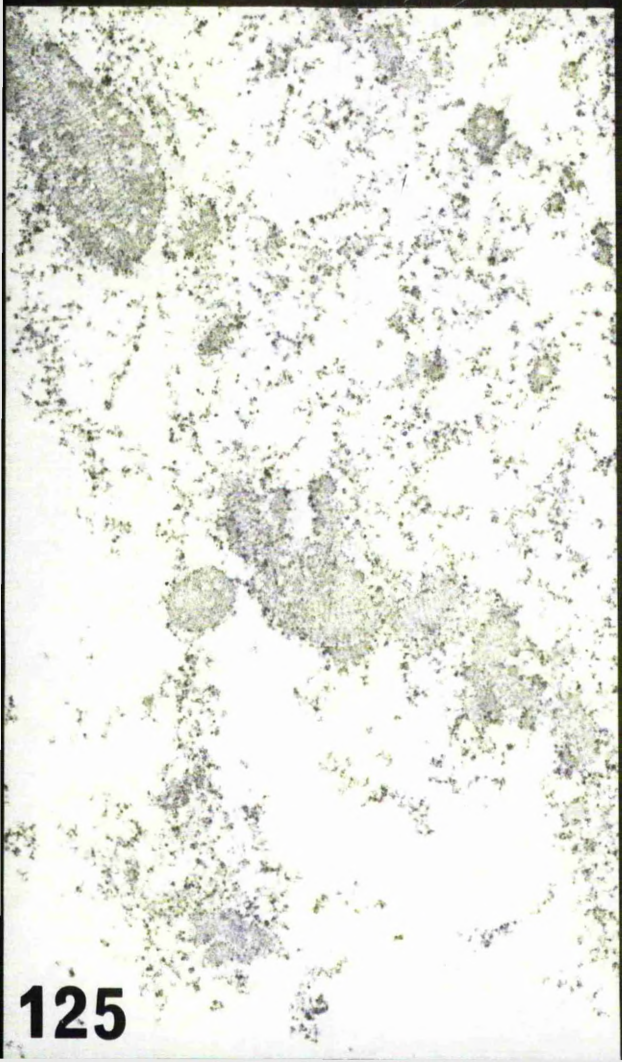
125

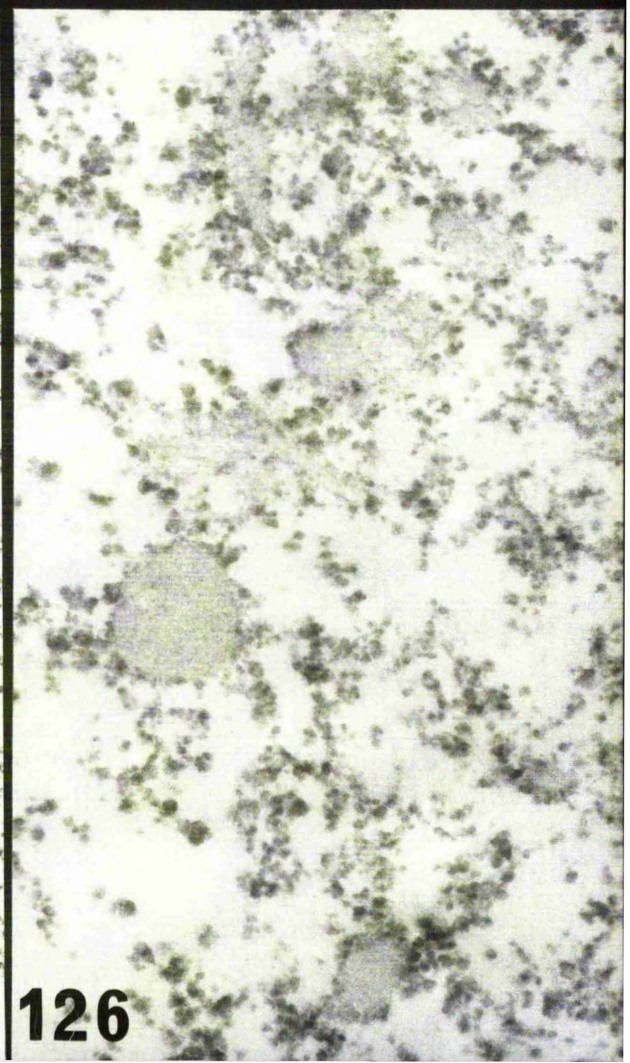
126

Figure 127. Banded fibre. Lead haematein, pH 3.0. x 33,000

Figure 128. Electron-dense masses. Lead haematein, pH 3.0. x 33,000

Figure 129. Banded fibre. Staining solution had a lead:haematein molar ratio of 0.4:1.0. x 33,000

Figure 130. Banded fibre. Staining solution had a lead:haematein molar ratio of 6.8:1.0. x 33,000

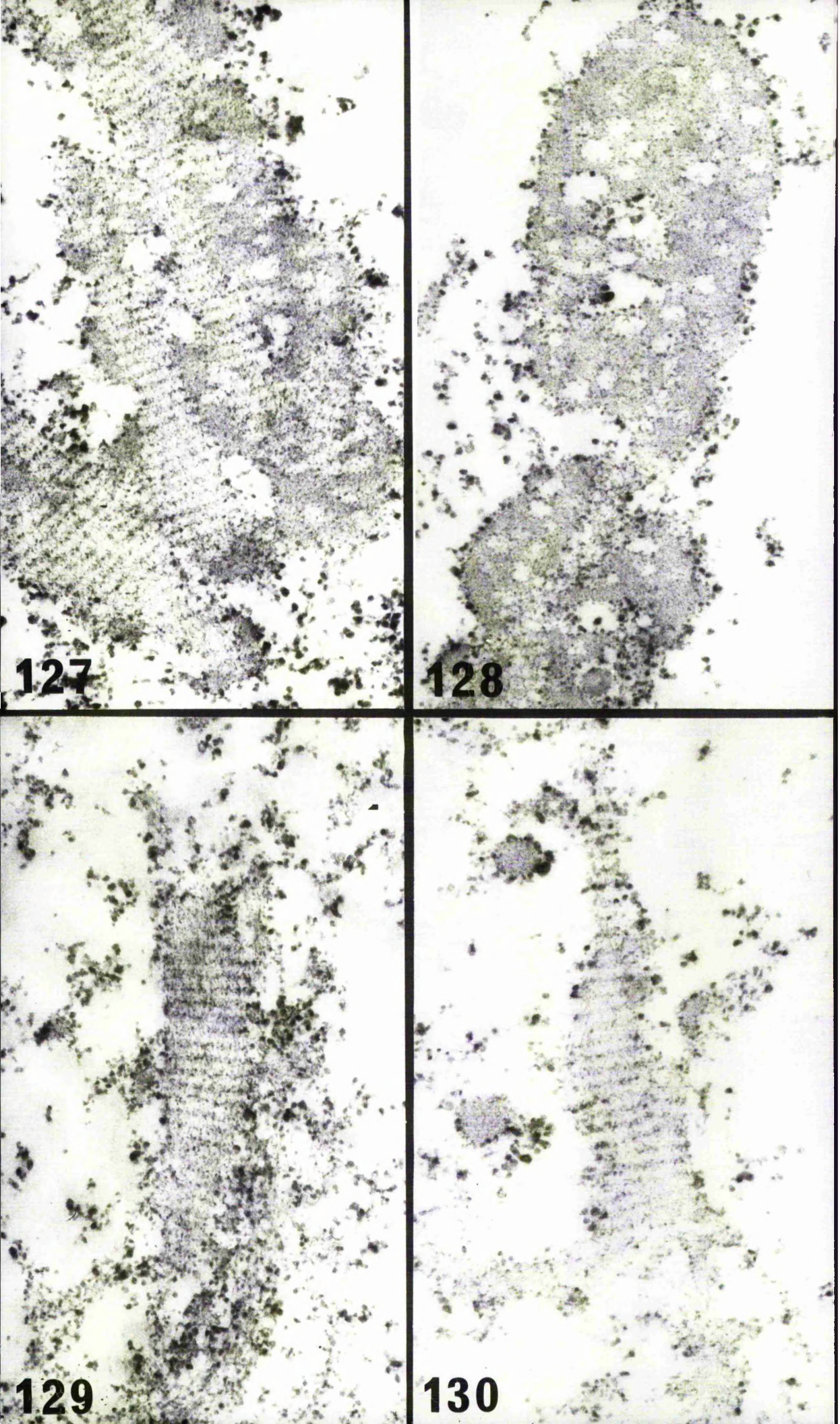
127
128
129
130

Figure 131. Appearance of notochordal cells and extracellular matrix after staining in lead haematein, pH 0.5. x 7,800

Figure 132. Banded fibre. Lead haematein, pH 0.5. x 33,000

Figure 133. Electron-dense masses. Lead haematein, pH 0.5. x 33,000

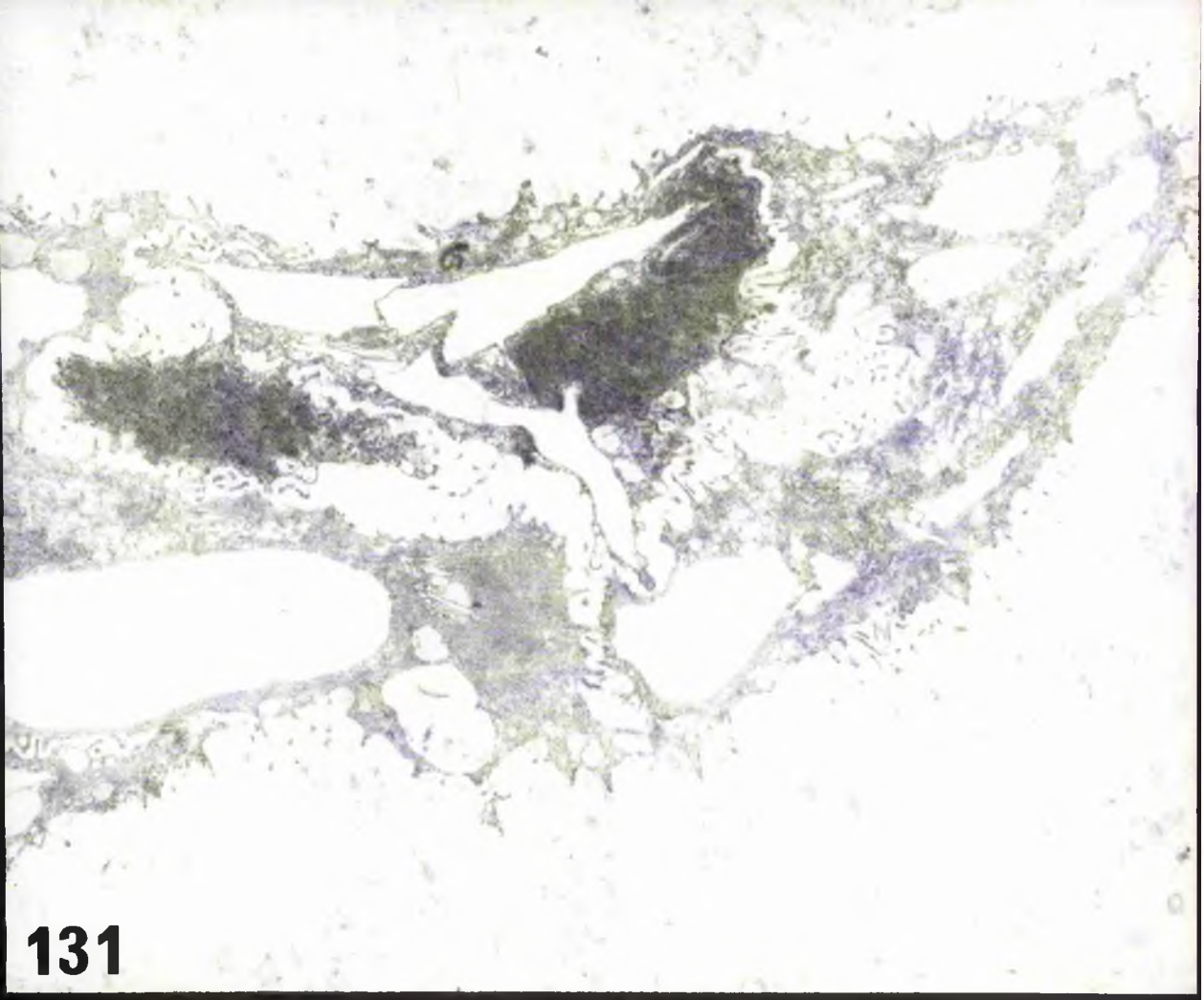

131

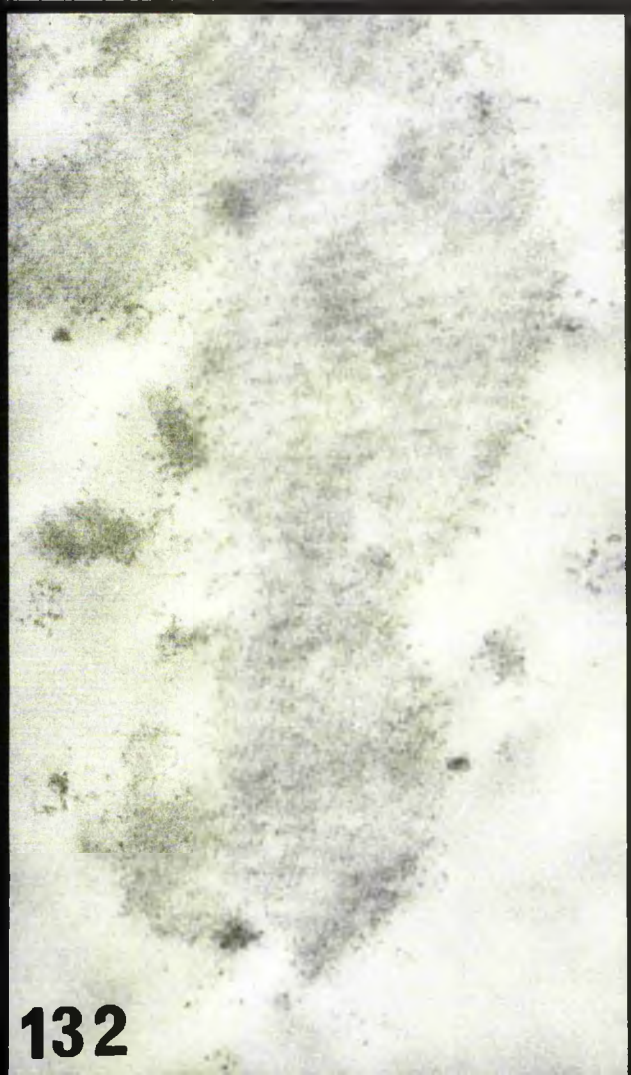

132

133

Figure 134. Appearance of notochordal cells and extracellular matrix after staining in lead haematein, pH 3.0. x 7,800

Figure 135. Banded fibre. Lead haematein, pH 3.0. x 33,000

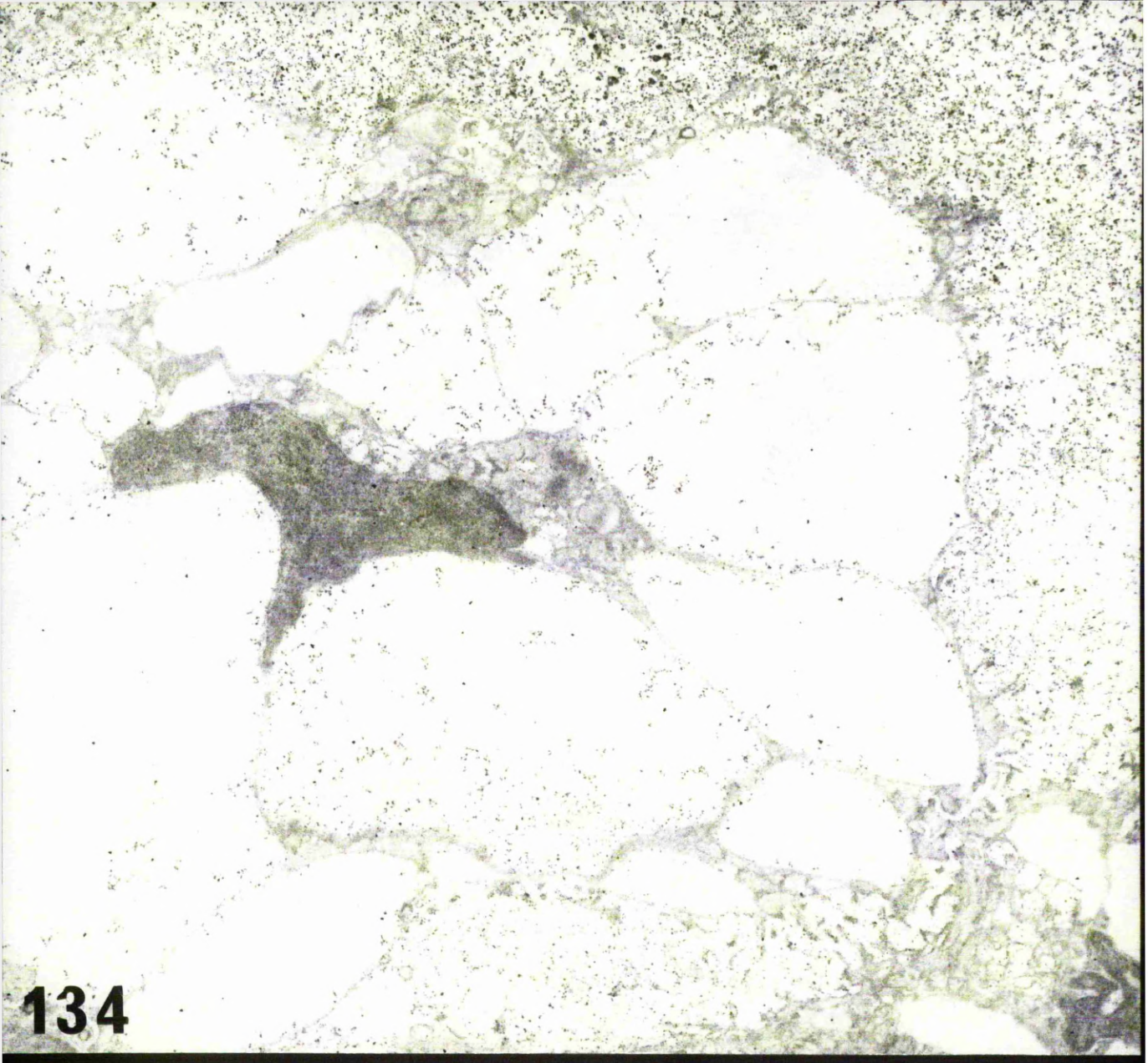

134

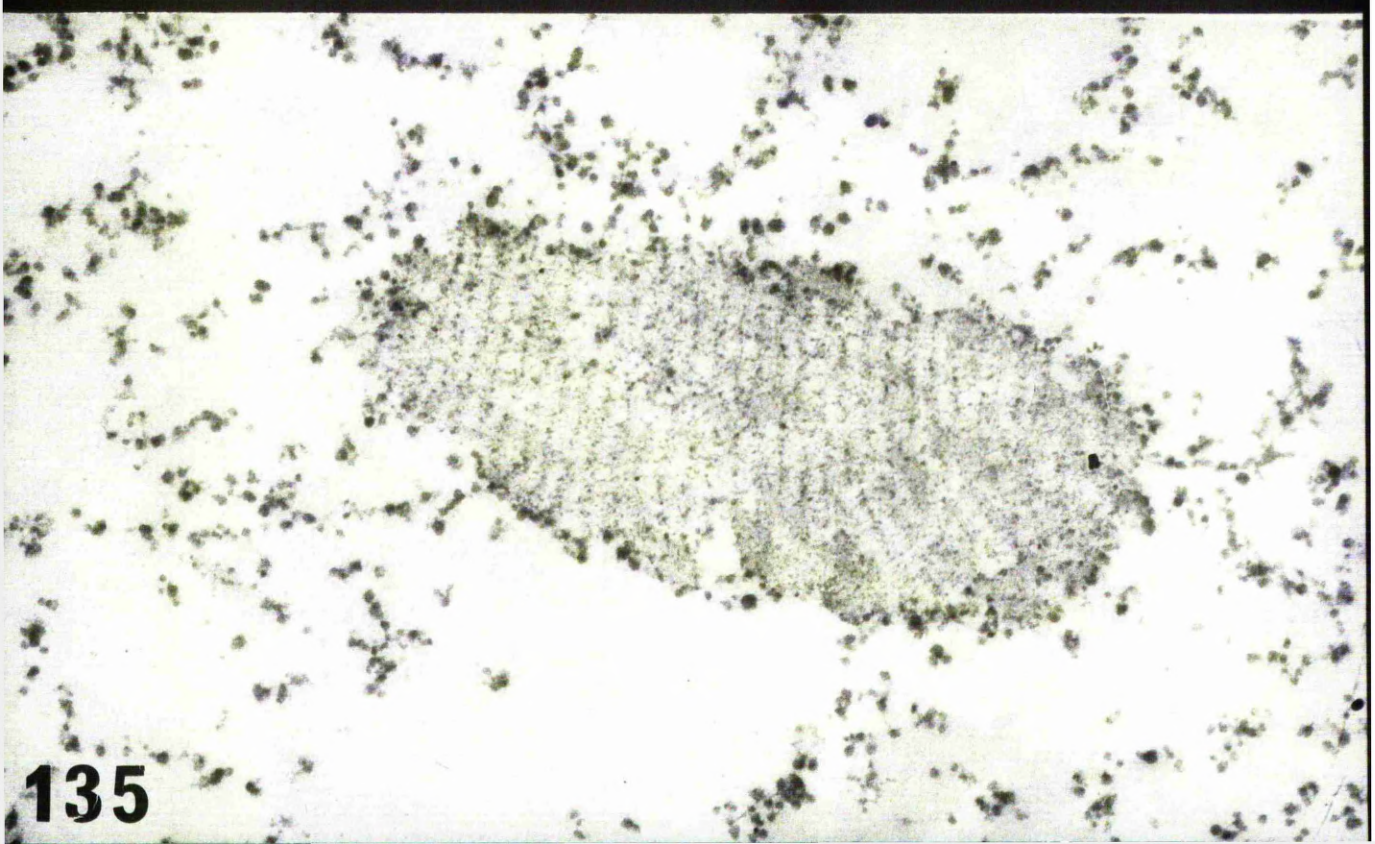

135

Figure 136. Banded fibre. Lead haematein + 0.6M $NaNO_3$. x 33,000

Figure 137. Banded fibre. Lead haematein + 1.6M $NaNO_3$. x 33,000

Figure 138. Banded fibre. Lead haematein + 1.7M $NaNO_3$. x 33,000

Figure 139. Banded fibre. Lead haematein + 2.0M $NaNO_3$. x 33,000


136


137

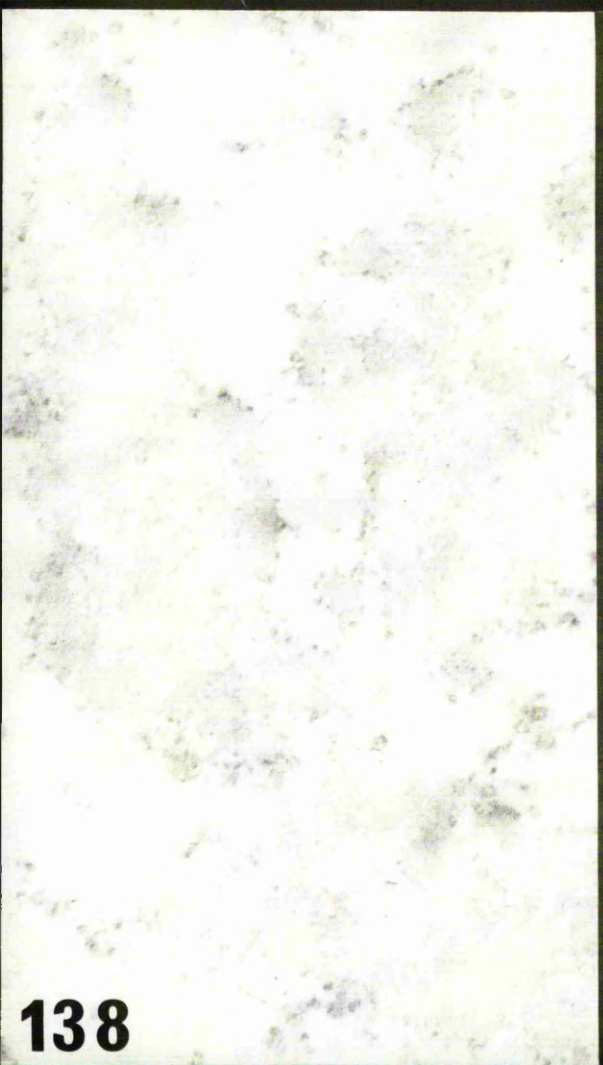
138

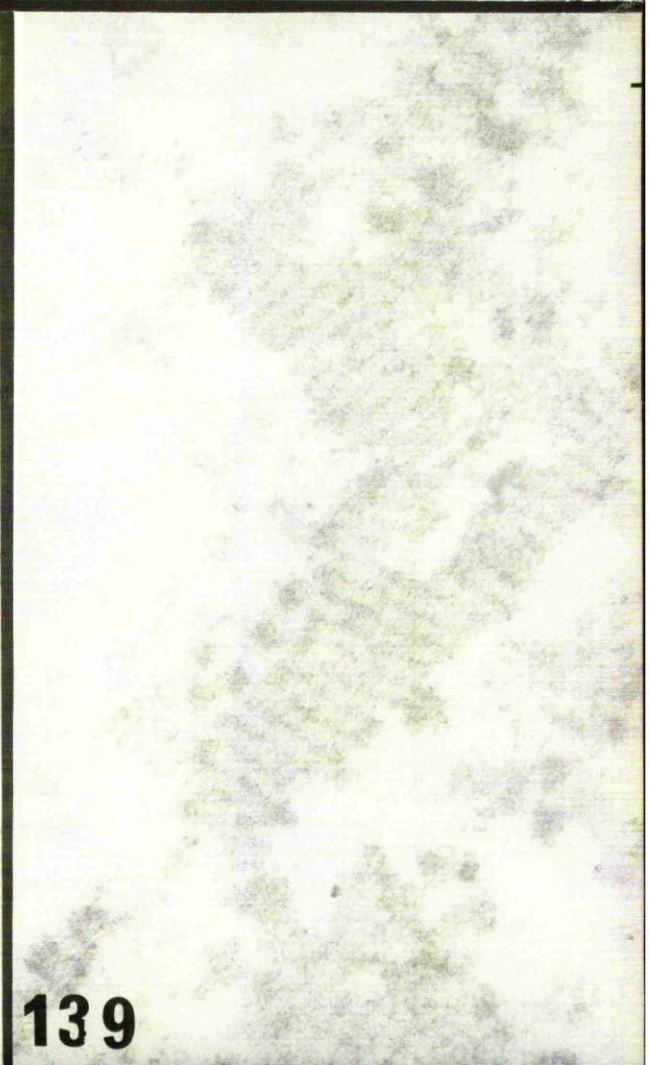
139

Figure 140. Appearance of notochordal cells and extracellular matrix after staining with lead haematein + 2.0M $NaNO_3$. x 10,000

Figure 141. Banded fibre. 5% lead nitrate. x 33,000

Figure 142. Electron-dense mass and matrix material. 5% lead nitrate + 2.0M $NaNO_3$. x 33,000

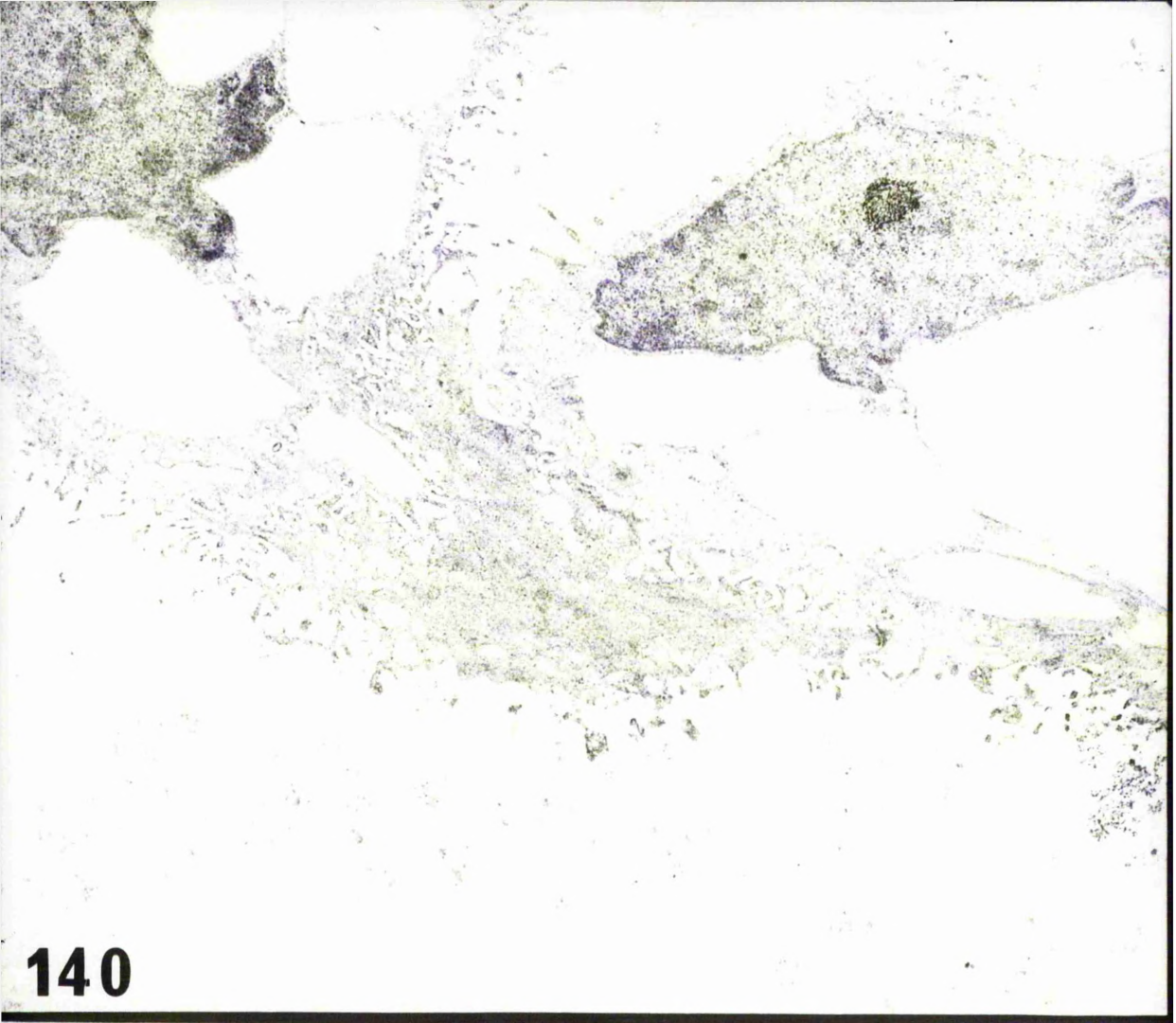

140

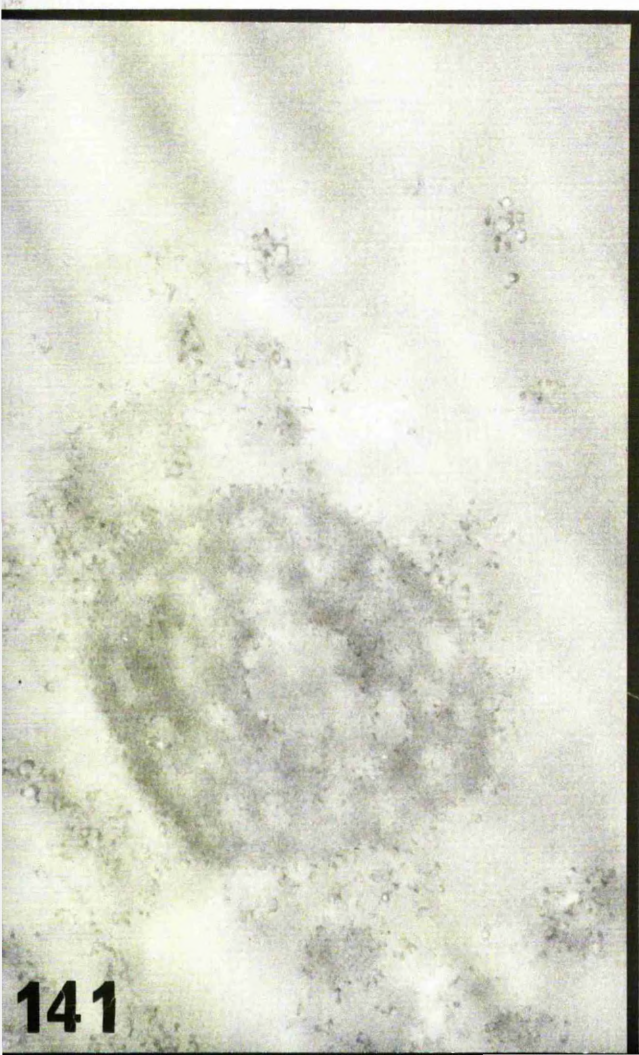

141

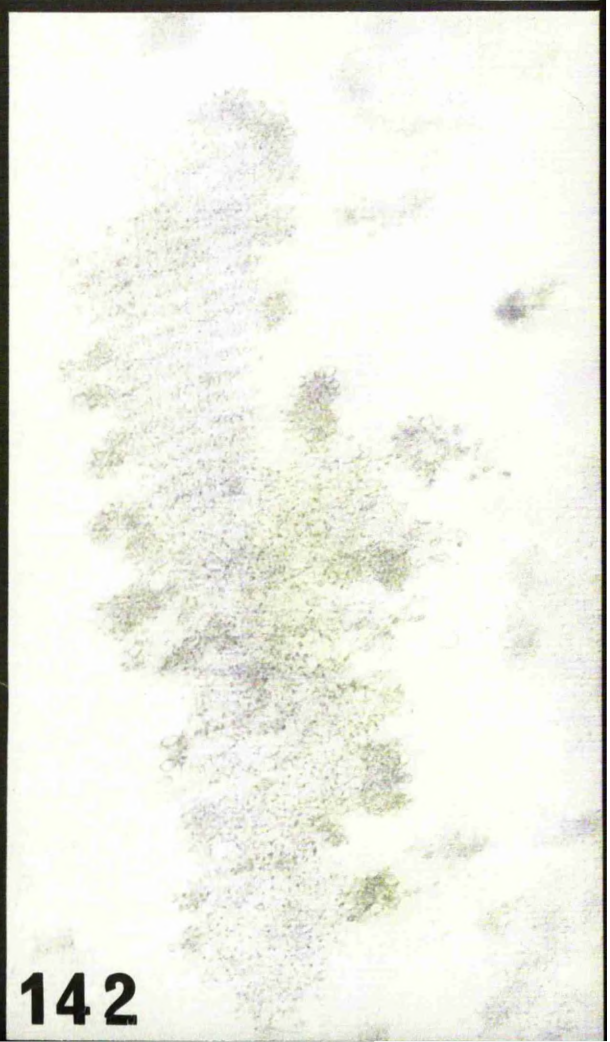

142

Figure 143. Absorption spectra of 0.6% uranyl acetate (a), 2% haematoxylin (b), and 0.4% uranium haematein (c).

Figure 144. Quantitative estimation of removal of uranium haematein from solution by chondroitin sulphate.

Absorption spectra of 0·6% uranyl acetate (a), 2% haematoxylin (b), and 0·4% uranium haematein (c)

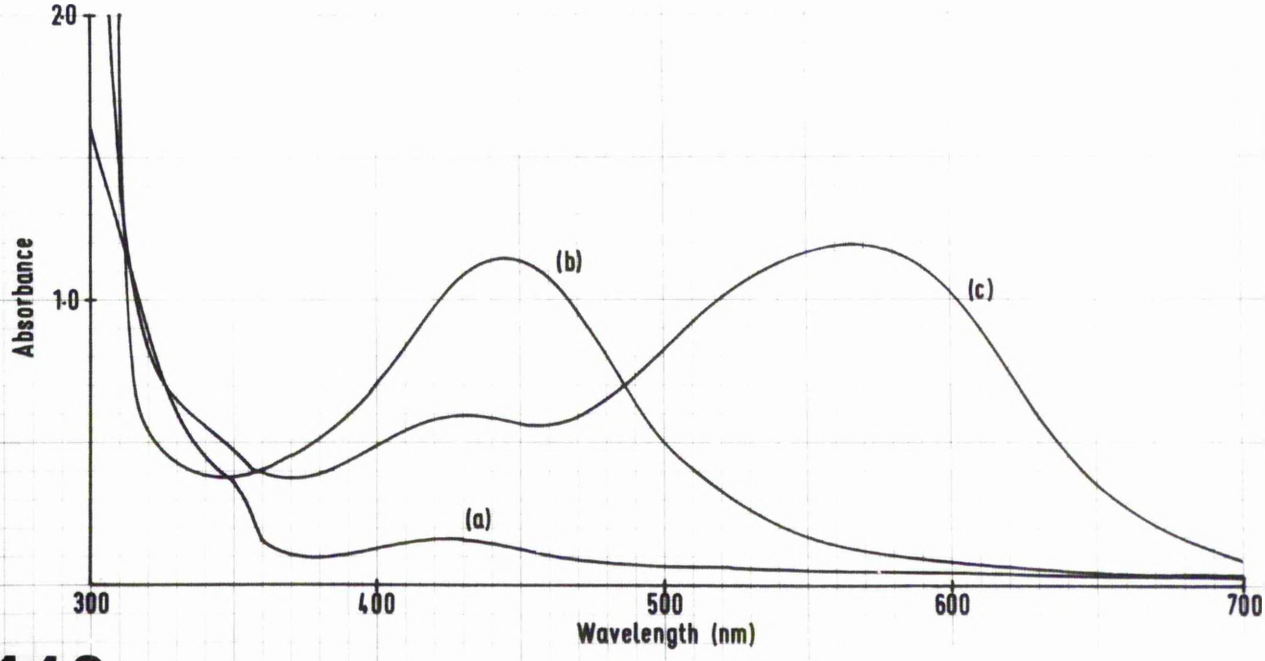

143

Quantitative estimation of removal of uranium haematein from solution by chondroitin sulphate

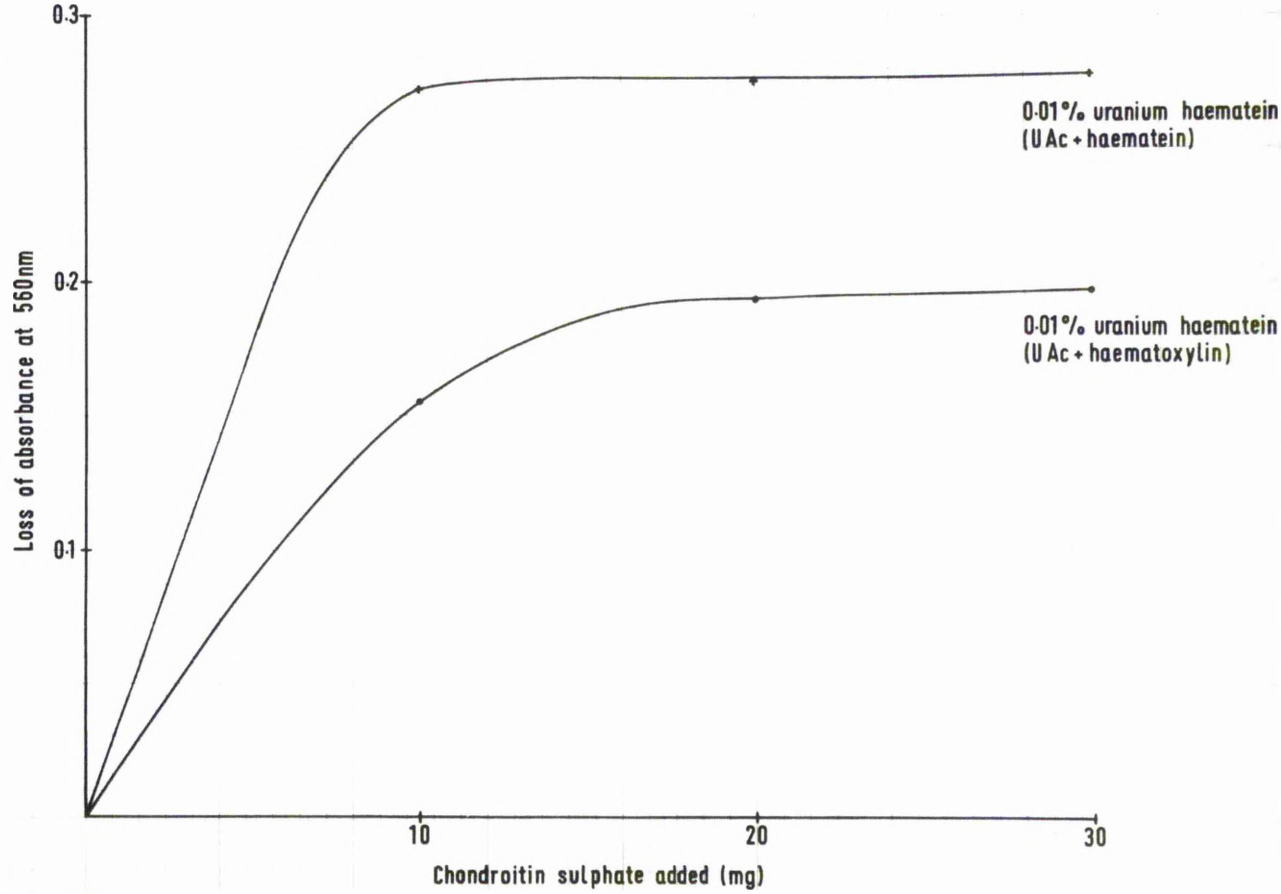

144

Figure 145. The absorbence at various wavelengths of solutions containing different proportions of uranium and haematein.

Figure 146. The absorbence at 560 nm. of solutions containing different molar ratios of uranium:haematein.

The absorbance at various wavelengths of solutions containing different proportions of uranium and haematein

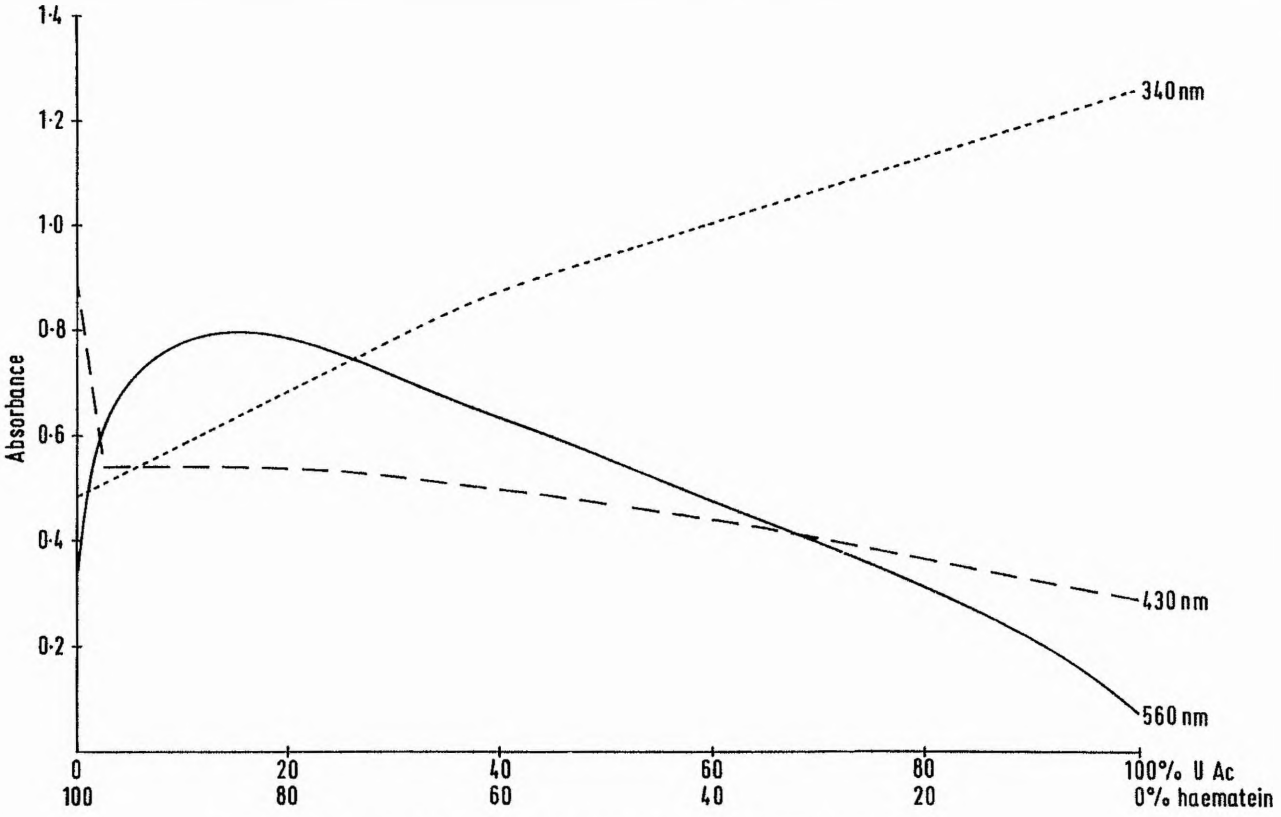

Proportion of $0{\cdot}66 \times 10^{-3}$ M haematein and $4{\cdot}71 \times 10^{-3}$ M uranyl acetate

145

The absorbance at 560nm of solutions containing different molar ratios of uranium:haematein

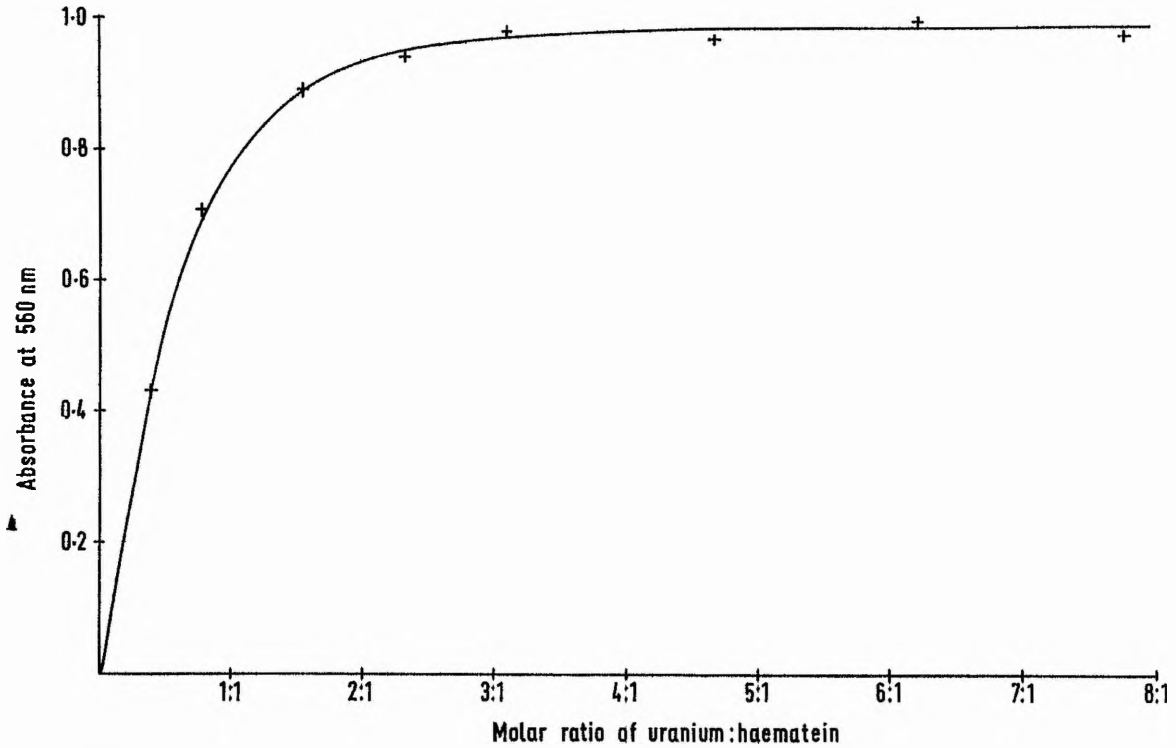

146

Figure 147. Chondrocyte in transitional zone between annulus fibrosus and nucleus pulposus. Uranium haematein (Molar ratio 2:1) pH 4.2.

x 20,000

Figure 148. Banded fibre within extracellular matrix. Uranium haematein (Molar ratio 2:1), pH 4.2. x 33,000

Figure 149. Unfixed collagen stained with uranium haematein (Molar ratio 2:1), pH 4.2.

x 150,000

Figure 150. Unfixed collagen conventionally stained with lead citrate and uranyl acetate.

x 150,000

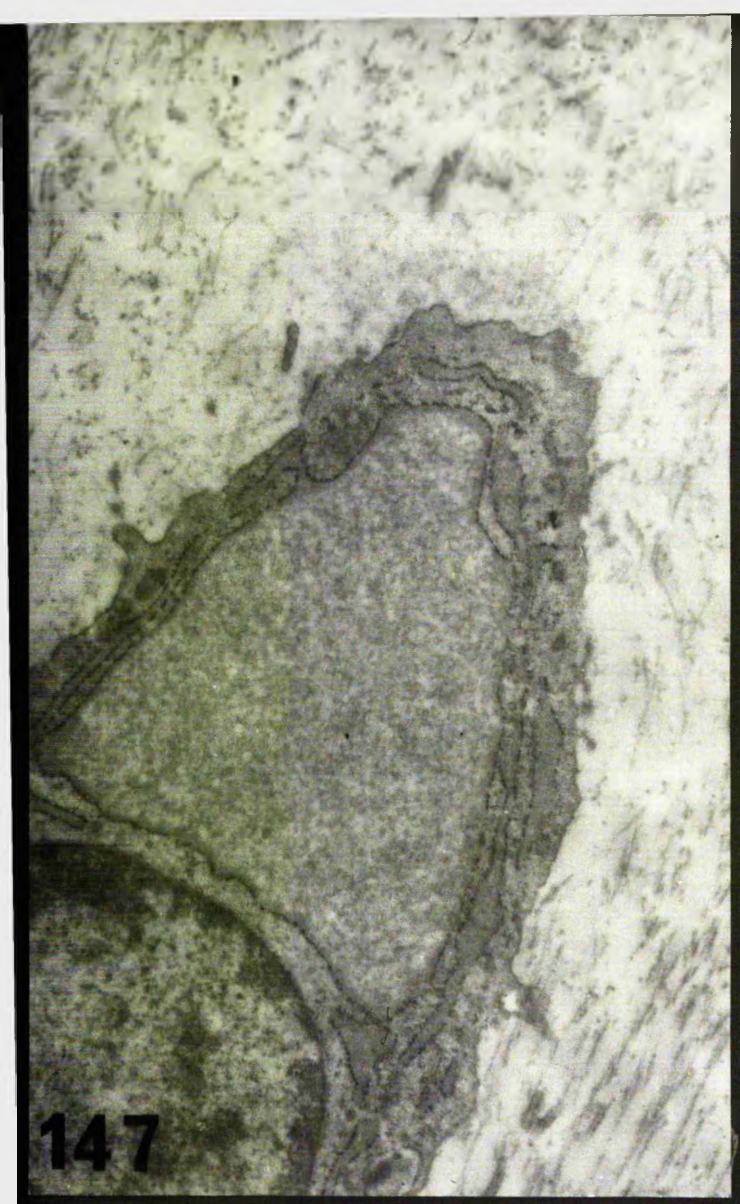

147

148

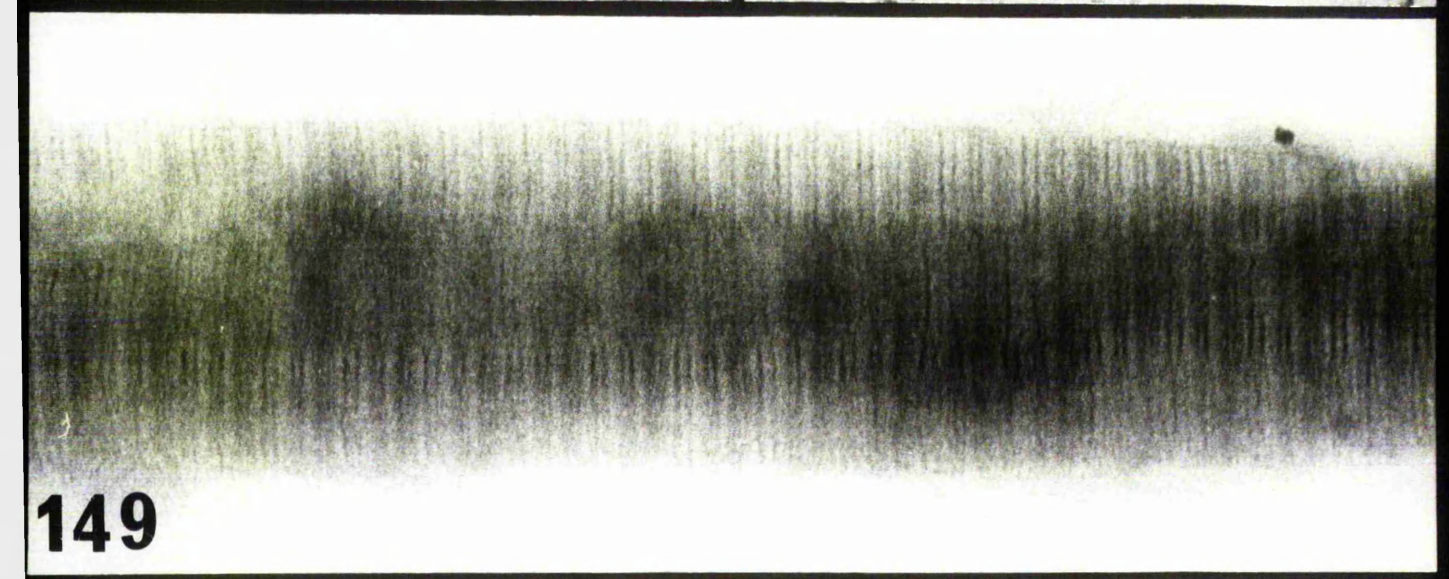

149

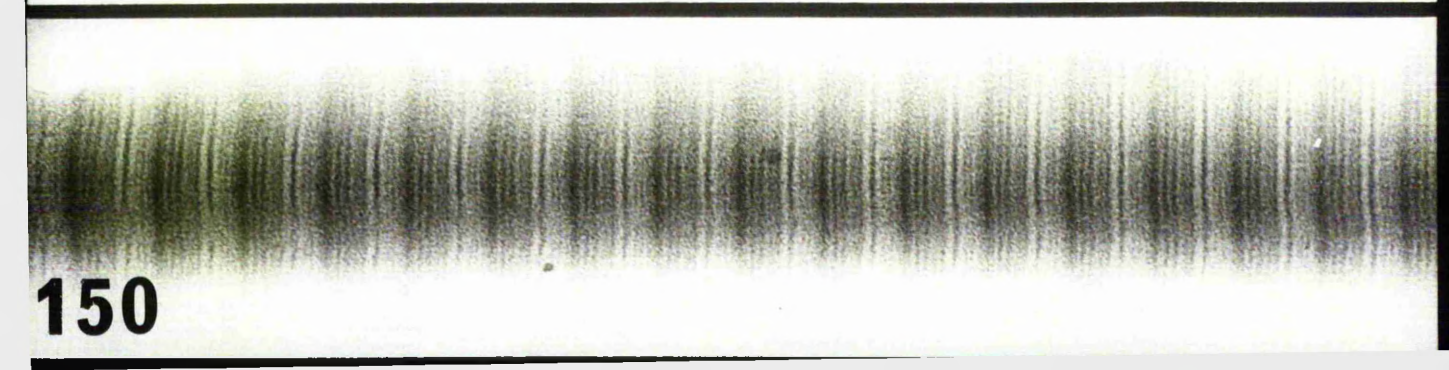

150

Figure 151. Quantitative estimation of removal of uranium haematein from solution by freeze-dried collagen.

Figure 152. Loss of absorbence at 560 nm. upon incorporation of salt into 0.5M acetate buffered uranium haematein, pH 5.6.

Quantitative estimation of removal of uranium haematein from solution by freeze-dried collagen

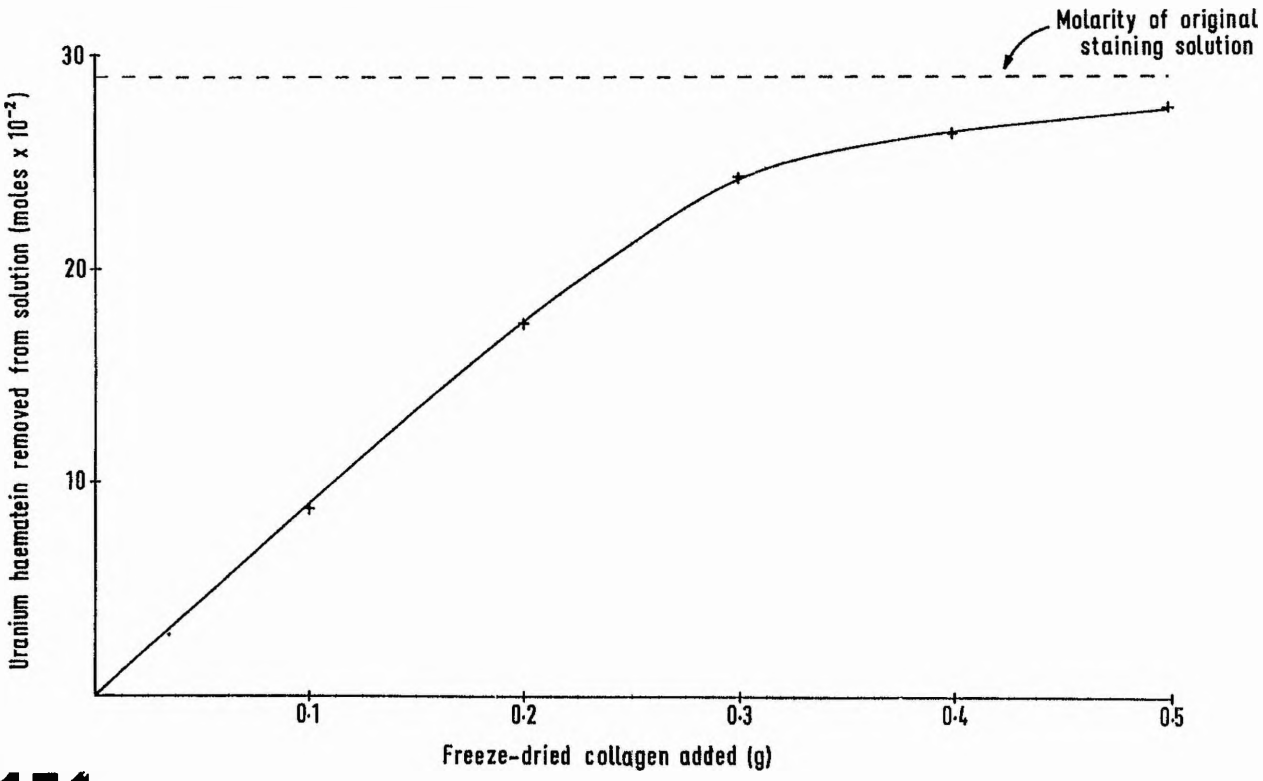

151

Loss of absorbance at 560nm upon incorporation of salt into 0·5M acetate buffered uranium haematein pH5·6

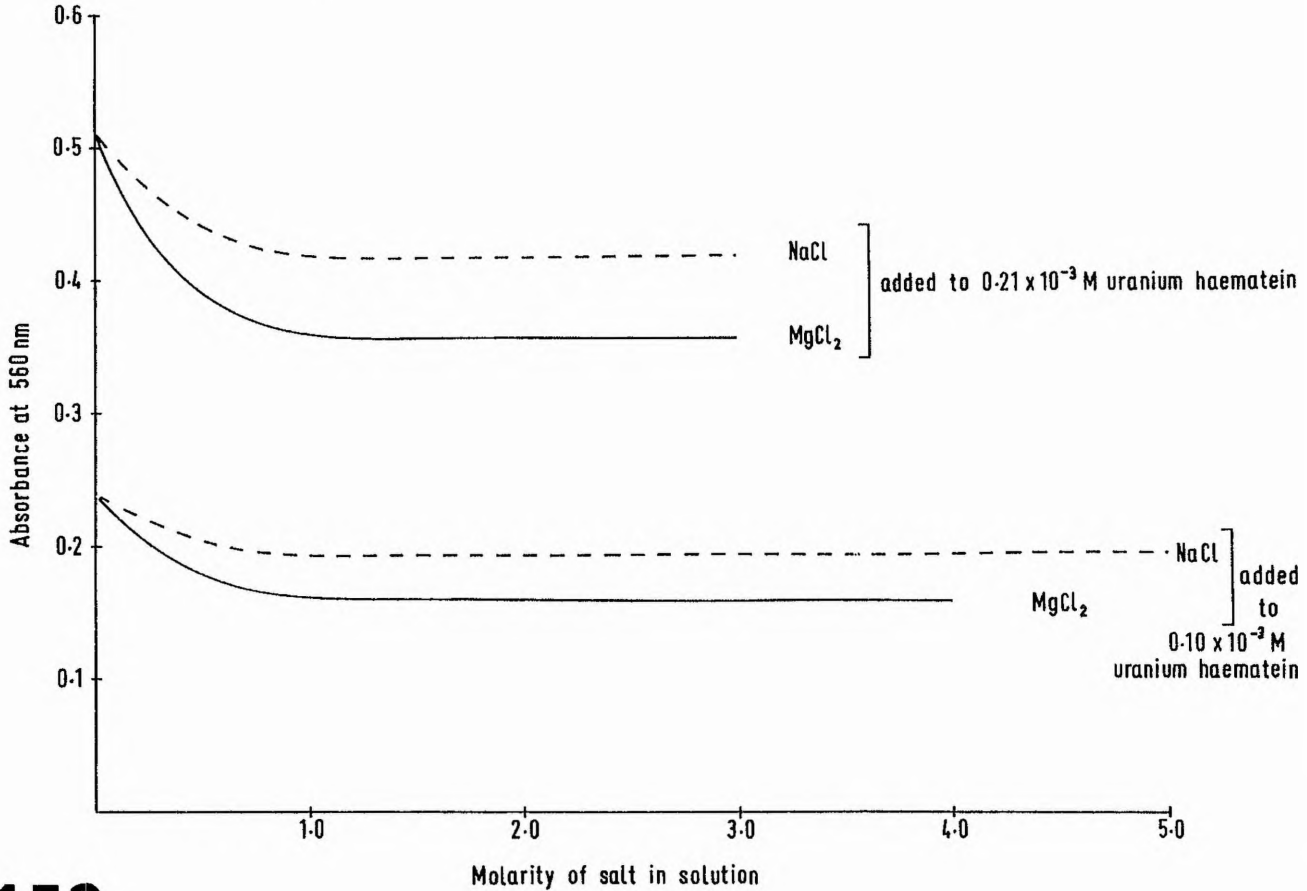

152